Impact of pH, temperature and dissolved organic matter on iron speciation and dissolved iron inventories in seawater

Dissertation

zur Erlangung des akademischen Grades eines Doktors der Naturwissenschaften

- Dr. rer. nat -

an der Mathematisch-Naturwissenschaftlichen Fakultät
der Christian-Albrechts-Universität zu Kiel

vorgelegt von

Kechen Zhu

Kiel, 2021

1. Gutachter: Prof. Eric P. Achterberg

2. Gutachter: Prof. David R. Turner

Tag der mündlichen Prüfung: 12.07.2021

Summary

Phytoplankton growth has been shown to be limited by a low supply of iron (Fe) in large parts of the world's surface ocean. In oxic seawater, the thermodynamically favored Fe form is Fe(III), which is rapidly precipitated and scavenged out of solution. Iron bound to organic matter has been shown to dominate Fe speciation and to buffer dissolved Fe (DFe) concentrations over the solubility of inorganic Fe (Fe´). Our current knowledge of Fe speciation suggests that an excess binding capacity of organic matter relative to Fe typically exists in seawater, but the sources, nature and residence time of the Fe-binding ligand pool are still largely unclear. Organic speciation of Fe is usually determined via competitive ligand exchange-adsorptive cathodic stripping voltammetry (CLE-AdCSV), but its data interpretation has some limitations, e.g. the absence of pH and temperature dimensions. The oceans are currently experiencing acidification, warming, deoxygenation and stratification, and therefore it is important to understand the impact of changing seawater chemistry conditions (e.g. decreasing pH) on Fe speciation. Therefore, I applied an ion paring-organic matter model (NICA-Donnan), to thermodynamically calculate ambient Fe speciation and derive the apparent Fe(III) solubility ($SFe(III)_{app}$).

Iron speciation is calculated by the competition between inorganic complexes and organic complexation with the NICA-Donnan model, using DFe concentrations from various seawater samples. The $SFe(III)_{app}$ is calculated in a oversaturated system by setting an input of DFe(III) to 10 nmol L^{-1}, at ambient ocean pH, temperature and dissolved organic carbon (DOC) concentrations. This will result in the precipitation of Fe hydroxide, as ferrihydrite assumed in our system. The $SFe(III)_{app}$ is defined as the sum of all aqueous inorganic species and Fe bound to organic matter at a free Fe (Fe^{3+}) concentration equal to the limiting solubility of Fe hydroxide ($Fe(OH)_3(s)$). I combined these predictions with observational DFe as well as Fe(II) data, to build a comprehensive picture on Fe speciation and DFe inventory in the ambient oceanic water column, with further feedbacks on primary productivity.

In Chapter 3, I first calibrated predictions of Fe speciation with four different NICA parameter sets representing a range of binding sites strengths and heterogeneities, by comparing those predictions to determinations of Fe speciation via CLE-AdCSV in samples collected from the

Celtic Sea. The results showed a constant low DOC concentration resulted in a slight improvement in the fit of titration data to the simulated titrations, suggesting that the changes in dissolved organic matter composition that occur alongside changes in DOC concentration dilute the Fe binding site pool. Using the optimized parameters, the calculated $SFe(III)_{app}$ was within the range of DFe concentrations observed after winter mixing on the shelf and in waters >1500 m depth at the furthest offshore stations. This supports the hypothesis that the ocean dissolved Fe inventory is controlled by the interplay between Fe solubility and Fe binding to organic matter.

In Chapter 4, I further derived Fe(III) NICA constants for marine DOM from samples collected across the Peruvian shelf and slope, via the approach PEST-ORCHESTRA. Using the constants, the modelled $SFe(III)_{app}$ showed a ca. 2 fold increase in the oxygen minimum zone compared to surface waters. The increase results from a one order of magnitude decrease in H^+ concentrations which impacts both Fe(III) hydroxide solubility and organic complexation. Using the Fe(II) measurements, I calculated the dissolved Fe(III) concentrations (DFe-FeII). The results highlight that the underlying distribution of ambient DFe(III) largely reflected the modelled $SFe(III)_{app}$ and an important role of ambient pH and temperature on the speciation and solubility of Fe.

Finally, I investigated correlations of predicted $SFe(III)_{app}$ and measured DFe at ocean basin scales, using data obtained during a series of GEOTRACES cruises (Chapter 5). A similar trend was observed in the vertical distributions of horizontally averaged $SFe(III)_{app}$ and DFe. Combining the regression analysis and proportions of DFe relative to predicted $SFe(III)_{app}$ at the basin scale, the results suggest the distribution of DFe is not solely a function of sinking organic matter remineralization processes, but also regulated by relative changes in ambient pH and temperature. pH has a larger impact on $SFe(III)_{app}$ than DOM at basin scales, based on a solubility gradient of Fe hydroxide that is driven by ambient temperature. Therefore, consideration of the impact of pH and temperature on organic Fe complexation is as important for the speciation and solubility of Fe as the characterization of Fe-binding ligands, since the global distributions Fe-binding ligand (and DOC concentrations) are relatively invariant at the basin scale.

Zusammenfassung

Das Wachstum von Phytoplankton wird nachweislich durch ein geringes Angebot an Eisen (Fe) in weiten Teilen der Weltmeere begrenzt. In oxischem Meerwasser ist die thermodynamisch bevorzugte Fe-Form Fe(III), das schnell ausgefällt wird und somit nicht mehr in Lösung vorliegt. An organisches Material gebundenes Fe dominiert nachweislich die Fe-Speziation und puffert die Konzentration von gelöstem Fe (DFe) über die Löslichkeit von anorganischem Fe (Fe´). Unser derzeitiges Wissen über die Fe-Speziation deutet darauf hin, dass im Meerwasser typischerweise ein Überschuss an Bindungskapazität von organischem Material relativ zu Fe besteht. Jedoch sind die Quellen, Arten und Verweilzeiten der Fe-bindenden Liganden noch weitgehend unklar. Die organische Speziation von Fe wird in der Regel mittels kompetitiver Ligandenaustausch-adsorptiver kathodischer Stripping-Voltammetrie (CLE-AdCSV) bestimmt, deren Dateninterpretation jedoch einige Einschränkungen aufweist, z.B. das Fehlen von pH- und Temperaturdimensionen. Die Ozeane erfahren derzeit eine Versauerung, Erwärmung, Desoxygenierung und Schichtung. Daher ist es wichtig, die Auswirkungen der sich ändernden chemischen Bedingungen (z. B. sinkender pH-Wert) auf die Fe-Speziation zu verstehen. Im rahmen der vorliegenden Arbeit wurde ein Ionenparing-Modell für organische Materie (NICA-Donnan) angewendet, um die Fe-Speziation thermodynamisch zu berechnen und die scheinbare Fe(III)-Löslichkeit ($SFe(III)_{app}$) abzuleiten.

Die Fe-Speziation wird durch die Konkurrenz zwischen anorganischen Komplexen und organischer Komplexierung mit dem NICA-Donnan-Modell berechnet, wobei DFe-Konzentrationen aus verschiedenen Meerwasserproben verwendet werden. $SFe(III)_{app}$ wird in einem übersättigten System berechnet, indem eine DFe(III) Konezentration von 10 nmol L^{-1}, bei ambienten ozeanischem-pH Werten, Temperaturen und gelösten organischen Kohlenstoff (DOC)-Konzentrationen eingestellt wird. Dies führt, wie in unserem System angenommen, zur Ausfällung von Fe-Hydroxid als Ferrihydrit. $SFe(III)_{app}$ ist definiert als die Summe aller wässrigen anorganischen Fe-Spezies und des an organisches Material gebundenen Fe bei einer freien Fe (Fe^{3+})-Konzentration, die gleich der begrenzten Löslichkeit von Fe-Hydroxid ($Fe(OH)_3(s)$) ist. Ich habe diese Vorhersagen mit beobachteten DFe- und Fe(II)-Daten kombiniert, um ein umfassendes Bild der Fe-Speziation und des DFe-Inventars in der

ozeanischen Wassersäule, mit weiteren Rückkopplungen auf die Primärproduktivität, zu erstellen.

In Kapitel 3 habe ich zunächst Vorhersagen der Fe-Speziation mit vier verschiedenen NICA-Parametersätzen kalibriert, die einen weiten Bereich von Bindungsstellenstärken und Heterogenitäten repräsentieren, indem ich diese Vorhersagen mit Bestimmungen der Fe-Speziation über CLE-AdCSV in Proben aus der Keltischen See verglichen habe. Die Ergebnisse zeigten, dass eine konstante niedrige DOC-Konzentration zu einer leichten Verbesserung der Anpassung der Titrationsdaten an die simulierten Titrationen führte, was darauf hindeutet, dass die Änderungen in der Zusammensetzung der gelösten organischen Substanz, die zusammen mit Änderungen der DOC-Konzentration auftreten, den Pool an Fe-Bindungsstellen verdünnen. Unter Verwendung der optimierten Parameter lag die berechnete $SFe(III)_{app}$ innerhalb des Bereichs der DFe-Konzentrationen, die nach der Winterdurchmischung auf dem Schelf und in Gewässern mit einer Tiefe >1500 m an den am weitesten entfernten Offshore-Stationen beobachtet wurden. Dies unterstützt die Hypothese, dass der Bestand an gelöstem Fe im Ozean durch das Zusammenspiel von Fe-Löslichkeit und Fe-Bindung an organisches Material gesteuert wird.

In Kapitel 4 habe ich mit Hilfe des PEST-ORCHESTRA Ansatzes weitere Fe(III)-NICA-Konstanten für marine gelöste organische Materie (DOM) aus Proben abgeleitet. Unter Verwendung der Konstanten zeigte die modellierte $SFe(III)_{app}$ in der Sauerstoffminimumzone einen ca. 2-fachen Anstieg im Vergleich zum Oberflächenwasser. Der Anstieg resultiert aus einer Abnahme der H^+-Konzentration um eine Größenordnung, die sowohl die Fe(III)-Hydroxid-Löslichkeit als auch die organische Komplexierung beeinflusst. Mit Hilfe der Fe(II)-Messungen habe ich die gelösten Fe(III)-Konzentrationen (DFe-FeII) berechnet. Die Ergebnisse zeigen, dass die zugrundeliegende Verteilung von DFe(III) in der Umgebung weitgehend die modellierte $SFe(III)_{app}$ widerspiegelt und dass der pH-Wert und die Temperatur der umgebenden Wassermasse eine wichtige Rolle für die Speziation und Löslichkeit von Fe spielen.

Schließlich untersuchte ich Korrelationen von vorhergesagtem $SFe(III)_{app}$ und gemessenen DFe Konzentrationen auf Ozeanbecken-Größenordnungen, unter Verwendung von Daten, die

während einer Reihe von GEOTRACES-Forschungsausfahrten gewonnen wurden (Kapitel 5). Ein ähnlicher Trend wurde bei den vertikalen Verteilungen von horizontal gemitteltem $SFe(III)_{app}$ und DFe beobachtet. Kombiniert man die Regressionsanalyse und die Anteile von DFe relativ zu vorhergesagtem $SFe(III)_{app}$, deuten die Ergebnisse darauf hin, dass die Verteilung von DFe nicht nur eine Funktion sinkender Remineralisierungsprozesse von organischem Material ist, sondern auch durch relative Änderungen des pH-Werts und der Temperatur in der Umgebung reguliert wird. Der pH-Wert hat einen größeren Einfluss auf $SFe(III)_{app}$ als DOM, basierend auf einem Löslichkeitsgradienten von Fe-Hydroxid, der durch die Umgebungstemperatur bestimmt wird. Daher ist die Berücksichtigung des Einflusses von pH und Temperatur auf die organische Fe-Komplexierung für die Speziation und Löslichkeit von Fe ebenso wichtig wie die Charakterisierung von Fe-bindenden Liganden, da die globalen Verteilungen Fe-bindender Liganden (und DOC-Konzentrationen) auf Ozeanbecken-Größenordnungen gesehen relativ unveränderlich sind.

Thanks to Dr. Felix Geißler on the German translation.

Acknowledgements

Firstly, I would like to thank my supervisor Prof. Eric P. Achterberg and my co-supervisor Dr. Martha Gledhill for giving me this opportunity, and your guidance and support. All your help has been extremely appreciated. I would also like to acknowledge the China Scholarship Council for financially supporting me during my PhD study.

Special thanks to Dr. Martha Gledhill, for sharing your knowledge and helping me to improve my research skills, and also your constant encouragement and patience regardless of any mistake I made during my work. I would never have been able to finish my dissertation without your guidance and patience. I am also grateful to Dr. Mark J. Hopwood, for your help on my first cruise, lab work and also your meaningful comments on my work.

I would like to express my thanks to all the great people of my working group. I thank Birgit Reiner, Peter Streu, Andre Mutzberg, Tim Steffens, Dominik Jasinski and Boie Bogner for all the administrative and technical support. Ali Alhashem, Jaw Chuen Yong, Münevver Nehir, Dr. Mario Esposito, Dr. Maria Martinez, Dr. Pablo Lodeiro, Dr. Xunchi Zhu and Xuechao Wang offered me great help for my lab work. Thanks to Dr. Aaron Beck, Dr. Christian Schlosser, Dr. Dagmara Rusiecka, Dr. Evangelia Louropoulou, Dr. Felix Geißler, Dr. Insa Rapp, Dr. Jan-Lucas Menzel, Jing Liu, Dr. Lucia Vieira, Dr. Ruifang Xie, Siao Jean Khoo, Stephan Krisch, Te Liu, Dr. Thomas Browning and so on. Also, I would like to show my appreciations to all the Chinese colleagues and friends who I met in GEOMAR and Kiel. They let me feel not alone and I'm really enjoying the wonderful time together.

Finally, my deepest thanks to my parents, who have provided infinite support and encouragement.

Contents

Abbreviations

AL	Artificial ligand
A_T	Total Alkalinity
CSV	Cathodic Stripping Voltammetry
CLE-AdCSV	Competitive Ligand Exchange-Adsorptive Cathodic Stripping Voltammetry
C_T	Dissolved inorganic carbon
DFe	Dissolved Fe
DFe*	The non-labile fraction of Fe (DFe*= total Fe – $FeNN_3$)
DO	Dissolved oxygen
DOC	Dissolved organic carbon
DOM	Dissolved organic matter
DW	The detection window (DW) describes the range over which competition between NN^- and natural ligand can be detected. It is traditionally defined as ±1 or 1.5 log units of $\alpha_{FeNN3,Fe'}$ (Van Den Berg et al., 1990)
Fe´	Inorganic Fe complexes
Fe^{3+}	Free iron concentration
FIA	Flow injection analysis
HEPES	N-(2-Hydroxyethyl)piperazine-N´-(2-ethanesulfonic acid)
HNLC	High nutrient low chlorophyll
I	Ionic strength
ICP-MS	Inductively coupled plasma mass spectrometry
$K_{Fe(III)DOM}$	Fe(III) NICA binding affinity
$k^{cond}_{FeNN3,Fe',or\ Fe3+}$	Conditional stability constants describing the strength of a complex $FeNN_3$ relative to inorganic Fe (Fe´) concentration or free Fe (Fe^{3+}) concentrations
$k^{cond}_{FeL,Fe',or\ Fe3+}$	Conditional stability constants describing the strength of a complex FeL (i.e. Fe binding to natural ligand) relative to inorganic Fe (Fe´) concentration or free Fe (Fe^{3+}) concentrations

$k_{FeNN3,H+}$	The stability constant of HNN used in an ion pairing model, that would account for competition between NN^-, H^+, Fe^{3+} and OH^- at the ionic strengths and pH relevant to our study
LDPE	Low-density polyethylene
$n_{Fe(III)DOM}$	Non-ideal constant for Fe(III)
NICA-Donnan	Non-ideal competitive adsorption in Donnan-like gels
HNN	1-nitroso-2-naphthol
NOM	Natural organic matter
OMZ	Oxygen minimum zone
pFe´	Inorganic Fe complexes in log scale ((-log($\sum Fe(OH)_i^{3-i}$))
pH_{NBS}	pH on the IUPAC/NBS scale
pH_{tot}	pH on the total scale
POPSO	Piperazine-1,4-bis(2-hydroxypropanesulfonic acid)
Q_{max,H^+}	Total amount of proton binding sites in dissolved organic matter
$SFe(III)_{app}$	The apparent solubility of Fe(III) calculated using the NICA-Donnan model by setting the total Fe(III) to 10 nmol L^{-1}, at ambient ocean pH, temperature and DOC concentrations.
WHAM	Windermere humic acid model
$\alpha_{FeNN3,Fe',or\ Fe3+}$	Side reaction coefficient for $FeNN_3$ expressed relative inorganic Fe (Fe´) or free Fe (Fe^{3+}) concentrations
$\alpha_{FeL,Fe',or\ Fe3+}$	Side reaction coefficient for Fe-natural ligand expressed relative inorganic Fe (Fe´) or free Fe (Fe^{3+}) concentrations

1 Introduction

Iron (Fe) is the fourth most abundant element in the earth's crust (Wedepohl, 1995), but it is present as a trace element (less than 1 mg kg^{-1}) in the modern oxygenated ocean. Early in the 1930s experimental data firstly showed that Fe enrichment stimulated the growth of phytoplankton providing evidence of Fe limitation to phytoplankton in seawater (Ruud, 1930; Gran, 1931; Hart, 1934). In 1990, Martin. (1990) proposed the 'Fe hypothesis' which postulated that increased inputs of Fe from dust into Southern Ocean during glacial periods resulted in enhanced utilization of nutrients and significant drawdown of carbon dioxide from the atmosphere. Iron enrichment experiments ranging from bottle incubations (Hutchins et al., 2002; Browning et al., 2018) to large-scale open ocean studies (Boyd et al., 2007) suggest Fe supply could stimulate phytoplankton growth in the high nitrate low chlorophyll (HNLC) regions, which currently make up 30% of the surface ocean (de Baar et al., 2005). Furthermore, Moore et al. (2009) suggests Fe could also have the potential to regulate nitrogen fixation by diazotrophs in nitrogen poor low latitude waters. Therefore, low supply of Fe could affect as much as half of the surface ocean.

1.1 Iron solubility and bioavailability in seawater

1.1.1 Iron solubility

Iron can exist in two oxidation states in seawater, the soluble ferrous form (Fe(II)) and ferric form (Fe(III)). In oxic seawater the thermodynamically favored form, Fe(III), is strongly hydrolyzed, and tends to precipitate as particulate Fe(III) hydroxides. Inorganic Fe has a poor solubility at near a seawater pH of 8.0 (0.01 nmol L^{-1}, 25°C) (Liu and Millero, 2002), but dissolved Fe (DFe) concentrations are much higher than inorganic Fe solubility (Johnson et al., 1997). Previous work has shown Fe bound to organic matter plays a critical role in Fe speciation and significantly enhances Fe solubility (Kuma et al., 1996; Liu and Millero, 2002; Gledhill and Buck, 2012). The more soluble form, Fe(II) is found in oxic waters as a transient species, and is thus present at low concentrations (Croot et al., 2008; Croot and Heller, 2012). In some cases, Fe(II) forms an important fraction of DFe concentrations, e.g. in low pH or low oxygen waters such as porewaters, hydrothermal vent fluids and oxygen minimum zone (Rickard and Luther,

2007). The rate of Fe(II) oxidation is dependent primarily on dissolved oxygen (DO) concentrations, pH and other reactive oxygen species (e.g. H_2O_2), as well as temperature and salinity (Millero et al., 1987; Millero and Sotolongo, 1989). Production of Fe(II) via several different processes should be considered in addition to oxidation rate only in seawater. Photochemistry is the dominant source of Fe(II) in surface seawater (Rose and Waite, 2005; Barbeau, 2006), in addition to processes such as biological release (Croot et al., 2008). In bottom seawater, Fe(II) can diffuse from porewaters to overlying waters with rates largely dependent on the DO gradient and biological activity (Homoky et al., 2012; Schlosser et al., 2018).

Dissolved Fe is operationally defined as Fe passing through a 0.2 µm filter (or 0.45 µm used in earlier literature). This fraction will include Fe(II), inorganic Fe(III) complexes, Fe(III) complexed by organic matter, small colloids and nanoparticles (Turner and Hunter, 2001; Raiswell and Canfield, 2012). These different Fe species are difficult to separate via filtration as their size ranges overlap (Figure 1.1). In oxic seawater, the physical distribution of Fe based on mass balance can be summarized as

$$Fe_{total} = Fe_{particulate} + Fe_{colloid} + Fe_{soluble} \quad (1)$$

Where $Fe_{colloid}$ is usually defined as the size range between 0.02 µm and 0.2 µm, and $Fe_{soluble}$ represents the <0.02 µm fraction. However, some of colloidal fractions of Fe may decrease Fe bioavailability and facilitate Fe removal through transformation of the colloidal fraction into larger particles (Wu et al., 2001). In contrast, using the chemical perspective, the distribution of Fe on the mass balance can be summarized as

$$Fe_{total} = Fe' + FeL + Fe_{inert} \quad (2)$$

Where Fe' represents labile inorganic Fe complexes, FeL represents Fe organic ligand complexes exchangeable with a time scale of < 1 day, and Fe_{inert} represents the Fe fraction bound up in matrices that are essentially non-labile over a period of 1 day or more. Although the organic complexation determines Fe speciation and strongly buffers DFe concentrations, the overall physico-chemical speciation of DFe is more complex in ambient seawater (Gledhill and Buck, 2012). In addition, the balance between the supply of Fe and removal processes primarily determines DFe distributions in the ocean (Boyd and Ellwood, 2010), where the organic complexation predominantly keeps Fe in soluble.

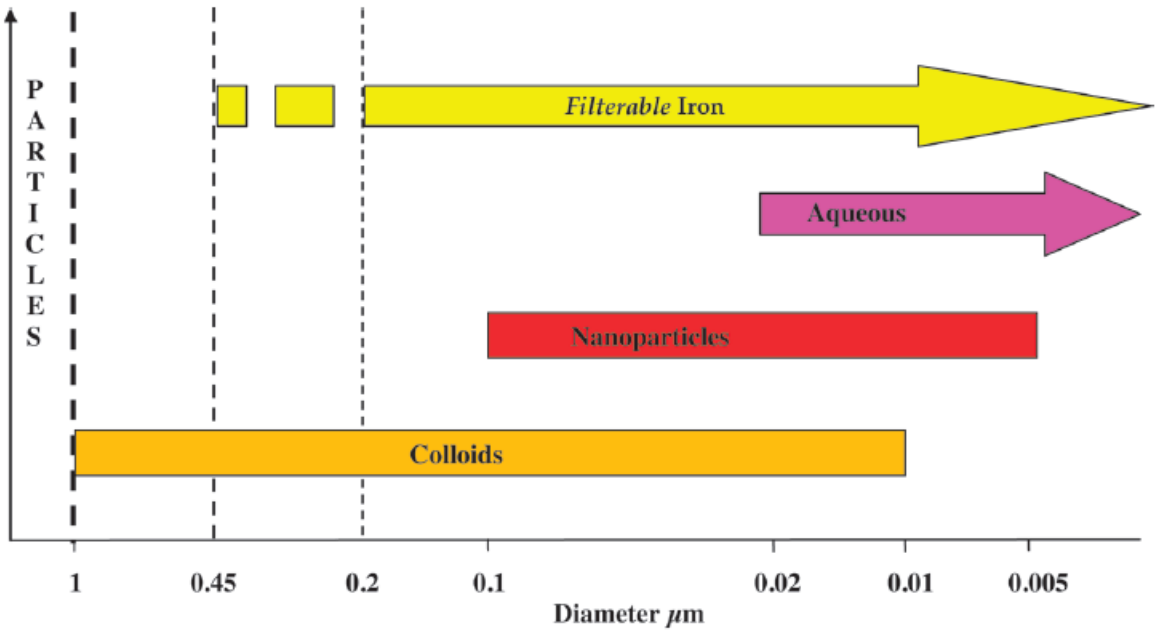

Figure 1.1. Size ranges of particles, colloids, nanoparticles and aqueous species in relation to filterable iron, which is regenerated from Raiswell and Canfield (2012).

The supply/sinks of iron in seawater

The Fe cycle is driven by the rates of supply and removal in seawater. Within the Fe supply, Boyd and Ellwood (2010) suggests it could be divided into two parts, 'new' (i.e. adding to oceanic inventory) and 'recycled' (i.e. turnover of the inventory). Within the Fe removal, it could also be divided into two parts, scavenging as a result of adsorption, precipitation and aggregation process leading to soluble phases being converted into colloidal and particulate forms, and biological uptake. The 'recycled' Fe and the biological part of Fe sinks, are driven by the internal cycling that mostly depends on primary production in the ocean. In the Fe supply, there are multiple sources of 'new' Fe, including e.g. rivers, icebergs, dust, sediments and hydrothermal sources, which are present from surface to deep water, and coast to open ocean.

River inputs are the dominant source of Fe to estuarine waters (Bruland and Lohan, 2006) and their immediate surroundings. The overall DFe flux from rivers into the world ocean is estimated to be 26 x 10^9 mol y^{-1} (Turner and Hunter, 2001). Much of this DFe is removed during estuarine mixing (Boyle et al., 1977; Sholkovitz et al., 1978; Hunter and Leonard, 1988) as charged Fe-

binding colloids aggregate to form larger particles and thus flocculate as salinity increases, and this removal process may be influenced by particle size in river water (Dai and Martin, 1995; Wen et al., 1999). Previous works have shown that organic Fe complexation plays a key role in Fe transport over great distances from river sources to the open ocean as well as in Fe availability to biological utilization (Powell and Wilson-Finelli, 2003; Rijkenberg et al., 2006b; Muller, 2018). Recently, Vieira et al. (2020) used both radium isotope and trace element data, and showed that Fe delivery from Congo River significantly contribute to offshore Fe availability in South Atlantic gyre, possibly resulting from rapid transport and additional benthic sources of Fe as well as the stabilization by organic ligands.

Atmospheric dust is a dominant external input of Fe to the surface open ocean, e.g. the western north Atlantic ocean receives about 43% of global oceanic dust inputs (Jickells et al., 2005). Volcanic dust can also act as a source of Fe and natural fertilization of Fe-depleted surface waters through volcanic-derived ash particles has been shown to stimulate phytoplankton growth and completely drawdown the macro nutrients nitrate and phosphate in the North Atlantic (Achterberg et al., 2013). Previous studies have shown that Fe has a short residence time in surface waters (Sarthou et al., 2003; Bergquist and Boyle, 2006), e.g. 17 to 28 days in the northeast Atlantic Ocean, so that Fe is rapidly removed from surface waters by precipitation and/or colloidal aggregation (Sarthou et al., 2003). On the other hand, photo-reduction of colloidal Fe has been observed in surface waters (Barbeau et al., 2003; Rijkenberg et al., 2006a), and could be an important process for maintaining elevated DFe in surface waters.

Icebergs are thought to be one of the largest Fe sources (3.9-30.5 Gmol Fe yr^{-1}) to both the Arctic and Southern Oceans (Boyd et al., 2012). Smith et al. (2007) reported increased iceberg fluxes could result in enrichment of iceberg derived terrigenous material (e.g. organic matter and Fe), and thus increase the abundance of phytoplankton. However, Hopwood et al. (2019) suggested that inputs of DFe from icebergs could also be influenced by the properties of the icebergs themselves and particularly by the speciation of released Fe from melt ice (e.g. dissolved-particulate size and distributions of Fe content). In addition to the properties of the icebergs, Fe complexation by organic matter is also expected to play a role and previous work has reported that Fe is undersaturated compared to the binding capacity of organic matter in Southern Ocean

waters (Boye et al., 2001; Croot et al., 2004a). Iron complexed by organic matter could therefore have the potential to facilitate the stability of iceberg Fe fluxes to the overall DFe inventory.

Resuspended shelf sediments and porewaters release combined with upwelling process are likely dominant sources of Fe to coastal surface waters (Johnson et al., 1997; Moore et al., 2004). Previous work has reported high DFe fluxes from reduced sediments in the Peruvian upwelling region (Bruland et al., 2005; Scholz et al., 2011, 2014; Vedamati et al., 2014) where very low oxygen concentrations lead to the predominance of Fe(II) in DFe pool in upwelled waters (Schlosser et al., 2018; Croot et al., 2019). On the other hand studies of Fe speciation in OMZs suggest the organic Fe complexation could shift the redox equilibrium away from Fe(II) (Witter et al., 2000; Hopkinson and Barbeau, 2007; Kondo and Moffett, 2015) and promote Fe(II) oxidation, thus minimizing the spatial extent of strong sedimentary Fe sources. The mechanism of DFe supply to surface water could therefore be strongly influenced by Fe complexed by organic matter. Furthermore, a recent study has shown that shelf humic substances potentially complex and transport sedimentary Fe for at least 4000 km in the North Pacific, suggesting the key role of organic complexation in shaping the distribution of Fe (Yamashita et al., 2020).

In the deep ocean, hydrothermal vents have been observed to strongly influence the DFe pool, e.g. in South Atlantic Ocean and South Pacific Ocean hydrothermal fluids have been shown to be enriched in Fe by more than several orders of magnitude relative to ambient DFe concentrations (Saito et al., 2013; Fitzsimmons et al., 2014, 2017). On one hand, the study of the DFe fraction that transports Fe from hydrothermal vents by Fitzsimmons et al. (2014, 2017) and the investigations of ligand characteristics by Buck et al. (2018) in the South Pacific Ocean, suggest Fe bound to organic matter could increase the stabilization of this DFe source and buffer it against scavenging. On the other hand, studies of Fe speciation near hydrothermal vents have shown that only small amount of hydrothermal Fe may be stabilized by complexation and that this will limit the increase in the DFe pool in deep water (Bennett et al., 2008; Hawkes et al., 2013; Kleint et al., 2016). Nevertheless, Fe complexed by organic matter could constrain the input of Fe from hydrothermal vents, thus influencing the transport of this Fe and further utilization by primary producers.

Comparing to new Fe supply, scavenging is the main removal mechanism of Fe from seawaters (Johnson et al., 1997). Iron is generally removed by scavenging on settling particles and vertical export of biogenic material from the surface ocean. It has been shown that Fe scavenging is a two-stage process, with reversible absorption to smaller and colloidal particles, and followed by aggregation and removal on large particles (Bruland and Lohan, 2006). In surface waters, Croot et al. (2004b) has reported an extremely short residence time with 6 to 62 days for Fe in the equatorial Atlantic due to rapid removal by aggregation and subsequent sinking of particles. A fraction of scavenged Fe is added to the sinking particulate Fe pool and will remineralize at depth throughout the water column, which is also an important source of Fe in the deep ocean. In intermediate water, Tagliabue et al. (2019) using a global model has shown that the accumulation of Fe is largely controlled by opposing fluxes of regeneration and scavenging, suggesting internal cycling is the main control on Fe stocks within intermediate waters. In deep ocean, Kuma et al. (2003) has shown that DFe depth profiles are a result of sinking particulate organic matter (POM), remineralization of sinking POM and ambient Fe solubility, suggesting ambient Fe solubility primarily determines DFe concentrations in deep ocean. Nevertheless, the residence time of Fe affects the DFe inventory in seawater, which is mainly driven by the process of regeneration and scavenging, and ambient Fe solubility that is influenced by complexed by organic matter.

1.1.2 Iron bioavailability

There is an well-defined recognition that limited availability of Fe lowers phytoplankton pigment content and light harvesting capacities, hinders photosynthesis and growth rates, and subsequently diminishes the production of organic matter and biogenic minerals (Boyd et al., 2007). Shaked and Lis, (2012) defined Fe bioavailability as the degree to which a certain Fe compound can be accessed and utilized by phytoplankton and this definition is followed in this thesis. However, quantifying Fe bioavailability is difficult in the marine environment, since Fe speciation is dynamic in time and space and Fe exists as a multitude of different compounds with substantially different chemical and physical properties (Turner and Hunter, 2001; Raiswell and Canfield, 2012). Compared to particulate Fe (pFe) or colloidal Fe (cFe), dissolved Fe is generally regarded as a more bioavailable fraction, but there is also evidence that pFe and cFe could be

utilized by phytoplankton (Sunda, 2001). Reductive dissolution of pFe in the presence of siderophores could be a potential Fe source for phytoplankton (Vraspir and Butler, 2009). In addition, phytoplankton physiology, light, temperature and microbial interactions could also affect Fe bioavailability (Worms et al., 2006; Shaked and Lis, 2012), e.g. Fe limitation caused the upregulation of high affinity Fe acquisition systems allows changes in access to different Fe pool (Maldonado and Price, 2001; Maldonado et al., 2006; Allen et al., 2008).

In the dissolved Fe pool, previous results from both laboratory and field culture experiments suggest inorganic Fe complexes (Fe´), are highly bioavailable fraction compared to most organically bound iron forms and small colloids (Morel et al., 2008; Shaked and Lis, 2012). However, in addition to the most readily available fraction Fe´, organically complexed Fe is important for phytoplankton, either via siderophore mediated Fe acquisition (Kazamia et al., 2018; Coale et al., 2019) or a reductive iron uptake pathway (Maldonado and Price, 2001; Shaked et al., 2005). Taken with the chemical perspective on the Fe speciation (equation 2), Fe solubility and bioavailability are thus both a function of its chemical speciation, which is largely influenced by the organic complexation (Boyd and Ellwood, 2010; Gledhill and Buck, 2012; Shaked and Lis, 2012).

1.2 Iron complexed by organic matter in seawater

Marine dissolved organic matter (DOM) accounts for 90% of organic carbon in the ocean that is approximately equal to the atmosphere's CO_2 load (Siegenthaler and Sarmiento, 1993; Hansell and Carlson, 2002). Marine DOM is operationally defined as the fraction passing through a filter of a nominal pore size (usually between 0.1 and 1.0 µM), where a major part is refractory and resistant to chemical decomposition and the bulk of its chemical structure remains largely unknown (Dittmar and Kattner, 2003; Koch et al., 2005; Zark and Dittmar, 2018). Interactions between dissolved trace elements (i.e. Iron in this thesis) and organic matter not only affect trace element availability to biota but also their mobility in biogeochemical cycles in the ocean, with strong feedback to climate change (Figure 1.2) (Zhang et al., 2019). Primary productivity produces organic matter that is the potential component of the Fe-binding ligand pool (Mawji et al., 2008; Vraspir and Butler, 2009), while in turn primary productivity is potentially limited by

insufficient Fe supply in large areas of the global surface ocean, e.g. in HNLC regions. Although the diverse sources and molecular structures of marine DOM lead to the complex composition of the Fe-binding ligand pool, knowledge on Fe binding to organic matter is typically acquired in two different ways, one using comparative ligand exchange-adsorption cathodic stripping voltammetry to directly focus on organic complexation (Gledhill and Buck, 2012), and the other one using mass spectrometry to determine the chemical composition of organic matter (Dittmar and Kattner, 2003; Koch et al., 2005; Zark and Dittmar, 2018).

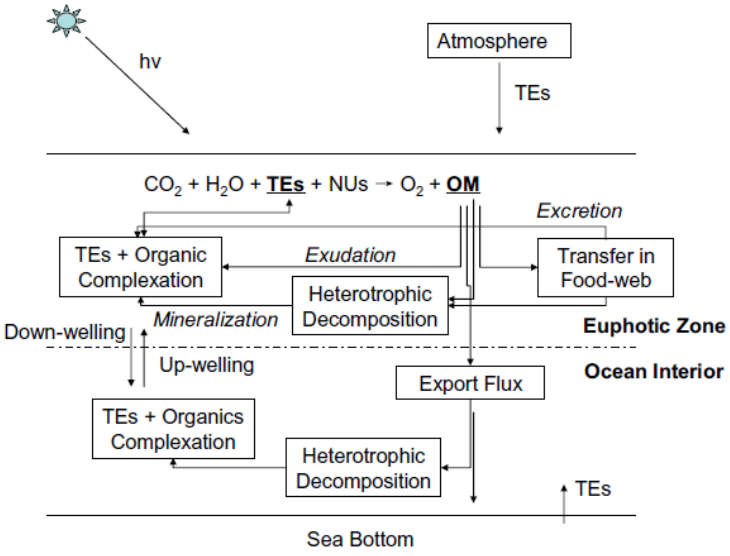

Figure 1.2. Interactions between dissolved trace elements (TEs) and organic matter (OM) in seawater, which is regenerated from Zhang et al. (2019). Nus: macro-nutrient includes N, P, Si; TEs: trace elements.

1.2.1 Determination of the organic iron complexation in seawater

Determination of organic speciation in seawater is based on either anodic stripping voltammetry (ASV) (Plavšić et al., 1982) or cathodic stripping voltammetry (CSV) (Van Den Berg, 1984). The organic Fe complexation is usually studied via competitive ligand exchange-adsorptive cathodic stripping voltammetry (CLE-AdCSV), by titrating water with increasing Fe concentrations in the presence of an added artificial ligand with known stability constants (Gledhill and Buck, 2012). The added competing ligand must form an electro-active complex with Fe(III) at a certain pH, and the complex should be adsorbed onto a mercury electrode

(hanging mercury drop electrode) at a set potential. The current generated from reduction of Fe bound to the complex is determined by a reducing (cathodic) potential scan and this current is assumed to be directly proportional to the concentration of Fe bound to the added ligand. Two steps are performed during the measurement, a preconcentration step and a stripping step. During the preconcentration step, the complex is collected on the surface of the working electrode (i.e. a mercury drop). Then, following a brief equilibrium period, the complex is reduced from the electrode surface back into the solution by scanning in a negative direction. An increase in the cathodic current is observed when the potential is negative enough to reduce the Fe in the complex on the Hg drop. The height of this peak in current is recorded for each Fe additions as a titration point and plotted against the added Fe concentrations to generate a titration curve.

This raw titration data is interpreted in terms of the Langmuir adsorption isotherm and is dependent on several assumptions, including an assumption of equilibrium, equal binding of each site to Fe, no competition from other metals and reversibility of the binding between natural ligand and added ligand (Gerringa et al., 2014). There are four artificial ligands typically used for CLE-AdCSV titrations with Fe, 1-nitroso-2-napthol (HNN) (Gledhill and van den Berg, 1994), salicylaldoxime (SA) (Rue and Bruland, 1995), 2-(2-thiazolylazo)-p-cresol (TAC) (Croot and Johansson, 2000), and dihydroxy-naphthalene (DHN) (Berg and van den Berg, 2006). In this thesis, HNN is used in the titrations and that data is interpreted as follows:

The Langmuir equation combines the equilibrium expression and the mass balance of the natural ligands. The equilibrium expression is given by

$$K'_{FeL} = [FeL]/([Fe^{3+}][L']) \qquad (3)$$

where FeL is the complex of Fe bound to ligand (L), and L´ is the concentration of L that is not bound to Fe. K'_{FeL} is the conditional stability constants of L with respect to Fe^{3+}. The mass balance of natural ligand is given by

$$[L_t] = [FeL] + [L'] \qquad (4)$$

where L_t is the total ligand concentration. Then inserting L´ from equation 2 into 1 gives the Langmuir equation:

$$[FeL] = K'_{FeL}[L_t][Fe^{3+}]/(K'_{FeL}[Fe^{3+}] + 1) \qquad (5)$$

In the presence of an artificial ligand, HNN, the new mass balance of Fe in the titrations is given by

$$[Fe]_T = Fe_{free} + \sum FeL + \sum FeNN_3 \quad (6)$$

where $[Fe]_T$ is the total Fe concentration, and Fe_{free} is the concentration of Fe not complexed by L or HNN. $\sum FeL$ and $\sum FeNN_3$ are the total concentration of Fe bound to L and HNN, respectively. Here, the fraction Fe_{labile} is the concentration of Fe detected in CSV titrations, and equal to the total concentration of Fe bound to HNN and inorganic Fe complexes, given by

$$[Fe_{labile}] = [Fe'] + \sum FeNN_3 \quad (7)$$

The CSV peak height is related to the labile Fe concentration via the sensitivity S:

$$i_P = S[Fe_{labile}] \quad (8)$$

S is obtained from the slope of the titration curve where L is saturated. The ratio of free to complexed species gives the side reaction coefficient (α) for the reaction, which is also related to the conditional stability constants as shown in equation (9),

$$\frac{[FeNN_3]}{[Fe^{3+}]} = \alpha_{FeNN3} = [KFeNN_3] * [NN'] \quad (9)$$

Species can only compete when their side reaction coefficient are within one order of magnitude of each other (van den Berg and Donat, 1992). Thus ligands detectable via CLE-AdCSV are restricted to those with side reaction coefficients within this 'detection window' (Ringbom and Still, 1972). In addition, Fe^{3+} is directly related to the labile concentrations by α, the overall α-coefficient for inorganic complexation and organic complexation by HNN with respect to Fe^{3+}, given by

$$[Fe^{3+}] = [Fe_{labile}]/\alpha \quad (10)$$

The CLE-AdCSV titration is an indirect approach to determine Fe complexed by organic matter, and produces two conditional parameters (i.e. conditional on pH), conditional stability constant and ligand concentrations. These results are required at certain conditions (i.e. pH and temperature) in given samples, which maybe not adequate to represent characteristics of Fe-binding ligand in real seawater. Furthermore, since the rapidly changing seawater chemistry conditions, characteristics in the organic Fe complexation using ambient pH and temperature is urgent to assess the changes in Fe solubility with further feedback on the availability of Fe to phytoplankton.

1.2.2 Iron binding ligands pool

It has been shown that Fe-binding ligands are present everywhere from the surface to deep ocean, and usually have the excess binding capacity relative to DFe concentrations in most seawaters (Gledhill and Buck, 2012). The chemical identity of Fe-binding ligands in seawater remains largely unknown and likely shows an intrinsic chemical heterogeneity. The possible sources of Fe-binding ligands are generally related to terrestrial inputs (Muller, 2018), produced by marine biota (e.g. siderophores and saccharides) (Mawji et al., 2008, 2011) and microbiological activity (e.g. breakdown of sinking particulate organic matter (Hwang et al., 2004). Laglera and Van Den Berg (2009) have shown that humic substances from terrestrial origin plays a dominant role in buffering DFe concentrations in coastal waters. Phytoplankton can release several ligands including domoic acid, exopolymeric substances and saccharides (Hassler et al., 2011a; Norman et al., 2015). Siderophores as a stronger Fe-binding ligand, has been found at low concentration across the oceans, ranging from several pmol L^{-1} to nmol L^{-1} (Mawji et al., 2011; Boiteau et al., 2016; Bundy et al., 2018).

Studies of the molecular composition of organic matter suggest many different kind of binding sites are present, where most organic ligands form coordination complexes with Fe in which Fe is attached to one or multiple non-covalent binding sites (Zhang et al., 2019). Binding sites of organic matter likely include amines, hydroxamates, hydroxyl, phenols and carboxyl groups. These functional groups, are present in both terrestrial and marine DOM. Furthermore, investigations into the molecular structure of DOM in marine and freshwater environments using Fourier-transform ion cyclotron resonance mass spectrometry, suggest a universal structural backbone exists possibly due to common microbial degradation process (Zark and Dittmar, 2018). This indicates that metal-organic matter competition models (e.g. NICA-Donnan model (Kinniburgh et al., 1999) and WHAM (Tipping et al., 2011)), originally applied in freshwater environment, could also be used to investigate the Fe speciation in seawaters as a first step, since these models incorporates complexation changes with pH and temperature.

1.3 Application of the NICA-Donnan model in seawater

The global ocean is experiencing the significant impact from climate change, e.g. accelerating acidification, warming, stratification and deoxygenation. The release of anthropogenic CO_2 has resulted in an increase in atmospheric CO_2 concentrations from 280 ppm at the beginning of industrial revolution (~1750) (Feely et al., 2009) to ca. 416 ppm at present (https://climate.nasa.gov/vital-signs/carbon-dioxide/). About one-quarter of this released anthropogenic CO_2 is absorbed by the ocean, which already resulted in ca. 0.1 unit decreased pH in the surface ocean, referred to as ocean acidification (Caldeira and Wickett, 2003). This situation will be even worse under the current trends of anthropogenic CO_2 emissions and ocean CO_2 uptake, with a further 0.3-0.5 unit decrease in pH projected by 2100 (Feely et al., 2004; Orr et al., 2005; Doney, 2006). Decreasing seawater pH affects biological processes (Doney, 2006), and also the biogeochemical cycles of trace metals (e.g. Fe) (Millero et al., 2009; Gledhill et al., 2015; Zhang et al., 2019). Increasing anthropogenic CO_2 into atmosphere has also resulted in ocean warming, since ocean has absorbed more than 90 percent of all the excess heat energy trapped by CO_2 (Stocker et al., 2013). Furthermore, ocean warming could thus lead to water stratification (Li et al., 2020) and deoxygenation (Matear et al., 2000). Seawater chemistry conditions are thus changing rapidly, and knowledge of ambient Fe speciation is essential to evaluate the potential changes in DFe inventory with further impacts on primary productivity.

1.3.1 The NICA-Donnan model

Natural organic matter (NOM) has the tendency of changing both chemical and physical properties of waters and NOM refers to a highly complex mixture of different organic compounds (Adusei-Gyamfi et al., 2019). Due to its high reactivity, NOM is thought to control the bioavailability and biogeochemical cycling of trace elements in freshwater and soil environments (Xia et al., 1997) and also in seawaters (Zhang et al., 2019). Humic and fulvic acids (humic substances) are widely believed to be representatives of NOM behavior in fresh aquatic environment, since those are the most abundant colloidal and dissolved fractions of NOM, respectively (Dudal and Gérard, 2004; Koopal et al., 2005). Carboxylic and phenolic groups are usually major binding sites of humic and fulvic acids. Acid-base titrations of purified humic and fulvic acids from terrestrial environments clearly show two broad peaks, with a first maximum around pH 3-5 probably associated with carboxylic groups and second maximum at

higher pH probably associated with phenolic groups (de Wit et al., 1993; Milne et al., 1995). The binding site distribution is heterogeneous and two chemical equilibrium models, WHAM/Model VII and NICA-Donnan have been developed to describe the distribution of the deprotonated carboxylic and phenolic groups and their metal binding affinities. Both models have been shown to reasonably describe experimental results obtained for proton and metal binding to NOM (Dudal and Gérard, 2004). WHAM/Model VII uses a discrete site approach but minimizes the number of parameters that need to be estimated by a priori assumption of a certain shape for the distribution, which results in four types of low binding affinity (carboxylic-type groups) sites and four types of high binding affinity (phenolic-type groups) sites (Tipping et al., 2011). Four parameters are needed to describe the complexation of any metal cations with each type of binding sites at carboxylic and phenolic-type groups, including two median intrinsic stability constants and two heterogeneity values, resulting in sixteen parameters to be estimated in total. The NICA-Donnan model characterizes binding site heterogeneity by using continuous distribution of competitive adsorption sites (carboxylic- and phenolic-type groups, NICA component) together with an electrostatic model component (Donnan model), which also leads to a reduction in the number of model parameters that needs to be estimated compared to WHAM VII (Kinniburgh et al., 1999; Koopal et al., 2005).

The theory of the NICA-Donnan model has been described in detail elsewhere (Kinniburgh et al., 1999; Koopal et al., 2005). The NICA model describes the specific interactions between cations (i.e. protons and metals - Fe in this study) and negatively charged surface functional groups within NOM (i.e. marine DOM in this study). The amount of protons bound is described using the Freundlich-Langmuir isotherm, Q_H, can be written as

$$Q_H = Q_{max1,H} \cdot \frac{(K_{H1}C_H)^{m1}}{1+(K_{H1}C_H)^{m1}} + Q_{max2,H} \cdot \frac{(K_{H2}C_H)^{m2}}{1+(K_{H2}C_H)^{m2}} \qquad (11)$$

where the subscript number associated with each constant (1,2) denotes groups with different affinities for the proton. In this case 1 denotes carboxylic type groups and 2 phenolic type groups. $Q_{max,H}$ is the total number of proton binding sites while K_H is the median value of the binding affinity distribution for protons. C_H is the local concentration of proton near the binding sites, and m defines the width of the distribution. Then following equation (11), the amount of metal (i.e. Fe) bound, Q_{Fe} can be written as

$$Q_{Fe} = \frac{n_{Fe1}}{n_{H1}} \cdot Q_{max1,H} \cdot \frac{(K_{Fe1}C_{Fe})^{n_{H1}}}{\sum(K_{Fe1}C_{Fe})^{n_{H1}}} \cdot \frac{[\sum(K_{Fe1}C_{Fe})^{n_{H1}}]^{p1}}{1+[\sum(K_{Fe1}C_{Fe})^{n_{H1}}]^{p1}} + \quad (12)$$
$$\frac{n_{Fe2}}{n_{H2}} \cdot Q_{max2,H} \cdot \frac{(K_{Fe2}C_{Fe})^{n_{H2}}}{\sum(K_{Fe2}C_{Fe})^{n_{H2}}} \cdot \frac{[\sum(K_{Fe2}C_{Fe})^{n_{H2}}]^{p2}}{1 + [\sum(K_{Fe2}C_{Fe})^{n_{H2}}]^{p2}}$$

where p_1, p_2 represent the widths of the distribution and thus the intrinsic heterogeneity of DOM. K_{H1}, K_{H1}, K_{Fe1}, K_{Fe2} are the median binding affinity for protons and Fe respectively. The constants n_{H1}, n_{H2}, n_{Fe1}, n_{Fe2} define the non-idealities of proton or metal ion binding to each group type. In the case where n=1, the proton or metal ion binds to binding sites in a 1:1 ratio. Proton binding constants can thus be derived from three parameters (K_H, n_H, p) for each type of group and for metal ion binding only two parameters, K_{Fe} and n_{Fe}, are estimated for each type of group.

The Donnan model describes the nonspecific electrostatic binding to any residual negative charge. In practice, the Donnan model assumes that a humic substance behaves like a uniform gel, where the net negative charges attract excess cations, and the ratio of the concentration of cations in the gel to that in the bulk solution defines a Boltzmann factor and a corresponding Donnan potential (Benedetti et al., 1996). In the Donnan model, the critical constant is called the Donnan volume, V_D, which is usually estimated using the empirical equation

$$\log V_D = b(1 - logI) - 1 \quad (13)$$

where I is the ionic strength of the bulk solution and b is the empirical parameter. In seawater, the relatively high ionic strength (I = 0.7) reduces the overall contribution of electrostatic binding. Furthermore recent work suggests that the Donnan model does not adequately describe the impact of ionic strength on the size and charge distribution of marine DOM (Lodeiro et al., 2020; Pinheiro et al., 2021), and ultimately use of other electrostatic models might be more appropriate for describing e.g. changes in metal and proton binding in estuaries, where large gradients in ionic strength are observed.

1.3.2 Speciation tools incorporating the NICA-Donnan model

Ultimately, the study of the chemical speciation of any metal aims to reliably predict the concentration of metal species of particular importance to the biogeochemistry of the metal, e.g. free Fe (Fe^{3+}), the sum of inorganic complexes (Fe´) or the apparent Fe(III) solubility. Such

predictions require calculations of both inorganic and organic speciation and are typically performed using equilibrium calculation tools. There are several available equilibrium calculation tools accounting for interactions between metals and DOM, in combination with the NICA-Donnan model, e.g. visual MINTEQ (Gustafsson, 2014) and ORCHESTRA (Meeussen, 2003) as well as PHREEQC (https://www.usgs.gov/software/phreeqc-version-3/). Visual MINTEQ combines state-of-the-art descriptions of sorption and complexation reactions with easy-to-use menus and options for importing and exporting data to/from Excel. The source code was originally developed from MINTEQA2 (United States Environmental Protection Agency, https://www.epa.gov/ceam/minteqa2-equilibrium-speciation-model). The NICA-Donnan model has been incorporated with visual MINTEQ to predict Fe speciation in seawater (Gledhill et al., 2015; Avendaño et al., 2016). ORCHESTRA is a Java based program and all equations are defined in text format, which makes model definitions accessible and extendible by users in addition to visual MINTEQ. The thermodynamic database of ORCHESTRA is originated from MINTEQA2. Furthermore, PHREEQC is another software to perform aqueous geochemical calculations and includes the Pitzer model and is designed for high ionic strength systems (e.g seawater), but without the application of the NICA-Donnan model.

The impact of high ionic strength on the calculation

In chemical equilibrium calculations, activity is a key parameter that describes how ions in solution interact with each other as well as with water molecules. The importance of these interactions increases with salt concentration. At higher ionic strength (I), ions behave chemically like they are less concentrated than they really are, and the activity coefficient is used to calculate the actual concentration. Speciation tools incorporate several equations for calculating individual ion activity coefficients, e.g. Dehye-Hückel/Davies equation and the Pitzer ionic model. The Debye-Hückel equation describes the ionic strength dependence of the activity coefficient of species in dilute aqueous solutions using two equations, one for the molar activity coefficient of an aqueous ion and another for the activity of solution. The key assumption of Debye-Hückel equation is that the central ion is a point charge and that the other ions are spread around the central ion with a Gaussian distribution. But the range of the Debye-Hückel equation is limited to $I < 0.1$, which is not suitable to seawater ($I=0.72$). Davis equation is a purely

empirical method based on the Debye-Hückel equation, by manually adding a simple term to fit higher ionic strengths, but its range is limited (I<0.5) and not suitable for seawater. In contrast, the Pitzer ionic model is valid to be used in high ionic strength systems, and contains a set of equations to calculate activity coefficient and these equations are derived from a single expression for the excess Gibbs energy of the solutions (Pitzer, 2018). Parameters in these equations of the Pitzer ionic model are a function of temperature and pressure. Gledhill et al. (2015) has reported that carbonate speciation produced by visual MINTEQ was different from CO_2SYS (Pierrot et al., 2006), as a result of calculation of ionic strength. Calculations via CO2SYS, a specific software for seawater, are used a set of mass-conservation equations within equilibrium constants as function of salinity, temperature and pressure and derived from seawater (Lewis and Wallace, 1998). This leads to underestimation of carbonate concentration in vMINTEQ that would result in a bias for copper speciation since the inorganic speciation of copper is strongly influenced by carbonate complexation (Millero et al., 2009).

1.3.3 Optimization of NICA parameters

Currently, the NICA-Donnan model has been widely used to describe metals bound organic matter in freshwater environments, within some level of accuracy (Dudal and Gérard, 2004; Koopal et al., 2005; Town and Van Leeuwen, 2016; Town et al., 2019), and also examined predictions of Fe speciation in seawater (Hiemstra and van Riemsdijk, 2006; Gledhill et al., 2015; Avendaño et al., 2016). In addition, a biotic ligand model which determines the competition for free trace metal ions between inorganic/organic ligands and biotic ligands, originally used in fresh waters (Worms et al., 2006), has also been examined to assess Cu speciation in seawater (Sander et al., 2015). However, standard approaches for modelling metal speciation in marine waters are still being developed (Turner et al., 2016), and those that are available mostly focus on the carbonate system (CO2SYS, Lewis and Wallace. 1998; Pierrot et al. 2006), and have not been extended to seawater. Ulfsbo et al. (2015) has reported a complete combination of WHAM/Model VII and Pitzer ionic model to predict organic alkalinity in seawater. However, since the parameters used in the Pitzer ionic model are still needed to specifically be derived from each single experiment, the combination between Pitzer model and metal/organic matter competition model (e.g. the NICA-Donnan model and WHAM), is

expected to improve the predictions of seawater metal speciation in future (Turner et al., 2016). Furthermore, the flexible definitions in ORCHESTRA makes it available to further combine the NICA-Donnan model with the Pitzer ionic model for seawater.

Recently, Lodeiro et al. (2020) successfully derived new proton-binding constants for the NICA-Donnan model for brackish seawater DOM, suggesting that binding sites of marine DOM behave less heterogonous and more ideal in binding behavior, compared to generic constants (Milne et al., 2001). Since the generic constants of the NICA-Donnan model were used in previous studies of Fe speciation in seawater (Hiemstra and van Riemsdijk, 2006; Gledhill et al., 2015; Avendaño et al., 2016), therefore, it is important to derive new NCIA constants for describing Fe binding to organic matter in marine environment, in combination with these new findings (Lodeiro et al., 2020). An empirical method has been applied to examine the impact of Fe NICA parameters with generic constants (Milne et al., 2001) on Fe speciation in seawater, via chemical speciation software visual MINTEQ (Gledhill et al., 2015; Avendaño et al., 2016). However, currently only surface complexation model under the visual MINTEQ interface could be utilized with mathematical parameter estimation software. Chemical speciation software ORCHESTRA in combination with parameter estimation program PEST has been reported to successfully optimize the parameters for Cd and Zn binding to standard Laurentian fulvic acid (Janot et al., 2017). Due to the advantages of accessibility and extendibly model definitions in ORCHESTRA and the available mathematical estimation method of PEST-ORCHESTRA, derivations of NICA parameters for metal binding to marine DOM that incorporate with new experimental design, are necessary and useful to understand the biogeochemical cycling of these metals.

1.4 Aim and structure of thesis

In the oxygenated seawater, the thermodynamic favored form Fe(III) is rapidly precipitated and constrains the supply of Fe for phytoplankton growth in large area of the ocean. Our current knowledge suggests that Fe complexed by organic matter largely controls the Fe speciation, buffering Fe against precipitation in seawater. Iron solubility and bioavailability are a function of chemical speciation, which is largely influenced by pH, temperature, and the concentration and binding affinity of binding sites of organic matter. However, the impact of currently rapid

changing seawater chemistry on Fe speciation and the dissolved Fe inventory remains largely unknown, since the available analytical methodology does not incorporate with changes in ambient pH and temperature. The overall aim of this study was to use intrinsic thermodynamic constants to calculate ambient Fe speciation and apparent Fe(III) solubility as a function of pH, temperature and DOC concentrations, and improve our understanding of biogeochemical cycling of Fe in the ocean. In order to achieve my aim, I combined laboratory speciation experiments using comparative ligand exchange-adsorption cathodic stripping voltammetry with theoretical equilibrium calculations using an ion paring-organic matter model (NICA-Donnan) in two different ocean areas, Celtic Sea and Peruvian shelf and slope region. I further examined the potential impact of pH and temperature on ambient Fe speciation and the apparent Fe(III) solubility at basin scales using data collected from the international GEOTRACES program. My specific objectives were to:

- Examine the applicability of the NICA-Donnan model to the calculation of Fe speciation in seawater via comparison of experimental results obtained with CLE-AdCSV with predictions of Fe speciation obtained via application of the NICA-Donnan model in the Celtic Sea.
- Derive NICA constants for Fe(III) binding to marine DOM, and apply these new constants to calculate ambient Fe speciation and the apparent Fe(III) solubility in combination with measurement of Fe(II), to investigate the impact of pH and DOM on the speciation and solubility of Fe in the Peruvian shelf and slope region.
- Investigate basin scales changes in the apparent Fe(III) solubility as a function of pH, temperature and DOC concentrations by applying the NICA-Donnan model in combination with observational data obtained during a series of GEOTRACES cruises.

2 Methods

This chapter will describe both experimental protocols for determination of Fe speciation and modelling protocols for derivation of Fe(III) NICA constants and calculations of ambient Fe speciation and apparent Fe(III) solubility. The aim of this chapter is to provide further details on the methodology presented in later chapters of this thesis.

2.1 Determination of iron speciation via competitive ligand exchange-adsorptive cathodic stripping voltammetry

Two different titration approaches were used in this thesis, one for analysis of seawater samples collected in Celtic Sea that used an overload titration approach (Kogut and Voelker, 2001), and the other for analysis of seawater samples in the Peruvian shelf that used a novel pH-Fe two dimensional titration approach.

2.1.1 Reagents and standards

All experiments used low density polyethylene (LDPE, Nalgene) bottles, and general labware (e.g. measuring cylinders) was cleaned prior to the preparation of regents and standards solutions. The cleaning procedure followed protocols recommended by GEOTRACES (Cutter et al., 2017). New bottles were soaked in Mucasol detergent (Sigma Aldrich) then 6.7 mol L^{-1} hydrochloric acid (HCl; reagent grade, Fisher Scientific) followed by 8.3 mol L^{-1} nitric acid (HNO3; reagent grade, Fisher Scientific), for one week for each step. Bottles were rinsed thoroughly with deionized water (18.2 MΩ cm^{-1}, Milli-Q, Millipore) between steps. All chemicals were prepared in a trace metal clean laboratory, and further diluted under a Class 1000 laminar flow bench at room temperature (20°C).

The stock solution of the added ligand, 1-nitroso-2-naphthol (HNN; Sigma Aldrich), was prepared by dissolving 0.173 g HNN in 100 mL methanol (Fisher, LC-MS grade), to give a final concentration 10 mmol L^{-1}. The two diluted HNN solutions used in titrations (0.1 and 1 mmol L^{-1}) were prepared from this stock solution with methanol.

A standard solution of Fe(III) was prepared from a 1 mg mL^{-1} ICP-MS stock solution (Fisher Scientific) and diluted with deionized water to a final concentration 0.1 mmol L^{-1}. The standard solution was then acidified to pH_{NBS} 2 (on the NBS scale) using trace metal clean hydrochloric acid (HCl; Romil, SpA grade). A further diluted Fe standard solution (100 nmol L^{-1}) was prepared for titrations with deionized water and subsequently acidified to pH_{NBS} 2.

In the overload titrations, a solution of N-2-hydroxyethylpiperazine-N´-ethanesulphonic acid (HEPES; Fisher Aristar grade) was used to buffer titration pH. 23.85 g HEPES was dissolved in deionized water up to 100 mL volume with a final concentration of 1 mol L^{-1}, which was subsequently adjusted to pH_{NBS} 8 using trace metal clean ammonia solutions (Romil, SpA grade). The HEPES stock solution (1 mol L^{-1}) was cleaned by HNN with the following procedure: a concentration of 20 µmol L^{-1} HNN was added to HEPES solution and left to equilibrate for overnight (>12 h). The buffer was then passed through a previously activated C_{18} SepPak column (Whatmann) (activation by 10 ml of methanol, 10 ml of deionized water and 10 ml of HCl) using the peristaltic pump, until the solution was clear (Avendaño et al., 2016).

In the pH-Fe two dimensional titrations, a solution of Piperazine-1,4-bis(2-hydroxypropanesulfonic acid) (POPSO; Sigma-Aldrich), was used to buffer pH during titrations. 16.31 g POPSO was dissolved with deionized water and a NaOH solution (1 mol L^{-1}) up to 90 mL volume, with final concentration 0.5 mol L^{-1}. The stock solutions of POPSO (0.5 mol L^{-1}) were adjusted to six different pH_{NBS} values, 7.0, 7.3, 7.6, 7.9, 8.2, 8.5 using trace metal clean ammonia solutions (Romil, SpA grade). The pH buffer solutions were cleaned as described for HEPES.

2.1.2 Importance of pH expression on the different scales, IUPAC and total scale

In this thesis, two different pH scales were used to report the seawater carbonate chemistry. As suggested for seawater (Dickson, 2010), pH is typically calculated from dissolved inorganic carbon (C_T) and total alkalinity (A_T) at ambient water column (i.e. salinity, temperature and pressure) within a high level of accuracy, via CO2SYS (Pierrot et al., 2006), a speciation

software for seawater, defined as the total scale (pH_{tot}). However, we used the NBS pH scale (pH_{NBS}) because it is consistent with the NIST database (Hummel et al., 2019) based speciation constants used in the NICA-Donnan model, via the speciation calculation tools (e.g. ORCHESTRA, Meeussen (2003). The relationship between different pH scales for seawater can be defined as follows,

$$aH = 10^{-pHNBS} = fH * Hsws \quad (1)$$

$$\frac{Htot}{1+TS/K2SO4} = \frac{Hsws}{1+TS/K2SO4+TF/KF} \quad (2)$$

where aH is the activity and fH is the activity coefficient of the H^+ ion (this includes liquid junction effects), TS and TF are the concentrations of SO_4^{2-} and fluorine, and $K2SO4$ and KF are the dissociation constants of $H2SO4$ and KF in seawater. For CO2SYS, we used constants from Mehrbach et al. (1973; refitted by Dickson and Millero (1987)) and Dickson (1990) to describe the carbonate and sulphate equilibrium with hydrogen ions, and from Uppström (1974) to account for boron. In this thesis, the total scale (pH_{tot}) is used to report ambient changes in the seawater carbonate chemistry, whilst the NBS scale (pH_{NBS}) is used to incorporates with the speciation calculations at ambient pH.

2.1.3 The Overload titration

The application of competitive ligand exchange adsorption cathodic stripping voltammetry typically assumes that peak currents are proportional to the sum of Fe binding to added ligand (AL) and would define the concentrations of metal species measured by CLE-AdCSV (Gledhill and Buck, 2012; Pižeta et al., 2015). When the weakest ligands in the sample are completely titrated, the slope that the top of peak current plotted against the total metal concentrations is equal to sensitivity (S), which is thus used to calculate the concentrations of FeAL (i.e. FeNN3 in this thesis). Kogut and Voelker (2001) has shown that a high enough concentration of AL in system could outcompete all natural ligands and improve the estimation of S in the presence of humic substance concentrations typical of coastal waters, called 'overload titrations'. Therefore, the 'overload titration' approach is thus adopted in the analysis of samples from Celtic Sea coastal waters. In this thesis (See Chapter 3), three different concentrations of HNN (1, 5 and 20 µmol L^{-1}) with detection windows ($\alpha FeNN3(Fe')$= 1.5, 184.6 and $1.2x10^4$), were used to titrate the binding sites in each seawater samples. Each sample was separated into 19 vials with 10 mL

volume in each vial. The pH_{NBS} of each vial was buffered to 8 via addition of HEPES to a final concentration 0.01 mol L^{-1}. Two blank vials were prepared via addition of 1 µmol L^{-1} HNN with no Fe addition at the beginning of each sample analysis. A series of Fe concentrations (0.4, 0.8, 1.5, 2, 3, 4, 5 nmol L^{-1}) were added into seven vials for each of the two low detection windows ([HNN]= 1, 5 µmol L^{-1}; $\alpha FeNN3(Fe')$= 1.5, 184.6). The last three vials were prepared for the highest detection window ([HNN=20 µmol L^{-1}; $\alpha FeNN3(Fe')$= $1.2x10^4$), with added Fe concentrations (5, 10, 15 nmol L^{-1}) with the aim of determination of the sensitivity according to the overtitration method. Samples were the left to equilibrate for overnight (>12 h). Voltammetic analysis was performed the following day using a hanging mercury drop electrode stand model VA663 (Metrohm, Switzerland) connected to a µAutolab voltammeter (Metrohm Autolab B.V., the Netherlands). The electrodes included a double-junction Ag/AgCl electrode, a reference electrode filled with 3 mol L^{-1} KCl solution, a standard Hg drop as a working electrode and a glassy carbon electrode as an auxiliary electrode. The current generated from reduction of $FeNN_3$ was determined after de-aeration of the sample with nitrogen gas (240 s). A deposition potential of -0.15 was used with a deposition time (240 s). The scanning mode was sample-DC from -0.3V to -0.7V at a scan rates of 50 mV s^{-1}. The reduction peak appeared at approximately -0.48V.

2.1.4 The pH-Fe two dimensional titration

This approach incorporates changes in pH and was used to derive Fe(III) NICA constants, in terms of any shift in Fe binding to carboxylic- or phenolic-type groups that can be driven by pH changes (Koopal et al., 2005). In this thesis (See Chapter 4), a single detection window ([HNN]= 2 µmol L^{-1}) was used to titrate the binding sites in each seawater samples. Each sample was separated into 30 vials, with six different pH_{NBS} values (7.0, 7.3, 7.6, 7.9, 8.2, 8.5) and five different added Fe concentrations (0, 0.5, 1.5, 5, 7.5, 10 nmol L^{-1}) for each pH_{NBS} value. To calibrate the analysis, the titration performed at pH_{NBS} 7.9 was typically assumed to reflect binding of all added Fe to the added ligand and thus used to calculate the sensitivity for each sample. Samples were left to equilibrate for overnight (>12 h).

Voltammetric analysis was performed using different instrumental conditions compared to the overload titration. The concentrations of $FeNN_3$ were determined after de-aeration of the sample with nitrogen gas (180 s for first scan and 30 s for second and third scans). A deposition potential of -0.15 was used with a deposition time (120 s). The scanning mode was sample-DC from -0.3V to -0.7V at a scan rate of 50 mV s^{-1}. The reduction peak appeared at approximately -0.47V.

2.1.5 The calibration of sensitivity from titrations

In this thesis, either the overload titration or pH-Fe two dimensional titration was aimed to incorporate the predictions of the NICA-Donnan model by a comparison of measured and modelled $FeNN_3$. Once a titration is completed, as a first step, the measured peak current for each aliquot is plotted against the total Fe concentrations for each sample and a line fitted through the high Fe concentrations part of the curve. Once the weakest ligands in the sample are completely titrated, the slope of this line is equal to the sensitivity (S). Then, $FeNN_3$ is calculated by the peak height divided by the sensitivity. In order to assess potential changes in the sensitivity of analysis at different HNN concentrations or pH values, we undertook a series of measurements using UV-irradiated seawater over the range of Fe concentrations used in our experiments, at different HNN concentrations (Chapter 3) or different pH values (Chapter 4). Details have been shown in the following chapter 3 and 4.

Variations in the sensitivity of titrations that are dependent on the added artificial ligand (i.e. HNN in this thesis) concentrations have been reported previously and are potentially problematic for our approach if they cannot be ascribed to actual changes in chemical speciation in the sample (Hudson et al., 2003). Our results have shown there is a difference between lower HNN concentrations (1 µmol L^{-1}) and higher HNN concentrations (5 and 20 µmol L^{-1})., and that is because of the competition from inorganic complexation is strong and leading to conditional stability constants of Fe binding to HNN that are indeed lower than previously used (Avendaño et al., 2016).

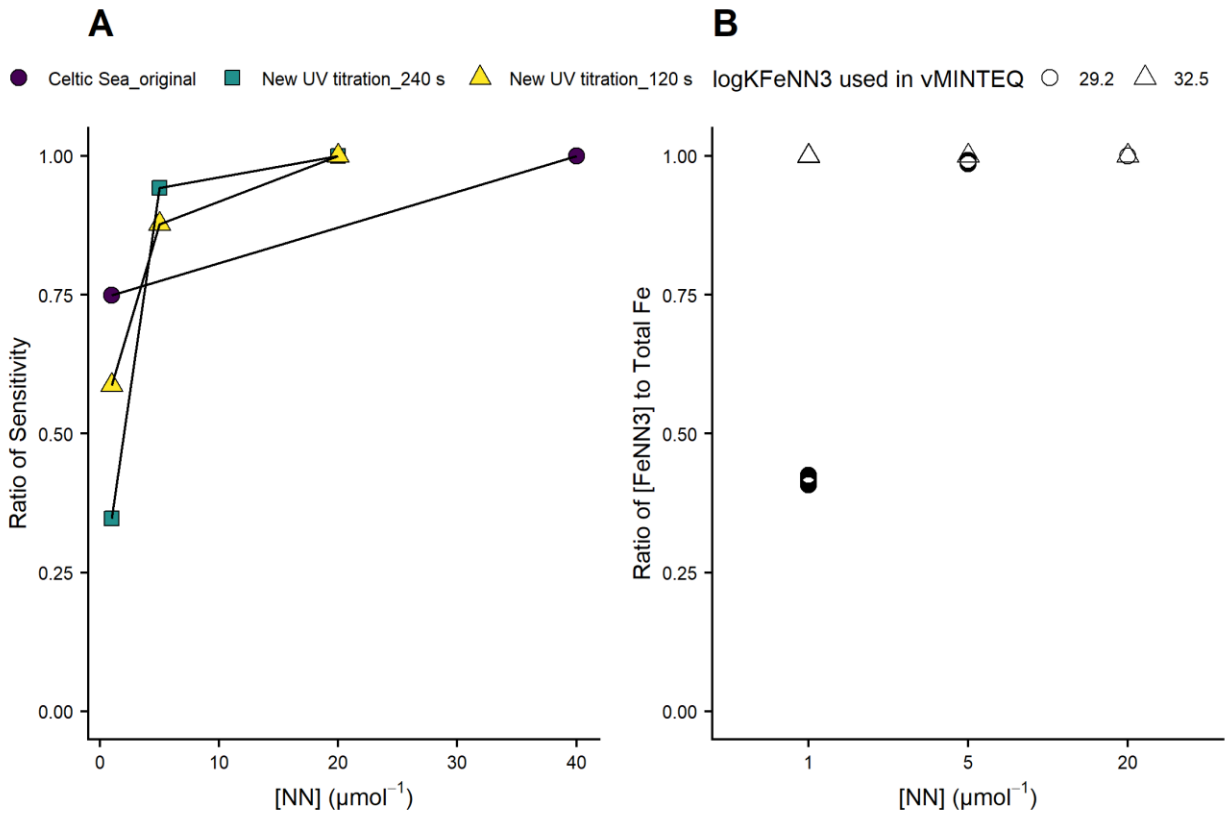

Figure 2.1. Sensitivity of voltammetric analysis using UV-irradiated seawater at each HNN concentrations was normalized to highest HNN concentration (Panel A). Original test undertaken before this work is indicated as circle points with deposition time (240 s), whilst new tests after this work are indicated as square points with deposition time (240 s) and triangle points with deposition time (120 s). Plot of simulated titrations via ORCHESTRA using the NICA-Donnan model is shown in panel B. Modelled FeNN3 was normalized to total Fe concentration at each titration point, which circle points indicated as input of $k_{FeNN3,H+}$ in ORCHESTRA with 29.2 (in log scale) and square points indicated as input of $k_{FeNN3,H+}$ in ORCHESTRA with 32.5 (in log scale).

In the pH-Fe two dimensional titrations (Chapter 4), the sensitivity is assumed not to vary with pH. Figure 2.2 has shown there is no real difference between the sensitivity versus pH dimensional in the UV-irradiated seawater, in the presence of two different HNN concentrations, 1 and 5 µmol L^{-1}. Measured FeNN3 is thus calculated using the average sensitivity of all pH values in each sample in the Peruvian shelf work.

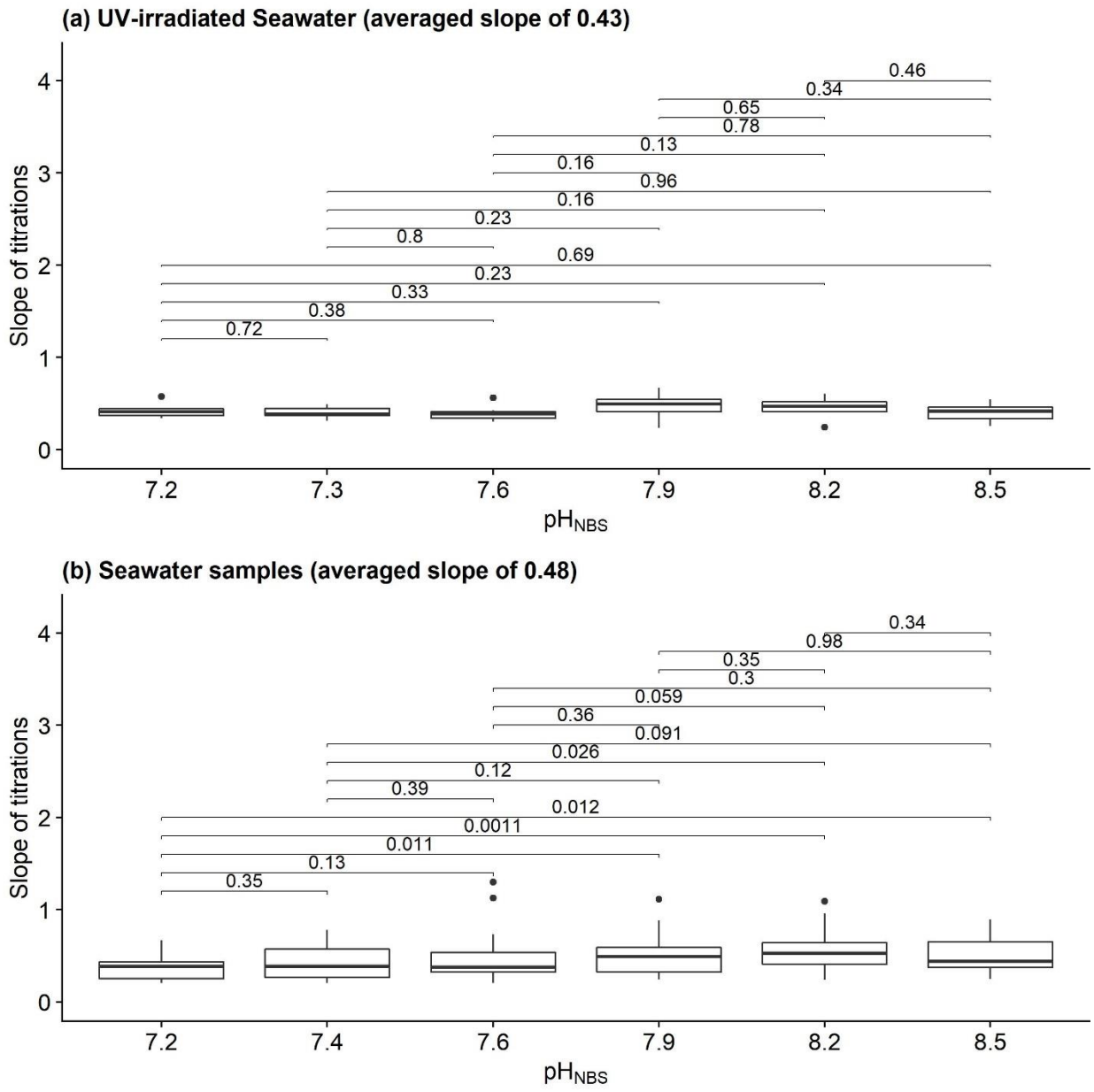

Figure 2.2. The calculated slopes from pH-Fe titrations are shown at each titration pH level, where (a) is shown as pH-Fe titrations performed in UV-irradiated seawater (n= 8), and (b) is shown as pH-Fe titrations performed in seawater samples collected in the Peruvian shelf and slope region (n= 31). We did the significance test by comparing the mean of slopes, via software R using the non-parametric Wilcoxon test that shown with p-values.

2.2 The application of PEST-ORCHESTRA to the estimation of parameters in the NICA-Donnan model in seawater

The chemical speciation software ORCHESTRA (Meeussen, 2003) is used together with the parameter estimation and uncertainty analysis package PEST (Doherty, 2019), to derive NICA constants for Fe(III) binding to marine DOM. This approach was successfully described by Janot et al. (2017) for deriving NICA constants for Cd and Zn binding to standard Laurentian fulvic acid. The general procedure of the approach is shown in Figure 2.3. The approach starts by simulating experimental titrations within ORCHESTRA, then the ORCHESTRA output data is passed to PEST and compared to experimental results. The Levenberg-Marquardt algorithm is used to re-estimate the NICA constants, which are passed back to ORCHESTRA. The process is repeated until a reproducible minimum in the least square error is obtained. Here we describe how to start with the calculation via ORCHESTRA only and then describe how to combine PEST and ORCHESTRA to estimate the constants.

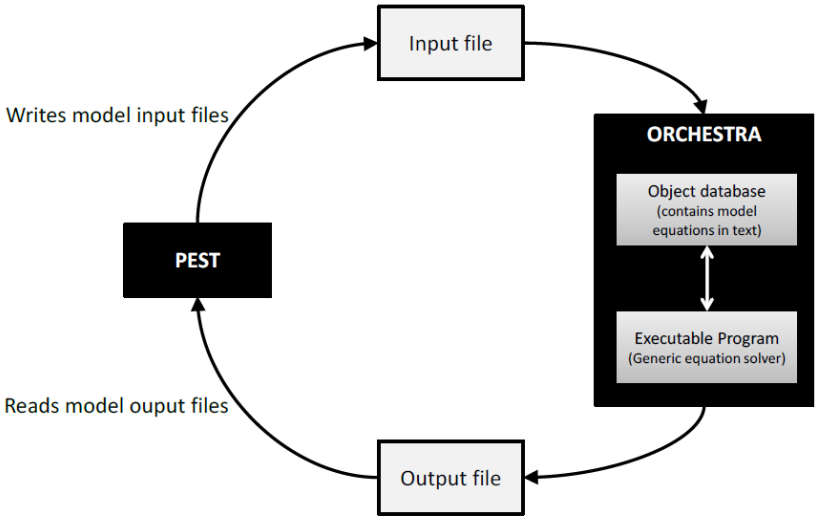

Figure 2.3. General structure of PEST-ORCHESTRA approach, was regenerated from Janot et al.(2017).

2.2.1 ORCHESTRA

ORCHESTRA is a computer program for stimulating chemical speciation and reactive transport processes, which is written in Java (hence Java must be installed on a computer) and runs on

Windows, ***Linux*** and ***Apple OSX*** (http://www.orchestra.meeussen.nl/model/). In ORCHESTRA, all source codes written in text format incorporate a user-friendly GUI (Figure 2.4). A complete equilibrium calculation via ORCHESTRA generally includes six processing files, ***Input.dat***, ***Output.dat***, ***Chemistry.inp***, ***Composer.inp***, ***Documentations.inp***, ***Concert.xml*** and the general database that includes ***objects.txt***, ***minteqv4.txt*** and ***adsmodels.txt***. We describe how to set up the calculations in ORCHESTRA.

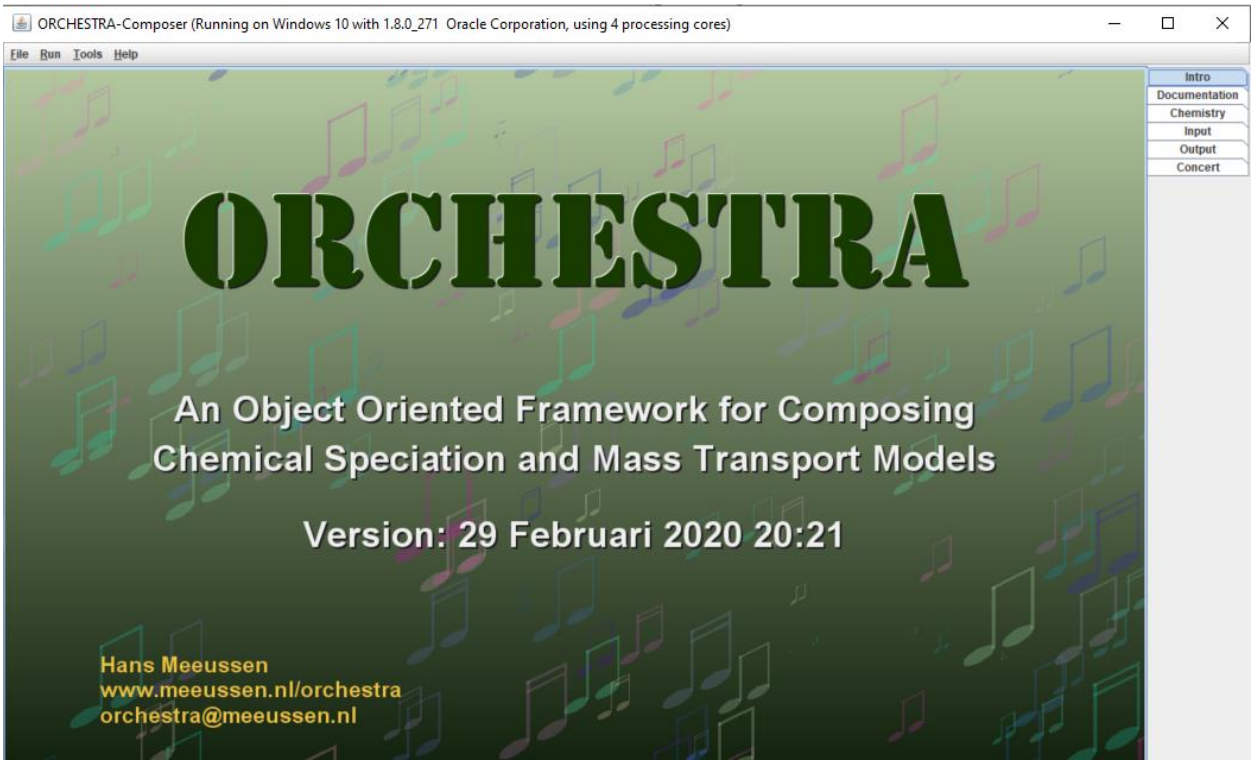

Figure 2.4. User Interface in ORCHESTRA when files are set up and connected.

Set up essential files and its links in ORCHESTRA

At the beginning of any calculation in ORCHESTRA, we need to firstly write each file in text format and set up the links. The general structure of folders and files used in ORCHESTRA and the way to store them on your computer is shown in Figure 2.5. Two sub-folders clearly contain different files used for calculations.

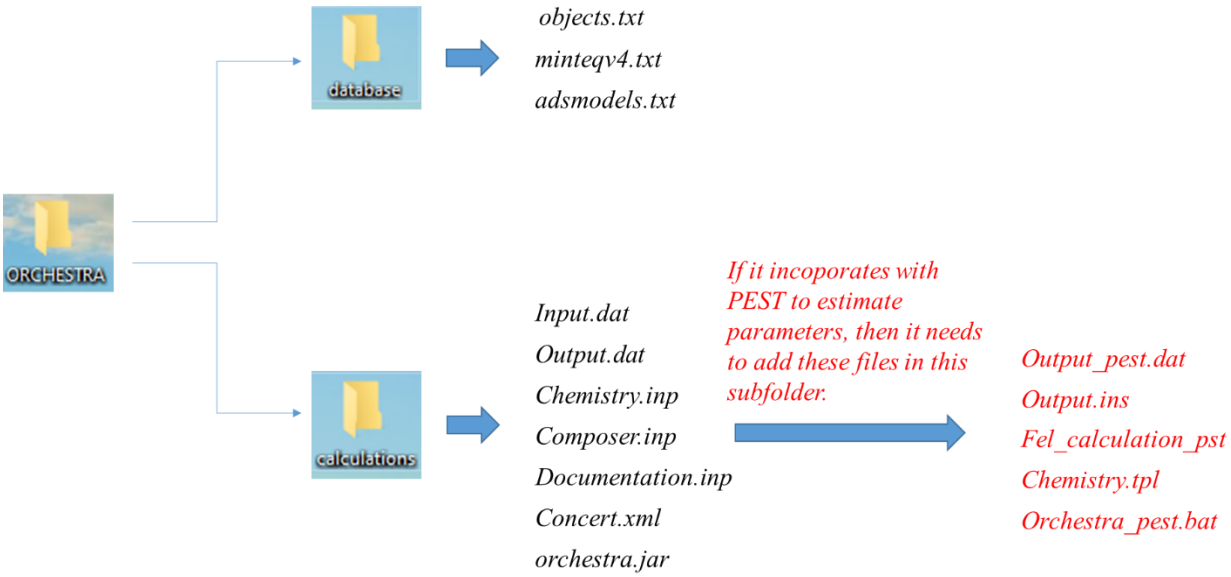

Figure 2.5. Structure of the established folders containing files used in ORCHESTRA.

In the sub-folder ***database***, all basic program information is written in ***objects.txt***, e.g. object class definitions or calculations of ionic strength. All chemical reactions and thermodynamic constants of chemical components are written in ***minteqv4.txt*** that is mostly re-written from original database of MINTEQA2 V4.0 (https://www.epa.gov/ceam/minteqa2-equilibrium-speciation-model). It is always wise to double check constants in the literature for any element of interest since improved estimations of constants continue to be published and mistakes can be made with database entries. The file ***adsmodels.txt*** contains all necessary information of the NICA-Donnan model as well as some other adsorption simulation models. These three original files can be found in the website (*http://www.orchestra.meeussen.nl/model/*).

In the sub-folder ***calculations***, we can define any chemicals with a certain value in ***Input.dat***, and select calculated chemical species as results in ***Output.dat***. All chemicals used in ***Input.dat*** and ***Output.dat*** are in units of mol L^{-1}. All definitions of chemicals, reaction equations and information on the NICA-Donnan model used for calculations are written in ***Chemistry.inp***. Generally, both ***Composer.inp*** and ***Documentations.inp*** are unchanged, since they are not related to any calculations. ***Concert.xml*** describes the basic procedure for how each file is read and executed in ORCHESTRA and is only re-written when ORCHESTRA is combined with PEST in order to estimate parameters. These above files can be found along with the original

descriptions on the website (*http://orchestra.meeussen.nl/model/*) and along with the original paper (Meeussen, 2003). Finally, all files can be linked and run for calculation in ORCHESTRA, by the Java executable file ***orchestra.jar***.

Calculations within the User Interface in ORCHESTRA

After the set-up of all essential files, one can start the calculation by running ***orchestra.jar*** or ***runorchestra.bat***, which will open the User Interface (Figure 2.4). Every calculation is executed by clicking the ***Run*** button in the main menu. In the User Interface, one can select or unselect chemicals as well as change the data input and output. Furthermore, one can re-define the parameters (e.g. ***reactions*** or ***constants*** used in the NICA-Donnan model) in ***Chemistry.inp*** file within the User Interface by clicking the ***GUI View*** button (See Figure 2.6).

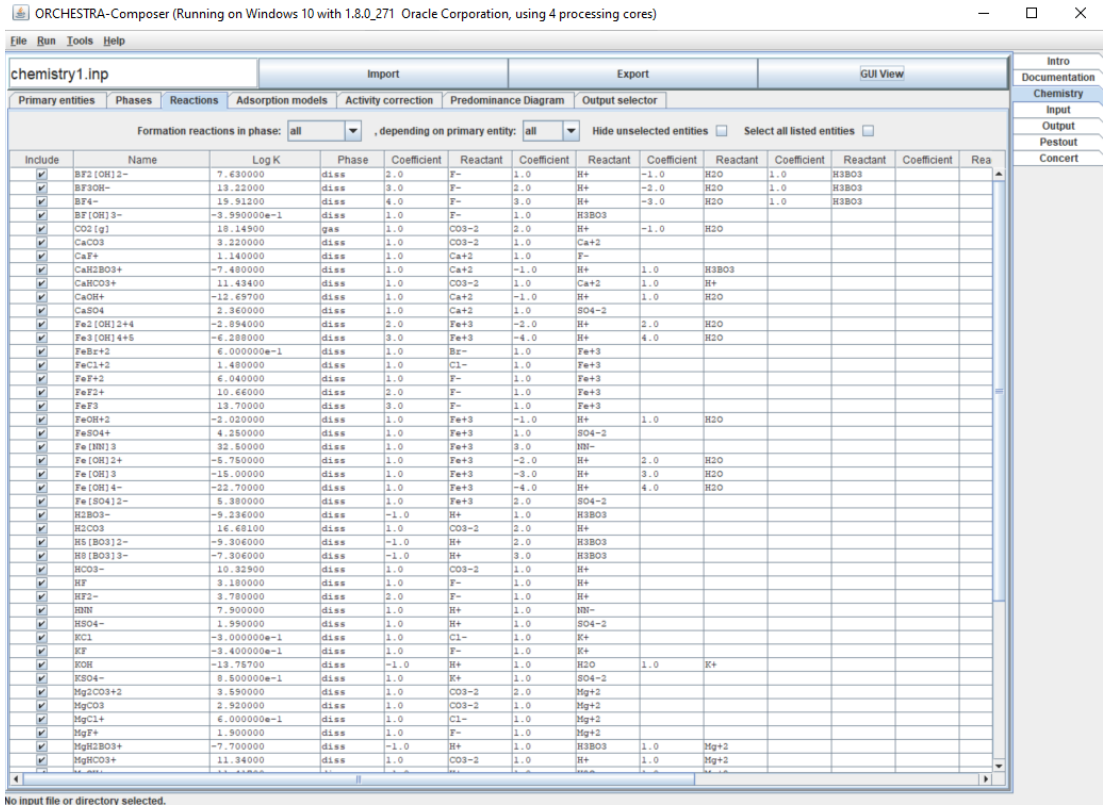

Figure 2.6. User Interface within the function of GUI View to re-define codes.

Things to consider when undertaking calculations via ORCHESTRA:

1) The default setting of temperature used in ORCHESTRA is 298.15 K (i.e. equal to 25°C). To calculate the impact of temperature on chemical reactions (i.e. equilibrium constant, k), we need to re-write the ***Chemistry.inp*** file. A function for temperature can be added to calculate equilibrium constant $k_{ambient}$ at a given temperature according to van't Hoff equation (3),

$$k_{ambient} = k_0 * 10^{\left(\frac{\Delta H}{2.303*R}\right)*\left(\frac{1}{T_0}-\frac{1}{T_{ambient}}\right)} \quad (3)$$

where k_0 is the standard equilibrium constant, and the reaction enthalpy ΔH is constant. R is the ideal gas constant. Details can be found in source codes in the appendix to the manual.

2) The NICA-Donnan model scales metal binding to DOC concentrations via knowledge of the concentration of binding sites per kg of dissolved organic matter ($Q_{max,H1}$ and $Q_{max,H2}$) in mol.kg DOM. To calculate the concentration of binding sites in any given sample, it is necessary to estimate the concentration of DOM in the sample in kg L^{-1}. In the marine environment, we typically determine concentrations of dissolved organic carbon (DOC) in µmol L^{-1}, since concentrations of DOM are too low to determine gravimetrically. We therefore need to know the mass of DOM equivalent that contains 1 µmol C in kg/µmol to convert from DOC concentration in units µmol L^{-1} to DOM concentrations in units kg L^{-1}. An estimate appropriate for the applied values of $Q_{max,H1}$ and $Q_{max,H2}$ are selected for use in the model. For example the ratio from Lodeiro et al. (2020) for marine DOM with $Q_{max,H1}$ and $Q_{max,H2}$ of 2.52 and 0.8 mol (binding sites) is 4.07 $\times 10^{-8}$ kg (DOM).µmol^{-1} (C), whilst for generic parameters for FA from Milne et al., (2013) where $Q_{max,H1}$ and $Q_{max,H2}$ of 5.88 and 1.86 mol (binding sites).kg^{-1} (DOM), then a value of 1.98 $\times 10^{-8}$ kg (DOM).µmol^{-1} (C) should be used.

3) In ***Input.dat*** file, DOC concentrations are input as ***DFA_kgl***. This is for convenience since it saves having to make a new adsorption model in ORCHESTRA using the NICA-Donnan equations named Marine DOM. You must also make sure that pH is fixed and not calculated, but the ionic strength is calculated and not fixed.

4) Since ORCHESTRA calculates activities via ion pairing using NIST thermodynamic constants, pH in ORCHESTRA should be given on the IUPAC/NBS scale (pH_{NBS}). We calculate

the pH_{NBS} in seawater samples from dissolved inorganic carbon (DIC) and total Alkalinity (TA) via a specific seawater speciation model CO2SYS (Pierrot et al., 2006).

5) There is one known bug: If the calculation produces nonsense values (i.e. very large values for ionic strength or other species are obtained), then you need to reduce the value of the pH stepwise by 0.1 units in the first line of your input data until you obtain a solution. This is possibly because ORCHESTRA has difficulty with balancing the charge in high ionic strength media with many ions (i.e. seawater) when the pH is fixed.

2.2.2 PEST

PEST, the software package, interacts with another model through the model's own input and output files, which assist and complement model parameter estimation and uncertainty analysis (https://www.pesthomepage.org/). Before using the PEST-ORCHESTRA approach, one needs to download the package of PEST (i.e. ***version 17.1 of the PEST suite***) from the website (https://pesthomepage.org/software-0), and directly unzip the package and store in a folder without any installation. In order to use PEST with ORCHESTRA, one needs to set up three main files within PEST, a template file (*.tpl, e.g. ***Chemistry.tpl***), an instruction file (*.ins, e.g. ***Output.ins***) and a control file (*.pst, e.g. ***Fel.pst***). The meaning of the code in these three files is explained generally in the appendix, and more details can be found in the User Manual Part I of PEST (Doherty, 2019).

Chemistry.tpl

This file is identical to the ORCHESTRA chemistry file, except the parameters to be optimized are written in between hash signs (#) within the expressions and model equations. Within each iteration step, PEST writes the chemistry file in which the variable between the hash signs are replaced with the updated estimates of the parameter values.

Output.ins

This file instructs PEST where and how to read the ORCHESTRA output from each model simulation.

Fel.pst

This file gives the instructions to PEST for performing the parameter fitting, i.e., gives the names of the template and instruction files, names of the parameters to be optimized with their minimum and maximum values, observation data and number of data points to be used in the fit, options and criteria for the parameter optimization and the instruction lines to run the model.

2.2.3 Procedure for running PEST-ORCHESTRA in *Windows*

Figure 2.7 shows how to start the estimation using PEST-ORCHESTRA step by step. I have only used PEST-ORCHESTRA in ***Windows***. Firstly, I set up the calculation in ORCHESTRA. Then, I ran the calculation in ORCHESTRA to be certain a successful solution to the problem can be obtained. After the successful calculation in ORCHESTRA, I set up the files for PEST. Importantly, all PEST files need to be written and stored in the same sub-folder used for the ORCHESTRA calculation (i.e. ***calculations***, see Figure 2.5). Finally, I started PEST-ORCHESTRA directly via the ***Command Prompt*** in ***Windows***.

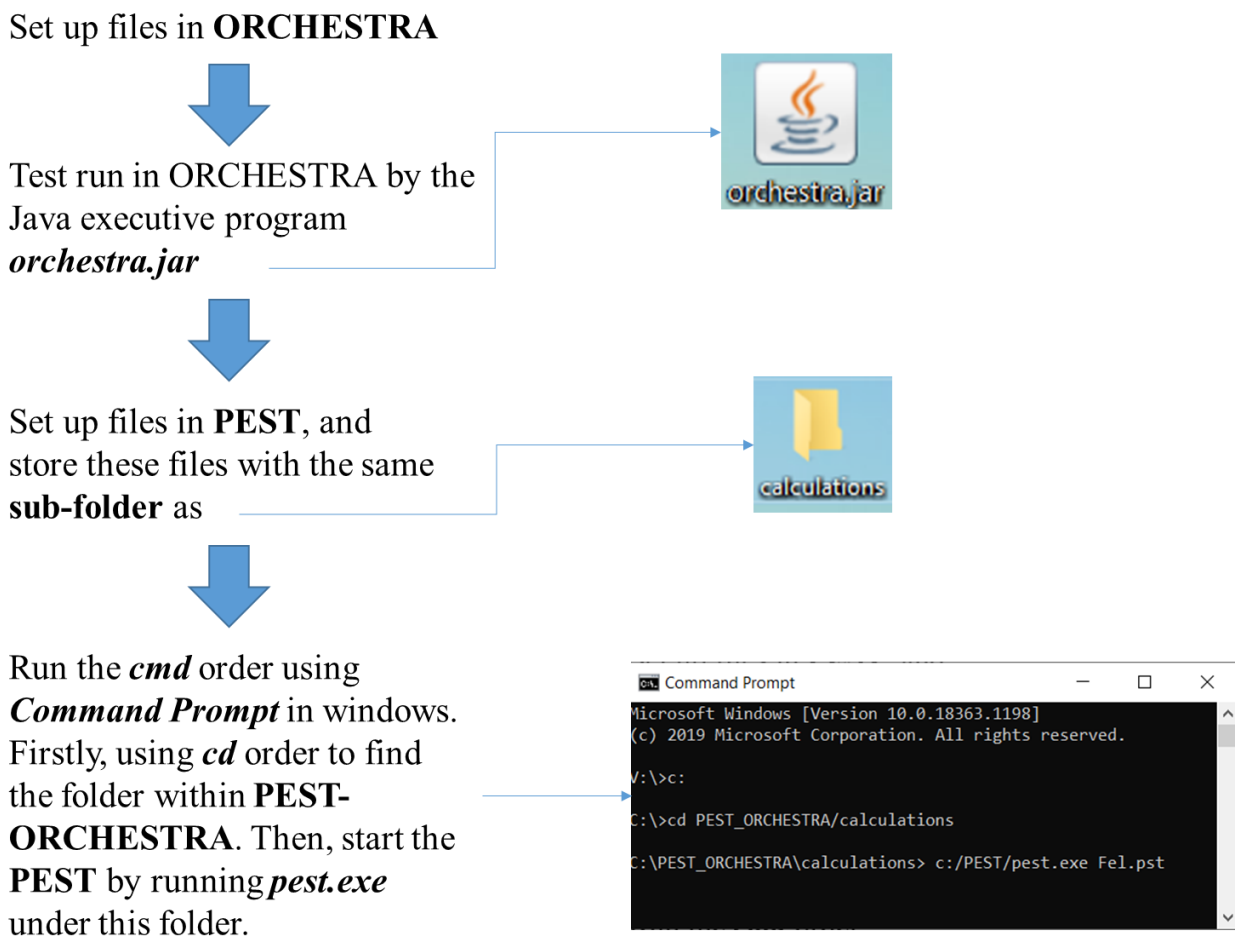

Figure 2.7. Procedure for running PEST-ORCHESTRA in ***Windows***.

2.2.4 Processing the results from PEST-ORCHESTRA

The derivation takes several minutes (e.g. ca. 10 mins for the example given with this protocol) and a suitable fit may not be obtained with the first run. Initial guesses need to be adjusted until constants with reasonable confidence intervals can be obtained. After the successful derivation, one will have several files for results. Results files can be read with a text reader like ***Notepad***. One uses the ***.rec*** file. In ***.rec*** file, and one can find details for the whole derivation process, e.g. iterations, estimated constants and residuals, which are all automatically calculated during the run.

2.3 Calculations of ambient Fe speciation and apparent Fe(III) solubility in seawater

Fe speciation and apparent Fe(III) solubility ($SFe(III)_{app}$) were thermodynamically calculated using the NICA-Donnan model at ambient seawater conditions (i.e. pH, DOC concentrations and temperature) based on methods described previously (Gledhill et al., 2015; Avendaño et al., 2016). The main changes during the modelling calculations is that the chemical speciation software ORCHESTRA was used in this thesis instead of visual MINTEQ applied previously (vMINTEQ; Gustafsson (2014). Simulated titrations using the NICA-Donnan model via both softwares ORCHESTRA and vMINTEQ were compared, suggesting there is no significant differences between the result outputs from these two softwares (See chapter 4). The procedure of calculations of Fe speciation and $SFe(III)_{app}$ were shown as follows.

The stability constants of inorganic and organic complexes used in ORCHESTRA were taken from NIST database (Smith et al., 2004), which are based on the pH_{NBS} scale. The salinity of each sample was used to derive the molality of major ions in seawater, Na^+, K^+, Mg^{2+}, Ca^{2+}, Sr^{2+}, Cl^-, $SO4^{2-}$, Br^-, $BO3^{3+}$, F^-, for the temperature 20°C and a density 1025 kg m^{-3}. The Davies equation was used to correct for ionic interactions. The ionic strength of seawater is at the upper end of the valid range for this correction method, which leads to an underestimation of ion activities and thus the ionic strength. Gledhill et al. (2015) has reported carbonate concentration was underestimated via vMINTEQ comparing to calculations produced by CO2SYS (Pierrot et al., 2006). Therefore, total CO_3^{2-} concentrations input into ORCHESTRA was forced as the relationship described in (Gledhill et al., 2015).

To calculate ambient Fe speciation (i.e. Fe(III) species) without consideration of non-equilibrium process such as the production of Fe(II), all data including major ion concentrations, total CO_3^{2-} concentrations, temperature, pH, DOC concentration as well as DFe concentration in seawater samples, were directly input into ORCHESTRA. In addition to calculation of ambient Fe speciation, the $SFe(III)_{app}$ with respect to ferrihydrite was calculated at ambient seawater conditions. The DFe(III) concentrations in the calculation were set to a constant level (10 nmol L^{-1}) that resulted in binding sites saturation and precipitation of $Fe(OH)_3$ as ferrihydrite. This hypothetical system results in 'precipitation' of ferrihydrite when the concentration of Fe^{3+}

increases to the point that the solubility product for ferrihydrite is exceeded. Thus the $SFe(III)_{app}$ is defined as the sum of aqueous inorganic Fe(III) species and Fe(III) bound to DOM at a free Fe (Fe^{3+}) concentration equal to the limiting solubility of Fe hydroxide ($Fe(OH)_3(s)$). The solubility of Ferrihydrite was defined by the solubility constants derived by (Liu and Millero, 1999). Our calculations does not account for the effects of pressure, which can also be expected to affect metal solubility (Moore and Millward, 1984).

3 Equilibrium calculations of iron speciation and apparent iron solubility in the Celtic Sea at ambient seawater pH using the NICA-Donnan model

Kechen Zhu[1], Antony Birchill[2], Angela Milne[2], Simon Ussher[2], Matthew P. Humphreys[3], Nealy Carr[4], Claire Mahaffey[4], Maeve C. Lohan[5], Eric P. Achterberg[1] and Martha Gledhill[*1]*

[1] GEOMAR Helmholtz Center for Ocean Research Kiel, Wischhofstr. 1-3, Kiel, Germany

[2] School of Geography, Earth and Environmental Sciences, University of Plymouth, Plymouth, UK

[3] NIOZ Royal Netherlands Institute for Sea Research, Department of Ocean Systems (OCS), Texel, The Netherlands

[4] School of Environmental Sciences, 4 Brownlow Street, University of Liverpool, L69 3GP, UK

[5] School of Ocean and Earth Science, University of Southampton, Southampton, UK

Submitted to Marine Chemistry

Abstract

We used a combined ion pairing - organic matter speciation model (NICA-Donnan) to predict the organic complexation of iron (Fe) at ambient pH and temperature in the Celtic Sea. We optimized our model by direct comparison with Fe speciation determined by Adsorptive Cathodic Stripping Voltammetry using the added Fe-binding ligand 1-nitroso-2-naphthol (HNN) in the presence and absence of natural organic matter. We compared determined Fe speciation with simulated titrations obtained via application of the NICA-Donnan model with four different NICA parameter sets representing a range of binding site strengths and heterogeneities. We tested the assumption that binding sites scale to dissolved organic carbon (DOC) concentrations in marine waters. We found that a constant low DOC concentration resulted in an improved fit of our titration data to the simulated titrations, suggesting that inputs of fresh DOM may not increase the heterogeneity or concentrations of Fe binding sites. Using the optimal parameter set, we calculated pFe(III)´ ($-\log(\sum Fe(OH)_i^{3-i})$) and apparent Fe(III) solubility ($SFe(III)_{app}$) at ambient pH and temperature in the water column of the Celtic Sea. $SFe(III)_{app}$ was defined as the sum of aqueous inorganic Fe(III) species and Fe(III) bound to DOM formed at a free Fe (Fe^{3+}) concentration equal to the limiting solubility of Fe hydroxide ($Fe(OH)_3(s)$). $SFe(III)_{app}$ was within range of the determined dissolved Fe concentrations observed after winter mixing on the shelf and in waters >1500 m depth at our most offshore stations. Our study supports the hypothesis that the ocean dissolved Fe inventory is controlled by the interplay between Fe solubility and Fe binding by organic matter, although the overall number of metal binding sites in the marine environment may not be directly scalable to DOC concentrations.

Keywords: trace metals, ocean acidification, intrinsic binding constants.

3.1 Introduction

Iron (Fe) is an essential micronutrient for marine phytoplankton growth, and its low supply and solubility limits primary productivity in large parts of the world's ocean (Boyd and Ellwood, 2010). Iron limitation mostly occurs in high–nitrate, low-chlorophyll (HNLC) regions, which make up approximately 30% of the surface ocean (Boyd et al., 2007). However, both Fe limitation and the potential for seasonal Fe limitation have also been reported for coastal regions and shelf seas, including European shelf seas (Birchill et al., 2017; Hogle et al., 2018; Hutchins & Bruland, 1998). The bioavailability and solubility of Fe in seawater is a function of its chemical speciation (Boyd & Ellwood, 2010; Gledhill & Buck, 2012; Hutchins et al., 1999). Inorganic Fe(III) is the thermodynamically favoured form of Fe in oxygenated seawater but, as a result of hydrolysis (equation 1), it has a low solubility that reaches a minimum between pH 7 and 9 (Byrne et al., 2000; Kuma et al., 1996; Liu & Millero, 2002). Hydrolysis competes with binding by organic matter (equation 2), thus complexation by dissolved organic ligands (i.e. those <0.2 μm in size) has the potential to reduce free Fe^{3+} concentrations and consequent formation of insoluble iron hydroxides ($Fe(OH)_3(s)$) and thereby increase the concentration of Fe(III) observed in the dissolved fraction (<0.2 μm) (Kuma et al., 2000, 1996; Liu and Millero, 2002).

$$Fe^{3+} + 3OH^- \rightarrow Fe(OH)_3(s) \quad (1)$$

$$2Fe^{3+} + (3-i)OH^- + DOM^{x-} \leftrightarrow Fe(OH)_i^{3-i} + Fe(DOM)^{3-x} \quad (2)$$

Reduction to Fe(II), via e.g. photolysis or biological activity, can also change Fe speciation, potentially increasing both the bioavailability and solubility of Fe (Barbeau, 2006; Rose and Waite, 2005; Schlosser et al., 2018). Complexation by organic matter, hydrolysis, and redox speciation thus all play important roles in ocean Fe biogeochemistry, and as a result the global Fe cycle is influenced by ocean acidification, water column stratification, warming and deoxygenation (Hutchins & Boyd, 2016). Given the role of Fe as an essential micronutrient, there is thus a need to develop reliable approaches that can be used to predict the impact of environmental change on oceanic Fe speciation and biogeochemistry (Ye et al., 2020). Ideally, such approaches would be based on a set of intrinsic thermodynamic and kinetic equations that would describe the chemical speciation and rates of

reaction of all Fe species in seawater according to ambient temperature, salinity and pH (Turner et al., 2016; Ye et al., 2020).

With respect to Fe(III) speciation in seawater, the work of Liu and Millero (1999) and Byrne et al. (2000) has provided a set of intrinsic thermodynamic constants that describe Fe hydrolysis and the formation of fresh Fe(III)-hydroxide colloidal precipitates (retained on a 0.02 µm filter). In contrast, for organic complexation, determination of metal speciation in seawater has traditionally adopted an approach where the observed strength and concentrations of metal-binding ligands were related to specific conditions of the sample (i.e. salinity, dissolved Fe concentration) and analysis (i.e. pH typically 8.0-8.2 depending on the method employed). Ocean sections of conditional ligand concentrations published as part of the GEOTRACES research programme (Buck et al., 2018, 2015; Gerringa et al., 2015) showed that, at pH 8 and room temperature, average conditional ligand concentrations range from 1-2 nEq of M Fe, and typically correlate with dissolved Fe concentrations, exceeding them by an average of ca.1 nEq of M Fe (Caprara et al., 2016). This covariance can at least partially be explained by application of analytical experimental designs and mathematical transformations that simplify a heterogeneous group of binding sites to an "average" site that can be observed under the applied experimental conditions (for further information see e.g. Gledhill and Buck, (2017); Town and van Leeuwen, (2005)). Whilst assuming two or more binding sites could overcome the covariance between ligand and dissolved iron concentrations (Buck et al., 2018), results are still specific to the titration pH rather than the sample pH and such assumptions come at the cost of increased parameter uncertainty (Pižeta et al., 2015). Thus, whilst the conditional approach demonstrates that organic complexation is important for the biogeochemistry of Fe, the conditional nature of the obtained results constrains our ability to predict how Fe(III) speciation is likely to change in a future ocean, since it provides no mechanistic knowledge of how Fe(III) binding to organic matter is influenced by pH or temperature.

Exactly how Fe(III) binding to organic matter changes as a function of pH depends on the functional group characteristics of the metal binding components of marine dissolved organic matter (DOM) (Shi et al., 2010; Zhang et al., 2019). Dissolved organic matter is a highly diverse mix of compounds (Koch et al., 2008) that will also potentially change in a future ocean (Lønborg et al., 2020). Metal binding components likely make up only a minor subset of the overall DOM pool (Zhang et al.,

2019). Previous studies have shown that bacteria and phytoplankton can release Fe binding ligands, including siderophores and polysaccharide exudates into their environment (Hassler et al., 2011a; Hassler et al., 2011b; Mawji et al., 2011; Vraspir and Butler, 2009). In addition, ligands can be released following viral lysis (Poorvin et al., 2011) or delivered by terrigenous sources in the form of humic-like substances (Muller, 2018). The organic ligand pool thus shows an intrinsic chemical heterogeneity, which is still not well understood (Gledhill and Buck, 2012), but is likely analogous to metal binding to natural organic matter in terrestrial and freshwater environments (Lodeiro et al., 2020).

Binding models for describing metal binding to organic matter using intrinsic constants (i.e. independent of pH) that account for heterogeneity are widely applied in terrestrial and freshwater environments. Perhaps the most widely used models are the Non-Ideal Competitive Adsorption (NICA)-Donnan model (Kinniburgh et al., 1999), Windermere humic acid model (WHAM) (Tipping et al., 2011), and Stockholm humic model (SHM) (Gustafsson, 2001). A primary assumption in these models is that binding sites scale proportionally to the concentration of dissolved organic carbon (DOC; 'dissolved' in this context is typically defined as <0.7 μm in size). The appeal of such an approach lies in the potential for describing the influence of Fe(III) binding to organic matter as a function of ambient pH and DOC concentrations, using a limited set of constants that could be applied to the estimation of Fe speciation across the whole ocean (Hiemstra and van Riemsdijk, 2006; Stockdale et al., 2016). Indeed, a step in this direction has recently been made in Ye et al. (2020), where the NICA-Donnan model has been used to parameterise the impact of future changes in ocean pH on ocean productivity in a global biogeochemical model. The NICA-Donnan model describes the binding behavior of metal ions to a heterogeneous mix of binding sites using a continuous bimodal distribution based on the Langmuir-Freundlich adsorption isotherm (Kinniburgh et al., 1999), while both the WHAM and SHM models rely on a set of empirically derived relationships and a set number of binding sites with different affinities to calculate metal speciation (Gustafsson, 2001; Tipping et al., 2011). A further key difference between the three approaches relates to the application of electrostatic sub-models to describe the impact of ionic strength on binding of metals to the organic matter phase. In the NICA-Donnan model, the Donnan component is used to describe non-specific electrostatic interactions on metal binding to DOM, while the SHM model uses the Basic Stern model (Gustafsson, 2001) and WHAM uses a correction based on the

Debye-Hückel and Gouy-Chapman theory (Tipping et al., 2011). All three approaches have been successfully used to predict metal speciation in seawater (Avendaño et al., 2016; Hiemstra & van Riemsdijk, 2006; Ndungu, 2012; Stockdale et al., 2011, 2015; Tipping et al., 2016). However, since a direct intercomparison study has yet to be undertaken, it is not known if one model is superior to the others in seawater applications.

In order to further test the applicability of such heterogeneous models to Fe(III) speciation in the marine environment, we wished to examine predicted and observed relationships between DOC concentrations and Fe speciation in more detail. In this study, we tested the underlying assumption that Fe speciation determined with a given set of intrinsic NICA constants could be scaled to DOC concentrations, at least within the range of DOC concentrations typically observed in marine waters. In coastal waters, average DOC concentrations are ca. 300 µmol L^{-1} because of enhanced productivity or localized DOC inputs from terrestrial sources (Barrón and Duarte, 2015), while in the open ocean DOC concentrations are lower and vary by at most a factor of two (40-80 µmol L^{-1}, Hansell, 2013). Since DOC composition changes with concentration (Hansell, 2013), we also implicitly tested a second assumption, that the changes in DOC composition resulting from microbial production and utilization of organic matter does not significantly impact the binding properties of DOM. We used samples collected on three cruises in the Celtic Sea during three different seasons. The Celtic Sea is a productive, temperate sea located on the northwest European shelf (Carr et al., 2018; Muller-Karger et al., 2005). Our three cruises transected from a productive shelf environment out to the open ocean and our samples therefore incorporated a range of DOC concentrations and DOM compositions from fresh DOM produced during phytoplankton bloom conditions to aged DOM from deep waters (>500 m). To test scalability to changing DOC concentration, we compared the concentrations of observed Fe species to those predicted using two sets of NICA constants previously described in the literature (Gledhill et al., 2015; Hiemstra and van Riemsdijk, 2006) and two sets more specific to DOM in our research area that we re-derived from raw titration data obtained in a previous study in our region (Avendaño et al., 2016). We used the NICA/Donnan model to calculate the equilibrium speciation of Fe(III) at ambient pH and temperature in our region. We estimated the impact of Fe bound to organic matter on the inorganic Fe fraction (Fe´) in our study region. Since Fe(III) solubility is also directly related to Fe speciation, we also examined the saturation state of Fe at ambient pH and temperature in our study region by calculating the apparent

Fe(III) solubility ($SFe(III)_{app}$). We define $SFe(III)_{app}$ as the sum of aqueous inorganic Fe(III) species and Fe(III) bound to DOM formed at a free Fe (Fe^{3+}) concentration equal to the limiting solubility of Fe hydroxide ($Fe(OH)_3(s)$; Zhu et al., 2021). We discuss the observed trends in the context of observed total dissolved Fe concentrations in order to understand the relative importance of different physico-chemical drivers that influence Fe speciation.

3.2 Materials and Methods

Sampling

Samples were collected during three cruises: DY018 in autumn (November 2014), DY029 in spring (April 2015) and DY033 in summer (July 2015) in the Celtic Sea on board the RRS Discovery as part of the UK Shelf Sea Biogeochemistry programme (Birchill et al., 2017; Rusiecka et al., 2018). Here, we examine Fe speciation at the central Celtic Sea site (CCS), a shelf edge station (CS2) and an off-shelf transect through a submarine canyon (C01-06) (Figure 1). Salinity, depth and temperature were measured using a Seabird CTD attached to a titanium rosette frame equipped with 24 x 10 L Ocean Test Equipment bottles (Birchill et al., 2017). Trace metal samples were collected following GEOTRACES protocols (Cutter et al., 2017). Samples for the determination of Fe speciation were filtered (0.2 µm cartridge filters; Sartobran-300, Sartorius) into acid-cleaned 250 ml low density polyethylene (LDPE) bottles (Nalgene) and frozen immediately (-20 °C). Samples were subsequently analyzed in a trace metal clean laboratory at GEOMAR.

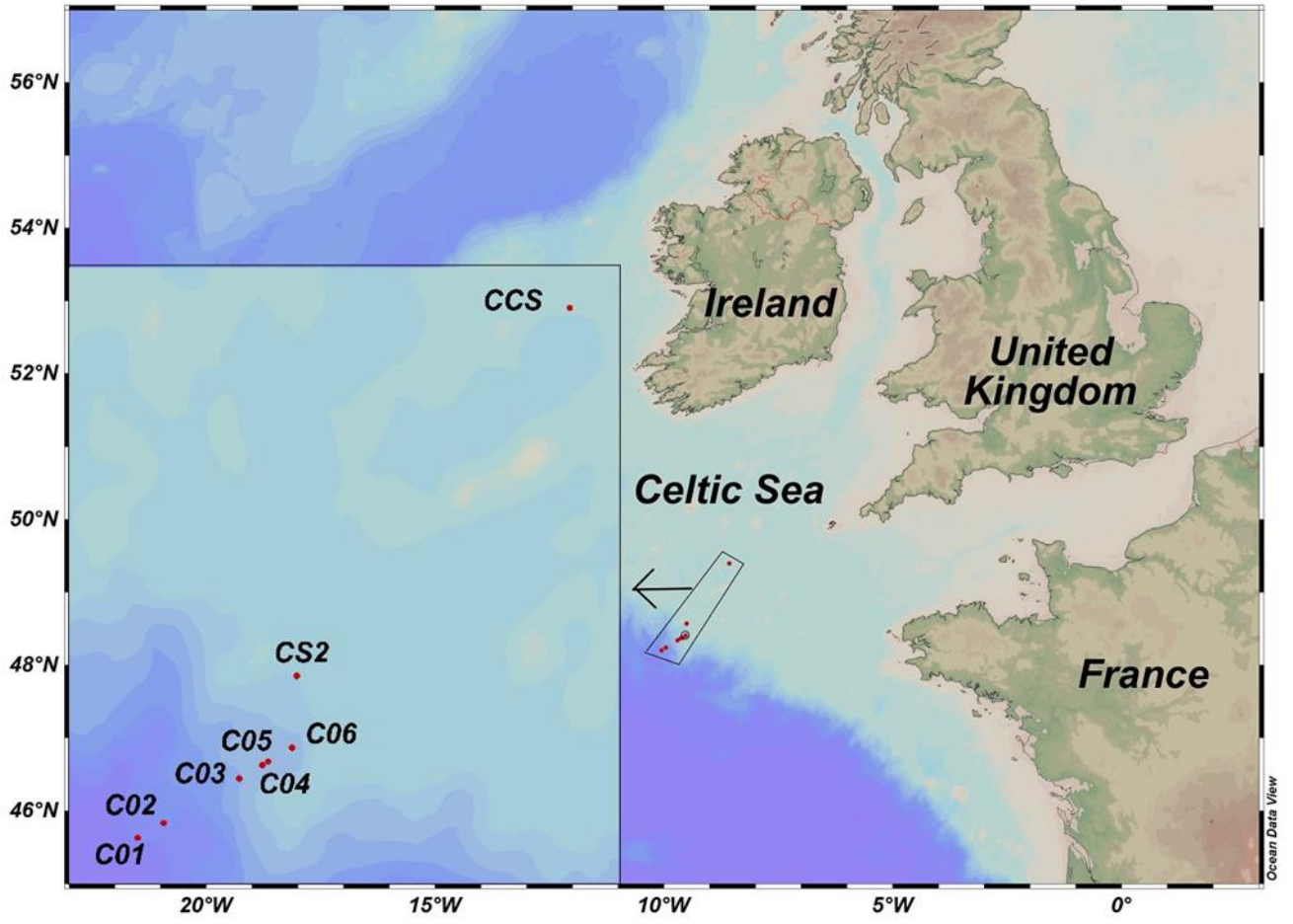

Figure 1. Map of study area with stations indicated by red dots. Map generated using Ocean Data View (Schlitzer, 2015).

Determination of dissolved Fe, dissolved organic carbon and pH

Samples for DFe analysis were collected after filtration through 0.2 µm cartridge filters. The samples were stored in acid cleaned LDPE bottles (Nalgene) and acidified to pH 1.7 (0.024 mol L^{-1} HCl, Romil-UpA). Dissolved Fe concentrations were determined using flow injection with chemiluminescence detection (Birchill et al., 2017; Obata et al., 1993). The accuracy and analytical uncertainty of the method was assessed by applying the top down NordtestTM approach to the analysis of SAFe and GEOTRACES consensus materials, the combined uncertainty was calculated to be 9.5 % (Worsfold et al., 2019).

Samples for the determination of DOC were collected after filtration (ashed glass fibre filters, 0.7 µm nominal pore size, Whatman), and acidified to pH 2 using hydrochloric acid. The DOC samples were analyzed onshore using high temperature catalytic oxidation on a Shimadzu TOC-VCPN. Consensus reference materials (CRM; University of Miami) were used to determine accuracy and precision of analysis daily, which were both better than 4 %.

Samples for dissolved inorganic carbon (C_T) and total alkalinity (A_T) were collected via silicone tubing into 250 ml borosilicate glass bottles following established protocols (Dickson, 2010). For the off-shelf transect, samples for C_T and A_T were collected only during DY018 and DY033. Each bottle was sealed shut with a greased ground glass stopper after introducing a 2.5 ml air headspace and sterilising the sample with 50 µl of saturated mercuric chloride solution. All samples were stored in the dark until analysis with VINDTA 3C instruments (Marianda, Germany). The C_T and A_T measurements were calibrated using measurements of certified reference material obtained from Prof A. G. Dickson (Scripps Institution of Oceanography, USA) (Humphreys et al., 2019). The pH of our seawater samples was calculated on the IUPAC/NBS scale (pH_{NBS}) from C_T and A_T using CO2SYS (Pierrot et al., 2006). In CO2SYS, the constants describing the carbonate and sulphate equilibrium with hydrogen ions were from Mehrbach et al. (1973) (refitted by Dickson and Millero (1987)) and Dickson, (1990), respectively, and the total boron concentration was estimated from salinity following Uppström, (1974). We used the NBS pH scale because it is consistent with the speciation constants in the applied NICA-Donnan and ion pairing models.

Determination of iron speciation via adsorptive cathodic stripping voltammetry

Iron speciation was determined by competitive ligand equilibrium with adsorptive cathodic stripping voltammetry (CLE-AdCSV), using 1-nitroso-2-naphthol (HNN) as the added ligand (van den Berg, 1995). HNN (Sigma-Aldrich) was diluted in methanol (Fisher, HPLC grade) to make a stock solution. To clean the stock buffer solution of N-(2-Hydroxyethyl)piperazine-N′-(2-ethanesulfonic acid) (HEPES; Sigma-Aldrich), HNN was added and equilibrated with the buffer overnight. HNN and $FeNN_3$ were subsequently removed using a pre-activated C18 SepPak column (Whatman). The pH_{NBS} of the buffer solution was adjusted to 8 prior to the titration work with ammonium hydroxide

(20-22%) (Optimal, Fisher Scientific), and the pH_{NBS} of each buffered sample was determined to be between 7.9 and 8.1, with an overall average of 8.00±0.08 (n=93).

Since the speciation measurements are thermodynamic, it is important that voltammetric peaks are stable and equilibrium is achieved (Laglera & Filella, 2015; Van Leeuwen & Town, 2005). In previous studies, a reaction time of > 6 h was assumed to be sufficient to reach equilibrium conditions (Avendaño et al., 2016; Boye et al., 2001; Boye et al., 2003; Gledhill & van den Berg, 1994). However, Wu and Luther (1994, 1995) waited 24 h to reach the equilibrium condition between FeL (i.e. Fe bound to natural ligand) and HNN. Here, we tested equilibration time prior to analyzing Fe speciation in our seawater samples. Our test indicated that a reaction time > 12h was needed to obtain consistent, reproducible peak heights, which we took to approximate equilibrium conditions between FeL and HNN for our method and we therefore allowed for a 16 h equilibration period.

Our speciation measurements are based on establishing an equilibrium between HNN, Fe^{3+}, binding sites (L^-) and the remaining inorganic Fe species (e.g. hydroxides) in the solution. The ratio of free to complexed species gives the side reaction coefficient (α) for the reaction (Ringbom and Still, 1972), which is also related to the conditional stability constant ($k^{cond}_{FeNN3,Fe3+}$) and the concentration of ligand not bound to Fe ([NN´]), as shown for the formation of $FeNN_3$ in equation (3).

$$\frac{[FeNN_3]}{[Fe^{3+}]} = \alpha'_{FeNN3,Fe3+} = k^{cond}_{FeNN3,Fe3+} \times [NN']^3 \qquad (3)$$

Species can only compete when their side-reaction coefficients are within an order of magnitude of each other, hence ligands detectable in a CLE-AdCSV titration are restricted to those with side reaction coefficients (α'_{FeL}) within this "detection window" (Van Den Berg et al., 1990; Hudson et al., 2003; Kogut & Voelker, 2001). However, there may be a considerable range of ligand strengths in seawater and the use of at least two detection windows has previously been recommended to ensure the full range of ligand strengths can be accounted for (Buck et al., 2012; Pižeta et al., 2015; Sander et al., 2011). We therefore used three different total HNN concentrations, $[HNN_T]$ = 1, 5 and 20 µmol L^{-1}.

We combined our different HNN concentrations with seven different Fe additions between 0 and 5 nmol L^{-1} at the two lower HNN concentrations (1 and 5 µmol L^{-1}) and 3 concentrations (5, 10, 15 nmol L^{-1}) at the highest HNN concentration (20 µmol L^{-1}) to create a matrix of 18 titration points. All titration data for one sample were obtained on the same day. Our aim was to estimate the slope using our highest HNN concentration and calculate [$FeNN_3$] according to the "overload titration" method (Kogut and Voelker, 2001). Examination of the sensitivity observed for each HNN concentration in seawater in our samples at Fe concentrations ≥ 3 nmol L^{-1} showed no significant difference between sensitivity at 5 and 20 µmol L^{-1} HNN (details in supplementary information, Figure S1). On the other hand, the titration point with the highest added Fe concentration (15 nmol L^{-1}) was often lower than expected, suggesting non-linearity in the titration at higher Fe concentrations, possibly caused by adsorption of the hydrophobic $FeNN_3$ complex on the walls of the voltammetric cell (Supplementary Figure S2). We thus used the data with 5 and 20 µmol L^{-1} HNN and added Fe concentrations from 3 to 10 nmol L^{-1} to calculate the sensitivity of our analysis and determine the $FeNN_3$ concentration.

The concentration of HNN not complexed by Fe ([NN´]) and the conditional stability constant ($k^{cond}_{FeNN3,Fe3+}$) of the $FeNN_3$ complex were used to derive the free Fe^{3+} concentrations in the sample at the fixed titration pH_{NBS} of 8.0 over the range of Fe concentrations according to equation (3). Since [HNN_T] >> [Fe], we assumed that [HNN_T] = [NN´]. The cumulative random error for Fe^{3+} is largely dependent on the random error in the $FeNN_3$ concentration, as the 95 % confidence interval for the estimation of $k^{cond}_{FeNN3,Fe3+}$ was 0.2 % of the determined value (see results). We estimated an average analytical precision for our determined $FeNN_3$ concentrations of 9 % based on the mean variability of observed peak areas. However, we note this estimate does not account for errors incurred during calculation of the sensitivity, which will result in an additional random error between titrations.

The difference between the total Fe present in the solution and [$FeNN_3$] were used to determine the non-labile dissolved Fe concentration (DFe*):

$$DFe^* = [TFe] - [FeNN_3] \quad (4)$$

where [TFe] is the concentration of total Fe (i.e. DFe + added Fe). DFe* is subject to error propagation from the determinations of both $FeNN_3$ (9 %) and dissolved Fe (7 %) and thus will be

subject to the combined error of 11.4 %. We therefore only report values of DFe* where [$FeNN_3$] is at least 11.4 % less than [TFe].

Derivation of equilibrium constant for $FeNN_3$ for application in ion pairing models for seawater

To ensure consistency between our observed $FeNN_3$ concentrations and our speciation calculations we derived an equilibrium constant valid for seawater (S=35) between pH_{NBS} 7.2-8.5 that accounts for competition between Fe and hydrogen ions for NN^-.

$$Fe^{3+} + 3HNN \leftrightarrow FeNN_3 + 3H^+ \quad (5)$$

We distinguish this constant from previously derived conditional stability constants ($\log k^{cond}_{FeNN3,Fe3+}$) by denoting it $\log k_{FeNN3,H+}$. We used the equilibrium constant for HNN of $10^{7.9}$ (NIST, Smith et al. 2004). Derivation was carried out by combining the chemical speciation program ORCHESTRA (Meeussen, 2003) with the parameter estimation software PEST (Doherty, 2019). Speciation calculations in ORCHESTRA were set up with input, chemistry and objects files as described previously (Janot et al., 2017; Zhu et al., 2021). Further details can be downloaded from protocols.io (dx.doi.org/10.17504/protocols.io.brc4m2yw). We used the Minteqv4 database for thermodynamic constants, which is consistent with the database used previously in visual MINTEQ (Avendaño et al., 2016; Gledhill et al., 2015) and we also verified that calculations in ORCHESTRA and visual MINTEQ were comparable. For the derivation of $\log k_{FeNN3,H+}$ we specified an initial estimate of 31, with an allowed range of 28 to 32. Parameter derivation is performed by calculation of the $FeNN_3$ concentration in ORCHESTRA for each measurement, which is then passed to PEST and compared to the observed values. PEST provides a new value for $\log k_{FeNN3,H+}$, which is then passed back to ORCHESTRA for a fresh calculation of $FeNN_3$. The procedure is iterated to minimize the residuals between observed and calculated $FeNN_3$ calculations via the Levenberg-Marquardt algorithm. The PEST output comprises a value for $\log k_{FeNN3,H+}$ with 95% confidence intervals, together with a full record of the optimization in the output file. Consistency was then further assessed by comparison between observed and calculated $FeNN_3$ and Fe^{3+} in UV irradiated seawater as a function of HNN concentration, within the HNN concentration range applied in this study.

Assessment of relationship between observed and calculated concentrations of iron species to DOC concentrations assuming binding sites behave according to the NICA-Donnan model.

The NICA-Donnan model was used to calculate the speciation of Fe at equilibrium for each titration point at pH_{NBS} 8.0, via speciation calculation tool ORCHESTRA (Meeussen, 2003). We tested the assumption that one set of NICA-Donnan parameters could describe variability in [$FeNN_3$] and [Fe^{3+}] by adding the "Fulvic acid" NICA-Donnan adsorption model to the dissolved ion pairing model used for the derivation of $\log k_{FeNN3,H+}$. Marine DOM was thus considered analogous to terrestrial and freshwater DOM (Gledhill et al., 2015; Laglera & Van Den Berg, 2009; Lodeiro et al., 2020). The applied NICA model assumes a continuous Sips bimodal distribution of binding sites. The distribution of the affinities of the two groups of binding sites (Denoted (1): Carboxylic-type groups, and (2): Phenolic-type groups) are described by three constants per binding site group: the width of the binding site distribution (p_1 and p_2), NICA affinity constant ($\log K_{Me1}$ and $\log K_{Me2}$ for a metal cation or $\log K_{H1}$ and $\log K_{H2}$ for the protonation constants) which represents the median of the distribution, and non-ideality constant which represents non-ideal behavior of ion adsorption (n_{Me1}, n_{Me2}, n_{H1}, n_{H2}), with n_{Hi} = 1 representing non-heterogeneous binding (i.e. one binding site per group; Kinniburgh et al., 1999). The binding of a metal by marine DOM, Q_{Me} is then described with reference to proton binding by marine DOM according to the following equation:

$$Q_{Me} = Q_{max1,T}\frac{n_{Me,1}}{n_{H1}}\cdot\frac{(K_{Me,1}.C_{Me})^{n_{Me,1}}}{(K_{H,1}.C_H)^{n_{H,1}}+(K_{Me,1}.C_{Me})^{n_{Me,1}}}\cdot\frac{\{(K_{H,1}.C_H)^{n_{H,1}}+(K_{Me,1}.C_{Me})^{n_{Me,1}}\}^{p1}}{1+\{(K_{H,1}.C_H)^{n_{H,1}}+(K_{Me,1}.C_{Me})^{n_{Me,1}}\}^{p1}} + Q_{max2,T}\frac{n_{Me,2}}{n_{H2}}\cdot\frac{(K_{Me,2}.C_{Me})^{n_{Me,2}}}{(K_{H,2}.C_H)^{n_{H,2}}+(K_{Me,2}.C_{Me})^{n_{Me,2}}}\cdot\frac{\{(K_{H,2}.C_H)^{n_{H,2}}+(K_{Me,2}.C_{Me})^{n_{Me,2}}\}^{p2}}{1+\{(K_{H,2}.C_H)^{n_{H,2}}+(K_{Me,2}.C_{Me})^{n_{Me,2}}\}^{p2}} \quad (6)$$

where $Q_{max1,T}$, $Q_{max2,T}$ refer to the total number of proton binding sites per binding site type, and C_H and C_{Me} are the concentrations of protons and metal, respectively.

In the NICA-Donnan model, electrostatic interactions are described by the Donnan component of the model which is based on the Boltzmann equation (Benedetti et al., 1996). However, at the ionic strength of seawater the apparent Donnan volume becomes very small and concentrations of metals electrostatically associated with DOM become negligible (Lodeiro et al., 2020; Pinheiro et al., 2021).

In this study, we used two previously published sets of NICA constants and two new NICA parameter sets (Table 1). The previously published sets were derived from surface waters collected in the Sargasso Sea (Set A: Hiemstra and van Riemsdijk, 2006) and surface waters obtained from an estuarine system on the English south coast (Set B: Gledhill et al. 2015), whilst the new parameter sets C and D were re-derived from surface waters in the Northwest European Shelf Sea based on titration data obtained in Celtic Sea samples first reported in Avendaño et al. (2016). We re-derived the set C and D values because the original reported values were empirically estimated using a $\log k_{FeNN3,H+}$ of 32.5, which was considerably higher than the value we derived in this study (see results). We used PEST-ORCHESTRA to re-derive the NICA constants following a similar procedure used for the derivation of $\log k_{FeNN3,H+}$ and described in Zhu et al., (2021). Since this work was focused on the Celtic Sea, we only used the titration data obtained from Celtic Sea samples in this derivation (samples collected at stations 1, 3, 4, 5, 6 18, 19, 20 from Avendaño et al. (2016)). We provide the raw titration data, required input files and a description of the protocol used in this derivation on protocols.io (dx.doi.org/10.17504/protocols.io.brc4m2yw). We followed the PEST-ORCHESTRA approach that was first used to derive NICA constants for Cd and Zn binding to Laurentian fulvic acid by Janot et al. (2017). Typically, both equilibrium constants and non-ideality constants are derived from experimental data. However, we found during preliminary derivations that since titrations were undertaken at only three pH_{NBS} values (7.2, 7.6, 8) and encompassed a relatively narrow pH range, data from Avendaño et al. (2016) were not sufficiently well constrained in pH space to reproducibly derive all four parameters. We therefore fixed $n_{Fe(III)1}$ and used the relationship between n_1 and n_2 from Milne et al. (2003) ($n_2 = 0.76 \times n_1$) to calculate $n_{Fe(III)2}$. We then estimated $\log K_{Fe(III)1}$, $\log K_{Fe(III)2}$ using initial estimates of 3 and 9, and allowed ranges of 2 to 4 and 8 to 10, respectively. Generic parameters from Milne et al. (2003), (2001) were used to describe binding of proton and major cations (H^+, Ca^{2+}, Mg^{2+}, Sr^{2+}) to be consistent with parameter sets A and B.

To investigate goodness of fit at different ambient DOC concentrations, we compared our observed $FeNN_3$ concentrations with $FeNN_3$ concentrations calculated in ORCHESTRA. We then compared Fe^{3+} calculated from observations using equation (3) with those calculated in ORCHESTRA and

observed versus calculated DFe* calculated using equation (4). For speciation calculations, pH was set to the analysis pH_{NBS} (= 8.00±0.08).

Prediction of apparent Fe(III) solubility and inorganic Fe concentrations at ambient pH and temperature in our study region

We predicted Fe speciation in our study area at ambient pH and temperature using the NICA constants with the best fit to our observed titration data. To calculate $SFe(III)_{app}$ we set our total Fe(III) concentration to 10 nmol L^{-1} and allowed for the formation of $Fe(OH)_3(s)$ (ferrihydrite) within ORCHESTRA. We use a solubility product of $\log K_s = 3.2$, derived from (Liu and Millero, 1999) to determine iron solubility according to equation (7).

$$^{*}K_S = [Fe^{3+}] \div [H^+]^3 = 10^{3.2}, \Delta H_r = -100.4 \text{ kJ mol}^{-1} \quad (7)$$

We therefore consider organically bound Fe as soluble, but freshly precipitated $Fe(OH)_3(s)$ as insoluble. We compare our $SFe(III)_{app}$ with observed dissolved Fe concentrations. However, given the potential size of both freshly formed $Fe(OH)_3(s)$ (defined in Liu and Millero (1999) as >0.02 µm) and organic matter (determined in the < 0.7 µm fraction), the Fe associated with both DOM and $Fe(OH)_3(s)$ may both be colloidal in nature (>0.02 but <0.2 µm) and this should be kept in mind when comparing the absolute values.

We calculated the sum of soluble inorganic species and express these concentrations as pFe(III)´ using:

$$pFe(III)' = -Log\ ([FeOH^{2+}] + [Fe(OH)_2^+] + [Fe(OH)_3] + [Fe(OH)_4^-]) \quad (8)$$

In these calculations, we set the total Fe concentration to be equal to the determined DFe concentration, but $Fe(OH)_3(s)$ was also allowed to form to account for possible formation of insoluble iron hydroxides when Fe^{3+} becomes oversaturated, according to equation (7).

3.3 Results and Discussion

3.3.1 Establishing consistency between observations and calculations in the absence of organic matter.

An understanding of how pH and temperature might influence trace element speciation at equilibrium can be obtained via iterative algorithms based on thermodynamic principles using sets of thermodynamic constants valid for the physico-chemical conditions to be explored in the study. We applied "off the shelf" ion pairing software packages in our study that incorporate ionic strength corrections based on the extended Debye-Hückel equation, but we highlight this is not fully optimal and warn that absolute values predicted via our speciation calculations will be affected by systematic bias as a result of overestimation of activities. The impact of the ion pairing approach is illustrated by an approximate 15% underestimation in ionic strength in our calculation (I=0.6 M), which is consistent with previous estimates of the error introduced by application of the Debye-Hückel equation (Stockdale et al., 2016). Nevertheless, valuable information – with respect to the extent that changes in physico-chemical properties such as pH and temperature may have on metal speciation – can be obtained if a system can be calibrated such that its observed and calculated values are consistent for a given critical species. In our study, we used a value for $\log k_{FeNN3,H+}$ within an ion pairing model, which would account for competition between NN^-, H^+, Fe^{3+} and OH^- at the ionic strengths and pH relevant to our study. In previous work, a first attempt at such a system was made by manually changing constants to obtain an empirical estimate for $\log k_{FeNN3,H+}$ (Avendaño et al., 2016). In this study, we sought to improve on this by first calibrating $\log k_{FeNN3,H+}$. We particularly focused on establishing consistency between determined and calculated Fe^{3+} and $FeNN_3$ concentrations, since $FeNN_3$ is the measured species from titrations and Fe^{3+} is the Fe species that reacts with the added ligand, hydroxide ion and natural organic matter.

Estimation of $\log k_{FeNN3,H+}$ using the parameter estimation software package PEST (Doherty, 2019) in combination with the ion pair speciation program ORCHESTRA (Meeussen, 2003) resulted in a $\log k_{FeNN3,H+}$ of 29.5±0.1. With this value, the Pearson correlation coefficient between observed and calculated log[$FeNN_3$] was 0.962 with a root mean squared error (RMSE) of 1.12 nmol L^{-1} over the pH_{NBS} range 7.2-8.5 and at an HNN concentration of 2 µmol L^{-1}. Predicted Fe^{3+} concentrations

(Fe^{3+}_{calc}) correlated with Fe^{3+} calculated from the observed $FeNN_3$ concentrations ($Fe^{3+}_{titration}$) ($\log[Fe^{3+}]_{calc} = 0.95 \times \log[Fe^{3+}]_{titration} -0.83$, $r^2= 0.97$, n=456) (Figure 2a). The modelled distribution of the relative proportion of Fe present as $FeNN_3$ as a function of pH suggests that $FeNN_3$ will be the dominant species between pH_{NBS} 7 and 8, with a maximum predicted response at pH_{NBS} 7.5 (Figure 2b), which is consistent with the relationship between pH and the voltammetric response for $FeNN_3$ previously reported by van den Berg (1991). However, our derived value of 29.5 for $\log k_{FeNN3,H+}$ is three orders of magnitude lower than the empirical estimate of 32.5 given by Avendaño et al. (2016). Further comparison with literature values showed that our calculated conditional stability constant at pH_{NBS} 8 is within the reported range after calibration against hydroxide and EDTA but lower than obtained at pH_{NBS} 6.9 (Supplementary Table 1). The difference between the calibrated constants could be explained by the ionic strength corrections applied during the calculations, the choice of conditional constants for Fe binding to EDTA, and the applied inorganic side reaction coefficient for Fe (Laglera et al., 2011).

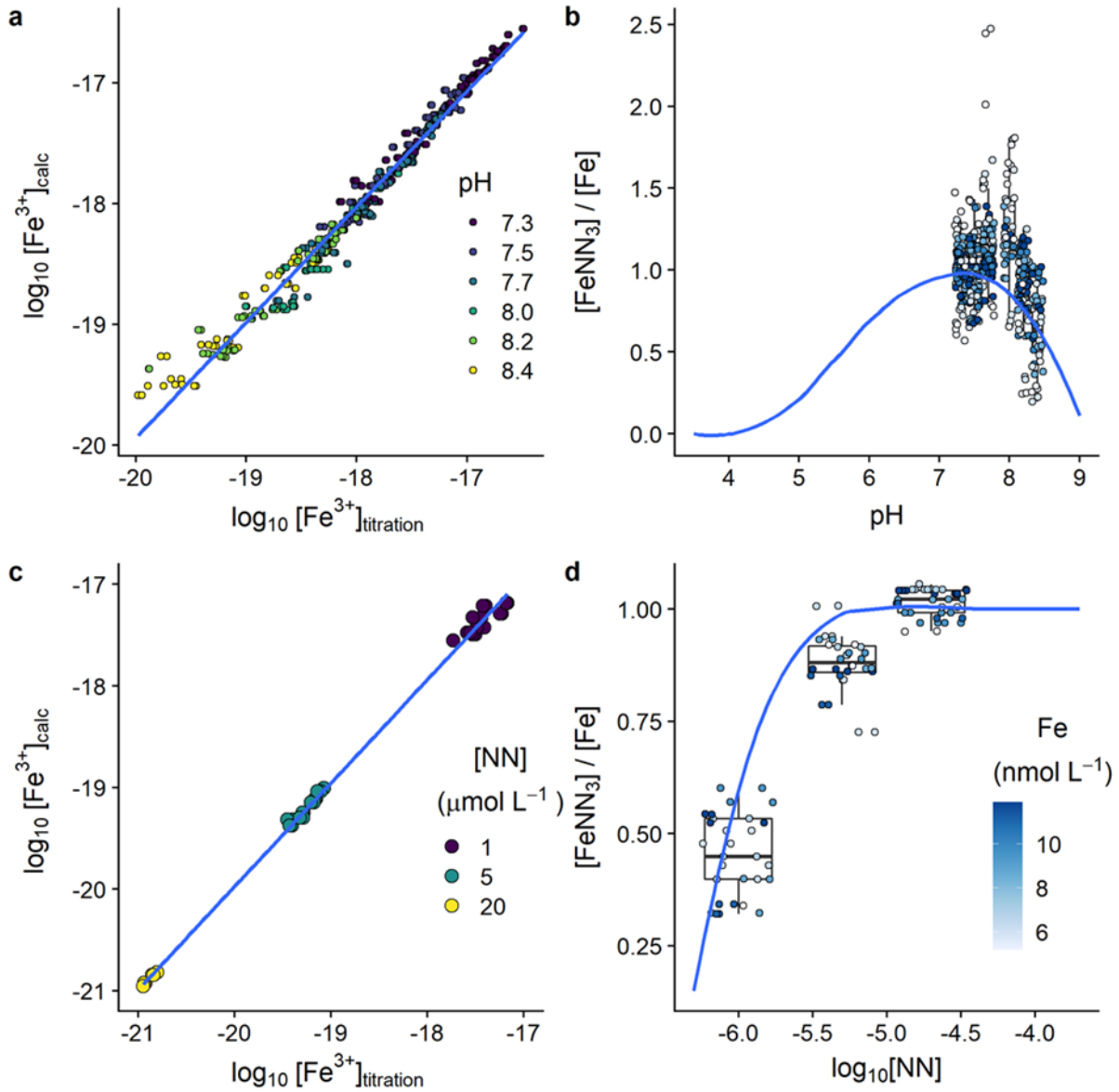

Figure 2 Predicted Fe^{3+} and $FeNN_3$ for seawater after ultra violet irradiation to destroy organic matter. (a) Predicted Fe^{3+} is plotted versus determined Fe^{3+} from titrations using HNN concentrations at 2 and 5 µmol L^{-1} over the pH_{NBS} range 7.2-8.5. (b) The proportion of $FeNN_3$ relative to total Fe from titrations using HNN concentrations at 2 and 5 µmol L^{-1}, is shown over the pH_{NBS} range 7.2-8.5, where measured $FeNN_3$ is indicated as colored points and predicted $FeNN_3$ is shown by the solid line. (c) Predicted Fe^{3+} is plotted versus determined Fe^{3+} from titrations undertaken at constant pH_{NBS} (~8.0) over the range of HNN concentrations. (d) The proportion of $FeNN_3$ relative to total Fe from titrations undertaken at constant pH_{NBS} (~8.0), is shown over the range of HNN concentrations, where measured $FeNN_3$ concentrations are shown as colored points and predicted $FeNN_3$ is shown by the solid line.

We next examined the relationship between calculated and determined $FeNN_3$ and Fe^{3+} concentrations using the derived $\log k_{FeNN3,H+}$ over the range of HNN concentrations (1, 5 and 20 µmol L^{-1}) employed in this study at pH_{NBS} 8.0 using the 'overload titration' method. We obtained a linear relationship between observed and calculated $[Fe^{3+}]$ ($\log[Fe^{3+}]_{calc}=1.07\pm0.03 \times \log[Fe^{3+}]_{titration} + 8.7\times10^{-20}\pm6.5\times10^{-20}$, $r^2=0.93$, n=98, Figure 2c). The positive intercept implies a slight systematic overestimate of $FeNN_3$ by the ion pairing model, which is supported by the relationship between the proportion of Fe bound to $FeNN_3$ and the HNN concentration (Figure 2d). The observed proportion of Fe(III) that was detected as $FeNN_3$ at both 1 and 5 µmol L^{-1} HNN was thus slightly lower (by an average of 10 and 15 % respectively) than predicted by the ion pairing model. Our calculated side reaction coefficients were $\log\alpha'_{FeNN3,Fe3+}$ = 9.1, 11.2 and 13 for 1, 5 and 20 µmol L^{-1} HNN, respectively. These values compared to a $\log\alpha'_{Fe}$ of 8.95 calculated by the ion pairing model at pH_{NBS} 8.0. The similarity between $\log\alpha'_{FeNN3,Fe3+}$ and $\log\alpha'_{Fe}$ at an HNN concentration of 1 µmol L^{-1} means that hydroxide ions will compete with HNN at our lowest HNN concentration (Figure 2c). Given the low solubility of Fe hydroxides (at pH_{NBS} 8.0 and 293 K, $Fe(OH)_3(s)$ is predicted to form at an $[Fe^{3+}]$ concentration of 7.58×10^{-20} mol L^{-1}, equivalent to pFe(III)′ = 10.2), the relatively high proportion of Fe^{3+} (maximum calculated Fe^{3+} in UV irradiated seawater = 5.7×10^{-18} mol L^{-1}) should theoretically result in formation of $Fe(OH)_3(s)$ at both 1 and 5 µmol L^{-1} HNN concentrations. Nevertheless, the linear relationship between observed and calculated Fe^{3+} suggests that $Fe(OH)_3(s)$ formation did not impact on the determination of $FeNN_3$, possibly because we always added HNN prior to addition of Fe. The binding of Fe to HNN therefore occurred more quickly than formation of $Fe(OH)_3(s)$. If we assume no formation of $Fe(OH)_3(s)$ occurred, then Fe^{3+} concentrations are consistent over the range of pH and HNN values examined here.

We concluded that our experiment - speciation calculation framework was adequately consistent within the time frame of our titration experiments. However, we caution that our experiments are likely not at true equilibrium, and while it was not detectable over the <24-hour equilibration period of our titrations, we cannot completely rule out formation of $Fe(OH)_3(s)$. Although our calculations simplify the complex kinetic and thermodynamic processes that influence chemical Fe speciation in aqueous solutions, we argue that they are sufficiently consistent to be used to investigate the relationship between DOC concentration and Fe speciation predicted by the NICA-Donnan model.

As a final step in the development of our experimental framework for examining the relationship between DOC concentrations and the fit of observed Fe speciation to different sets of NICA parameters, we re-derived the NICA constants from Avendaño et al. (2016). We carried out this re-derivation to improve upon the empirical nature of the original estimates and to account for the difference in $\log k_{FeNN3,H+}$ used to generate the estimates for the NICA affinity constants reported by Avendaño et al. (2016). When fitting for four parameters ($n_{Fe(III)1}$, $n_{Fe(III)2}$, $\log K_{Fe(III)1}$, $\log K_{Fe(III)2}$) we found that repeated estimations (n>3) using the same initial arbitrary parameter values did not produce reproducible results, likely as a result of overfitting the data set. The value of n_i and its relationship to n_H as described in equation (6) have been related to reaction stoichiometry between H^+ and the metal ion (Hiemstra and van Riemsdijk, 2006), thus determination of n_i requires experimental data with sufficient density and range in pH space (Zhu et al., 2021). Unfortunately, we found that this criterion was not satisfied by the data of Avendaño et al. (2016), since titrations at only 3 pH values within a relatively restricted range (less than one pH unit) were undertaken. We therefore initially set the value for $n_{Fe(III)1}$ to 0.31 based on previously reported values available for marine organic matter (Avendaño et al., 2016; Gledhill et al., 2015; Hiemstra and van Riemsdijk, 2006). The value of $n_{Fe(III)2}$ was calculated using the formula $n_2 = 0.76 \times n_1$ which has previously been shown to describe the covariance between n_1 and n_2 observed for multiple cations (Milne et al., 2003). Our re-derived NICA affinity constants (set C) are presented in Table 1 along with a further two sets of constants (sets A and B) taken from the literature (Gledhill et al., 2015; Hiemstra and van Riemsdijk, 2006) that we use directly. As expected, the combination of fixing n_i, the mathematical rederivation and the change in $\log k_{FeNN3,H+}$, resulted in differences in the derived $\log K_{Fe(III)1}$ and $\log K_{Fe(III)2}$ used in this study compared to the values empirically estimated (0.26, 3.6, 0.23 and 8.3 for $n_{Fe(III)1}$, $\log K_{Fe(III)1}$, $n_{Fe(III)2}$, $\log K_{Fe(III)2}$ respectively) by Avendaño et al. (2016).We further examined the impact of n_i by increasing the value of n_1 and n_2 (set D) to consider the possibility that marine DOM is less heterogeneous than typically observed for terrestrial organic matter (Lodeiro et al., 2020; Zhu et al., 2021). As well as influencing the effective competition between the metal and protons (Milne et al., 2003), the non-ideality constant influences the relationship between the free metal ion concentration and the total dissolved metal concentration (also termed the concentration dependency, Milne et al. 2003). Incorporation of heterogeneity results in an exponential increase in Fe^{3+} as DFe concentrations increase, which arises because stronger binding sites in the distribution

are occupied first. Higher values of n_i result in a shallower exponential curve for the relationship between Fe^{3+} and DFe concentrations.

Table 1. Four sets of constants for Fe(III) binding to the two dissolved organic matter binding site types of the NICA-Donnan model. Parameter sets A and B were taken from the literature, Hiemstra and van Riemsdijk (2006) and Gledhill et al. (2015), respectively. Parameter sets C and D were re-derived for this study based on raw titration data obtained in Celtic Sea samples previously reported in Avendaño et al. (2016). We fixed the non-ideal constants ($n_{Fe(III)}$) to derive the binding affinity ($\log K_{Fe(III)}$) for both parameter sets C and D. The goodness of fit is indicated as root mean square error (RMSE).

Fe(III) NICA constants	set A	set B	set C	set D
FA1: Carboxylic-type groups				
$\log K_{Fe(III)1}$	2.8	3.6	2.81±0.36	3.16±0.001
$n_{Fe(III)1}$	0.36	0.3	0.31	0.4
FA2: Phenolic-type groups				
$\log K_{Fe(III)2}$	8.3	11.2	9.04±0.01	9.80±0.01
$n_{Fe(III)2}$	0.23	0.15	0.24	0.3
RMSE for parameters rederived in this study	NA		0.7908	0.2149

3.3.2 Influence of dissolved organic carbon concentration on determined and calculated Fe speciation at constant pH

In this work, we analyzed 106 samples from three cruises undertaken in November (DY018, 47 samples), April (DY029, 34 samples) and July (DY033, 28 samples) by CLE-AdCSV and present raw titration data in the SI (Supplementary Figure S2). We first compared $FeNN_3$ concentrations calculated with the NICA-Donnan model using parameter sets A-D with the observed $FeNN_3$ concentrations for the whole data set (Table 2, Supplementary Figure S3). Simulated $FeNN_3$ using parameter set B systematically underestimated the observed $FeNN_3$ concentrations, resulting in a

larger RMSE in comparison to sets A, C and D (Table 2). Parameter set B thus overestimated the binding strength of organic matter in our study region. The stronger binding represented by parameter set B could reflect the estuarine nature of the samples used for the parameter estimation, which might be more strongly influenced by terrestrial organic matter. However, we caution that the data set used for the estimation in Gledhill et al. (2015) was based on analysis of one sample and the authors of that study emphasized that it was intended as a proof of concept.

Table 2. Relationships between calculated (y) and observed (x) $FeNN_3$ concentrations obtained using four sets of NICA constants. Sets A and B and are taken from the literature, Hiemstra and van Riemsdijk (2006) and Gledhill et al. (2015), respectively. Sets C and D were re-derived for this study based on titrations data taken from Avendaño et al. (2016). The number of observations was 643. The goodness of fit is indicated as root mean square error (RMSE).

Fe(III) NICA constants	set A	set B	set C	set D
Linear equation	y=1.03x+0.36	**y**=8.05x-0.79	y=1.03x+0.50	y=1.03x+0.39
r^2	0.85	0.78	0.84	0.85
RMSE (nmol L^{-1})	0.95	1.52	0.89	0.98

$FeNN_3$ is a dominant species at 5 and 20 µmol L^{-1} HNN in our titration experiments, and variability in less abundant species might be expected to be more sensitive to changes in binding site concentrations and better highlight systematic bias with respect to DOC concentrations. Therefore, we next compared the relationship between $[Fe^{3+}]_{titration}$ and total Fe with calculated values for Fe^{3+} obtained from combining the ion-pairing and NICA model ($[Fe^{3+}]_{NICA}$) using our four sets of NICA constants for samples binned into three different DOC concentrations: 45-55, 55-65, and >65 µmol L^{-1} (Figure 3). The DOC bins broadly align with concentrations typically observed for semi-refractory, semi-labile and labile DOC respectively (Hansell, 2013), although the division between the different DOC fractions is likely less well defined than implied here. Figure 3 shows that the relationship between $[Fe^{3+}]_{titration}$ and total Fe was quite well described by A, C and D, but not well described by parameter set B, although some differences between Fe^{3+} at 1 µmol L^{-1} HNN at low total Fe

concentrations was evident for all sets at DOC concentrations > 55 µmol L^{-1}. Results of correlation between $[Fe^{3+}]_{titration}$ and $[Fe^{3+}]_{NICA}$ are given in Table 3. Calculated $[Fe^{3+}]_{NICA}$ using parameter sets A, C and D again showed better agreement with $[Fe^{3+}]_{titration}$ (Table 3) than parameter set B. Combining information from intercept, slope and r^2 and Akaike Information Criteria (AIC), A and D were found to be a better fit to the data than C.

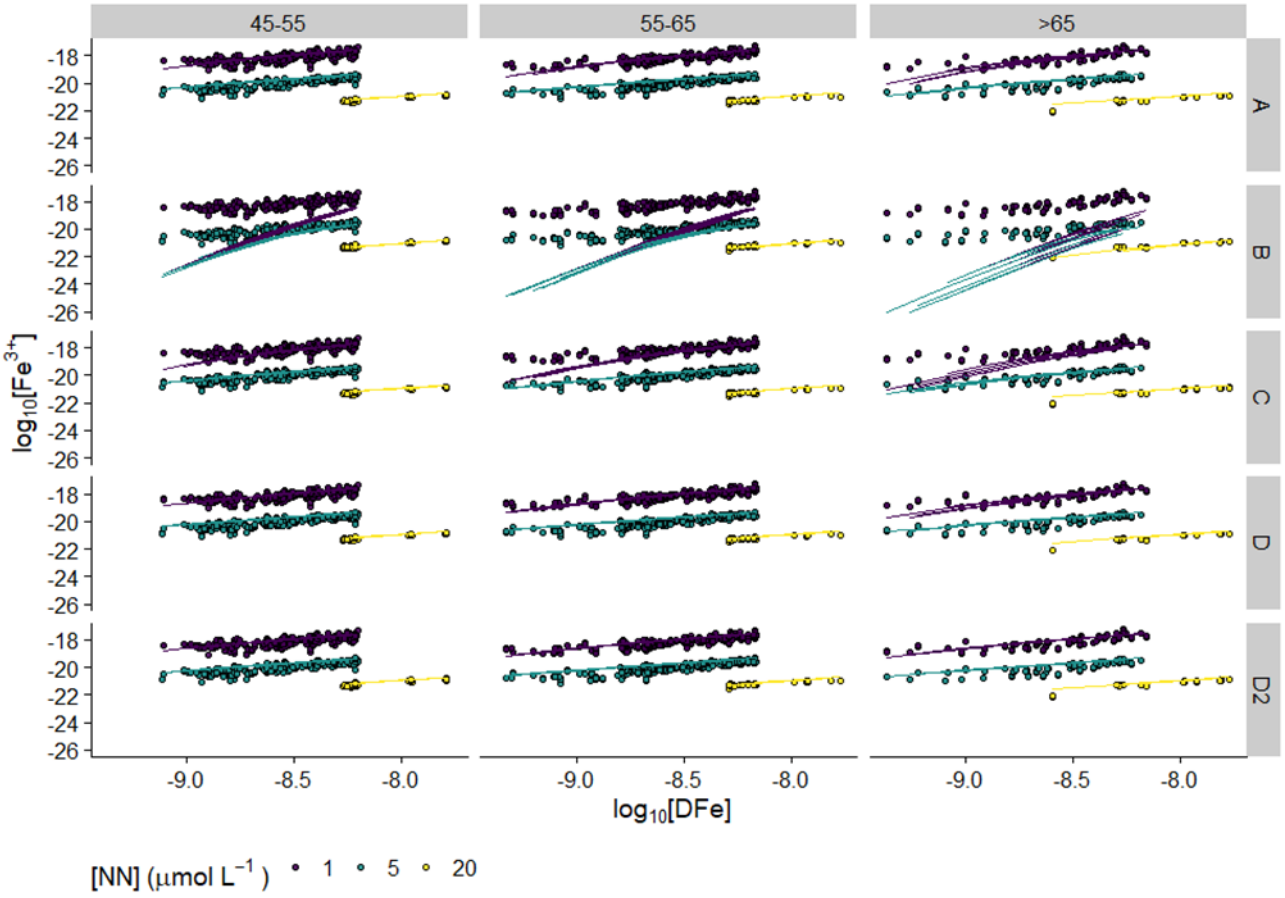

Figure 3. Plots of Fe^{3+} versus total Fe concentrations obtained for titrations binned into three DOC concentration ranges (45-55, 55-65 and >65 µmol L^{-1}). Points show Fe^{3+} concentrations obtained from measured $FeNN_3$ concentrations at three different HNN concentrations: 1, 5 and 20 µmol L^{-1}. Lines show Fe^{3+} concentrations calculated using the NICA-Donnan model combined with an ion-pairing model. Four different NICA parameter sets were applied: parameter set A was reported in Hiemstra and van Riemsdijk, (2006), B in Gledhill et al. (2015), whilst C and D were re-derived for this study based on titration data from Avendaño et al. (2016) (Table 1). Scenario D2 used NICA parameter set D, but assumed that DOC concentrations were constant at 43.7 µmol L^{-1}.

We noted that goodness-of-fit of $[Fe^{3+}]_{NICA}$ to $[Fe^{3+}]_{titration}$ tended to decrease with increasing DOC concentration (Table 3). We therefore further examined the scenario that binding sites did not scale with DOC concentration by calculating the Fe speciation using parameter set D and fixing the DOC concentration to the lowest value observed in our study (43.7 µmol L^{-1}). We found similar goodness-of-fit results for this fixed-DOC scenario (D2) across the whole range of DOC concentrations observed in our study, suggesting that binding sites are not necessarily more abundant at higher DOC concentrations.

Table 3. Correlations of $\log[Fe^{3+}]_{titration}$ (x) observed in titrations undertaken at different HNN concentrations with $\log[Fe^{3+}]_{NICA}$ (y) calculated using a combined ion-pair/NICA-Donnan model. Sets A and B and are taken from the literature, Hiemstra and van Riemsdijk (2006) and Gledhill et al. (2015), respectively. Sets C and D were rederived for this study based on titration data taken from Avendaño et al. (2016). The D2 scenario used parameter set D but assumed a constant DOC concentration of 43.7 µmol L^{-1}.

DOC concentration (µmol L^{-1})	NICA parameter set	Intercept	Slope	R^2	AIC
45-55 (n=612)	A	-1.21±0.16	0.93±0.01	0.95	-55
	B	-10.8±0.6	0.50±0.03	0.27	1655
	C	-2.67±0.18	0.85±0.01	0.93	116
	D	-1.24±0.16	0.93±0.01	0.96	-80
	D2	-1.05±0.16	0.93±0.01	0.96	-89
55-65 (n=643)	A	-1.34±0.14	0.92±0.01	0.96	-138
	B	-10.0±0.8	0.55±0.03	0.23	2008
	C	-2.83±0.2	0.85±0.01	0.91	289
	D	-1.38±0.14	0.92±0.01	0.97	-202
	D2	-1.04±0.13	0.93±0.01	0.97	-249
65-200 (n=234)	A	-2.06±0.32	0.89±0.02	0.92	117
	B	-13.1±1.7	0.43±0.09	0.09	881
	C	-4.20±0.48	0.79±0.03	0.80	303

D	-2.04±0.29	0.89±0.01	0.94	62
D2	-1.18±0.25	0.92±0.01	0.96	-16

For our final assessment employing our titration data, we examined the relationship between the non-labile Fe concentrations (DFe*) and $[Fe^{3+}]_{titration}$ observed in our titrations and compared the relationship to values calculated using the NICA model. For both titration data and simulated results using the NICA-Donnan model, DFe* was calculated using equation (4); at 1 µmol L^{-1} HNN, this fraction therefore incorporates a portion of the Fe bound to hydroxides. Figure 4 shows the relationship between DFe* and Fe^{3+} of measured ($DFe^*_{titration}$) and calculated data (DFe^*_{NICA}), binned according to DOC concentration. We observed larger scatter in the calculations of DFe* at each HNN concentration and weak correlations ($r^2 < 0.2$, data not shown) between $DFe^*_{titration}$ and DFe^*_{NICA}, which likely reflects increased error propagation and the limited range of DFe* values that can be observed using AdCSV. However, for the most part, observed $DFe^*_{titration}$ fell between calculated values obtained for parameter set B and those obtained in the absence of organic matter (no DOM) and overlapped with parameter sets A, C and D. The overload titration method assumes that DFe* will be negligible at 20 µmol L^{-1} HNN, and indeed we rarely observed DFe* values greater than 11 % of total Fe (the threshold of uncertainty) at this HNN concentration. Data points where DFe* was detected at 20 µmol L^{-1} HNN were scattered through the data set and thus result from random error rather than systematic offsets associated with individual samples. Furthermore, we note that at 5 µmol L^{-1} HNN, concentrations of $[FeNN_3]_{calc}$ were overestimated in our UV seawater experiments (Figure 2d), which could contribute further to discrepancies between $DFe^*_{titration}$ and DFe^*_{NICA}. The analytical limitations of CLE-AdCSV should also be considered here, since its results are known to be influenced by the estimation of sensitivity, lack of equilibrium conditions, and the number and distribution of titration points (Gledhill and Gerringa, 2017; Hudson et al., 2003; Pižeta et al., 2015; Town and Filella, 2000). In particular, the calculation of DFe* is sensitive to bias in estimation of the slope (Hudson et al., 2003), and the ability to detect significant concentrations of DFe* is strongly influenced by the sensitivity of the method. In our case, we note that HNN is one of the least sensitive ligands that can be used to detect Fe by CLE-AdCSV (Ardiningsih et al., 2021), although it has the advantage that it forms one dominant species (Waska et al., 2016), which simplifies application over a range of added ligand concentrations (Abualhaija and van den Berg, 2014). Importantly, the $FeNN_3$ complex can also be detected over a relatively wide pH range (van

den Berg, 1991), allowing speciation analysis to be applied over a range of pH values (Avendaño et al., 2016; Gledhill et al., 2015).

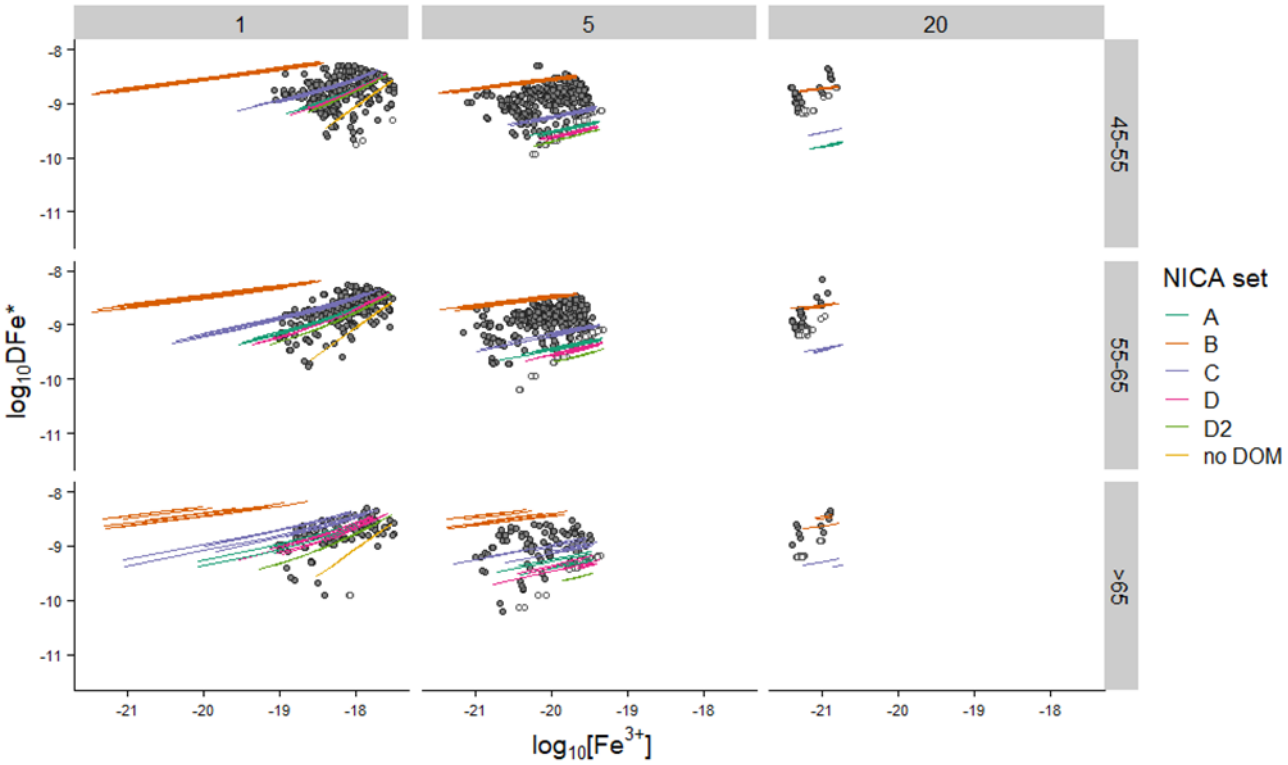

Figure 4. Plot of DFe (i.e. total Fe - $FeNN_3$) versus Fe^{3+} concentrations. Calculated DFe* and Fe^{3+} from titrations are shown as grey points. Open symbols show values where DFe* was below detection and are set to the value of the detection limit. Lines show values predicted for each titration using the NICA-Donnan parameter sets (A-D), at pH 8.0 and temperature 20° C with ambient DOC concentrations. Scenario D2 is the same as set D but with a constant DOC concentration of 43.7 µmol L^{-1} whilst no DOM shows the expected result in the absence of Fe bound to organic matter. Data is faceted according to HNN concentration (horizontal facet, µmol L^{-1}) and DOC concentration range (vertical facet, µmol L^{-1}).*

Taken together, the calculated $[Fe^{3+}]_{NICA}$ values in our titrations suggest parameter sets A and D provide the best approximations of $[Fe^{3+}]_{titration}$. Examination of DFe* suggests that NICA parameters A, C and D predict DFe* within the range of observed values. Considering NICA sets A and D, binning the data into three different DOC concentrations showed that goodness of fit decreased slightly with increasing DOC concentration (Table 3). The increase in negative intercept with increased DOC concentration suggests that this was because the NICA model slightly overestimated Fe binding to DOM at higher DOC concentrations, and this effect was largely eliminated by

assuming a constant DOC concentration of 43.7 µmol L^{-1} with scenario D2. The overestimation of the impact of increasing DOC concentrations could point to dilution of the Fe-binding functional groups by input of fresh DOM with a lower binding site density. Since the main source of fresh DOC in our study area is phytoplankton (Carr et al., 2018; Davis et al., 2018), this would imply that the overall binding affinity of DOM produced by phytoplankton is lower than the aged DOM pool. However, such a trend could also be observed if the use of generic NICA constants from Milne et al., (Milne et al., 2003) results in an overestimation of binding site heterogeneity for marine DOM. There is a paucity of data investigating the acid-base binding characteristics of marine DOM, so we recommend further investigation of total binding site concentrations and binding site heterogeneity as a function of DOM mass (Lodeiro et al., 2020), particularly with respect to the changes in DOM composition as a function of productivity. Furthermore, we recommend that alternative experimental designs for titrations are explored for their ability to derive intrinsic, rather than conditional, metal binding constants (e.g. titrations over a wider range of pH values (Avendaño et al., 2016; Gledhill et al., 2015) or with higher pH resolution (Zhu et al., 2021)).

3.3.3 Prediction of Fe(III) speciation in the Celtic Sea using ambient pH and dissolved organic carbon concentrations

3.3.3.1 The combined impact of variability in pH and DOC concentration and choice of NICA constants on calculated Fe speciation.

For a heterogeneous group of binding sites, DFe, pH, and DOC all influence pFe(III)´. We illustrate the relative importance of the key parameters for driving variability in pFe(III)´ with model experiments (Figure 5a and b). We calculated pFe(III)´ with three scenarios based on the minimum and maximum observed values for pH and DOC we encountered in our study area: i) pH_{NBS} = 8.1, DOC = 45 µmol L^{-1} ii) pH_{NBS} = 8.3, DOC = 45 µmol L^{-1} and iii) pH_{NBS} = 8.3, DOC = 150 µmol L^{-1}. We compare these scenarios with values calculated using ambient pH and DOC, without considering the formation of $Fe(OH)_3$(s). The different scenarios show that the DOC range encountered in our study area has a greater potential impact on pFe(III)´ than pH does, especially for parameter set D, where scenarios (i) and (ii) overlap. The low impact of pH arises because pH did not vary greatly in

the study region (range of ~0.2) and because the lower heterogeneity described by parameter set D reduced the impact of pH.

We compared the data points and the solid curve in Figure 5 (a) and (b) and observed a decrease in pFe(III)´ of approximately 1 and 0.5 log units at our lowest DFe concentrations and 2 and 1 log units at our highest DOC concentrations for parameter sets A and D, respectively. These values provide an estimate of the likely error in pFe(III)´ introduced by scaling to DOC and, not surprisingly, show that the greatest impact will occur at the highest DOC concentrations. The differences between the magnitude of the estimates for sets A and D relate to the degree of heterogeneity, as described by the non-ideality constant, with set D describing a less heterogeneous distribution of binding sites than set A.

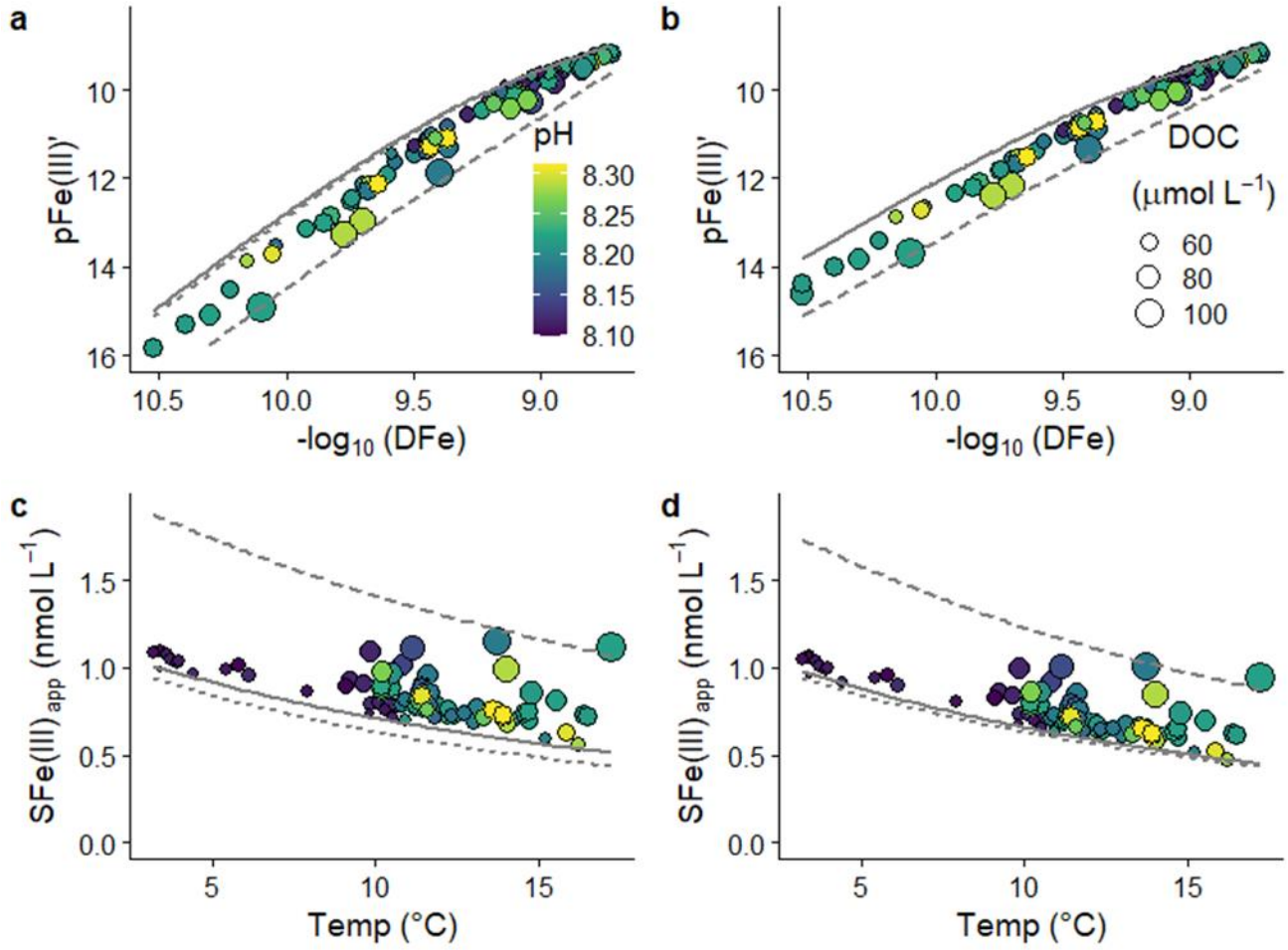

Figure 5 (a), (b) Plots of pFe(III)´as a function of dissolved Fe concentration (DFe) and (c),(d) apparent Fe(III) solubility ($SFe(III)_{app}$) as a function of temperature for NICA parameter sets A and D respectively. The

impact of pH and DOC concentration are shown by the colour and size of the points, respectively. The lines show the trend if pH and DOC are assumed constant at (i) solid line: pH = 8.09 and DOC =43.7 µmol L^{-1} (ii) short dashes: pH = 8.31 and DOC =43.7 µmol L^{-1} and (iii) long dashes: pH = 8.31 and DOC =150 µmol L^{-1}.

3.3.3.2 Impact of pH, DOC and temperature on apparent Fe(III) solubility in the Celtic Sea

Fe(III) solubility strongly influences the overall Fe inventory in the ocean (Johnson et al., 1997) and in the absence of ligands the oceanic DFe inventory would be significantly lower (Hunter and Boyd, 2007; Liu and Millero, 2002). Previous work has suggested that the ocean is saturated with respect to Fe(III) hydroxide (Byrne & Kester, 1976; Kuma et al., 1996, 1998, 2003). However, CLE-AdCSV determinations suggested that ligand concentrations are in excess of DFe, which implies that Fe(III) hydroxide might be undersaturated at the pH of the measurement (Caprara et al., 2016). The saturation state of Fe in the ocean is thus subject to some uncertainty. Furthermore, the interplay between scavenging and solubility is poorly constrained (Tagliabue et al., 2016), and the potential impact of changes in ambient seawater pH on Fe solubility has rarely been considered (Millero et al., 2009; Ye et al., 2020).

Our calculations of [Fe^{3+}] at the ambient pH and DOC concentrations described above resulted in a maximum value of 4.5×10^{-19} nmol L^{-1} for both parameter sets A and D, obtained at the highest DFe concentration of 1.9 nmol L^{-1}. At pH_{NBS} 8.0 and 20°C, our ion pairing model predicts formation of $Fe(OH)_3(s)$ at an Fe^{3+} concentration of 7.58×10^{-20} mol L^{-1}. Therefore our predicted Fe^{3+} concentrations were oversaturated with respect to $Fe(OH)_3(s)$. We therefore used iterative speciation calculations to investigate the potential interaction between Fe(III) solubility, temperature, pH and Fe binding to DOM in our study area. We calculated apparent Fe(III) solubility ($SFe(III)_{app}$) by setting the total Fe(III) concentrations to 10 nmol L^{-1} for all samples in the model, thereby ensuring formation of the insoluble $Fe(OH)_3(s)$ species. $SFe(III)_{app}$ was then expressed as the sum of the concentrations of aqueous inorganic Fe(III) species and Fe(III) bound to DOM.

Figure 5 (c) and (d) shows the variation of calculated $SFe(III)_{app}$ plotted as a function of temperature for parameter sets A and D respectively. Trends for $SFe(III)_{app}$ for both parameter sets were similar and the highest $SFe(III)_{app}$ was observed at maximum DOC concentrations. Whilst DOC was an important influence on $SFe(III)_{app}$, decreased temperature and pH also both lead to increasing

$SFe(III)_{app}$ as a result of changes in the hydrolysis according to equation (1) (Figure 5, c and d). We assessed the relative importance of pH and temperature by calculating $SFe(III)_{app}$ using the same scenarios described for calculation of pFe(III)´ (section 4.3.2). We observed that pH had a greater impact on $SFe(III)_{app}$ than on pFe(III)´. However, in the scenario where Fe binding does scale with DOC concentration, DOC was more important than pH for our study area.

Comparisons between NICA parameter sets A and D showed that $SFe(III)_{app}$ was 0.05 nmol L^{-1} higher for parameter set A than for parameter set D at our lowest DOC concentration (43.7 µmol L^{-1}) and 0.2 nmol L^{-1} higher at our highest DOC concentration (111 µmol L^{-1}) (Figure 5, c and d). The difference was driven by changes in the affinity constant and the relative non-ideality of the binding sites, which effectively results in a lower binding affinity for parameter set D in comparison to parameter set A.

Both parameter sets predict maximum $SFe(III)_{app}$ values (1.2 and 1.1 nmol L^{-1}) that are lower than the determined maximum DFe concentrations (1.9 nmol L^{-1}). We emphasize that absolute values have to be compared with caution because of systematic errors in the calculations from e.g. ionic strength corrections. Here, we also need to consider the influence of physical size and filter size cut-off, since the solubility product used in this study was determined using 0.02 µm filter cut off (Liu and Millero, 1999), whilst Fe binding characteristics were determined with a 0.2 µm filter cut off range and DOC concentrations used in this study were determined in the <0.7 µm fraction. We note that fresh Fe hydroxide nanoparticles can be as small as 2-3 nm (Cismasu et al., 2011; Janney et al., 2000) and would thus be classed as dissolved when a 0.02 µm filter cut off is employed. In addition, scavenging processes in which DFe is potentially reversibly adsorbed onto solid phases present in the water column are thought to be an important influence on DFe concentrations (Achterberg et al., 2018; Fitzsimmons et al., 2017) but are not considered in our approach. It is therefore difficult to precisely map our predicted $SFe(III)_{app}$ onto DFe concentrations. Nevertheless, we considered being able to predict $SFe(III)_{app}$ to within 58 % of the determined DFe concentration as encouraging and hence further examined the temporal and spatial variability of Fe species calculated at ambient pH, DFe and DOC in the Celtic Sea.

3.3.3.3 Calculated Fe speciation at ambient pH and temperature in the Celtic Sea

We examined spatial and temporal variability in Fe speciation that results from changes in DFe and pH in our study region using parameter set D. However, we note that the differences in both calculated pFe(III)´ and $SFe(III)_{app}$ between A and D were limited (maximum for pFe(III)´ of 1.2 log units and 0.2 nmol L^{-1} for $SFe(III)_{app}$), especially at low DOC concentrations (negligible for pFe(III)´ and 0.05 nmol L^{-1} for $SFe(III)_{app}$). We re-calculated Fe speciation using ambient DFe concentrations and allowed for formation of $Fe(OH)_3(s)$ where DFe > $SFe(III)_{app}$. We first examined the temporal variability in $SFe(III)_{app}$ and pFe(III)´ on the Celtic Sea Shelf and then spatiotemporal variation across the shelf break using i) ambient DOC and ii) a fixed DOC concentration set to the lowest deep-water DOC concentration observed in our study area (43.7 µmol L^{-1}).

Seasonal variability in the Central Celtic Sea (site CCS) on the shelf.

The hydrography and the seasonal cycles of DFe, DOC and pH of the Celtic Sea during our sampling period has been described in detail elsewhere (Birchill et al., 2017; Carr et al., 2018; Humphreys et al., 2019; Rusiecka et al., 2018). Briefly, DFe concentrations varied both in the surface mixed layer and deeper waters, with the spring bloom resulting in significant drawdown of DFe in surface waters (0.08 ± 0.01 nmol L^{-1}, n= 2) to levels similar to observations in open ocean regions, while in deeper waters DFe increased from 0.82 ± 0.02, n= 3 (April) to 1.48 ± 0.06 nmol L^{-1}, n= 3 (July) (Birchill et al., 2017). In the surface mixed layer, DOC concentrations were highest in April (73.3 ± 2.9 µmol L^{-1}, n= 3) and lowest in July (57.7 ± 4.0 µmol L^{-1}, n= 5) (Figure S4). DOC concentrations tended to decrease with increasing depth in April and November, and concentrations in all three samples below the thermocline were 64.8 ± 0.0 µmol L^{-1} (n= 3) in April and 58.7 ± 1.8 µmol L^{-1} (n= 4) in November. In July, the trend of DOC was opposite, such that above the thermocline DOC decreased with increasing depth, whilst higher DOC was observed below the thermocline (67.6 ± 4.6 µmol L^{-1}, n= 2). pH was higher in surface waters compared to deeper waters during all three sampling campaigns (Figure S4). A vertical gradient in pH was observed in November with a difference of 0.11 between the surface mixed layer and below the mixed layer.

The changes in DFe, pH and temperature throughout the seasonal cycle resulted in changes in both $SFe(III)_{app}$ and pFe(III)´ (Figure 6). In surface waters in July and November, DFe was consistently lower than calculated $SFe(III)_{app}$ and as expected, DFe was thus undersaturated with respect to $Fe(OH)_3(s)$ formation in our calculations (Figure 6a). Below the mixed layer (>75 m), remineralization of sinking organic matter in the bottom mixed layer resulted in increased DFe (Birchill et al., 2017) and formation of $Fe(OH)_3(s)$ in our calculations (Figure 6a). With the constant DOC scenario, $SFe(III)_{app}$ changed by < 0.03 nmol L^{-1} at station CCS. For the ambient DOC scenario $SFe(III)_{app}$ was overall higher by 0.3 nmol L^{-1} as a result of the increased DOC concentrations (Figure S4), however variability was also low (<0.02 nmol L^{-1}). We found that the $SFe(III)_{app}$ determined by our speciation model for the bottom mixed layer were very similar (0.54-0.87 nmol L^{-1}, Figure 6a) to the concentrations of DFe determined throughout the well-mixed water column in April (0.82 ± 0.04 nmol L^{-1}, n=6). Our results therefore suggest that when the water column is stratified, water below the mixed layer is oversaturated with Fe as a result of constant supply of DFe by remineralization. Winter mixing subsequently resets the DFe inventory to one that our results suggest could be based on Fe solubility.

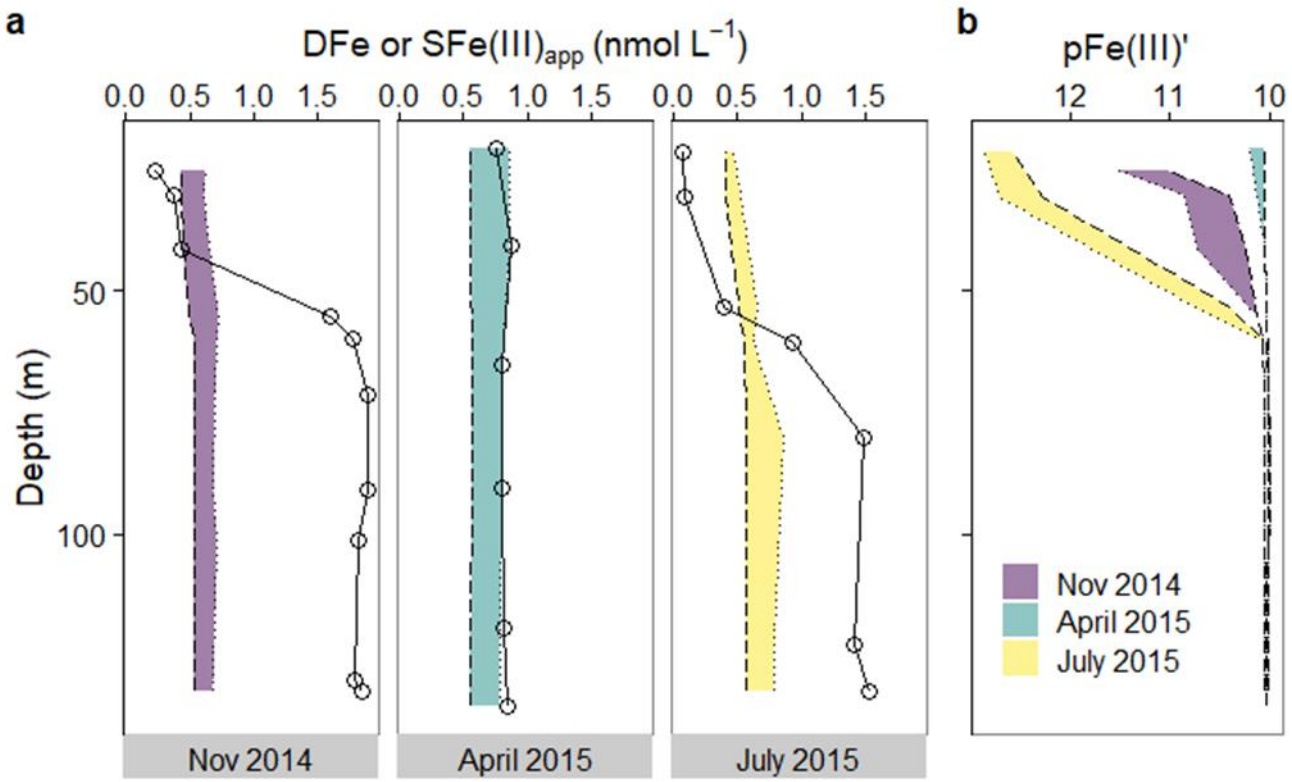

Figure 6. (a) Seasonal changes in the vertical distribution of observed dissolved Fe (<0.2 µm, point and solid line) and calculated apparent Fe(III) solubility ($SFe(III)_{app}$ = Fe(III)′+Fe bound to DOM) using NICA parameter set D. Lines show values calculated using a fixed DOC concentration of 43.7 µmol L^{-1} (long dashes) or ambient DOC concentration (dotted line) and the shaded area highlights the difference between the two scenarios. For calculation of $SFe(III)_{app}$, we assumed a total Fe(III) concentration of 10 nmol L^{-1} in our calculations and DFe was therefore not an input parameter in the calculations. (b) pFe´ ($-log_{10}(Fe(III))$) was calculated allowing for the formation of ferrihydrite when DFe was greater than $SFe(III)_{app}$ with ambient (dots) and fixed (dashes) DOC concentration scenarios. Calculations were performed using ambient pH and temperature for samples collected on the shelf in autumn (November 2014), spring (April 2015) and summer (July 2015).

Above the mixed layer, pFe(III)´ was primarily dependent on DFe concentrations, with pH having a minor influence (Figure 6b) because of the low degree of heterogeneity predicted by parameter set D (Figure 5b). Below the surface (>75 m), the over-saturation of Fe in July and November meant that pFe(III)´ was rather constant (10.04±0.02) and controlled by the formation of $Fe(OH)_3(s)$ in our calculations rather than by the strength of binding to organic matter. In April, surface water (<75 m) pFe(III)´ was similar to those in deeper waters as the water column was well-mixed, whilst a marked increase of pFe(III)´ was observed from surface to deeper waters in July and November (Figure 6b). pFe(III)´ was thus predicted to increase in surface waters from summer through to spring in both

constant and ambient DOC scenarios. The increase in pFe(III)´ was thus largely driven by the drawdown of DFe in April resulting from phytoplankton productivity (Birchill et al., 2017). After July, the slight increase in vertical exchange due to mixing and the on shelf circulation pattern resulted in a decrease surface water pFe(III)´ from July to November, even though the water column remained stratified.

Spatiotemporal variation in key variables and Fe speciation over the Shelf break

Temperature and salinity data over the shelf break are provided in Figure S5. Dissolved Fe ranged in concentration between 0.03-1.90 nmol L^{-1} along the transect and was lower in surface waters (0.22±0.12 nmol L^{-1} in November, 0.20±0.28 nmol L^{-1} in July), and enhanced in deeper waters below ~500 m (1.04±0.24 nmol L^{-1} in November, 0.87±0.14 nmol L^{-1} in July, Figure 7). The distribution and concentration of DFe are broadly consistent with previous observations in the Celtic Sea (Nedelec et al., 2007) and neighbouring Bay of Biscay (Laès et al., 2007; Ussher et al., 2007). A notable exception is that the DFe observed in this study during July 2015 in the surface mixed layer include the lowest reported DFe concentrations (< 0.1 nmol L^{-1}) for waters in this region. These are attributed to biological Fe uptake during the spring bloom coupled with low external inputs to the surface mixed layer (Birchill et al., 2017). In contrast to surface waters, concentrations of DFe in excess of 1.00 nmol L^{-1} (to a maximum of 1.90 nmol L^{-1}) were observed at inner shelf stations in November (C03-C06, CS2) and July (C04-06) at depths >500 m, which we attribute to a lateral flux of DFe from the Celtic Sea shelf slope (Nedelec et al., 2007).

Average DOC concentrations of 60.1 ± 9.2 µmol L^{-1} (n= 48) were observed in November, and 58.4 ± 14.2 µmol L^{-1} (n= 28) in July (Figure 7). Higher DOC concentrations were occasionally observed in surface waters (station C06 in November (98.23 µmol L^{-1}) and station C02 in July (111 µmol L^{-1})). Between 200-1000 m, DOC was higher at C03 station than at other stations in November, a feature that partly coincided with higher DFe concentrations. In the deep ocean (> 1000 m), DOC was slightly lower in July (49.2±3.19 µmol L^{-1}) than in November (52.3±3.3 µmol L^{-1}).

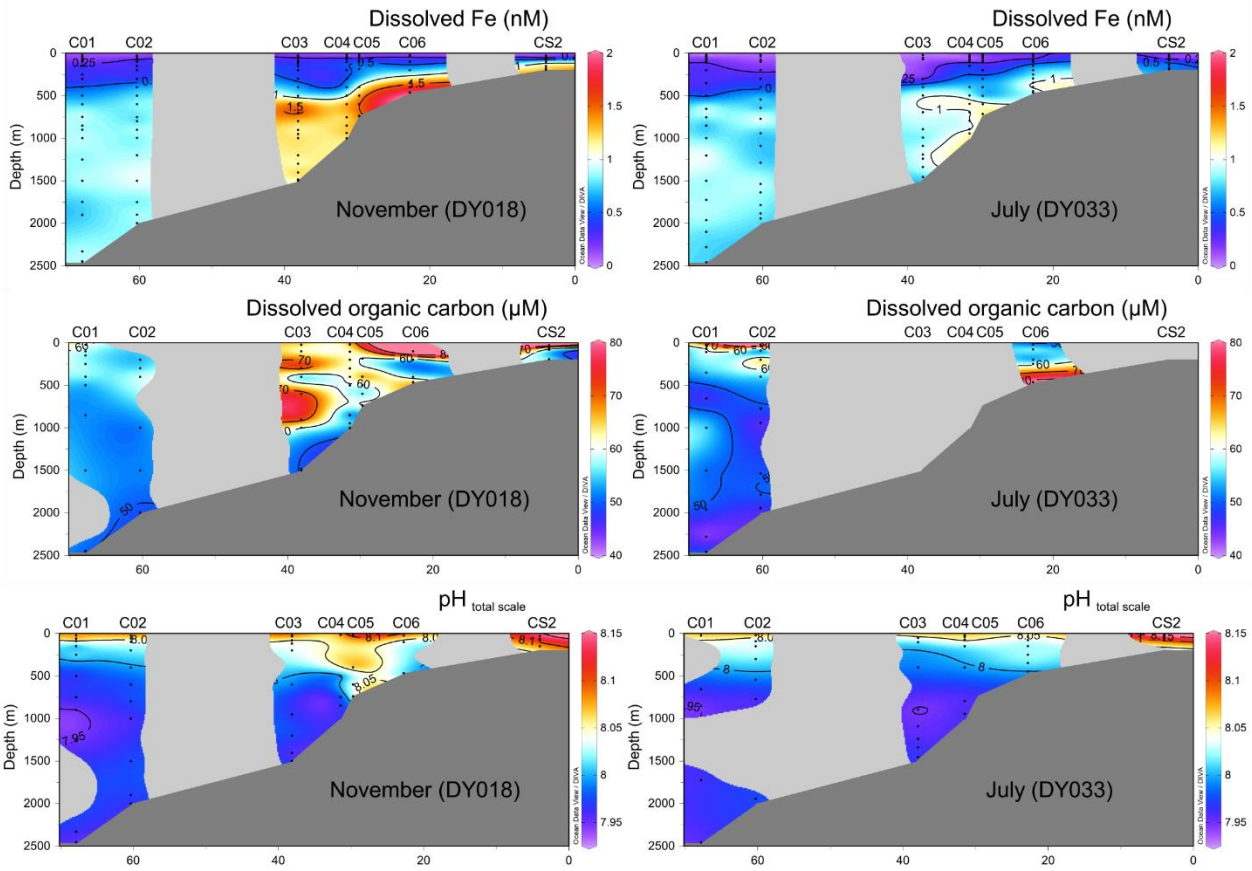

Figure 7. The distribution of dissolved Fe (DFe), dissolved organic carbon (DOC) , pH_{total} (on the total scale) during autumn (DY018, November 2014) and summer (DY033, July 2015) over the shelf break.

Surface waters in the area exhibited higher, relatively uniform pH (Figure 7). Higher surface water pH at C04-06 stations coincided with higher DOC in autumn, which suggest that both of these features were driven by increased productivity as observed at CCS. At depth (> 1000 m), changes in pH corresponded to changes in salinity and temperature and were thus likely influenced by water mass circulation and the biological carbon pump (Figure S5).

For both the ambient and constant DOC scenarios, $SFe(III)_{app}$ was >0.8 nmol L^{-1} in the deep ocean (>1500 m) at stations C01 and C02 in November and July (Figure 8). Mean $SFe(III)_{app}$ (0.96±0.08 and 0.88±0.08 nmol L^{-1} for the ambient and constant DOC scenarios respectively) was again remarkably close to the mean observed DFe concentrations (0.9±0.1 nmol L^{-1}). We emphasize here that the DFe concentration is not a parameter included in the calculations of $SFe(III)_{app}$, since the total Fe concentration is set to 10 nmol L^{-1} for all samples and our calculated $SFe(III)_{app}$ concentrations are thus independent of DFe. The potential impact of scaling to DOC concentration is

illustrated by increases in the difference between $SFe(III)_{app}$ calculated where ambient DOC concentrations were high (>70 µmol L^{-1}) relative to the assumed constant concentration scenario of 43.7 µmol L^{-1} at stations C03-CS2 in November or at station C06 in July (Figure 8). Nevertheless the difference between $SFe(III)_{app}$ calculated at constant DOC and ambient DOC was always less than 0.54 nmol $^{-1}$ (Figure 8) and scaling to DOC thus has a limited overall impact on determined $SFe(III)_{app}$.

In surface waters, DFe was consistently lower (<0.25 nmol L^{-1}) than $SFe(III)_{app}$ predicted using both DOC scenarios and Fe^{3+} was thus undersaturated with respect to $Fe(OH)_3(s)$ formation in our calculations (Figure 8), as observed for surface waters at CCS. The depth at which DFe became less than $SFe(III)_{app}$ shoaled with the DFe concentration (Figure 7 and 8). In waters close to the seafloor on the inner shelf (C03-C06), DFe concentrations were in excess of the $SFe(III)_{app}$ concentration. As described for station CCS and observed on the Peruvian Shelf (Zhu et al., 2021), we suggest that these waters were influenced by non-equilibrium processes. Our speciation calculations are considered to be at equilibrium and thus do not account for any non-equilibrium processes that may be occurring in the water column, such as remineralization, scavenging, inputs from sediments or changes in redox state. Our study region is known to experience inputs of DFe along with other metals in nepheloid layers that propagate offshore from the sediments over the shelf break (Laès et al., 2007; Rusiecka et al., 2018), and previous work found that the authigenic or scavenged fraction of particulate Fe becomes increasingly important close to the seafloor (Marsay et al., 2017). Such sediment-derived benthic inputs can be expected to be scavenged from the water column and adsorptive processes are likely to depend on particle concentrations (Bergquist and Boyle, 2006; Fitzsimmons et al., 2013; John et al., 2018). However, the mechanisms and processes governing scavenging in the ocean are poorly constrained (Boyd and Ellwood, 2010; Tagliabue et al., 2014) and scavenging rates are effectively treated as “free” parameters in biogeochemical models and thus tuned to achieve realistic Fe concentrations (Tagliabue et al., 2014). Our work confirms previous studies (Hiemstra and van Riemsdijk, 2006) suggesting that the solubility of Fe is an important constraint on the extent of Fe scavenging in the ocean.

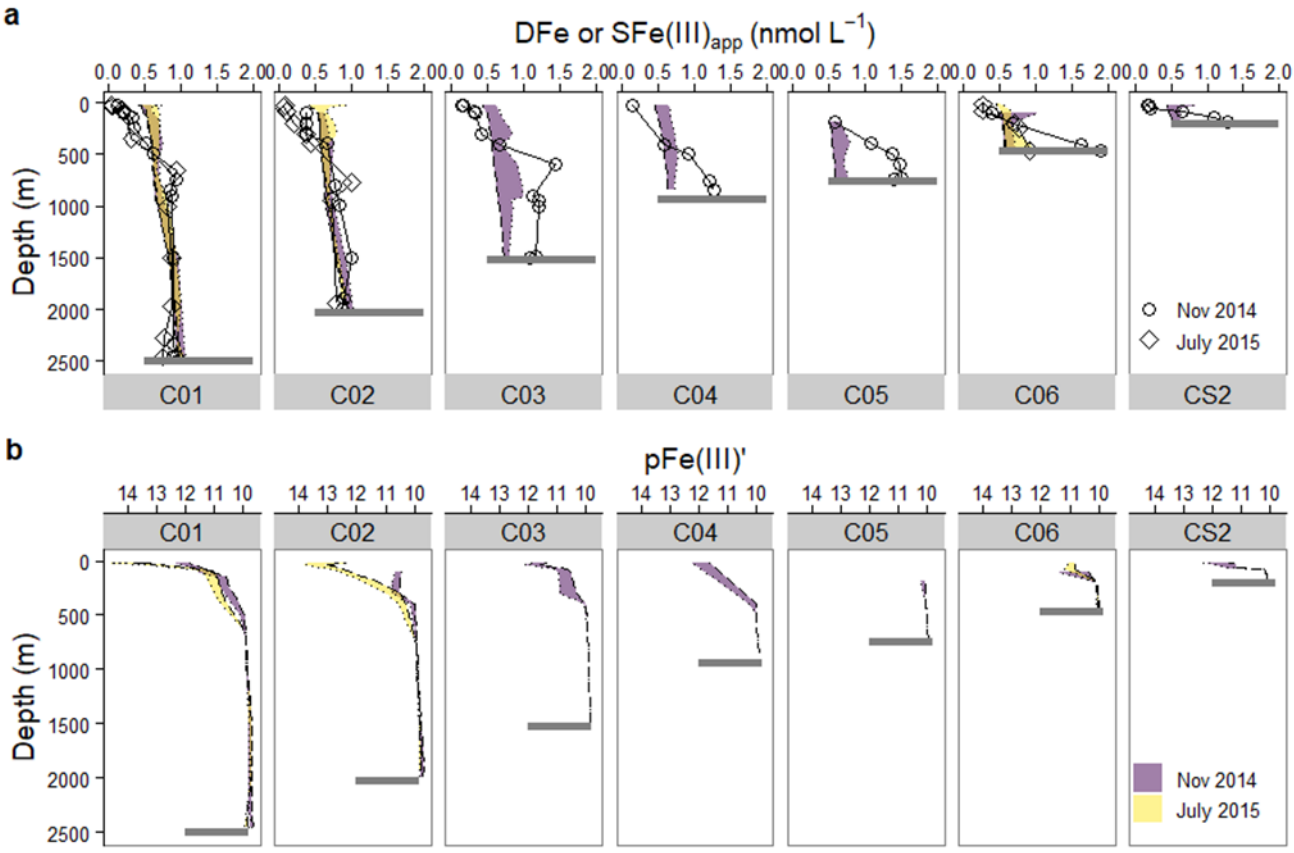

Figure 8. (a) Changes in the vertical distribution of calculated $SFe(III)_{app}$ using NICA parameter set D - observed dissolved Fe (<0.2 µm, point/diamond and solid line) are provided for reference. Lines show values calculated using a fixed DOC concentration of 43.7 µmol L^{-1} (long dashes) or ambient DOC concentration (dotted line) and the shaded area highlights the difference between the two scenarios. For calculation of $SFe(III)_{app}$, we assumed a total Fe(III) concentration of 10 nmol L^{-1} in our calculations and DFe was therefore not an input parameter in the calculations. (b) pFe(III)´ ($-\log_{10}(Fe(III))$) was calculated from DFe, or $SFe(III)_{app}$ when DFe > $SFe(III)_{app}$. Calculations applied the ambient pH and temperature for samples collected over the shelf break in autumn (November 2014) and summer (July 2015) seasons. DOC concentrations were not determined for C03-C05 and CS2 in July 2015. Grey bars show the depth of the water column at each station.

Calculated pFe(III)´ was lowest in deep waters and highest in surface waters indicating an increase in Fe(III)´ in deeper waters (Figure 8b, pFe(III)´ scale is reversed). Below ~500m, pFe(III)´ (10.04±0.02) was relatively constant throughout the water column in November and July and irrespective of the DOC scenario, largely because it is set by the solubility product of $Fe(OH)_3(s)$ in our calculations (i.e. pFe(III)´ □ $[Fe^{3+}]$ which in turn is limited by $Fe(OH)_3(s)$). In surface waters, when pFe(III)´ is dependent on the DFe concentration, pFe(III)´ increased towards the open ocean from a minimum of 10.8 (constant DOC) or 11 (ambient DOC) at C06 to a maximum of 13.2 (constant DOC) or 14.6 (ambient DOC) at C01 (Figure 8). For the stations furthest offshore, the

potential impact of scaling to DOC for calculation of pFe(III)′ was more important. For example, a 30 µmol L^{-1} increase in DOC resulted in an increase of two units in pFe(III)′ in surface waters at station C01. We found that values of pFe(III)′ predicted using parameter set D under both constant and variable DOC scenarios encompassed the range of values found to support both iron-replete and iron-limited growth in families of phytoplankton including cyanophytes, haptophytes and diatoms which have been observed in our study area (Blain et al., 2004). For example, reduction in growth of *Synechococcus* sp. was shown to begin at pFe′ values of 14 (Timmermans et al., 2005), close to the lowest values predicted by parameter set D with ambient DOC concentrations, while Sunda & Huntsman (1995) found onset of growth was limited at 20 pmol L^{-1} (pFe(III)′ = 10.7) for the small haptophyte *Emiliania huxleyi* and at 160 pmol L^{-1} (pFe(III)′ = 9.8) for the diatom *Thallassiosira weissflogii*. However, we have not considered the role of redox chemistry in our calculations. Fe(II) is known to be more readily available to phytoplankton (Shaked and Lis, 2012) and significant concentrations of Fe(II) can be formed via photochemical reduction in surface waters, with Fe(II) concentrations of up to 175 pmol L^{-1} previously reported for surface waters (<50 m) in this region (Ussher et al., 2007).

3.4 Conclusions

In this work, we combined analysis of Fe speciation by AdCSV with an ion-pairing/NICA-Donnan model to determine Fe(III) speciation at equilibrium in the Celtic Sea. We first calibrated our competing added ligand (HNN) in the absence of organic matter for the experimental conditions applied in our study. We then compared titration data obtained by varying both Fe concentrations and HNN concentrations with calculations of Fe speciation predicted via the NICA-Donnan model with four sets of parameters and found that the parameter sets that predicted relatively weak binding with low heterogeneity best described our titration data. We further found that fits improved on application of a constant low DOC concentration of 43.7 µmol L^{-1} across the data set, rather than assuming that binding scaled to ambient DOC concentrations. This suggests that binding sites may be more strongly linked to the refractory component of marine DOM and fresh inputs of DOM that result from phytoplankton productivity may not result in increased binding site concentration or heterogeneity.

We used the NICA-Donnan parameters that fitted most closely to our titration data to predict $SFe(III)_{app}$ and pFe(III)´ at ambient seawater pH and temperature with both ambient and fixed DOC concentrations. Calculated $SFe(III)_{app}$ concentrations (ca. 0.9 nmol L^{-1}) were within the range of the water column DFe concentrations observed on the shelf after winter mixing and also the furthest off-shore deep water DFe concentrations. In surface waters DFe concentrations were lower than $SFe(III)_{app}$ as result of the drawdown of DFe by phytoplankton. On the shelf in July and November and over the shelf break DFe exceeded $SFe(III)_{app}$ in deeper waters close to the seafloor, which could potentially be ascribed to inputs of DFe from remineralization and sediments. Although the proximity of our calculated $SFe(III)_{app}$ to the observed DFe concentrations is very encouraging, we highlight that our calculations are a simplification of the real system since we do not account for non-equilibrium processes, and the physical size of our $SFe(III)_{app}$ fraction may not map directly onto the DFe concentration. Comparing the fixed and ambient DOC scenarios suggests that scaling binding site concentrations to DOC concentrations has a limited overall impact on Fe speciation and the impact was mostly restricted to surface waters where DFe concentrations are lower than $SFe(III)_{app}$. Since $SFe(III)_{app}$ is controlled by the solubility of $Fe(OH)_3(s)$, relative changes in $SFe(III)_{app}$ will depend on both pH and temperature. In our study region, changes in temperature resulted in a potential 0.5 nmol L^{-1} change in $SFe(III)_{app}$, whilst the pH range observed in our study area was too limited to detect a strong pH effect.

We also calculated pFe(III)´ in our study region and predicted values between 10 and 14, a range which encompasses the range of pFe(III)´ shown to limit growth in phytoplankton. The lower limit on pFe(III)´ was set by the solubility of $Fe(OH)_3(s)$. The upper limit and changes in pFe(III)´ were strongly influenced by the DFe concentration, although DOC concentrations also had an impact if binding site concentrations are scaled to DOC. The limited pH range and low binding site heterogeneity meant that pH did not have a strong influence on pFe(III)´ in this study region.
We suggest that the use of intrinsic binding parameters for Fe binding to DOM has the potential to improve understanding of the influence of organic matter on Fe solubility at ambient pH and temperatures and allow for more confident disentangling of the different processes affecting the DFe inventory, although further work is required to refine NICA constants for Fe in seawater.
Furthermore, our results suggest it may be possible to further simplify calculations of Fe speciation in marine waters by assuming a constant binding site concentration, at least in waters remote from

terrestrial influences, although this finding should be confirmed in further work employing more sensitive analytical approaches for determination of Fe speciation than we applied in this study. A robust parameterization of the relationship between pH, DOC, temperature and DFe with respect to both Fe bioavailability and solubility also has the potential to provide for a more mechanistic description of Fe binding in global biogeochemical models.

Acknowledgement

The authors would like to thank Bert-Jan Groenenberg for his help with PEST-ORCHESTRA. We thank the captain and crew of the RSS Discovery. KZ was supported by a scholarship from the China Scholarship Council. The project was funded by the UK Natural Environment Research Council (NE/L501840/1 (A.B.), NE/K001779/1 (M.L., S.U., A.M.), NE/K002007/1 (N.C and C.M.), NE/K001973/1 (E.A. and M.G.) and the Helmholtz Association. The authors declare no competing financial interest. All data that supports the findings of this study have been submitted to the British Oceanography Data Centre. Raw titration data can be downloaded from dx.doi.org/10.17504/protocols.io.brc4m2yw.

Abbreviations

Terms	Description
$k^{cond}_{FeNN3,Fe',or\ Fe3+}$	Conditional stability constants describing the strength of a complex $FeNN_3$ relative to inorganic Fe concentration or free Fe^{3+} concentrations
$\alpha_{FeNN3,Fe',or\ Fe3+}$	Side reaction coefficient for $FeNN_3$ expressed relative to inorganic Fe concentration or free Fe^{3+} concentrations
$k^{cond}_{FeNN3,H+}$	Stability constants of HNN used in an ion pairing model, that would account for competition between NN^-, H^+, Fe^{3+} and OH^- at the ionic strengths and pH relevant to our study
Detection window	The detection window describes the range over which competition between NN^- and binding sites (L^-) can be detected. It is traditionally defined as ± 1 or 1.5 log units of $\alpha_{FeNN3,Fe'}$ (Van Den Berg et al., 1990)

$k^{cond}_{FeL,Fe'}$	Conditional stability constants describing the strength of a complex FeL relative to inorganic Fe concentration
$a_{FeL,Fe'}$	Side reaction coefficient for metal-natural ligand expressed relative to inorganic Fe concentration
$logK_{Fe(III)1\ or\ 2}$	The median value of distribution of binding affinity of Fe(III) binding to organic matter in the NICA-Donnan model
$n_{Fe(III)1\ or\ 2}$	The non-ideal constants describe the ratio of Fe(III) to binding sites
$[Fe^{3+}]_{titration}$	Free Fe concentrations determined in titrations
$[Fe^{3+}]_{cal}$	Free Fe concentrations calculated using an ion pairing model in the absence of organic matter
$[Fe^{3+}]_{NICA}$	Free Fe concentrations calculated using the NICA-Donnan model in the presence of organic matter
$DFe^*_{titration}$	The non-labile fraction of Fe determined in titrations (i.e. total Fe – $FeNN_3$)
DFe^*_{NICA}	The non-labile fraction of Fe calculated using the NICA-Donnan model in the presence of organic matter (i.e. total Fe – $FeNN_3$)

Supplementary Material

Pages: 8

Figures: 5

Tables: 1

Methodology for titration experiments

Titrations were carried out using a static mercury drop electrode (Metrohm, 663 VA stand), a saturated Ag/AgCl (in 3 M KCl) reference electrode and a glassy carbon counter electrode controlled by a potentiostat (µAutolab, Metrohm) via NOVA 2.0 software (Metrohm). For samples collected on Cruise DY029 we used an integrated autosampler (Model 858, Metrohm) to deliver titration aliquots to the FEP voltammetric cell. Titration aliquots were equilibrated in pre-conditioned 50 mL centrifuge tubes (FEP, Nalgene) which fitted directly into the autosampler. Vials were preconditioned using aged trace metal clean seawater and rinsed with high purity water (18.2 MΩ cm^{-1}, Milli-Q, Millipore) between titrations. The use of the autosampler required 15 mL sample volume (10 mL was added to the cell, the remaining solution was used for rinsing the tubing or remains in the vial), and thus 15 titration points in total. For analysis of samples from DY033 and DY018, we increased the number of titration points to nineteen × 10 mL, which meant that we could not use the autosampler. Equilibration was undertaken in the same vials and aliquots were directly added to the volatmmetric cell. Titration experiments started with cruise DY029, and ended with DY018. For DY033 and DY018 the sequence of Fe additions was 0, 0, 0.4, 0.4, 0.8, 0.8, 1.5, 1.5, 2, 2, 3, 3, 4, 4, 5, 5, 5, 10, 15 nmol L^{-1}. The concentration of $FeNN_3$ was determined after de-aeration of the sample with nitrogen gas (240 s). A deposition potential at -0.15 V was used with deposition time of 240 s. The scanning mode was sample-DC from -0.35 V to 0.80 V at a scan rate of 50 mV s^{-1}, the reduction peak of $FeNN_3$ appeared at approximately -0.46 V.

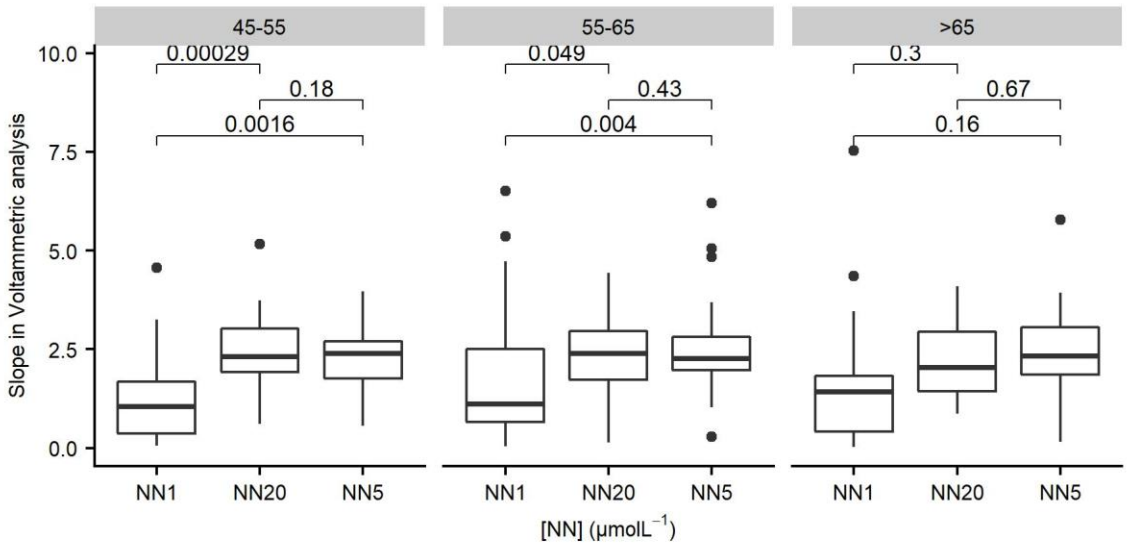

Supplementary Figure S1. Slopes observed for linear parts of the titrations (Fe additions > 2 nmol L^{-1}) at different HNN concentrations, binned according to DOC concentrations. Numbers in the plots refer to values for *p* obtained from a t-test used to estimate the impact of HNN concentration on slope.

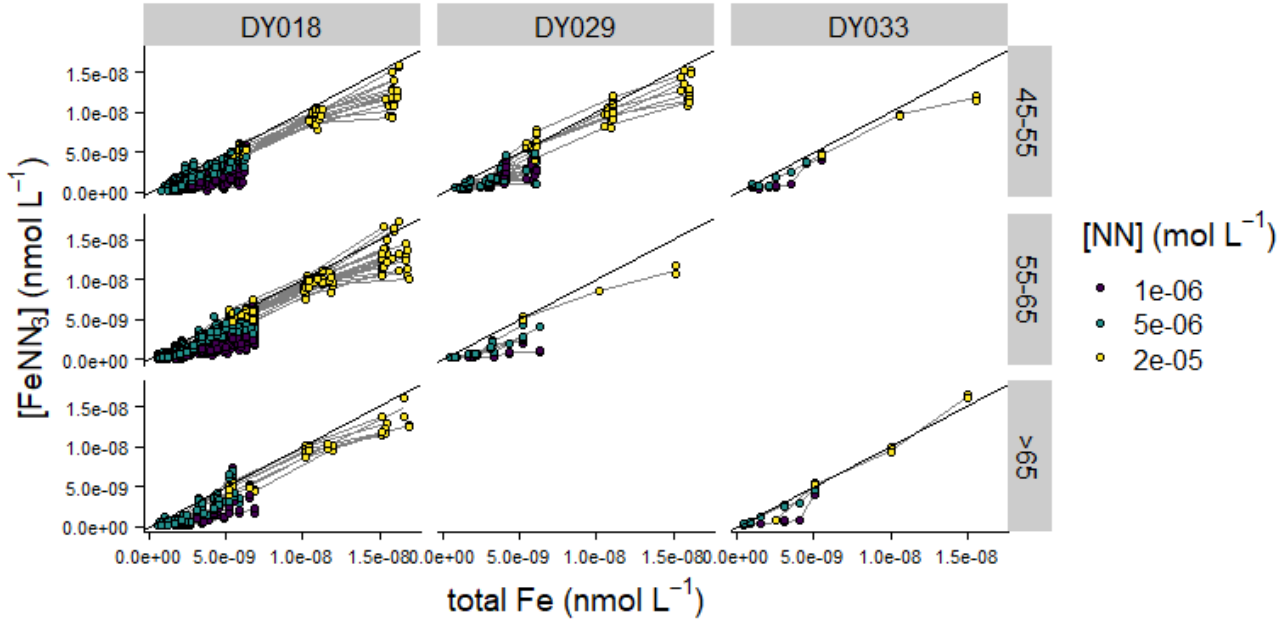

Supplementary Figure S2. Titration data plotted as measured $FeNN_3$ concentrations as a function of total Fe and binned according to DOC concentration. The solid line is a slope=1, intercept =0.

Supplementary Table 1. Comparison of literature values of conditional stability constant logK^{cond}_{FeNN3} with those calculations in the study at the same pH_{NBS}. The competing ligand used for the calibration is given in Column 1. A key factor influencing the discrepancy in the data is likely ionic strength. Ion pair models underestimate the activity of ions at high ionic strength, which leads to a lower estimated ionic strength in the ion pair model (e.g. I = 0.59 M calculate in ORCHESTRA at S=35), compared to that of seawater (I =0.7 M) assumed when K^{cond}_{FeEDTA} and logα'_{Fe} are calculated directly from intrinsic stability constants, even if the same ionic strength correction algorithm (e.g. the extended Debye Hückel or Davies equation) is applied in the calculations.

Competing ligand	pH_{NBS}	K^{cond}_{FeNN3} reported in the study	logα'_{Fe} reported in the study	K^{cond}_{FeEDTA} reported in the study	logα'_{Fe} calculated in this study at the same pH_{NBS}	Calculated K^{cond}_{FeNN3} at the same pH_{NBS}	Reference
Hydroxide	8.05	5.12×10^{26}	9.8	-	9.08	1.3×10^{27}	Hawkes et al. (2013)
EDTA	8.07	2.51×10^{28}	10	16.7	9.12	1.4×10^{27}	van den Berg (1995)
EDTA	6.9	6.31×10^{27}	8.3	16.7	6.69	8.3×10^{24}	Wu and Luther. (1995)
EDTA	6.9	3.16×10^{28}	8.45	16.34	6.69	8.3×10^{24}	Gledhill and van den Berg (1994)

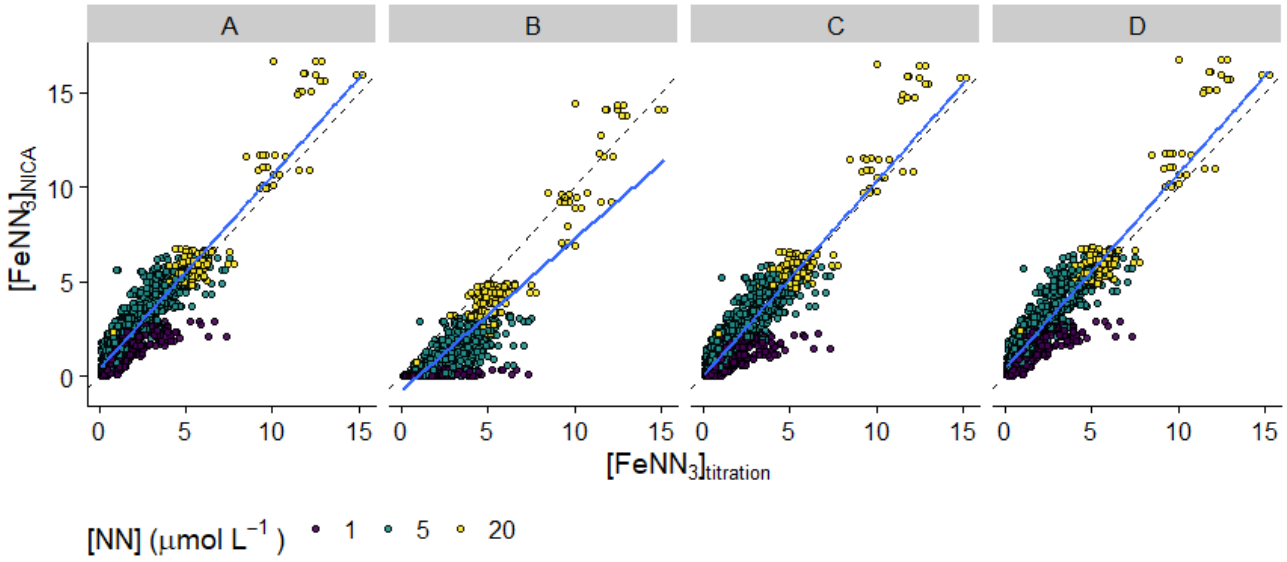

Supplementary Figure S3. Comparison of experimentally determined versus simulated $FeNN_3$ concentrations for titrations undertaken on seawater samples collected from the Celtic Sea. Determined $FeNN_3$ concentrations were obtained at three different HNN concentrations: 1 µmol L^{-1} (dark circles), 5 µmol L^{-1} (green circles) and 20 µmol L^{-1} (yellow circles). Simulated $FeNN_3$ concentrations were predicted using a combined ion-pair/NICA-Donnan model within the computer program ORCHESTRA. Four different NICA parameter sets were applied: parameter set A from Hiemstra and van Riemsdijk, (2006), B from Gledhill et al. (2015), and C and D rederived for this study based on titrations data taken from Avendaño et al. (2016). The solid blue lines are the fitted linear curve between experimental $FeNN_3$ and simulated $FeNN_3$ concentrations, while the dashed dark line represents a slope=1.

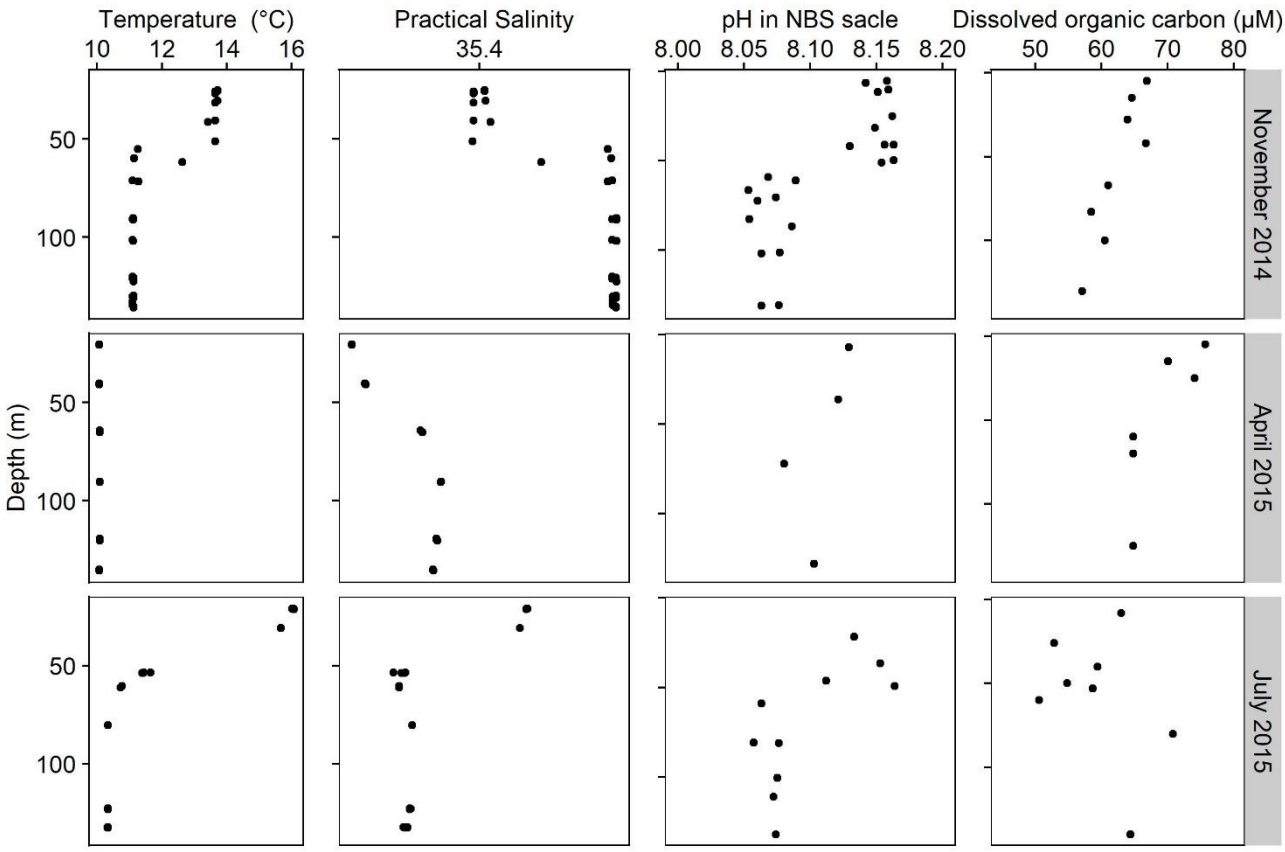

Supplementary Figure S4. Seasonal variation of temperature, salinity, pH and dissolved organic carbon (DOC) concentrations during autumn (November 2014), spring (April 2015) and summer (July 2015) at the shelf sea site (CCS).

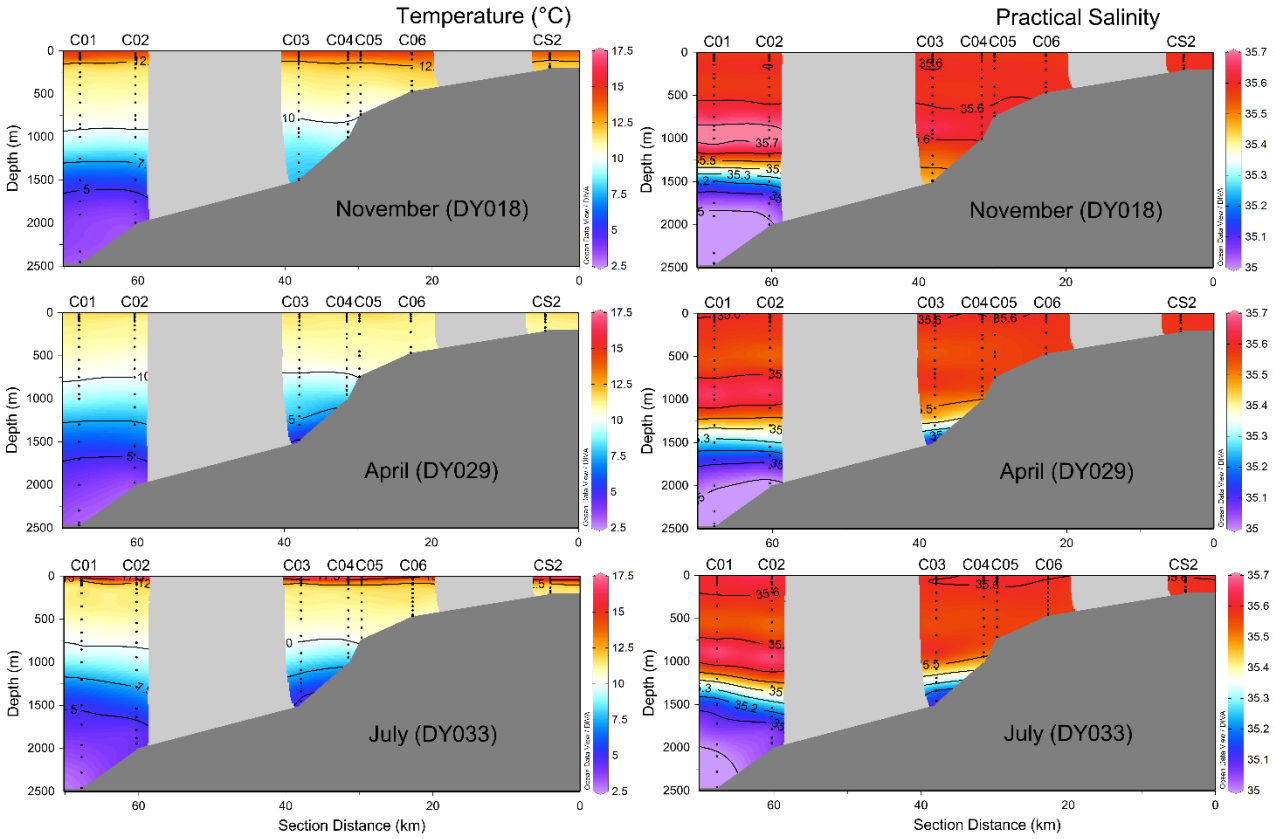

Supplementary Figure S5. Seasonal variation of temperature and salinity during autumn (November 2014), spring (April 2015) and summer (July 2015) at the shelf edge (CS2) and over the canyon transect stations (C01-C06).

4 Influence of pH and dissolved organic matter on iron speciation and apparent iron solubility in the Peruvian shelf and slope region

Kechen Zhu[*1], Mark J. Hopwood[1], Jan E. Groenenberg[2], Anja Engel[1], Eric P. Achterberg[1] and Martha Gledhill[1]*

[1] GEOMAR Helmholtz Center for Ocean Research Kiel, Wischhofstr. 1-3, 24148 Kiel, Germany

[2] Wageningen University, Department of Environmental Sciences, PO Box 47, 6700 AA Wageningen, The Netherlands

Submitted to Environmental Science & Technology

Under review

Abstract

The chemical speciation of iron (Fe) in the ocean is influenced by ambient pH and dissolved oxygen, and concentrations and strengths of binding sites of dissolved organic matter (DOM). We derived new NICA constants for Fe(III) binding to marine DOM via pH-Fe titrations. We used the constants to calculate Fe(III) speciation and derive the apparent Fe(III) solubility ($SFe(III)_{app}$) in the ambient water column across the Peruvian shelf and slope region. We define $SFe(III)_{app}$ as the sum of aqueous inorganic Fe(III) species and Fe(III) bound to DOM at a free Fe (Fe^{3+}) concentration equal to the limiting solubility of Fe hydroxide ($Fe(OH)_3(s)$). We predicted a ca. 2 fold increase in $SFe(III)_{app}$ in the oxygen minimum zone (OMZ) compared to surface waters. The increase results from a one order of magnitude decrease in H^+ concentration which impacts both Fe(III) hydroxide solubility and organic complexation. A correlation matrix suggests changes in pH have a larger impact on $SFe(III)_{app}$ and Fe(III) speciation than DOM in this region. Using Fe(II) measurements, we calculated ambient DFe(III) and compared this to predicted $SFe(III)_{app}$. The underlying distribution of ambient DFe(III) largely reflected the predicted $SFe(III)_{app}$ indicating decreased pH as a result of OMZ intensification and ocean acidification may increase $SFe(III)_{app}$ with potential impacts on surface DFe inventories.

Keywords: trace metal, ocean deoxygenation, Fe(II), humic substance, PEST, ORCHESTRA, biogeochemical cycling

4.1 Introduction

The Peruvian upwelling region comprises the largest oxygen minimum zone (OMZ) (i.e. dissolved oxygen (DO) <20 µmol L^{-1} at 100-1000 m) (Karstensen et al., 2008) in the world's ocean. Upwelled waters along the Peruvian coastline are known to act as a significant source of Fe along with other nutrients (e.g. N, P, Si) to surface waters (Carr and Kearns, 2003; Noffke et al., 2012). Previous work has shown that enhanced dissolved Fe (DFe) observed in bottom waters on the shelf and slope is primarily related to suboxic sedimentary inputs (Hong and Kester, 1986; Bruland et al., 2005; Vedamati et al., 2014; Rapp et al., 2020) due to exceptionally high benthic Fe fluxes in the region (Scholz et al., 2011, 2014). Whilst benthic Fe supply along the Peruvian shelf is clearly high in a global context, Fe limitation of primary productivity in proximal open ocean surface waters (Hutchins et al., 2002; Browning et al., 2017, 2018) suggests that a short residence time of any Fe supplied by benthic sources in the inner shelf may have limited impact on primary producers further offshore. This raises important questions about the mechanisms restricting the transport of Fe from OMZs to offshore surface waters and how this transport will respond to perturbations such as OMZ expansion and ocean acidification (Stramma et al., 2008b).

In oxic surface waters, Fe has a short residence time (e.g. hours (Scholz et al., 2016; Croot et al., 2019) to a few days to weeks (Croot et al., 2004b)) since Fe(III), the thermodynamically favored Fe form, is hydrolyzed and rapidly scavenged and precipitated, and thereby removed from solution (Boyd and Ellwood, 2010). Complexation by dissolved organic matter (DOM), which occurs predominantly in the <0.02 µm size fraction (Cullen et al., 2006; Boye et al., 2010; Fitzsimmons et al., 2015) reduces the concentration of free Fe^{3+}, and thus effectively reduces hydrolysis of Fe(III) and the formation of insoluble iron hydroxides ($Fe(OH)_3(s)$). One important consequence of Fe complexed by organic matter is thus an increase in the apparent solubility of Fe(III) ($SFe(III)_{app}$) in seawater, with $SFe(III)_{app}$ defined as the sum of aqueous inorganic Fe(III) species and Fe(III) bound to DOM at a free Fe (Fe^{3+}) concentration equal to the limiting solubility of Fe hydroxide ($Fe(OH)_3(s)$). Organic Fe(III) complexation thus plays a key role in determining the overall DFe inventory and residence time in the surface ocean (Kuma et al., 1996; Liu and Millero, 2002; Hiemstra and van Riemsdijk, 2006). A potential control on offshore Fe transport from the Peruvian upwelling region is thus the capacity for organic Fe(III) complexation to mitigate against

DFe scavenging and precipitation (Liu and Millero, 2002; Hiemstra and van Riemsdijk, 2006). A transient, minor fraction of DFe in oxic waters also exists as Fe(II) mainly due to photochemical reduction (Barbeau, 2006). This fraction also increases under suboxic conditions, with Fe(II) dominating DFe speciation close to sediments within OMZs (Hong and Kester, 1986; Vedamati et al., 2014; Schlosser et al., 2018).

The upwelling of nutrient rich deep waters off Peru results in enhanced primary productivity and dissolved organic carbon (DOC) concentrations in surface waters, with remineralization of sinking biogenic particles leading to oxygen depletion and reduced pH values. The OMZ is significantly more acidic (pH 7.5 on the total scale (Paulmier and Ruiz-Pino, 2009)) than surface waters (pH 8.1, total scale (Caldeira and Wickett, 2003)), whilst DOC varies from concentrations below 50 µmol L^{-1} in the OMZ to more than 120 µmol L^{-1} in surface waters (Loginova et al., 2016). Furthermore, acidification resulting from oceanic uptake of anthropogenic atmospheric CO_2 is more acute in upwelling regions since the upwelling process takes CO_2-rich intermediate water to the ocean surface with a consequent lowering of the buffering capacity (Feely et al., 2008, 2018; Osborne et al., 2019). A thorough investigation of Fe speciation and its influence on Fe biogeochemistry in the Peruvian coastal region should therefore account for variations in chemical Fe speciation driven by pH, DO and DOC.

The marine Fe(III)-binding ligand pool is known to be heterogeneous (Gledhill and Buck, 2012), and includes compounds that have properties similar to humic and fulvic acids (Laglera et al., 2007; Laglera and van den Berg, 2009; Muller, 2018) but also microbially produced siderophores (Mawji et al., 2008; Boiteau et al., 2016; Bundy et al., 2018). Whilst siderophores are very strong ligands, they are generally present at very low concentrations (<20 pmol L^{-1}) (Mawji et al., 2008; Boiteau et al., 2016; Bundy et al., 2018). Heterogeneous humic-like materials, have a weaker Fe binding strength, yet appear to be more widely distributed (Muller, 2018). These different pools of Fe binding ligands will exhibit different Fe binding affinities as a function of pH, which can be described by intrinsic Fe and proton binding constants (Millero et al., 2009; Gledhill et al., 2015; Zhang et al., 2019). Such competitive interactions can be accounted for via application of metal-binding models, e.g. the Non-ideal Competitive Adsorption (NICA) model (Kinniburgh et al., 1999) or Windermere humic acid model (WHAM) (Tipping et al., 2011), which have been

developed to describe interactions between cations and complex heterogeneous mixtures of binding sites in natural waters, and have been shown to be broadly comparable (Christensen et al., 1998; Dudal and Gérard, 2004). Recent work has shown that the proton binding behaviour of DOM derived from the brackish Baltic Sea can be described using the NICA-Donnan model (Lodeiro et al., 2020) and that this model is also consistent with Fe speciation measurements typically undertaken in seawater (Hiemstra and van Riemsdijk, 2006; Avendaño et al., 2016; Gledhill and Gerringa, 2017). Briefly, the NICA model describes the binding behaviour of metal ions to a heterogeneous mix of binding sites with varying binding strengths using a continuous bimodal distribution representing carboxylic-like groups and phenolic-like groups (here called DOM1 and DOM2, respectively), based on the Langmuir-Freundlich adsorption isotherm (Kinniburgh et al., 1999). The NICA model contains three key parameters, the median value ($\log K$), and width (p) of the distribution of binding affinity, and the non-ideal constants (n) that describe the ratio of ions to binding sites. The NICA model accounts for the impact of pH and DOC concentrations on metal-binding, allowing Fe speciation to be predicted for ambient conditions in the water column. The NICA model is combined with the Donnan model to describe electrostatic interactions; however the high ionic strength of seawater (I=0.72) reduces the volume of the Donnan phase which can then be neglected (Town and Van Leeuwen, 2016; Town et al., 2019; Pinheiro et al., 2021).

In this study, we aim to build a comprehensive picture of DFe speciation in the Peru upwelling region and assess implications for Fe biogeochemistry via determinations of Fe(II) concentrations and calculations of equilibrium Fe(III) speciation using the NICA-Donnan model under ambient conditions of pH, temperature and DOC. We applied a novel experimental design, varying pH and Fe concentrations, in titrations undertaken on samples collected on the Peruvian shelf and slope. We used the titration data to derive new intrinsic NICA constants for Fe(III) binding to marine DOM using the total proton-binding site concentrations determined for marine DOM ($Q_{max,H^+,DOM1}$ and $Q_{max,H^+,DOM2}$) (Lodeiro et al., 2020) in combination with the parameter estimation program PEST and speciation calculation software ORCHESTRA (Janot et al., 2017). We then applied our derived constants to calculate $SFe(III)_{app}$ and DFe(III) speciation at equilibrium across the Peruvian shelf and slope. We interpret our calculated equilibrium speciation within the context of observed changes in pH, DOC, DFe, and DFe(III) concentrations.

4.2 Materials and Methods

Samples were collected during RV METEOR cruise M136 (11 April - 3 May 2017) on the Peruvian shelf and slope. Samples from four stations (No. 54, 56, 58 and 66) were used for NICA constant derivations (Figure 1, panel a). Depth, temperature, salinity and DO were measured using Seabird CTD sensors attached to a powder-coated aluminum GEOTRACES compliant rosette system (Seabird) equipped with 24 x 12 L Ocean Test Equipment samplers. Sampling protocols and methods for determining DFe (Rapp et al., 2017), Fe(II) (Croot and Laan, 2002; Hopwood et al., 2017), DOC (Engel and Galgani, 2016) and pH (Dickson, 2010) have been described in detail elsewhere and are provided in the Supporting Information (SI).

Briefly, DFe samples were collected in acid-cleaned low-density polyethylene bottles (Nalgene) via filtration (0.8/0.2-µm AcroPak 500 cartridge filters) following GEOTRACES protocols (Cutter et al., 2017), acidified at sea to pH ~1.9 (adding 150 µl HCl (OPTIMAL grade, Fisher Scientific) per 125 ml sample) and determined >6 months later via inductively coupled plasma mass spectrometry after pre-concentration using a cation chelating resin on an automated SEAFAST system as per Rapp et al. (Rapp et al., 2017). The detection limit for Fe was 100 pmol L^{-1}. Samples for Fe(II) were collected unfiltered in acid-cleaned opaque high density polyethylene bottles (Nalgene) which were filled to overflowing and analyzed onboard via flow injection analysis using luminol chemiluminescence without preconcentration (Croot and Laan, 2002; Hopwood et al., 2017). Calibration via standard addition was conducted for each station on the day of sample analysis from at least four standard additions made to water from a mid-depth sample immediately after analysis of all Fe(II) samples for each station (total analysis time per station ~4 hours). The detection limit was ~200 pmol L^{-1}. Samples for DOC were collected after filtration with combusted GF/F filters (0.7-µm, Whatman), acidified with 80 µl of 85% phosphoric acid per 20 ml and stored at 4 °C in the dark, with analysis via Shimadzu TOC-VCPN following standard protocols (Engel and Galgani, 2016). Consensus reference materials (University of Miami) were used to determine accuracy and precision of analysis. The detection limit was 1 µmol L^{-1} C. Samples for dissolved inorganic carbon (C_T) and total alkalinity (A_T) were collected via silicone tubing into 250 ml borosilicate glass bottles following internationally established protocol (Dickson, 2010), and

stored in the dark until analysis with VINDTA 3C instruments (Marianda, Germany). The 1σ measurement precision was 2.74 µmol kg^{-1} for C_T and 0.45 µmol kg^{-1} for A_T.

pH expression on IUPAC and total scales

The pH of our seawater samples was calculated on the IUPAC/NBS scale (pH_{NBS}) from C_T and A_T using CO2SYS (Pierrot et al., 2006), a speciation model specific for seawater. We used the NBS pH scale because it is consistent with the NIST based speciation constants used in ORCHESTRA. We also used the total pH scale (pH_{tot}) to report the seawater carbonate chemistry. For CO2SYS, we used constants from Mehrbach et al. (Mehrbach et al., 1973) as refitted by Dickson and Millero (Dickson and Millero, 1987) and Dickson (Dickson, 1990) to describe the carbonate and sulphate equilibrium with hydrogen ions, and from Uppström (Uppström, 1974) to account for boron.

Determination of Fe(III) speciation via adsorptive cathodic stripping voltammetry

A pre-requisite for the derivation of Fe(III) NICA constants is to incorporate changes in pH in the experimental design. Therefore, we applied a two dimensional pH-Fe experimental design for titration experiments, using competitive ligand equilibrium with adsorptive cathodic stripping voltammetry (CLE-AdCSV) as the detection method. Fe(III) speciation was determined by CLE-AdCSV at room temperature (20 °C), using 1-nitroso-2-naphthol (HNN) as the added ligand (Gledhill and van den Berg, 1994) after a 16 h equilibrium period (Boye et al., 2001). The CLE-AdCSV method has been widely applied in seawater (Hunter, 2005; Laglera and van den Berg, 2009; Gledhill and Buck, 2012), and the limit of detection is 0.13 nM Fe when using HNN (Ardiningsih et al., 2021). We used a single window titration ($[HNN]$=2 µmol L^{-1}) with six different pH_{NBS} values (7.0, 7.3, 7.6, 7.9, 8.2, 8.5) and five different Fe concentrations (0, 0.5, 1.5, 5, 7.5, 10 nmol L^{-1}) for each pH_{NBS} value, resulting in a two dimensional pH-Fe titration matrix with a total of 30 titration data points per sample (an example titration is shown in Figure S1 in SI). We observed no significant difference in voltammetric sensitivity over the pH_{NBS} range 7.0-8.5 in seawater that had been irradiated with ultra violet light to remove DOM (Figure S2). For

our samples, we used the sensitivity determined at pH_{NBS} 7.9 to calculate the $FeNN_3$ concentration at each pH.

1-nitroso-2-naphthol (HNN; Sigma-Aldrich grade) was diluted in methanol (Fisher, HPLC grade) to make the stock solution of HNN (10 mmol L^{-1}). Piperazine-1,4-bis(2-hydroxypropanesulfonic acid) (POPSO; Sigma-Aldrich) was used to buffer the pH of samples in this work, since POPSO buffers over the pH_{NBS} range 7.2-8.5, which is close to the complete pH_{NBS} range applied in our study. To clean the stock buffer solution (POPSO, 0.5 mol L^{-1}), HNN(final concentration, 10 µmol L^{-1}) was equilibrated with the buffer solution overnight. HNN and $FeNN_3$ were subsequently removed using a pre-activated C18 SepPak column (Whatman) (Avendaño et al., 2016). The pH of the buffer solution was adjusted with ammonium hydroxide (20-22%, Optima, Fisher Scientific). pH_{NBS} was determined post titration for each titration point using a pH-meter (inoLab® pH 720, WTW).

Application of the NICA-Donnan model within the speciation program ORCHESTRA

A key assumption of the approach is that the bulk properties of marine DOM can be represented by a limited number of binding site coefficients that describe intrinsic affinities between cations and different types or groups of binding sites. Furthermore, it is assumed that both groups of marine DOM binding sites (i.e. via the NICA-Donnan model) scale proportionally with DOC. To date, there have been only a few derivations of NICA parameters for marine DOM. Available Fe(III) NICA constants for waters with salinities over 30 have been derived from solubility experiments undertaken in oligotrophic open ocean water from the Sargasso Sea (Liu and Millero, 1999, 2002; Hiemstra and van Riemsdijk, 2006), or empirically from titration experiments on samples from an estuary and a temperate shelf environment (Gledhill et al., 2015; Avendaño et al., 2016). The NICA-Donnan model scales metal binding to DOC concentrations via knowledge of the number moles of binding sites per kg of DOM ($Q_{max,H^+,DOM1}$ and $Q_{max,H^+,DOM2}$). Marine DOM has been shown to have a lower total amount of available proton binding sites (i.e. $Q_{max,H^+,DOM}$) within both the carboxylic and phenolic fractions (Lodeiro et al., 2020) in comparison to generic fulvic acid (Milne et al., 2001). We applied a value of 4.07×10^{-8} kg (DOM)/µmol (C) (Lodeiro et al., 2020) to convert the concentration of DOC (µmol L^{-1}) to DOM (kg L^{-1}) and values of 2.52 mol

/kg for DOM1 and 0.80 mol /kg for DOM2, for the concentration of each group of binding sites (Lodeiro et al., 2020). These values were combined with generic fulvic acid constants (Milne et al., 2001, 2003) for the remaining NICA-Donnan constants (all constants are shown in Table S2 in SI).

We provide full details of our procedure and the original code in an online protocol (DOI: dx.doi.org/10.17504/protocols.io.brc4m2yw). Speciation calculations in ORCHESTRA incorporate pH, DOC, temperature, Fe(III) and major ions of seawater (Na^+, K^+, Mg^{2+}, Ca^{2+}, Sr^{2+}, Cl^-, SO_4^{2-}, CO_3^{2-}, Br^-, B^{3+}, F^-) with molarities calculated from salinity and pressure. For inorganic ions, ionic strength corrections were made via the Davis equation (i.e. extended Debye-Hückel equation) within ORCHESTRA. Seawater ionic strength (I=0.72) is at the upper limit of the valid range of this correction method, which likely results in a systematic offset for ions with higher charge (e.g. 20% underestimation for the activity of the carbonate anion (Gledhill et al., 2015)). Stability constants for inorganic complexes were taken from the NIST database (Smith et al., 2004), whilst marine DOM was described using the NICA-Donnan model (Laglera and van den Berg, 2009; Gledhill et al., 2015; Muller, 2018). The impact of temperature on the inorganic complexes is calculated using the van't Hoff equation.

Derivation of Fe(III) NICA constants ($\log K_{Fe(III)DOM1,2}$ and $n_{Fe(III)DOM1,2}$) via PEST-ORCHESTRA

We used PEST-ORCHESTRA to derive the NICA binding affinity constants ($\log K_{Fe(III)DOM1}$, $\log K_{Fe(III)DOM2}$) and non-ideality constants ($n_{Fe(III)DOM1}$, $n_{Fe(III)DOM2}$) for Fe(III) binding to the carboxylic-like (DOM1) and phenolic-like (DOM2) binding sites of marine DOM. To derive the constants, we simulated the pH-Fe titration with assumed initial values for $logK_{Fe(III)DOM1}$, $logK_{Fe(III)DOM2}$, $n_{Fe(III)DOM1}$ and $n_{Fe(III)DOM2}$ and defined a range for their variability within ORCHESTRA. The simulated pH-Fe titration was then passed to PEST and Fe(III) NICA constants estimated iteratively to obtain the lowest sum of squared residuals between experimental and modelled $FeNN_3$ via a Levenberg-Marquardt algorithm. PEST adjusted the fitted constants in a step wise manner within the provided range and passed the new constants back to ORCHESTRA to complete the estimation loop. The procedure is repeated multiple times (n>10) with a range of

initial guesses and ranges until a given set of initial values produced a reproducible solution. We chose the solution with the lowest root mean square errors. We used the same approach to firstly derive the stability constant for $\log k_{FeNN3,H+}$ used in ORCHESTRA from titrations undertaken in UV-irradiated seawater (Details in SI).

Calculations of ambient dissolved Fe(III) speciation and apparent Fe(III) solubility using the NICA-Donnan model via ORCHESTRA

Derived Fe(III) NICA constants from our seawater samples were then used to calculate DFe(III) speciation in the ambient water column (pH_{NBS}, temperature, and DOC) across the Peruvian shelf and slope. We derived the apparent Fe(III) solubility ($SFe(III)_{app}$) by setting total Fe(III) concentrations to 10 nmol L^{-1} in each sample. This will result in precipitation of $Fe(OH)_3(s)$ (as ferrihydrite in our calculations) following Liu and Millero (Liu and Millero, 1999). Ferrihydrite formation was calculated using the solubility product ($\log K_{so}$ = 3.2) to determine iron solubility according to equation (1).

$$K_{so} = \frac{[Fe^{3+}]}{[H^+]^3} = 10^{3.2}, \Delta H_r = -100.4\ kJ\ mol^{-1} \quad (1)$$

The $SFe(III)_{app}$ is thus defined as the sum of aqueous and organic Fe species (equation 2) formed at an Fe^{3+} concentration equal to the limiting solubility of Fe hydroxide.

$$SFe(III)_{app} = \sum Fe(OH)_i^{3-i} + Fe(III)DOM \quad (2)$$

where Fe(III)DOM is the total concentration of Fe bound to DOM calculated using the NICA-Donnan model, and $\sum Fe(OH)_i^{3-i}$ is the sum of inorganic Fe complexes. The assumed total Fe concentrations of 10 nmol L^{-1} for the calculation of $SFe(III)_{app}$, means that neither DFe nor DFe(III) is an input term in our calculations and $SFe(III)_{app}$ is independent of observed DFe concentrations. Our approach does not account for the effects of pressure, which can also be expected to affect metal solubility (Moore and Millward, 1984).

4.3 Results and Discussion

4.3.1 Derivation of Fe(III) NICA constants ($\log K_{Fe(III)DOM1,2}$ and $n_{Fe(III)DOM1,2}$) for the Peruvian shelf and slope region

A total of 32 pH-Fe titrations were completed in this study and we derived one general set of Fe(III) NICA constants for the Peruvian shelf and slope region (Table 1). Results showing measured and predicted $FeNN_3$ concentrations and Fe bound to DOM are given in the SI (Figure S3).

For DOM1, the binding affinity ($\log K_{Fe(III)DOM1}$, with respect to Fe^{3+}) is lower than the value derived by Avendaño et al. (Avendaño et al., 2016), while higher than the value reported by Hiemstra and van Riemsdijk (Hiemstra and van Riemsdijk, 2006) (Table 1). For DOM2, the binding affinity ($\log K_{Fe(III)DOM2}$) is higher than that derived by Avendaño et al. (Avendaño et al., 2016) and Hiemstra and van Riemsdijk (Hiemstra and van Riemsdijk, 2006). The results indicate that organic matter in the Peruvian coastal region has a different Fe binding affinity from either oligotrophic open ocean water of the Sargasso Sea (Hiemstra and van Riemsdijk, 2006), or the shelf waters in the north east Atlantic (Avendaño et al., 2016). DOM in the Celtic Sea is likely more strongly influenced by terrestrially-derived organic matter (Carr et al., 2019), while DOM in the Peruvian coastal regime (Loginova et al., 2016, 2019) originates predominantly from autochthonous primary production. Furthermore, intense mineralization of organic matter, which can also generate dissolved organic ligands for Fe(III)-binding below the euphotic zone (Witter et al., 2000; Gerringa et al., 2006) could lead to differences in binding affinities between the Sargasso Sea and Peru coastal regime (Carlson et al., 2004). Our results also showed that the non-ideal constants (n) were higher than those reported in previous work, which suggests that binding sites in marine DOM are closer to ideal (n=1) and less heterogeneous than the literature values (Hiemstra and van Riemsdijk, 2006; Avendaño et al., 2016), consistent with recently derived proton binding constants for marine DOM (Lodeiro et al., 2020).

We point out that there are additional uncertainties with our derived constants. The pH range used in our titrations is limited in extent, a factor which is constrained by the pH range over which CLE-AdCSV method can usefully be applied. Furthermore the total binding site concentrations for marine DOM used in this study were derived from DOM isolated from brackish waters of the Baltic Sea and may not be fully representative of the Peruvian upwelling regime and might not fully account for phenolic-like groups (Li et al., 2016, 2017; Lodeiro et al., 2020). It should also be noted that the majority of our samples (n= 13) were obtained from below the surface mixed

layer, with only three samples originating from surface waters. The number of surface samples was insufficient for detection of systematic differences between fresher, surface DOM and deeper, more strongly remineralized DOM. Our derived constants in this study are thus likely more representative for aged, remineralized DOM since this would be expected to dominate the DOM pool at depth (Hansell and Carlson, 2001).

Table 1. Derived NICA constants for Fe(III) binding to marine DOM. Goodness of fit indicators are shown by the root mean square errors (RMSE) and correlation coefficient (r^2). Two available sets of Fe(III) NICA constants previously used in seawater with salinity over 30, are shown for comparison (Hiemstra and van Riemsdijk, 2006; Avendaño et al., 2016).

Fe(III) NICA constants			
DOM1: carboxylic-like groups			
	This work	Avendano et al. 2016 (Avendaño et al., 2016)	Hiemstra and van Riemsdjik. 2006 (Hiemstra and van Riemsdijk, 2006)
$\log K_{Fe(III)DOM1}$	2.94 ± 0.19	3.6	2.7 ± 1.1
$n_{Fe(III)DOM1}$	0.32 ± 0.0	0.26	0.36 ± 0.05
DOM2: phenolic-like groups			
$\log K_{Fe(III)DOM2}$	9.60 ± 0.0	8.3	8.3 ± 3.5
$n_{Fe(III)DOM2}$	0.30 ± 0.02	0.23	0.23 ± 0.09
RMSE	0.1792	NA	
Correlation coefficient (r^2)	0.9012		

4.3.2 Physico-chemical environment of the Peruvian shelf and slope region

The main hydrographic feature along this coastal region off Peru is upwelling that occurs all year round and was relatively strong in austral winter at the time of our cruise (Strub et al., 1998) (Figure S4). The upwelling results in a high supply of nutrients to surface waters, which promotes

enhanced primary productivity of marine phytoplankton (Carr, 2001; Carr and Kearns, 2003; Loginova et al., 2016). The enhanced productivity and subsequent organic matter remineralization impact DO, pH and DOC, which are thus intricately connected in this region (Jiao et al., 2010; Carr et al., 2019; Loginova et al., 2019). We observed higher pH_{tot} (> ~7.8) and DOC concentrations (> ~80 µmol L^{-1}) in oxic (DO> ~120 µmol L^{-1}) surface waters (<20 m) as a result of high productivity (Figure 1). In subsurface waters, sluggish ventilation and microbial remineralization of sinking phytoplankton biomass decreased DO and DOC concentrations (Brandt et al., 2015; Loginova et al., 2019), and pH_{tot} (Bates, 2018). Upwelled CO_2-rich acidic waters from the OMZ also affected the distribution of pH_{tot} in surface waters of the Peruvian shelf and slope (<200 km distance), leading to lower pH_{tot} (~7.8-8.0). The lowest pH_{tot} (7.04) in this work was observed close to sediments at the shelf break due to enhanced organic matter remineralization occurring at the sediment-water interface (Mosch et al., 2012; Dale et al., 2017).

Dissolved Fe and Fe(II) distributions

Dissolved Fe concentrations were rather constant throughout the water column at the station closest to the coast (ca. 3.6 km offshore) (5.78±2.41 nM, number of samples (n) =5, value expressed as mean ±1σ; Figure 1, panel e) as a result of enhanced mixing. On the shelf (between >15 km and <50 km offshore), DFe concentrations decreased (1.42±1.01 nM, n=9) in surface waters (<20 m). In subsurface waters, we observed elevated DFe (range from ca.1 to 35 nM), with highest DFe concentrations found in near-bottom waters over the shelf (35.5 nM). Offshore (>50 km from the coast), DFe in surface waters was consistently lower (0.69±0.22 nM, n=6) than on the shelf. In subsurface waters, DFe concentrations increased with depth reaching an average of 1.81±0.45 nM, (n=16) at depths >400 m, with the exception of station 58, where DFe reached 3.29 nM between 200~300 m.

On the shelf (<50 km off shore), Fe(II) concentrations were low (0.28±0.09 nM, n=3, Figure 1, panel f) in surface waters, and Fe(II) made up 27.0±5.3% of the DFe inventory. In subsurface waters, we observed elevated Fe(II) (ranging from ca.0.5 to 10.9 nM), with highest Fe(II) in near-bottom waters (10.9 nM), making up 31% of the DFe inventory. Offshore (>50 km), Fe(II) was consistently low (0.23±0.03 nM, n=3) in surface waters (<20 m) compared to onshore stations. In subsurface waters, enhanced Fe(II) and DFe concentrations were observed between 50~200 m

extending offshore to station 56 (DFe = 4.10±0.93 nM, n=6; Fe(II) =1.92±1.09 nM, n=3). Elevated Fe(II) concentrations were also observed between 200~300 m at station 58 (1.30 nM) where Fe(II) made up 40% of the DFe inventory.

Overall, DFe and Fe(II) concentrations on the shelf were in agreement with earlier observations for this area (Bruland et al., 2005; Vedamati et al., 2014; Rapp et al., 2020). The increased DFe inventory in shelf and offshore waters was likely influenced by higher Fe(II) concentrations as a consequence of the combination of the depleted oxygen conditions and upwelling (Croot et al., 2019). Enhanced DFe and Fe(II) concentrations observed at station 58 in the upper OMZ (200~300 m) can be related to laterally transported Fe from sediment sources (Heller et al., 2017; Cutter et al., 2018; Rapp et al., 2020). Sediments are known to be a dominant source of Fe(II) and DFe to the overlying waters in this area, caused by reductive dissolution of Fe oxyhydroxides in anoxic sediments and subsequent high diffusive Fe(II) fluxes from pore waters (Scholz et al., 2011, 2014), and also by resuspension of surface sediments (Noffke et al., 2012; Vedamati et al., 2014). Our work shows a marked decrease of DFe in bottom waters across the slope at depths between 300~500 m. This gradient was previously reported (Scholz et al., 2011; Vedamati et al., 2014), and is likely caused by lower benthic DFe and Fe(II) inputs into bottom waters despite low oxygen conditions (DO<20 µmol L^{-1}). The presence of reactive oxygen species may also accelerate Fe(II) oxidation (Barbeau, 2006; Croot et al., 2008) in the presence of strong organic ligands, even under low oxygen condition (Witter et al., 2000; Rose and Waite, 2002; Hopkinson and Barbeau, 2007; Kondo and Moffett, 2015). Furthermore, Fe(II) oxidation may have been facilitated by microbial nitrate reduction either enzymatically through anaerobic iron oxidation or by providing nitrite for an abiotic reaction (Scholz et al., 2016).

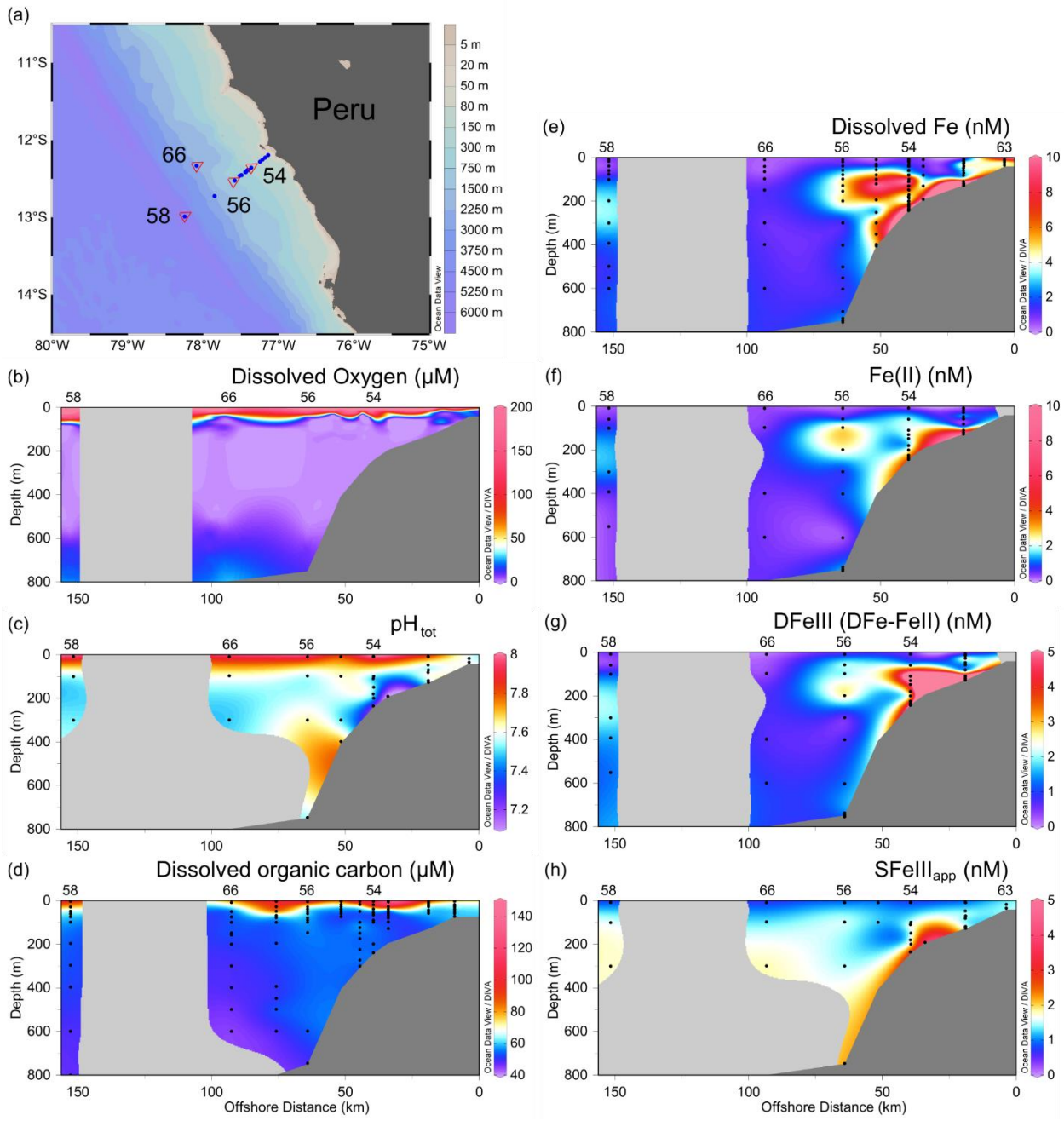

Figure 1. (a) Map of the Peruvian shelf and slope region with sampling sites. Samples for derivation of Fe(III) NICA constants were collected from two shallower sites (Station No. 54, 56 with water depth 243 and 749 m, respectively) and two deeper sites (Station No. 58, 66 with water depth 5410 and 2065 m, respectively). (b) The distribution of dissolved oxygen across the Peruvian shelf and slope region. Measured ambient (c) pH_{tot} (total scale) (d) Dissolved organic carbon concentrations, (e) dissolved Fe, (f) Fe(II), (g) DFeIII (DFe-FeII), and modelled (h) apparent

Fe(III) solubility ($SFe(III)_{app}$) for discrete samples from selected stations. Figures are generated by Ocean Data View (Schlitzer, 2015).

4.3.3 Equilibrium calculations of apparent Fe(III) solubility for the Peruvian shelf and slope region

The overall DFe inventory is determined by the interaction between organic Fe(III) complexation and Fe solubility as regulated by the precipitation of hydroxide or oxyhydroxides (Liu and Millero, 2002; Hiemstra and van Riemsdijk, 2006), which is influenced by pH and DOC concentrations. The application of chemical speciation models facilitates equilibrium calculations of $SFe(III)_{app}$ at ambient pH_{NBS}, temperature and DOC concentrations via the use of intrinsic binding constants and consideration of competition between binding by organic matter (in this case calculated via the NICA-Donnan model) and hydroxide ions with consequent $Fe(OH)_3(s)$ formation (See method section). We calculate $SFe(III)_{app}$ in this study based on solubility constants derived for $Fe(OH)_3(s)$ formation defined as the >0.02 µm fraction after one week of equilibrium) (Liu and Millero, 2002). However, given our DOM fraction was determined as the <0.7 µm fraction, it is not straightforward to map the chemical speciation calculations we made in this study onto size fractions (soluble, colloidal, dissolved) that are typically determined in field studies. The Fe predicted to be bound to DOM and the formed $Fe(OH)_3(s)$ in our calculations may both be colloidal in nature (>0.02 but <0.2 µm) and this should be considered when comparing the absolute values of $SFe(III)_{app}$ with DFe or DFe(III). For example, size-fractionation of the DFe pool suggests that as much as 50 % of the DFe pool could be present as colloids (0.02-0.2 µm) (Cullen et al., 2006; Boye et al., 2010; Fitzsimmons et al., 2015) and inert to coordination exchange. Although this significant colloidal fraction is suggested to comprise nanoparticulate Fe (oxyhdr)oxides, rather than complexed Fe(III) (Raiswell and Canfield, 2012), a portion of the dissolved ligand pool has nevertheless been found to occur in the colloidal fraction (Kondo et al., 2021).

We further emphasize that our calculations are equilibrium calculations and thus do not include non-equilibrium processes such as scavenging, biological uptake or redox processes. These processes can be expected to have an important impact on DFe inventory in the water column, with scavenging of DFe onto particles or biological uptake of DFe acting to reduce the DFe

inventory (Tagliabue et al., 2016; Ye et al., 2020) and redox process affecting the distribution of DFe in the Peruvian shelf and slope region (Croot et al., 2019).

Here, we use our derived constants to calculate $SFe(III)_{app}$ and compare its distribution to the measured ambient DFe(III) concentrations (Figure 1, panel g and h). In surface waters (<20 m), modelled $SFe(III)_{app}$ was consistently low (0.86±0.09 nM, n=6), and less than double the observed ambient DFe(III) (0.52±0.28 nM, n=4). Modelled $SFe(III)_{app}$ increased with depth in offshore waters (>50 km off shore), averaging 1.53±0.22 nM, n=7 in the top of the OMZ (80~400 m), and 2.2 nM in deeper waters (>400 m) of station 56. Observed DFe(III) increased with depth in offshore waters (>50 km) from ca. 0.5 nM in surface waters to ca. 1.2 nM at depth (>400 m), except at the furthest offshore station (58) where a maximum of 1.76±0.32 nM (n=2) between 200~400 m was observed. Near the coast, modelled $SFe(III)_{app}$ was near constant through the water column (1.38 and 1.42 nM). The maximum $SFe(III)_{app}$ (3.9 nM), was found in bottom waters, coincident with the lowest measured pH_{tot} (7.04, total scale) and highest observed DFe concentrations on the Peruvian shelf.

Overall modelled $SFe(III)_{app}$ showed good agreement to measured ambient DFe(III) in the Peruvian shelf region with a correlation coefficient ($r = 0.67$, n=14, $p< 0.05$, Figure S5). Ambient DFe(III) apparently exceeded the solubility of Fe as a result of enhanced benthic Fe fluxes in near-bottom waters (Figure 2, panel a) where DFe is under kinetic rather than thermodynamic control and thus out of equilibrium with ambient pH and ligand properties. We also observed a contrast between offshore stations 58 and 66 (Figure 1), where in subsurface waters (>100 m) the observed DFe (including DFe(II)), 1.81±0.73 nM, n=13) was close to modelled $SFe(III)_{app}$ (1.62±0.23, n= 4), and our coastal station 63 where observed DFe (including DFe(II)), 5.78±2.41 nM, n=5) concentrations were much higher than modelled $SFe(III)_{app}$ (1.40±0.03 nM, n=2). This contrast is again potentially a result of important non-equilibrium processes in coastal waters, where the transient Fe(II) species and elevated Fe inputs from sediments determine the DFe inventory. On the other hand, the similarity between measured DFe(III) and observed DFe concentrations in offshore waters (station 58 and 66), suggests a system that is close to our predicted equilibrium conditions in subsurface waters.

In surface waters, modelled $SFe(III)_{app}$ was higher than observed DFe(III) by 0.33±0.21 nM, n=4. This discrepancy is consistent with a role for biological Fe uptake and abiotic particle scavenging, with enhanced particle concentrations in surface waters (Moore and Braucher, 2007; Boyd and Ellwood, 2010; Heller et al., 2017). In the OMZ interior, modelled $SFe(III)_{app}$ overall exceeded measured DFe(III) by 0.5-1 nM. This difference is likely linked to excess Fe-binding capacity as reported previously in the OMZ, and caused by the release of Fe-binding ligands during organic matter degradation (Witter et al., 2000; Kondo and Moffett, 2015).

Our results show that the distribution of $SFe(III)_{app}$ is strongly influenced by pH throughout the water column (Figure 1 and 2). We examined the correlations among modelled $SFe(III)_{app}$, pH, DOC and temperature (Figure S5). pH showed a stronger correlation with $SFe(III)_{app}$ ($r = -0.95$, $n=21$, $p<0.05$) than temperature ($r = -0.82$, $n=21$, $p<0.05$) or DOC ($r = -0.72$, $n=21$ $p<0.05$). When expressed as a proportion of the $SFe(III)_{app}$ fraction, then inorganic Fe increased from 6% of $SFe(III)_{app}$ at pH_{NBS} 8.1 to 20% at pH_{NBS} 7.16, whilst the proportion bound to DOM decreased from 94% to 80% in our calculations (Figure 2, panel b and c). Thus the increase $SFe(III)_{app}$ was driven by increased $Fe(OH)_3$ solubility and not by stronger Fe binding. Modelled $SFe(III)_{app}$ values using the constants derived in this work were lower than would be predicted using NICA constants from the Celtic Sea (Avendaño et al., 2016), but higher than would be predicted using constants reported by Hiemstra and van Riemsdijk (Hiemstra and van Riemsdijk, 2006) for the Sargasso Sea (Figure 2, panel b). The change in solubilities between studies reflects changes in heterogeneity of the NICA binding sites (i.e. $n_{Fe(III)DOM1}$, $n_{Fe(III)DOM2}$) as well as changes in the binding affinity of the DOM2 group ($\log K_{Fe(III)DOM2}$) (Figure 2, panel b and d). This is consistent with recent work on protonation constants derived using the NICA-Donnan model, which showed marine DOM has different acid-base properties compared to terrestrial DOM (Lodeiro et al., 2020). Since the value of $logK_{Fe(III)DOM}$ represents the median of the binding affinity distribution via the NICA-Donnan model, differences in $\log K_{Fe(III)DOM}$ between studies could reflect the DOM pool changing from coastal environments to the oligotrophic open ocean environment (Hansell and Carlson, 2002; Seidel et al., 2017). However, since there are few Fe(III) NICA constants available for marine DOM, further work is required to confirm this preliminary finding. Nevertheless, even use of one set of Fe(III) NICA constants throughout the water column results in $SFe(III)_{app}$ within the range of observed DFe(III) concentrations and trends in $SFe(III)_{app}$ that are similar to observed trends for

DFe(III) concentrations, highlighting the importance of ambient pH and DOC conditions as important controls on changes in ambient DFe concentrations. Furthermore this link to pH and DOC, which will likely change as a result of increasing atmospheric CO_2 concentrations, has important implications for future shifts in Fe availability within OMZs but also other systems.

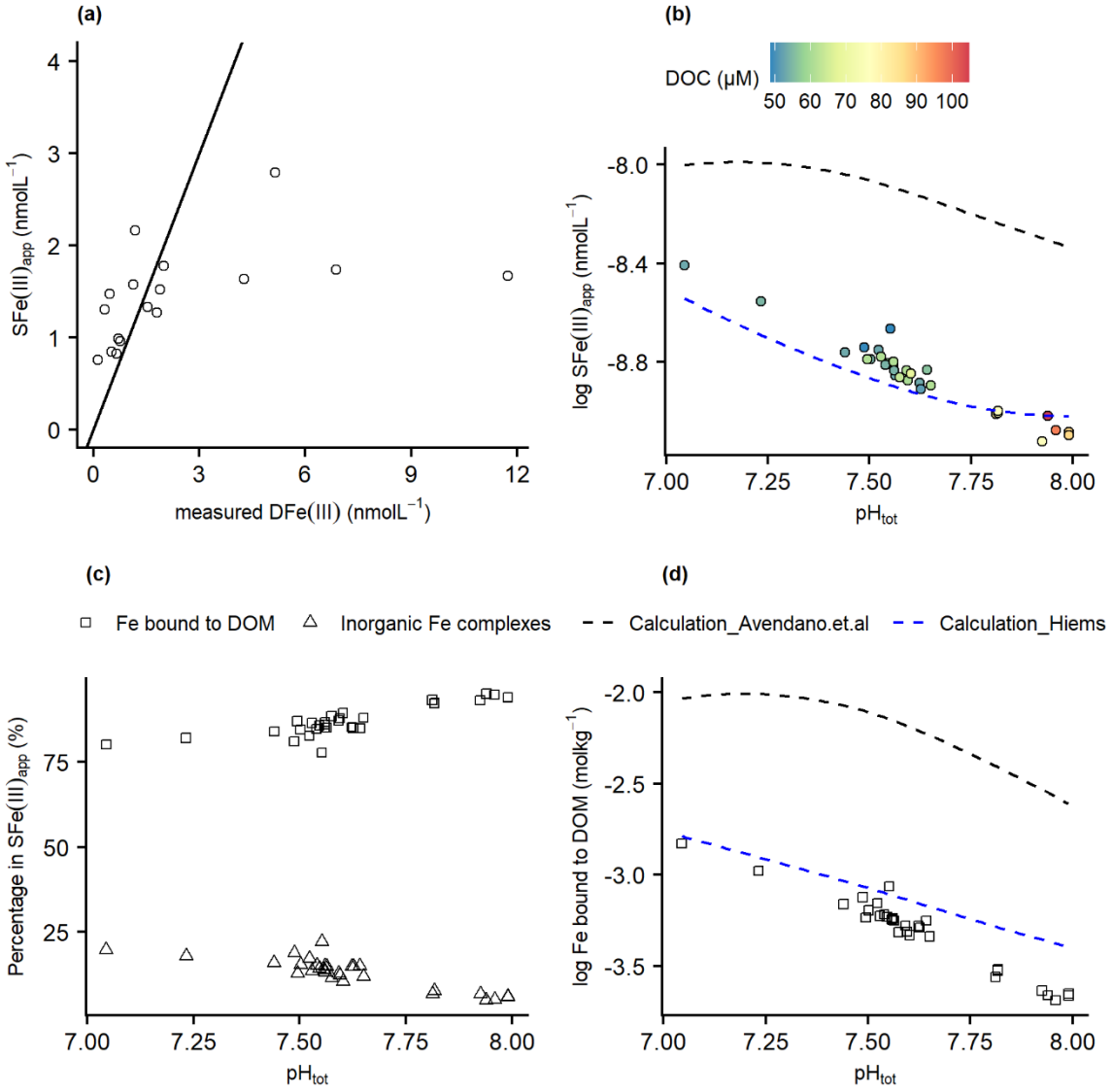

Figure 2. Modelled apparent Fe(III) solubility ($SFe(III)_{app}$) determined from competition between binding to DOM and assumed ferrihydrite precipitation. We used ambient pH_{NBS}, temperature and DOC concentrations, but assumed the total Fe(III) concentrations of 10 nmol L^{-1} in our calculations. (a) Modelled $SFe(III)_{app}$ plotted against measured ambient DFeIII (DFe-FeII), where the linear dark line is slope of 1. (b) Modelled $SFe(III)_{app}$ shown in log scale plotted as a function of pH_{tot} and DOC concentrations, where simulated dashed lines are the model results using two

previously reported sets of NICA constants (see Table 1) (Hiemstra and van Riemsdijk, 2006; Avendaño et al., 2016). (c) The proportion of inorganic and organic complexes of Fe relative to modelled $SFe(III)_{app}$ is shown as a function of pH_{tot}. (d) The amount of Fe bound to DOM (per kg DOM), is plotted as a function of pH_{tot}, where simulated lines are the modelling results using two previously reported sets of NICA constants (see Table 1) (Hiemstra and van Riemsdijk, 2006; Avendaño et al., 2016).

We conducted a sensitivity analysis of the NICA-Donnan model on derived values of $SFe(III)_{app}$ and evaluated percentage changes in $\Delta SFe(III)_{app}$ induced by 10% changes in both groups (DOM1 and DOM2) of the binding affinity and non-ideal constant (Figure S6). In our calculations a relatively constant 13±1% increase in $SFe(III)_{app}$ was induced by a 10% increase in $\log K_{Fe(III)DOM1}$, but $SFe(III)_{app}$ increased by 45% at higher pH_{tot} (~8.1) as a result of a 10% increase in $\log K_{Fe(III)DOM2}$. For the non-ideality constants, $SFe(III)_{app}$ was most sensitive to $n_{Fe(III)DOM1}$ (-33%) across the pH_{tot} range, whereas $SFe(III)_{app}$ decreased by 17% as a result of a 10% increase in $n_{Fe(III)DOM2}$ at higher pH_{tot} (~8.1).

4.3.4 Fe(III) speciation in the Peruvian shelf and slope region

The NICA model assumes the presence of two binding site groups, a low proton binding affinity group with a K_H in the range of carboxylic-like groups, and a higher proton binding affinity group with a K_H in the range of phenolic-like groups. Since the degree of proton occupation of each group of sites varies with Fe(III) NICA constants and pH, the importance of each group with respect to Fe(III) binding will vary through the water column (Lodeiro et al., 2020), with increasing pH resulting in increased binding to phenolic-like groups (DOM2). In Figure 3, the detailed speciation of Fe(III) bound to marine DOM (in log scale) calculated using the NICA-Donnan model with our derived constants, is provided as a function of pH. We also repeated these calculations using Fe(III) NICA constants from Hiemstra and van Riemsdijk (Hiemstra and van Riemsdijk, 2006) (Table 1) with generic constants (Milne et al., 2001). Our results show that both types of binding sites are important for Fe(III) speciation in the ocean, but the binding shift between DOM1 and DOM2 within the pH range reported in this work is different from previous work with generic constants (Hiemstra and van Riemsdijk, 2006). Firstly, the total amount of

binding sites derived for marine DOM (Lodeiro et al., 2020) is considered less than generic constants (Milne et al., 2001), and thus resulted in a difference in binding behaviour. Also the ratio of non-ideal constants $n_{Fe(III)DOM}/n_H$ could be interpreted as a reaction stoichiometry. For DOM1, a calculated ratio of $n_{Fe(III)DOM1}/n_{H1} \approx 1{:}2$ was similar between this work and Hiemstra and van Riemsdijk (Hiemstra and van Riemsdijk, 2006). For DOM2, the ratio of $n_{Fe(III)DOM2}/n_{H2}$ was 1:2.5 compared to that (1:3) reported in Hiemstra and van Riemsdijk (Hiemstra and van Riemsdijk, 2006). As discussed in Hiemstra and Riemsdijk (Hiemstra and van Riemsdijk, 2002), our derived ratio of $n_{Fe(III)DOM2}/n_{H2}$ (1:2.5) resulted in a larger difference between that ratio and the mean number of OH groups per Fe(III) ion in inorganic Fe species with increasing pH. Thus our calculations showed a lower Fe(III)-binding per kg DOM2, in combination with the effect of binding sites of marine DOM (Figure 3). We have assumed that both groups of marine DOM binding sites scale proportionally with DOC. However, the molecular composition of marine DOM (e.g. the aromaticity index, AI) is known to change during degradation (Koch and Dittmar, 2006; Hansen et al., 2016). Although we had insufficient sample numbers from surface waters to test the hypothesis that NICA constant change with DOM composition in this study, we cannot rule out this possibility.

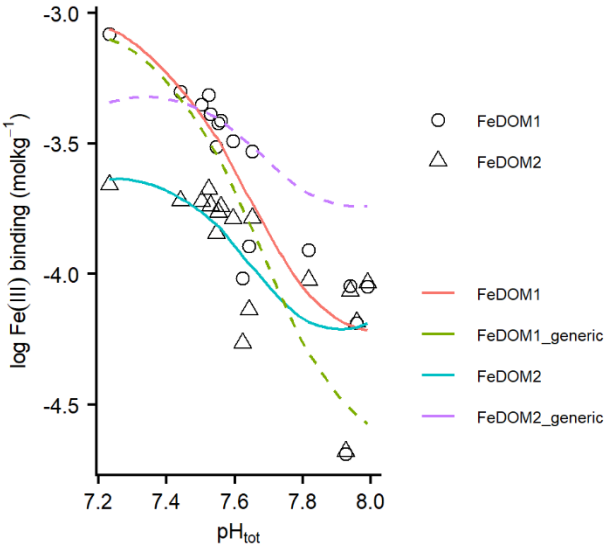

Figure 3. Dissolved Fe(III) speciation was calculated using the NICA-Donnan model with our derived Fe(III) NICA constants (Table 1) at ambient pH_{NBS} (the NBS scale), DOC and measured DFe(III) (DFe-FeII) in the case of equilibrium with ferrihydrite. The proportion of carboxylic-like (DOM1) and phenolic-like (DOM2) groups to ambient DFe(III) speciation plotted versus pH_{tot}

(total scale), are shown as data points (circle: Fe(III) binding to DOM1; triangle: Fe(III) binding to DOM2). The colored lines indicate the simulated curve via the NICA-Donnan model using all constants from this work (solid lines), and Fe(III) NICA constants derived by Hiemstra and van Riemsdijk (Hiemstra and van Riemsdijk, 2006) with generic constants (Milne et al., 2001) (dashed lines).

4.4 Environmental implications

We have applied a pH-Fe experimental titration design in combination with a speciation model and parameter optimization software to determine the binding affinities between Fe(III) and marine DOM in the Peruvian shelf and slope region. Subsequent calculations of DFe(III) speciation for the ambient water column show close agreement between measured DFe(III) concentrations and modelled apparent Fe(III) solubility ($SFe(III)_{app}$) in offshore waters, suggesting an important role for both pH and DOM as drivers of DFe distributions in the ocean. We observed a strong vertical gradient in pH distribution (ca.1 units) in this region, that will likely be influenced by on-going ocean acidification and deoxygenation. Our calculations suggest pH is more important for DFe(III) speciation and $SFe(III)_{app}$ than DOM, and that contributions from inorganic Fe complexation are more important than increased organic complexation at lower pH. We adopted a new way to account for the impact of both changes in pH and DOC, and redox process on DFe speciation in the Peruvian upwelling region, via a comparison of equilibrium calculations of DFe(III) speciation using the NICA-Donnan model and measured DFe(III) by in situ Fe(II) measurements. Although we predicted one set of Fe(III) NICA constants for the whole region, we cannot rule out a potential change in Fe binding characteristics between surface and deeper waters which should be explored in future studies.

Our work suggests that the combination of pH and DOM caps the maximum concentration of DFe that can be held within the shelf waters at equilibrium. Our findings work towards constraining the mechanisms that control Fe retention in the system but we note that the transfer of Fe to the water column is still controlled by benthic interactions, river and aeolian supply. On the Peruvian shelf, benthic DFe fluxes generally increase in response to deoxygenation, but our work suggests the corresponding DFe concentrations in the water column in contact with sediments are inherently

transient and will thus rapidly decline towards the maximum stable Fe(III) concentration. The lateral transfer of DFe offshore within the OMZ is therefore not necessarily increased by higher benthic DFe inputs on the shelf. However, it is possible that the lateral transfer of DFe will increase in response to ocean acidification. Such an increase could potentially be amplified by processes, such as increased productivity, that also drive ocean deoxygenation. Our approach provides a framework within which to explore the impacts of such feedbacks. Further determinations of intrinsic constants for marine DOM will likely improve our understanding of the influence of pH and DOM concentration and composition on DFe distributions in the ocean.

Acknowledgements

The authors would like to thank the captain, crew of FS meteor, chief scientist Marcus Dengler (M136), and Uwe Papenburg for support during cruise work. TA and DIC measurements were conducted by Jennifer Clarke (GEOMAR). KZ was supported by a scholarship from the China Scholarship Council. The project was funded by the Deutsche Forschungsgemeinschaft as part of Sonderforschungsbereich (SFB) 754: “Climate-Biogeochemistry Interactions in the Tropical Ocean”, and the Helmholtz Association. The authors declare no competing financial interest.

Supplementary information

Contents:

1 Sampling protocols and methods for determinations of dissolved Fe, Fe(II), dissolved organic carbon and pH in seawater samples

1.1 Sampling protocols

Seawater samples were collected following GEOTRACES protocols (Cutter et al., 2017) using a trace metal clean CTD (Sea-Bird SBE25) and a rosette frame equipped with 24 trace metal clean samplers (12 L, Ocean Test Equipment (OTE)). The bottles were transferred to a clean-laboratory container for sampling and filtration, and pressurized to 0.2 bar overpressure using filter N_2 gas. Samples for the determination of dissolved Fe (DFe) (<0.2 µm), Fe(II) (unfiltered), dissolved organic carbon (DOC, <0.7 µm) and total alkalinity (A_T)/dissolved inorganic carbon (C_T) were collected across the Peruvian shelf and slope region. All low density polyethylene (LDPE, Nalgene) bottles used for DFe sampling and high density polyethylene (HDPE, Nalgene) bottles for Fe(II) sampling, were acid washed according to the protocol (Achterberg et al., 2001b). New bottles were soaked in Mucasol detergent (Sigma Aldrich) then 6.7 mol L^{-1} hydrochloric acid (HCl; reagent grade, Fisher Scientific) followed by 8.3 mol L^{-1} nitric acid (HNO3; reagent grade, Fisher Scientific), for one week for each step. Bottles were rinsed thoroughly with deionized water (18.2 MΩ cm^{-1}, Milli-Q, Millipore) between steps. Samples were subsequently analyzed in the clean laboratories at GEOMAR, except Fe(II) samples which were analyzed immediately (within 10 minutes of collection of seawater from samplers, full details in Section 1.3) onboard.

1.2 Determination of dissolved Fe

Dissolved Fe samples were collected after filtration (AcroPak1000 capsule 0.8/0.2 µm filters) in trace metal clean low density polyethylene (125 ml LDPE, Nalgene) bottles and acidified to pH 1.9 by addition of 180 µL 32-35% HCl (ROMIL, UPA) per 125 ml. Dissolved Fe samples were preconcentrated using an automated SeaFAST (Elemental Scientific Inc.) with a cation chelating resin (WAKO, Wako Pure Chemical Industries, Japan), and determined by high resolution inductively coupled plasma-mass spectrometry (Element XR, Thermo Fisher Scientific) exactly as per Rapp et al. (2017) with calibration by isotope dilution. Briefly, DFe samples were UV-digested prior to preconcentration to breakdown organic complexation by organic matter. Samples were online buffered to pH 6.4 ± 0.5 using 1.5 mol L^{-1} ammonium acetate buffer, before loading

onto the resin. After preconcentrated on the resin, DFe was eluted into 1 mol L^{-1} distilled HNO_3, from supra-pure HNO_3 (SpA grade, Romil). Analysis of DFe via ICP-MS were achieved with a combined (buffer + manifold) analytical blank 20±25 pmol L^{-1}. The detection limit (3*standard deviation) of this method is 100 pmol L^{-1} for DFe. Reference materials were regularly analyzed alongside samples and were in good agreement with consensus values for DFe (Table S1).

Table S1. Certified and consensus reference materials (CRM) for dissolved Fe (DFe) concentrations determined in this study.

CRM	Measured concentrations	Certified/consensus concentrations	units
NASS-7	6.27 ± 0.75	6.16 ± 0.47	nmol kg^{-1}
CASS-6	27.17 ± 2.29	27.40 ± 2.15	nmol kg^{-1}
GSC	1.48 ± 0.023	1.54 ± 0.115	nmol L^{-1}

1.3 Determination of Fe(II)

Fe(II) samples were collected from GO-FLO bottles within the trace metal clean container on deck without filtration and immediately prior to other trace metal samples. Fe(II) samples were then passed to an analyst sequentially such that the time between subsampling from GO-FLO bottles and the completion of analysis (i.e. the completion of chemiluminescence peaks for a sample) was consistently <10 minutes for every sample. The order of sampling GO-FLO bottles was always deepest first for consistency.

Fe(II) samples were collected in trace metal clean opaque high density polyethylene (HDPE, Nalgene) bottles which were filled to overflowing. Analysis was via flow injection analysis using luminol chemiluminescence without preconcentration on a modified FeLume system as per Croot and Laan (2002) (Croot and Laan, 2002) using 10-port valves (Valco, Vici), a photonmultiplier tube (PMT, H9319-11, Hamamatsu) and a glass flow cell with a mirrored base (Waterville Analytical Products). Seawater, luminol reagent and deionized water were pumped using a peristaltic pump (MiniPuls 3, Gilson). The PMT was secured inside an electrical box to minimize background light, and all reagent and sample tubing was opaque (black PTFE, Global FIA, 0.8 mm internal diameter) except peristaltic pump tubing (PVC, Gradko). Luminol (5-

amino-2,3-dihydro-1,4-phthalazine-dione, Fluka) was used as received and luminol reagent prepared as per Croot and Laan (2002) (Croot and Laan, 2002) in opaque HDPE bottles. Luminol reagent was stored refrigerated in the dark for >2 days prior to use.

Fe(II) stock solutions were prepared from ammonium Fe(II) sulfate hexahydrate (99.997% Sigma Aldrich) in de-ionized water acidified with 0.1% by volume concentrated HCl (UPA grade, Romil). A diluted Fe(II) stock solution (1 µmol L^{-1}) was prepared daily. The detection limit (defined as 3 standard deviations of a blank measurement) varied slightly between analytical runs but was consistently <200 pmol L^{-1}.

Calibration via standard addition was conducted at each station on the same analytical run as sample analysis with peak height used to calibrate Fe(II) concentrations. Reported Fe(II) concentrations are derived from at least 3 chemiluminescence peaks obtained at 1 minute intervals. At least four standard additions were made to water from a mid-depth sample immediately after analysis of all Fe(II) samples for each station (total analysis time per station ~4 hours). Test with shallower/deeper water produced similar Fe(II) responses in the range 1-10 nmol L^{-1}. A notable exception to this was found with water collected from benthic landers, as per Plass et al., 2019 (Plass et al., 2019), from near-bottom depths (< 5 m) over some parts of the inner shelf where the luminol response to Fe(II) was markedly suppressed possibly due to insufficient O_2 in the reagent/seawater mixture within the flow cell. Attempts to quantify Fe(II) under these conditions were therefore abandoned.

1.4 Determination of dissolved organic carbon

Samples for the determination of dissolved organic carbon (DOC) were collected (20 ml) in combusted glass ampoules after filtration with combusted GF/F filters (Whatman) (8 h at 500°C). The filtered samples were acidified with 80 µL of 85% phosphoric acid per 20 ml, heat sealed immediately and stored at 4°C in the dark until analysis. DOC samples were analyzed onshore using high temperature catalytic oxidation on a Shimadzu TOC-VCPN following the protocol from Engel and Galgani. (2016). The calibration for instrument was conducted every 8-10 days by measuring the standard solutions of 0, 500, 1000, 1500, 2500 and 5000 µg C L^{-1}, prepared from a

potassium hydrogen phthalate standard (Merck). For each measurement day, deionized water (18.2 MΩ cm^{-1}, Milli-Q, Millipore) was determined for the blank of instrument, and standard solutions were determined between samples for quality control in the same day. The precision was <4% estimated as the standard deviation of replicate measurements divided by the mean. Consensus reference materials (University of Miami) were used to determine accuracy and precision of analysis daily, with the certified values ranged from 42-45 µmol C L^{-1}. The detection limit of DOC measurements was 1 µmol L^{-1}.

1.5 Determination of pH

Samples for dissolved inorganic carbon (C_T) and total alkalinity (A_T) were collected via silicone tubing into 250 ml borosilicate glass bottles following internationally established protocols (Dickson, 2010). Each bottle was sealed shut with a greased ground glass stopper after introducing a 2.5 ml air headspace and sterilising the sample with 50 µl of saturated mercuric chloride solution. All samples were stored in the dark until analysis according to the method (Humphreys et al., 2019). The determination of C_T was conducted using VINDTA 3C instruments (Marianda, Germany). Using 10% phosphoric acid to acidify seawater samples, then converted aqueous CO_2 from all C_T was transferred to the detector by nitrogen gas flow. A_T in samples was determined by potentionmetric titration, using 0.1 M hydrochloric acid (HCl), via VINDTA 3C instruments (Marianda, Germany). Both results of C_T and A_T were calibrated using measurements of seawater certified reference material (CRM) obtained from A.G. Dickson at Sripps Institution of Oceanography (Dickson et al., 2003). The 1σ measurement precision was calculated as the absolute difference between duplicates divided by $2/\sqrt{\pi}$ (Thompson and Howarth, 1973), within 2.74 µmol kg^{-1} for C_T and 0.45 µmol kg^{-1} for A_T.

The pH of our seawater samples was calculated on the IUPAC/NBS scale (pH_{NBS}) from C_T and A_T using CO2SYS (Pierrot et al., 2006), a speciation model specific for seawater. We used the NBS pH scale because it is consistent with the NIST based speciation constants used in the NICA-Donnan model via ORCHESTRA. We also used the total pH scale (pH_{tot}) to report the seawater carbonate chemistry. For CO2SYS, we used constants from Mehrbach et al. (Mehrbach et al., 1973) as refitted by Dickson and Millero (Dickson and Millero, 1987) and Dickson (Dickson,

1990) to describe the carbonate and sulphate equilibrium with hydrogen ions, and from Uppström (Uppström, 1974) to account for boron.

2 Determination of Fe(III) speciation via adsorptive cathodic stripping voltammetry

In this work, we combined a new experimental design of pH-Fe two dimensional titrations, by varying both pH and total Fe(III) concentrations, to derive new NICA constants for Fe(III) binding to marine dissolved organic matter (DOM) via the PEST-ORCHESTRA (Janot et al., 2017) (an example titration shown in Figure S1). We firstly derived the stability constant of $\log k_{FeNN3,H+}$ used in ORCHESTRA for describing the competition of Fe, H+ to HNN at our titration conditions (i.e. the NBS pH scale, temperature, salinity, DOC, HNN and total Fe(III) concentrations) (see section 4 in SI). To complete the NICA constants/stability constant of HNN estimation loop via PEST-ORCHESTRA, the analytical species $FeNN_3$, during pH-Fe titrations is firstly predicted using the NICA-Donnan model in ORCHESTRA, and then compared that with determined $FeNN_3$ via adsorption cathodic stripping voltammetry in PEST to obtain the lowest sum of squared residuals between experimental and modelled $FeNN_3$ calculated using a Levenberg-Marquardt algorithm. Therefore, the reliable measurements of $FeNN_3$ concentrations are important for confidential derivations.

Typically, measured $FeNN_3$ is calculated from peak height of titrations divided by the sensitivity. The sensitivity is calculated by plotting peak height versus total Fe concentrations, and equal to the slope of the part where organic matter is considered to be saturated with respect to Fe (Gerringa et al., 2014). In our case we observed a linear response at concentrations of added Fe > 1.5 nmol L^{-1}. The sensitivity is largely dependent on the artificial ligand concentrations used in the titrations, i.e. HNN in this work but can also be influenced by pH and sample matrix. We therefore examined the sensitivity at each individual pH for both UV-irradiated seawater and samples collected across the Peruvian shelf and slope region. Figure S2 shows there was no significant difference of slopes calculated from titrations with respect to varying pH in UV-irradiated seawater. In contrast we observed a significant difference in slope ($p > 0.01$) between pH_{NBS} (on the NBS scale) 7.2, 8.2 and 8.5 and between pH_{NBS} 7.4 and 8.5 in samples collected across the Peruvian shelf and slope region. We therefore assumed the

sensitivity of the $FeNN_3$ response did not vary with pH within the pH range used in this work and that the variability in sensitivity observed in the samples was a result of binding by weak binding sites present in the sample. To calculate the concentration of $FeNN_3$ observed at each titration point within each titration, we used the sensitivity determined at pH_{NBS} 7.9.

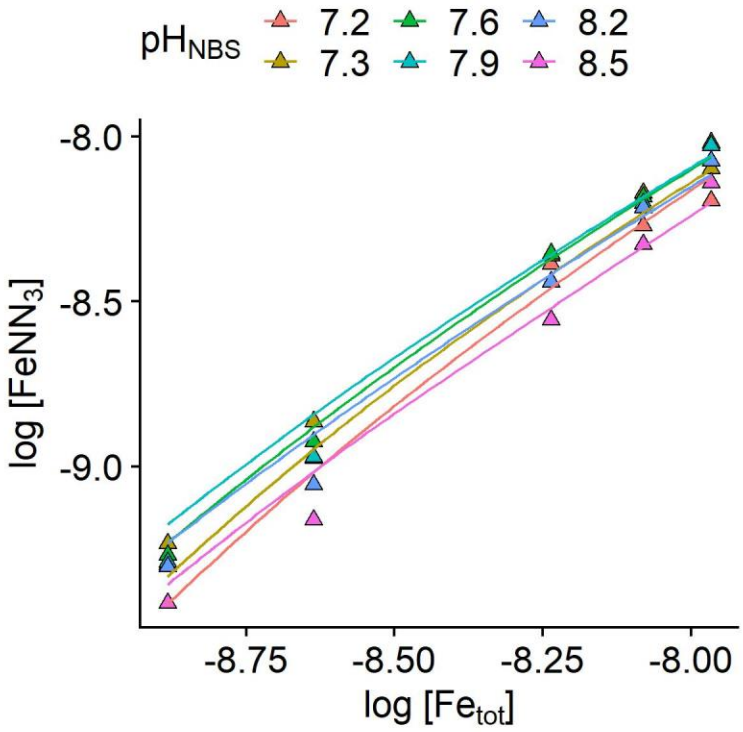

Figure S1. An example of pH-Fe titration undertaken on seawater samples collected in the Peruvian shelf and slope region, is shown as triangle data points. The simulated lines are the modelling results using the NICA-Donnan model with our derived Fe(III) NICA constants (Table 1 in main text). $[Fe_{tot}]$ and $[FeNN_3]$ are indicated as total Fe concentration (i.e. dissolved Fe + additional Fe) in each titration point and analytical species of voltammetry, respectively.

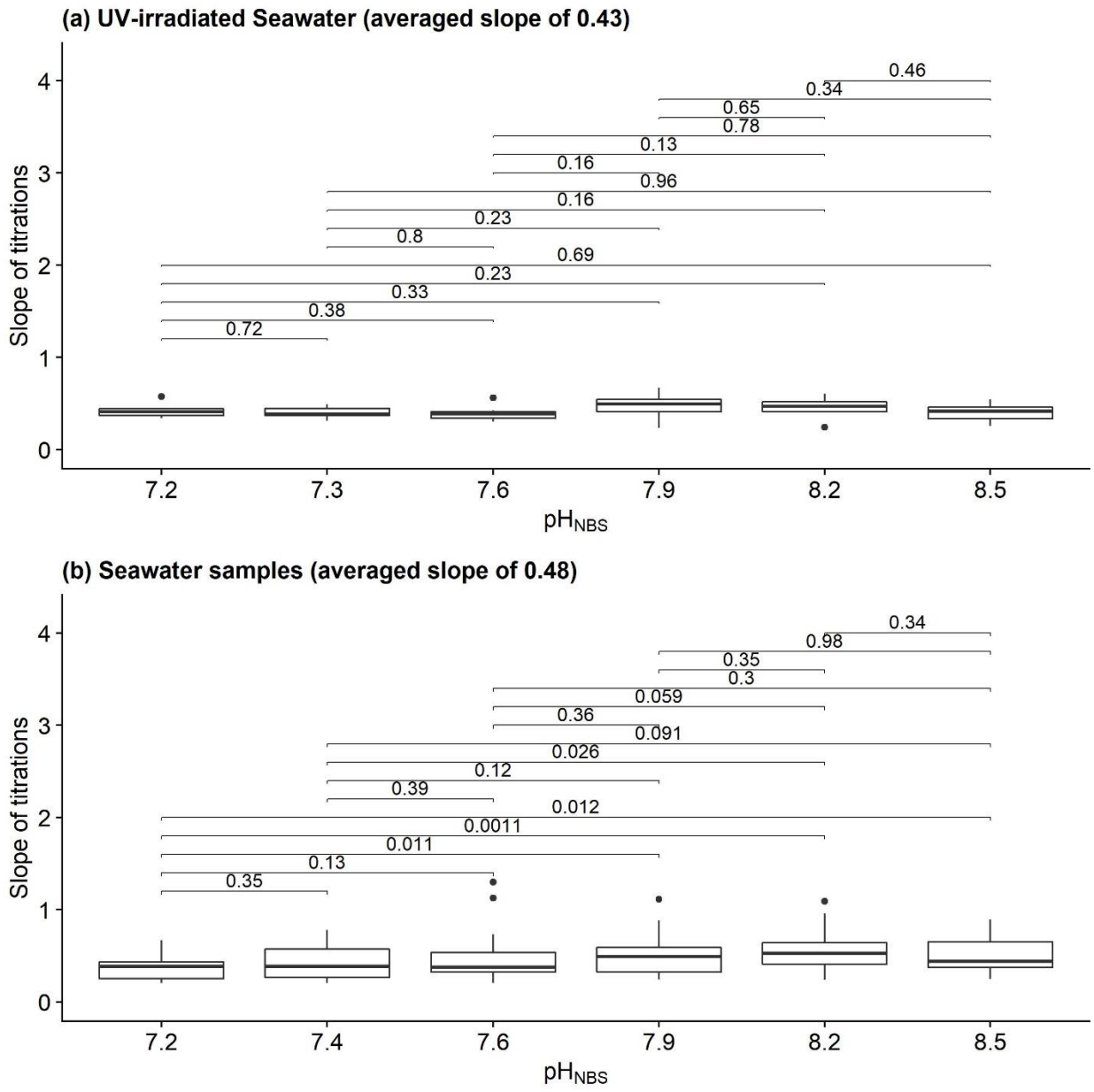

Figure S2. The calculated slopes from pH-Fe titrations are shown at each titration pH level, where (a) is shown as pH-Fe titrations performed in UV-irradiated seawater (n= 8), and (b) is shown as pH-Fe titrations performed in seawater samples collected in the Peruvian shelf and slope region (n= 31). We did the significance test by comparing the mean of slopes, via software R using the non-parametric Wilcoxon test that shown with p-values.

3 Application of the NICA-Donnan model within the speciation program ORCHESTRA

Table S2. All constants used in the NICA-Donnan model in order to derive Fe(III) NICA constants for marine dissolved organic matter (DOM) in the Peruvian shelf and slope region are shown. DOM1 represents carboxylic-like groups while DOM2 represents phenolic-like groups. a: taken from Lodeiro et al. (2020); b: taken from Milne et al. (2001, 2003).

	DOM1 (carboxylic-type groups)		DOM2 (phenolic-type groups)	
Ion i	$logk_{DOM1}$	n_{DOM1}	$logk_{DOM2}$	n_{DOM2}
H^+	2.34[b]	0.66[b]	8.60[b]	0.76[b]
Ca^{2+}	-2.13[b]	0.85[b]	-3.00[b]	0.80[b]
Mg^{2+}	-2.1[b]	0.77[b]	-2.4[b]	0.59[b]
Sr^{2+}	-2.5[b]	0.85[b]	-4.6[b]	0.70[b]
	Donnan constants: b = 0.57[b] $Qmax_{DOM1}$ = 2.52[a], $Qmax_{DOM2}$ = 0.80[a], p_1 = 0.59[b], p_2 = 0.70[b],			

4 Derivation of stability constant log$k_{FeNN3,H+}$ used in ORCHESTRA from UV-irradiated seawater

In this work, we applied sets of ion-paring model based on thermodynamic principles to understand how pH and temperature might influence trace element speciation at equilibrium (at least) valid for the physico-chemical conditions. Nevertheless, valuable information with respect to the extent that changes in physico-chemical properties such as pH and temperature might change metal speciation can be obtained if a system can be calibrated in such a way so that it is consistent between observed and calculated values for a given critical species.

To combine competitive ligand exchange with adsorption cathodic stripping voltammetry (CLE-AdCSV) method with derivation of Fe(III) NICA constants using the PEST-ORCHESTRA, both the reliable calculations and predictions of the analytical species FeNN3 from titrations, are required. We did the assessment of measured $FeNN_3$ in pH-Fe titrations prior to predictions (see

section 2 in SI). Therefore, we further attempted to achieve the reliable predictions via derivation of a specific $\log k_{FeNN3,H+}$ for application within an ion pairing model, that would account for competition between NN^-, H^+, Fe^{3+} and OH^- at the ionic strengths and pH relevant to our study. We distinguish this constant from previously derived conditional stability constants ($\log k^{cond}_{FeNN3,Fe3+}$) by denoting it $\log k_{FeNN3,H+}$.

Previous work suggested that the conditional stability for the complexation of Fe(III) by HNN ($\log k^{cond}_{FeNN3,Fe3+}$) resulted in little variability over the pH_{NBS} range 6.8-8.3 (Gledhill et al., 2015) and a value for the pH independent $\log k_{FeNN3,H+}$ of 32.5 for I = 0 was empirically estimated after taking into account the protonation constant for HNN ($pKaHNN$= 7.9, taken from NIST database (Smith et al., 2004)) and competition for Fe(III) between HNN and EDTA at different pH values (Gledhill et al., 2015). However, since this value was empirically derived and given that $\log k^{cond}_{FeNN3,Fe3+}$ has been shown to vary over three orders of magnitude in previous work (26.7 to 29.5) (Gledhill and van den Berg, 1994; van den Berg, 1995; Wu et al., 1995; Laglera et al., 2007; Hawkes et al., 2013), we chose to recalibrate $\log k_{FeNN3,H+}$ for the conditions applied in this study, utilizing the PEST parameter optimization method to derive $\log k_{FeNN3,H+}$. Thus, we firstly performed pH-Fe titrations undertaken in UV-irradiated seawater. Titrations were repeated over the pH_{NBS} range 7.2 to 8.5 at two different adding HNN concentrations ([NN]= 2 µmol L^{-1}, n=5; [NN]= 5 µmol L^{-1}, n=3).

Full details and files used in these derivations are described and can be downloaded from protocols.io (dx.doi.org/10.17504/protocols.io.brc4m2yw). Briefly, we assumed an initial value of 31(in log sacle) for the derivation of $\log k_{FeNN3,H+}$, with an allowed range of 28 to 32. Parameter derivation is performed by calculation of the $FeNN_3$ concentration in ORCHESTRA for each measurement, which is then passed to PEST and compared to the observed values. PEST guesses a new value for $\log k_{FeNN3,H+}$, which is then passed back to ORCHESTRA for a fresh calculation of $FeNN_3$. The procedure is iterated to minimize the residuals between observed and calculated $FeNN_3$ calculations via the Levenberg-Marquardt algorithm. The thresh-holds for obtaining an acceptable solution were also set in the PEST control file. The PEST output

comprises a value for $\log k_{FeNN3,H+}$ with 95% confidence intervals and the root mean squared error (RMSE), together with a full record of the optimisation in the output file.

The value of $\log k_{FeNN3,H+}$ (29.5, Table S3) determined in this study was lower than that used in previously in visual MINTEQ (32.5 (Gledhill et al., 2015; Avendaño et al., 2016)), but nevertheless within the range of error for $\log k^{cond}_{FeNN3,Fe3+}$ determined previously. The difference is likely due to the improved methodology used for parameter optimization, and also reflect the new derived $\log k_{FeNN3,H+}$ that account for competition between NN^-, H^+, Fe^{3+} and OH^- at the ionic strengths and pH relevant to this study.

Table S3. Derivation of $\log k_{FeNN3,H+}$ via the PEST-ORCHESTRA from pH-Fe titrations undertaken in UV-irradiated seawater. Goodness of fit indicators are shown by the root mean square errors (RMSE) and correlation coefficient (r^2).

$\log k_{FeNN3,H+}$	29.5 ± 0.09
Root mean square errors during the comparison of $FeNN_3$ (in log scale)	0.1202
Correlation coefficient (r^2)	0.9623

5 Further Figures and Tables in the Supplementary

Figure S3. Results of simulated titrations using the optimized parameters derived in this work (Table 1 in main text) compared with results obtained from experimental titrations. (a) Concentrations of $FeNN_3$ (in log scale) (y= 0.966±0.012 x – 0.284±0.099, RMSE= 0.176) and (b) concentration of the non-labile fraction of Fe that is not binding to HNN (in log scale) (named as DFe*, equal to total Fe – $FeNN_3$) (y= 0.524±0.029 x – 4.058±0.253, RMSE= 0.189). The dashed line in panel (b) is the detection limit of DFe* in this work and all values to the left of this line were thus below detection, which were removed from panel (b) (ca. 23%). Positive detection of a ligand relies on establishing a significant difference between expected Fe and determined Fe concentration in the linear part of the titration curve (>5 nmol L^{-1}). Taking our highest titration point (10 nmol L^{-1}) and the practical precision of our analysis, we estimate a cumulative error (σ) for total Fe – $FeNN_3$ of 0.36 nmol L^{-1}. The cumulative error results in an estimated detection limit (3σ) for binding sites of approximately 1.08 nmol L^{-1}.

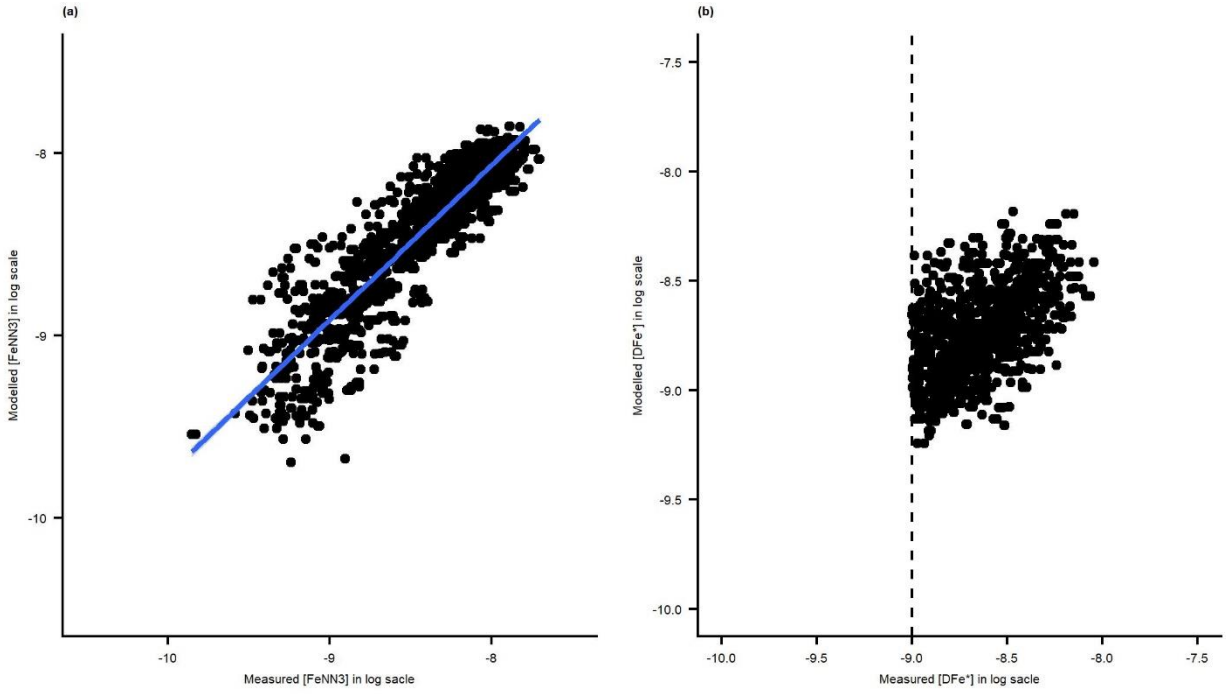

Figure S4. The distribution of temperature and practical salinity across the Peruvian shelf and slope region.

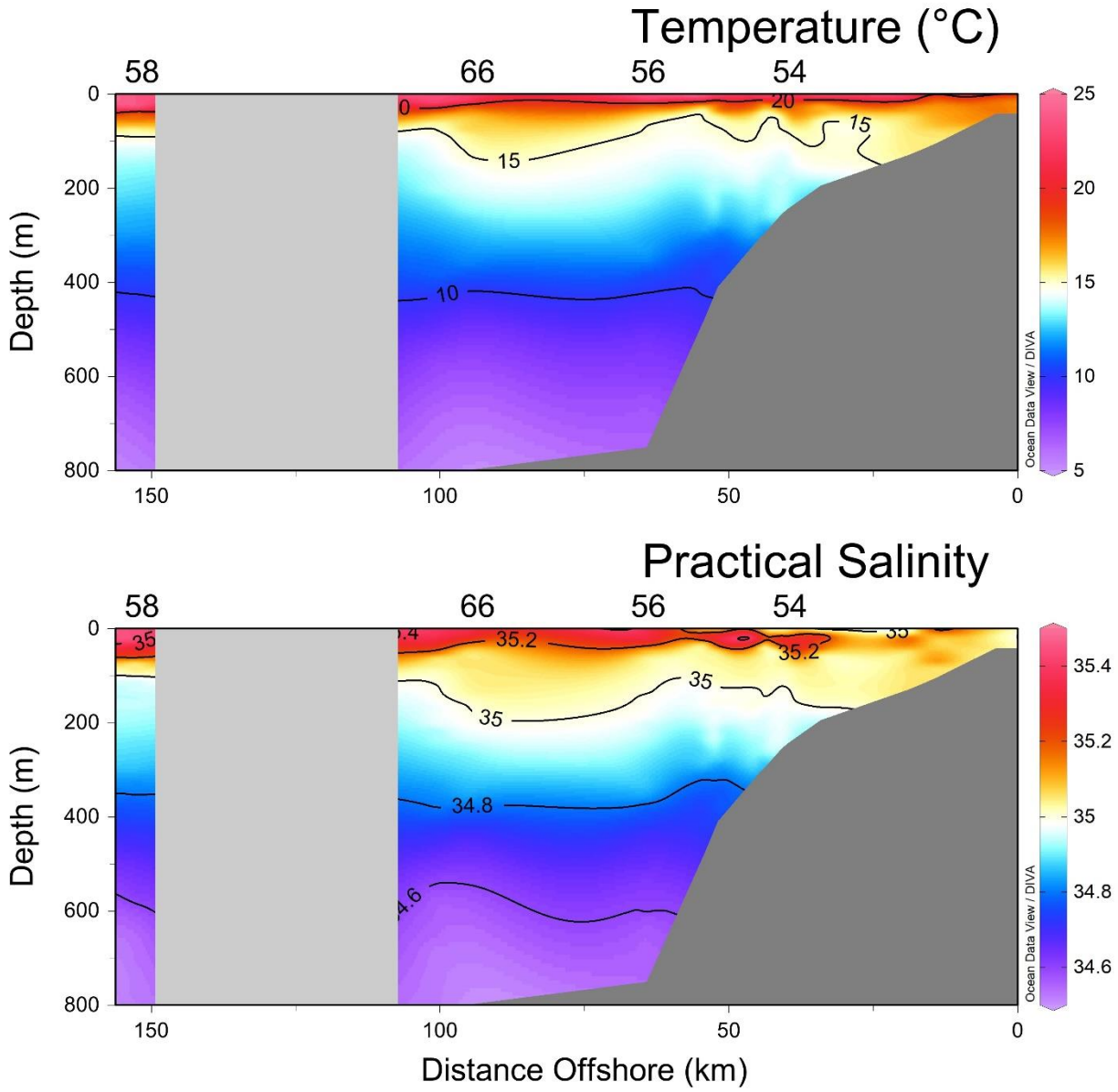

Figure S5. The correlation matrix of modelled apparent Fe(III) solubility ($SFe(III)_{app}$), dissolved Fe (DFe), ambient measured dissolved Fe(III) (DFe(III)= DFe - FeII) and ambient conditions (i.e. pH, temperature and dissolved organic carbon (DOC)) in discrete samples collected across the Peruvian shelf and slope region, which was generated via software R using the Spearman correlation method that shown with p-values. Not significant correlations ($p>0.05$) were cross out.

Figure S6. The Sensitivity analysis of the NICA-Donnan model for modelled apparent Fe(III) solubility ($SFe(III)_{app}$). We evaluated the percentage change in $\Delta SFe(III)_{app}$ induced by 10% and 20% in both the binding affinity and non-ideal constants. These parameters with changes are within the value range reported previously (Hiemstra and van Riemsdijk, 2006; Gledhill et al., 2015; Avendaño et al., 2016).

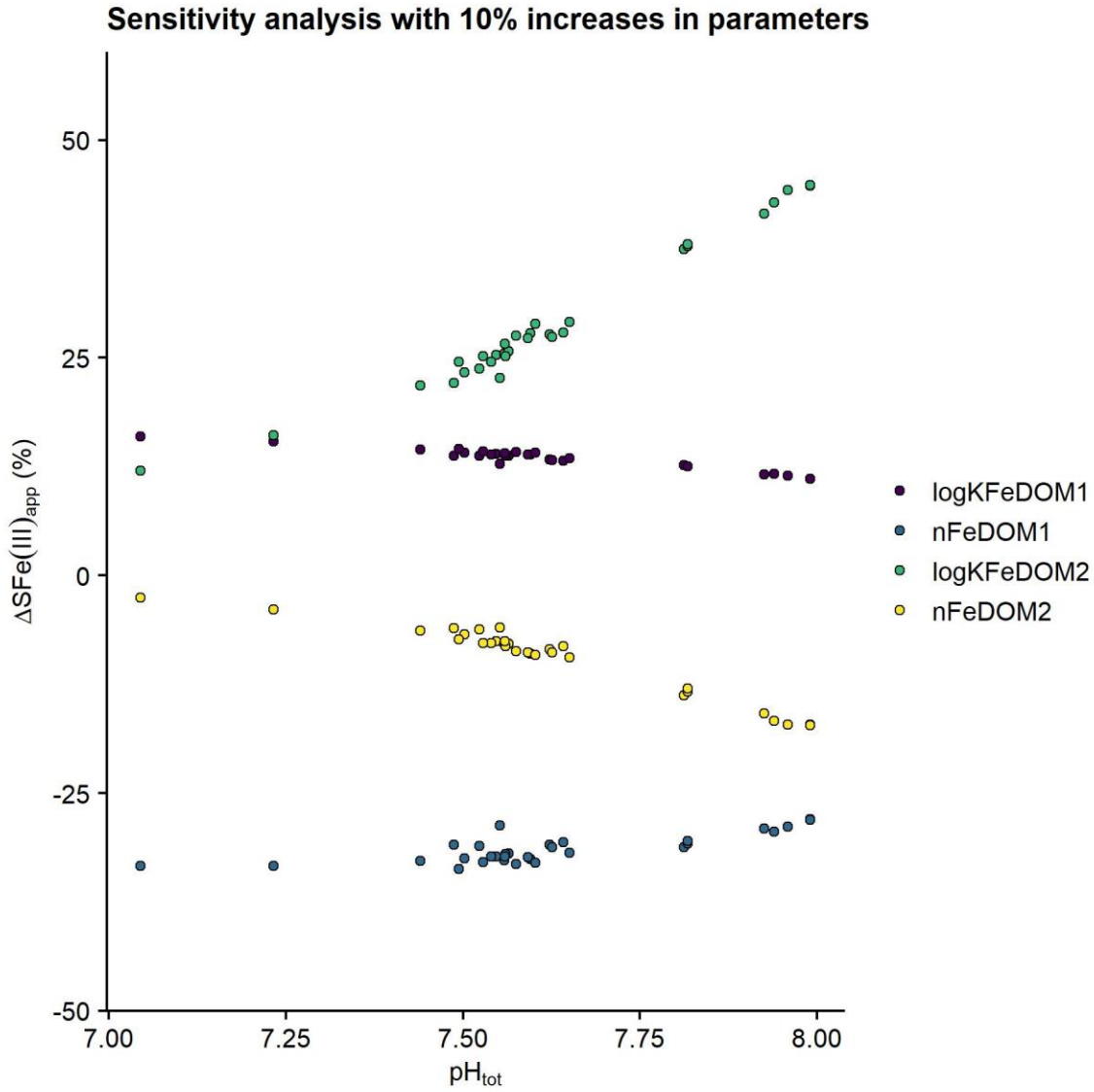

Table S4. All data of ambient pH, temperature, dissolved inorganic carbon (DIC), dissolved organic carbon (DOC) and measured ambient DFe(III) (DFe-FeII) used in the calculations for the side reaction coefficient $\alpha_{FeL,Fe'}$, with respect to inorganic Fe (Fe´) , using the NICA-Donnan model via ORCHESTRA.

Sampling stations	Depth (m)	Temperature (°C)	Dissolved inorganic carbon (µmol kg^{-1})	pH_{NBS} (the NBS scale)	Dissolved Organic carbon (µmol L^{-1})	DFe(III) (nmol L^{-1})	Calculated $\alpha_{FeL,Fe'}$ (in log scale)
58	8.46	23.77	2090.70	8.09	97.13	0.52	1.71
58	100.66	14.49	2269.84	7.66	57.56	1.13	1.03
58	300.67	11.79	2284.03	7.63	52.68	1.99	0.68
66	9.55	22.20	2134.64	8.06	76.33	0.13	2.80
66	97.05	14.33	2358.87	7.74	53.05	0.32	1.95
56	9.27	23.05	2121.15	8.07	104.65	0.76	1.50
56	97.66	14.82	2277.01	7.67	57.88	1.89	0.79
56	299.54	12.35	2253.89	7.75	55.95	0.46	1.73
56	746.22	6.58	2311.25	7.65	48.75	1.19	0.98
54	9.04	21.03	2092.95	8.12	86.90	0.66	1.39
54	109.79	14.80	2316.59	7.56	52.99	6.87	0.72
54	179.78	14.36	2277.16	7.62	54.11	4.27	0.74
54	235.15	13.58	2335.33	7.35	54.46	5.16	0.66
60	8.26	20.07	2183.80	7.94	76.71	0.70	1.38
60	47.31	16.82	2257.22	7.71	60.13	1.53	0.86
60	80.77	16.19	2252.16	7.77	60.91	1.80	0.87
60	119.89	14.91	2281.03	7.64	60.91	11.73	0.81

5 Impact of pH and temperature on apparent iron solubility and dissolved iron inventories in seawater

Kechen Zhu[1], Eric P. Achterberg[1], Nicholas Robert Bates[2,3], Loes J. A. Gerringa[4] and Martha Gledhill[1]

[1] GEOMAR Helmholtz Center for Ocean Research Kiel, Wischhofstr. 1-3, 24148 Kiel, Germany

[2] Bermuda Institute of Ocean Sciences, St. George's, Bermuda

[3] Department of Ocean and Earth Science, National Oceanography Centre, University of Southampton, Southampton, United Kingdom

[4] Department of Ocean Systems, NIOZ, Royal Netherlands Institute for Sea Research, Utrecht University, Texel, The Netherlands

To be Submitted to Global Biogeochemical Cycles

Abstract

A low supply of iron (Fe) limits phytoplankton growth in large parts of the global surface ocean, and thus restricts oceanic uptake of atmospheric carbon dioxide (CO_2). In turn, uptake of anthropogenic CO_2 by the ocean results in a decrease in pH, which influences the biogeochemical cycling of Fe. Here we used an ion paring - organic matter model (NICA-Donnan) to thermodynamically calculate the apparent Fe(III) solubility ($SFe(III)_{app}$) at ambient ocean temperature, pH and dissolved organic carbon (DOC) concentrations. The $SFe(III)_{app}$ is defined as the sum of aqueous inorganic Fe species and Fe complexed by organic matter at a free Fe (Fe^{3+}) concentration equal to the limiting solubility of Fe hydroxide ($Fe(OH)_3(s)$). $SFe(III)_{app}$ was calculated by setting total Fe(III) to 10 nmol L^{-1} and allowing for formation of $Fe(OH)_3(s)$ when the free ion concentration exceeded its solubility in seawater. Using data obtained during a series of GEOTRACES cruises, our results showed that there was a similar trend in the vertical distributions of horizontally averaged $SFe(III)_{app}$ and DFe, suggesting the underlying basin-scale distribution of DFe likely reflect relative changes in the $SFe(III)_{app}$. Regression analysis showed correlation coefficients of 0.44 and 0.55 for DFe-P and DFe-Si, respectively, and 0.5 for DFe-$SFe(III)_{app}$, suggesting the distribution of DFe is not solely a function of sinking organic matter remineralization processes, but also regulated by relative changes in ambient pH and temperature. This hypothesis was confirmed by the proportions of DFe relative to predicted $SFe(III)_{app}$, that were overall less variable through the water column at basin scales. In addition, changing pH was observed to be more important for determining $SFe(III)_{app}$ at basin scales, based on a solubility gradient of Fe hydroxide that is driven by ambient temperature. Therefore, consideration of the impact of pH and temperature on Fe speciation is as important for the speciation and solubility of Fe as the characterization of Fe-binding ligands, since the global distributions Fe-binding ligand (and DOC concentrations) are relatively invariant at the basin scale.

5.1 Introduction

Over the past 270 years, the ocean has taken up ca. 30% of the emitted anthropogenic carbon dioxide (CO_2), which has resulted in 0.1 unit pH decrease in the surface ocean relative to the preindustrial period, referred to as ocean acidification (Feely et al., 2009). This decrease in ocean pH is projected to continue and pH could drop by a further 0.33 pH unit by the end of this century under the IPCC RCP8.5 'business-as-usual' scenario (Jiang et al., 2019). Ocean acidification is known to affect biological processes, e.g. the ability of marine calcifiers to build shells or skeletal structures (Doney, 2006), but also has the potential to affect biogeochemical cycling of trace metals such as iron (Fe) (Millero et al., 2009; Gledhill et al., 2015; Stockdale et al., 2016; Ye et al., 2020).

Iron is an essential micronutrient and known to limit marine primary productivity (Boyd et al., 2007) as a result of a low supply and a low solubility of the thermodynamic favored form Fe(III) in oxic seawater (Liu and Millero, 2002). Iron is complexed by organic matter, which strongly increases Fe solubility and controls Fe speciation in seawater (Liu and Millero, 2002; Gledhill and Buck, 2012). Current understanding suggests there is an overall excess binding capacity for Fe, and only slight variations in binding characteristics are observed at basin scales, especially in deep waters (Buck et al., 2015, 2018; Gerringa et al., 2015). This indicates that the concentrations and characteristics of dissolved organic matter (DOM) that binds Fe may not vary greatly over spatial-temporal scales. Furthermore, the lack of variability in binding characteristics may be a reflection of a lack of variability in the composition and concentration of the overall DOM pool in time and space (Zark and Dittmar, 2018). Iron binding in the marine environment has been shown to be heterogeneous although the ligands still remains largely uncharacterized. Iron binding organic ligands likely include siderophores produced by bacteria and humic substances of terrestrial origin (Gledhill and Buck, 2012). Siderophores are present at very low concentrations and have a strong binding affinity for Fe (Mawji et al., 2008; Boiteau et al., 2016; Bundy et al., 2018), whilst humic substances are thought to dominate the Fe-binding DOM pool in estuarine and coastal areas, but with weaker binding strength (Muller, 2018).

The capacity of organic matter to bind Fe is not determined by the concentration and affinity of the binding sites alone, but also by changes in ambient physico-chemical conditions such as pH, temperature and ionic strength. Seawater pH varies by nearly one unit from ca. 8.2 (on the total pH scale) in the subpolar and polar surface waters (Takahashi et al., 2014) to ca. 7.6 (on the total scale) in the eastern boundary upwelling regions (Bates, 2018), whilst temperatures up to ca. 35°C are observed in the tropical surface waters compared to ca. 1°C in the subpolar and polar deep waters (Abraham et al., 2013). Iron complexed by organic matter is considered to buffer the dissolved Fe (DFe) concentrations and thus potentially regulate scavenging, suggesting the overall DFe inventory is dependent on the interaction between Fe solubility and the binding capacity of DOM (Johnson et al., 1997; Liu and Millero, 2002; Kuma et al., 2003), which in turn is strongly influenced by pH (Millero et al., 2009; Gledhill et al., 2015; Ye et al., 2020) and temperature (Liu and Millero, 2002).

Marine DOM contains acidic and basic binding groups which typically have different acidities and thus different relative affinities for H^+ and metal ions (Zhang et al., 2019). To account for changes in Fe speciation with pH given a heterogeneous Fe-binding ligand pool(Gledhill and Buck, 2012; Muller, 2018), intrinsic equilibrium constants are required. Such approaches are provided by e.g. the NICA-Donnan model (Kinniburgh et al., 1999) and WHAM/Model VII (Tipping et al., 2011). These models simulate competition between protons, major cations and metal ions binding to heterogeneous groups of binding sites such as fulvic acid and humic acids, which are considered to be the dominant form of organic matter in terrestrial and freshwater aquatic environments. Both models use two major types of binding sites, carboxylic-type (averaged pKa, ca. 4.5) and phenolic-type groups (averaged pKa, ca. 10) (Perdue, 1985). The NICA-Donnan model assumes continuous binding sites for each type, whereas the WHAM/Model VII employs four sets of discrete binding sites for each type. The parameters of both models are derived from experimental data of isolated humic substances, which thus leads to a key assumption that the binding properties of environmental DOM is similar to isolated humic substances. Both the NICA-Donnan model and WHAM/Model VII provide consistent results to Fe solubility and titration experiments in seawater (Hiemstra and van Riemsdijk, 2006; Stockdale et al., 2011, 2015; Gledhill et al., 2015; Avendaño et al., 2016). However, all of these aforementioned studies have used proton-binding characteristics of terrestrial DOM to determine

Fe binding in marine systems. Recently the first set of proton binding constants for marine DOM has been derived for the brackish Baltic Sea (Lodeiro et al., 2020). Combining these new constants, Zhu et al, (submitted) specifically derived NICA constants for Fe(III) binding to marine DOM and subsequently calculated Fe(III) speciation using the NICA-Donnan model in the water column of the Peruvian shelf and slope. Results indicated that decreased pH as a result of intense organic matter remineralization in the oxygen minimum zone (OMZ) and ocean acidification could increase the apparent solubility of Fe(III) and thus potentially facilitate the supply of DFe to surface waters. Furthermore, a global Fe model that incorporated a novel parameterization of organic Fe complexation derived using the NICA model, showed that accounting for the impact of pH and DOM improves the prediction of global DFe concentrations, suggesting that both pH and DOM could have an important influence on the global DFe inventory (Ye et al., 2020).

In this work, we used the NICA-Donnan model for cation binding to organic matter applying newly derived proton- and Fe(III)-binding constants for marine DOM (Lodeiro et al. 2020; Zhu et al., Submitted). We incorporated the chemical speciation tool ORCHESTRA (Meeussen, 2003) with its ion-pairing model to predict the apparent Fe(III) solubility ($SFe(III)_{app}$) in the Atlantic and Pacific Oceans at ambient pH, temperature and dissolved organic carbon (DOC) concentrations. Discrete samples for determinations of pH, DOC and DFe were collected during a series of GEOTRACES cruises, along a West Atlantic transect, Subtropical North Atlantic transect and Southeast Pacific transect. We compared the modelled $SFe(III)_{app}$ to measured DFe at basin scales, and then examined the correlations among the $SFe(III)_{app}$, DFe, pH, temperature and DOC and nutrients. Our work aims to account for the impact of changes in ambient conditions, such as pH and temperature, on the prediction of $SFe(III)_{app}$ with further impact on the overall DFe inventory in the ocean. We also discuss the combined impact of pH and low oxygen condition on Fe speciation (see Chapter 4).

5.2 Materials and Methods

5.2.1 Observational data

Observational data used in this work was collected during a series of GEOTRACES cruises, along a West Atlantic transect (GA02), Subtropical North Atlantic transect (GA06) and Southeast Pacific transect (GP16) (Figure 1). Depth, temperature, salinity and dissolved oxygen (DO) were measured using CTD sensors attached to rosette frames. pH, DOC and DFe were obtained from discrete sample data from the following sources. For cruise GA02, results of dissolved inorganic carbon (C_T), total alkalinity (A_T), DOC and DFe were directly taken from the GEOTRACES database IDP2017 (Schlitzer et al., 2018). For cruise GP16, results of DOC and DFe were directly taken from the GEOTRACES database IDP2017 (Schlitzer et al., 2018), while C_T and A_T in GP16 were obtained from a published database by Bates (2018). For cruise GA06, trace metal samples were collected using Ocean Test Equipment samplers on a Ti frame and deployed using a conducting Kevlar wire following the GEOTRACES protocol (Cutter et al., 2017). Samples for the determination of DFe were obtained after filtration using 0.2 µm Acropack filters with N_2 overpressure and acidified to pH 1.8 by addition of 140 µL ultraclean HCl (Romil, UpA) to 125 mL samples. Dissolved Fe was analyzed onboard using an online flow injection analysis (FIA) systems with a Toyopearl column with luminol chemiluminescence (Schlosser et al., 2014). Samples for the determination of C_T and A_T were collected following (Dickson et al., 2007), into 250 mL Schott Duran borosilicate glass bottles. C_T and A_T were analyzed onboard using a VINDTA 3C instrument, by coulometric titration and potentiometric titration, respectively (Tynan et al., 2016). Samples for the determination of DOC were filtered through combusted (450 °C, 4-6 h) glass fibre filters (Whatman, GF/F) into combusted (450°C, 4-6 h) glass ampoules and acidified with 30 µL of 50% (v/v) HCl (Romil, UpA). After acidification, the ampoules were flame-sealed. DOC was analyzed by high temperature catalytic oxidation following (Badr et al., 2003).

5.2.2 Calculations of the apparent iron solubility in the ambient water column

The NICA-Donnan model has been described previously for calculating dissolved Fe(III) speciation in seawater (Hiemstra and van Riemsdijk, 2006; Gledhill et al., 2015; Avendaño et al., 2016). The NICA-Donnan approach assumes that bulk properties of marine DOM can be represented by a limited number of binding site coefficients that describe intrinsic affinities between cations and different types or groups of binding sites in analogy to binding between

metals and humic substances (Gledhill and Buck, 2012; Muller, 2018). Briefly, the NICA model calculates the proton/metal competition within a heterogeneous mix of binding sites, which is generally defined as two major groups, carboxylic groups and phenolic groups (here called DOM1 and DOM2, respectively). The NICA model has three key parameters: median value of binding affinity distributions (logK) and their width (p), and non-ideal constants (n) for describing the exchange ratio of metal ions/protons to binding sites. The Donnan model accounts for any residual electrostatic interactions dependent on the specific volume of humic substances relative to ionic strength. The uniformly high ionic strength (I=0.72) in seawater limits the impact of electrostatic effects in the ocean (Lodeiro et al., 2020; Pinheiro et al., 2021). A further key assumption is that both groups of binding sites (DOM1 and DOM2) scale proportionally with DOC. The NICA-Donnan model scales metal binding to DOC concentrations via knowledge of the number moles of binding sites per kg of DOM ($Q_{max,H^+,DOM1}$ and $Q_{max,H^+,DOM2}$). We calculated a value of 4.07×10^{-8} kg (DOM)/µmol (C) (Lodeiro et al., 2020) and converted DOC (µmol L^{-1}) into binding sites (kg L^{-1}) using values of 2.52 mol /kg and 0.80 mol /kg for DOM1 and DOM2, respectively, derived for marine DOM (Lodeiro et al., 2020).

Full details of the calculations on the apparent Fe(III) solubility are described in the Method chapter of this thesis, and also can be downloaded from the online protocols.io (DOI: dx.doi.org/10.17504/protocols.io.brc4m2yw). Briefly, we use a uniform concentration of total Fe(III) of 10 nmol L^{-1} in our system and incorporate an inert insoluble phase of Fe hydroxide (as ferrihydrite, assumed in our calculations) defined by the solubility constants given in Liu and Millero (1999). The $SFe(III)_{app}$ is thus defined as the sum of aqueous inorganic Fe species and Fe complexed by organic matter at a free Fe (Fe^{3+}) concentration equal to the limiting solubility of Fe hydroxide ($Fe(OH)_3(s)$). We emphasize that the observed DFe concentrations are not an input term for the determination of $SFe(III)_{app}$. Our approach does not account for the effects of pressure, which can also be expected to affect metal solubility (Moore and Millward, 1984). Also, non-equilibrium processes such as Fe(II) production have not been calculated in this approach, though Fe(II) could also significantly enhance the DFe pool especially in e.g. OMZs (Croot et al., 2019).

5.2.3 Seawater carbonate chemistry reported on the total scale/IUPAC NBS scale

pH was calculated on the total scale (pH_{tot}) from C_T and A_T using CO2SYS (Pierrot et al., 2006), a speciation model specific for seawater. We also calculated pH on the IUPAC/NBS scale (pH_{NBS}), because the ion-pairing model used in this work is dependent on stability constants taken from NIST (Smith et al., 2004), which are derived relative to the IUPAC/NBS scale. The relationship between the NBS scale and total scale is linear and described by the following equations

$$aH = 10^{-pHNBS} = fH * Hsws \quad (1)$$

$$\frac{Htot}{1+TS/K2SO4} = \frac{Hsws}{1+TS/K2SO4+TF/KF} \quad (2)$$

Where aH is the activity and fH the activity coefficient of the H^+ ion (including liquid junction effects), TS and TF are concentrations of SO_4^{2-} and fluorine, and $K2SO4$ and KF are the dissociation constants of $H2SO4$ and KF in seawater. For CO2SYS, we used constants from Mehrbach et al. (1973; refitted by Dickson and Millero (1987)) and Dickson (1990) to describe the carbonate and sulphate equilibrium with hydrogen ions, and from Uppström (1974) to account for boron.

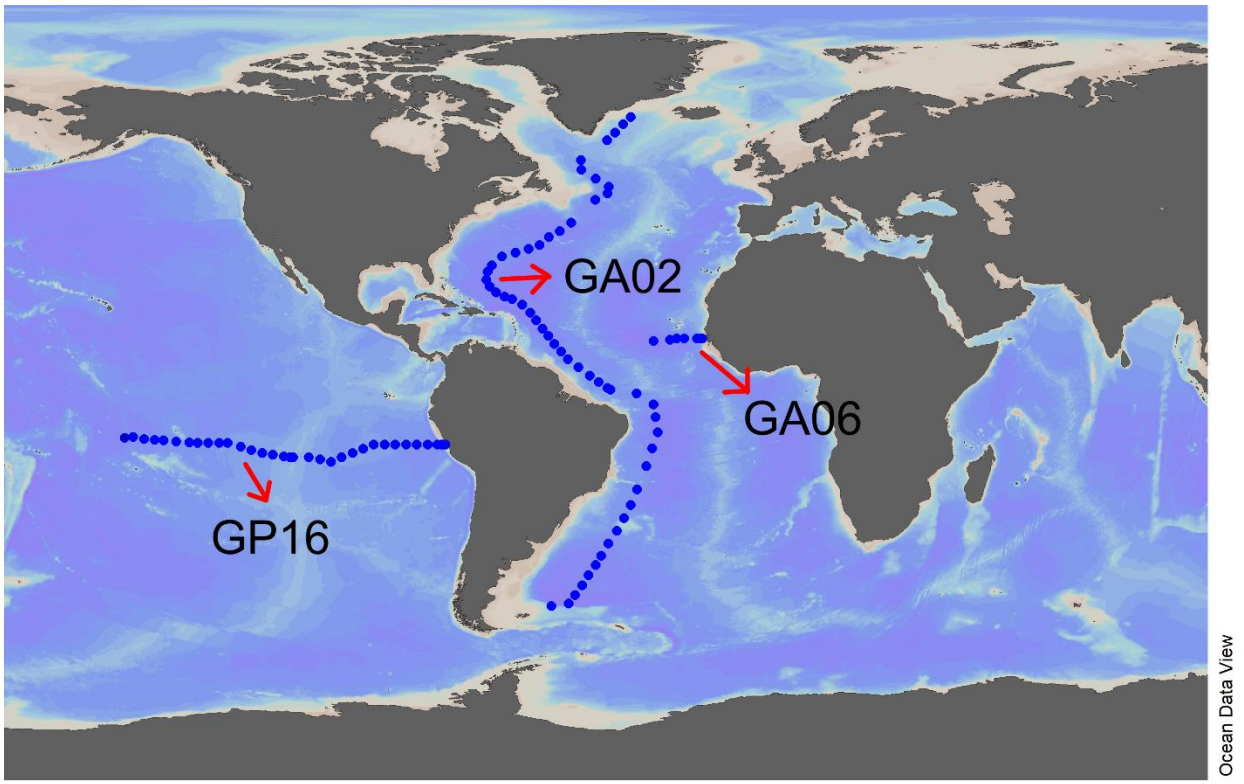

Figure 1. Map of the stations sampled during a series of GEOTRACES cruises, along a West Atlantic transect (GA02), Subtropical North Atlantic transect (GA06) and Southeast Pacific transect (GP16), was generated using Ocean Data View (Schlitzer, 2015).

5.3 Results

5.3.1 Modelled apparent iron solubility in the Atlantic and Pacific oceans

5.3.1.1 Ambient seawater chemistry conditions

pH

In the top 1000 m (Figure 2, 3 and 4), ocean pH_{tot} showed higher values (>8.05) in surface waters (<50 m) in highly productive regions of the Western North and South Atlantic during spring-summer months, and the Subtropical North Atlantic, compared to the Southeast Pacific (pH_{tot} >8). In subsurface waters (~100-1000 m), ocean pH_{tot} decreased with increasing depth in the Atlantic and Pacific Oceans, with minimum values found in OMZs in the Western Tropical Atlantic (<7.8), Subtropical North Atlantic (<7.7) and Southeast Pacific (<7.6). The low pH values are related to intense remineralization of sinking organic matter (Stramma et al., 2008a; Paulmier et al., 2011)(Bates, 2018). Below 1000 m (Figure 2, 3 and 4), ocean pH_{tot} distribution in the West Atlantic corresponded with water masses, while that pH_{tot} distributions in the Subtropical North Atlantic and Southeast Pacific were rather constant, with values of 7.92±0.04, n=43, and 7.80±0.04, n=232, respectively.

Dissolved organic carbon

In the top 1000 m (Figure 2, 3 and 4), concentrations of DOC were >80 µmol L^{-1} in surface waters (<50 m) in the Atlantic and Pacific Oceans and decreased with increasing depth. In subsurface waters (~100-1000 m), DOC concentrations decreased from ≤80 µmol L^{-1} at ~100 m, to values ≤50 µmol L^{-1} at ~1000 m in the West Atlantic and Subtropical North Atlantic, and to values ≤40 µmol L^{-1} at ~1000 m in the Southeast Pacific, respectively. There were exceptions of enhanced DOC concentrations (>60 µmol L^{-1}) observed at ~300 and 700 m between 10-20°S in the West Atlantic. Below 1000 m (Figure 2, 3 and 4), DOC concentrations were consistently low (~35-50 µmol L^{-1}) in the West Atlantic, and slightly decreased from north to south following the

path of the deep global thermohaline circulation. However, high DOC concentrations (>70 µmol L^{-1}) were observed at ~1000-2000 m at ~10-20°S in the West Atlantic. In the subtropical North Atlantic and Southeast Pacific, DOC concentrations were consistently low (<42 µmol L^{-1}) below 1000 m through the water column. The distributions of DOC in both ocean basins were consistent with previously reported data (Hansell et al., 2009).

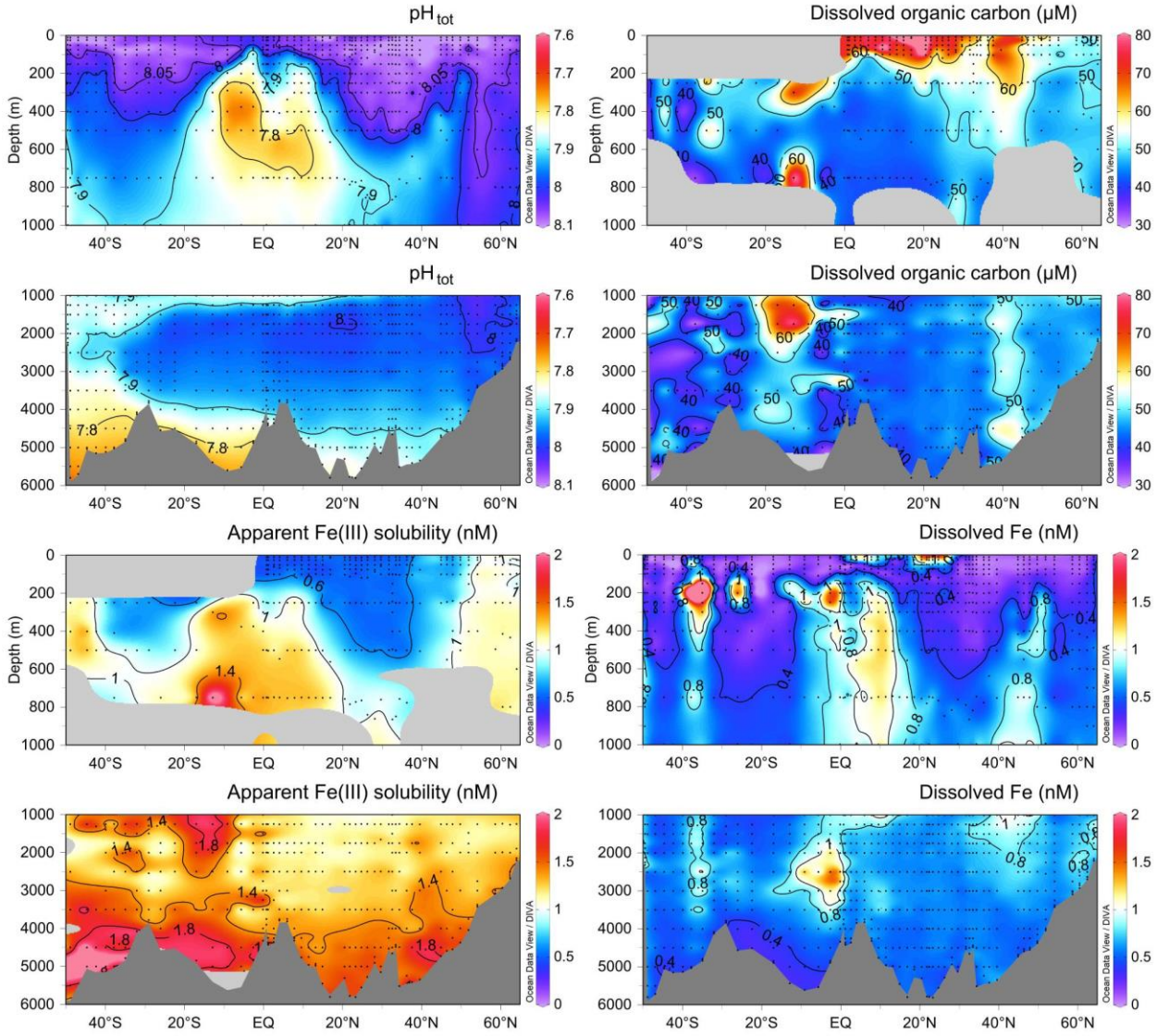

Figure 2. The distributions of pH_{tot} (total scale), dissolved organic carbon (DOC), modelled apparent Fe(III) solubility ($SFe(III)_{app}$) and dissolved Fe, were shown for full datasets along a West Atlantic transect (GA02). $SFe(III)_{app}$ was calculated using the NICA-Donnan model at ambient ocean temperature, pH_{NBS} (the NBS scale) and DOC concentrations.

5.3.1.2 Modelled apparent iron solubility

In the West Atlantic, values of modelled $SFe(III)_{app}$ were <0.6 nmol L^{-1} in the upper 200 m (Figure 2)and increased with increasing depth down to 1000 m and towards the north (~50-60 °N). Below 1000 m, values of modelled $SFe(III)_{app}$ were near constant between 1-1.4 nmol L^{-1} following the path of North Atlantic Deep Water, and slightly increased in the southern part of the West Atlantic transect and in Antarctic Bottom waters (>4000 m).

In the Subtropical North Atlantic (Figure 3), surface modelled $SFe(III)_{app}$ (<50 m) showed low values (<0.6 nmol L^{-1}) in offshore waters (in the west of 20°N) and slightly increased towards to the coast. In the subsurface waters (~100-1000 m), modelled $SFe(III)_{app}$ increased with increasing depth down to 1000 m with values >1.4 nmol L^{-1}. Values of $SFe(III)_{app}$ were similar (ca. 1.2 nmol L^{-1}) at ~1000-4000 m and slightly increased in the deep waters (>4000 m).

In the Southeast Pacific (Figure 4), surface modelled $SFe(III)_{app}$ (<50 m) showed low values (<0.6 nmol L^{-1}) in offshore waters (west of 90°W) and slightly increased towards to the coast. In subsurface waters (~100-1000 m), values of $SFe(III)_{app}$ increased with increasing depth, and were higher than 1.6 nmol L^{-1} below 400 m near the coast. Below 1000 m, values of $SFe(III)_{app}$ showed consistently high (>1.4 nmol L^{-1}) through the water column.

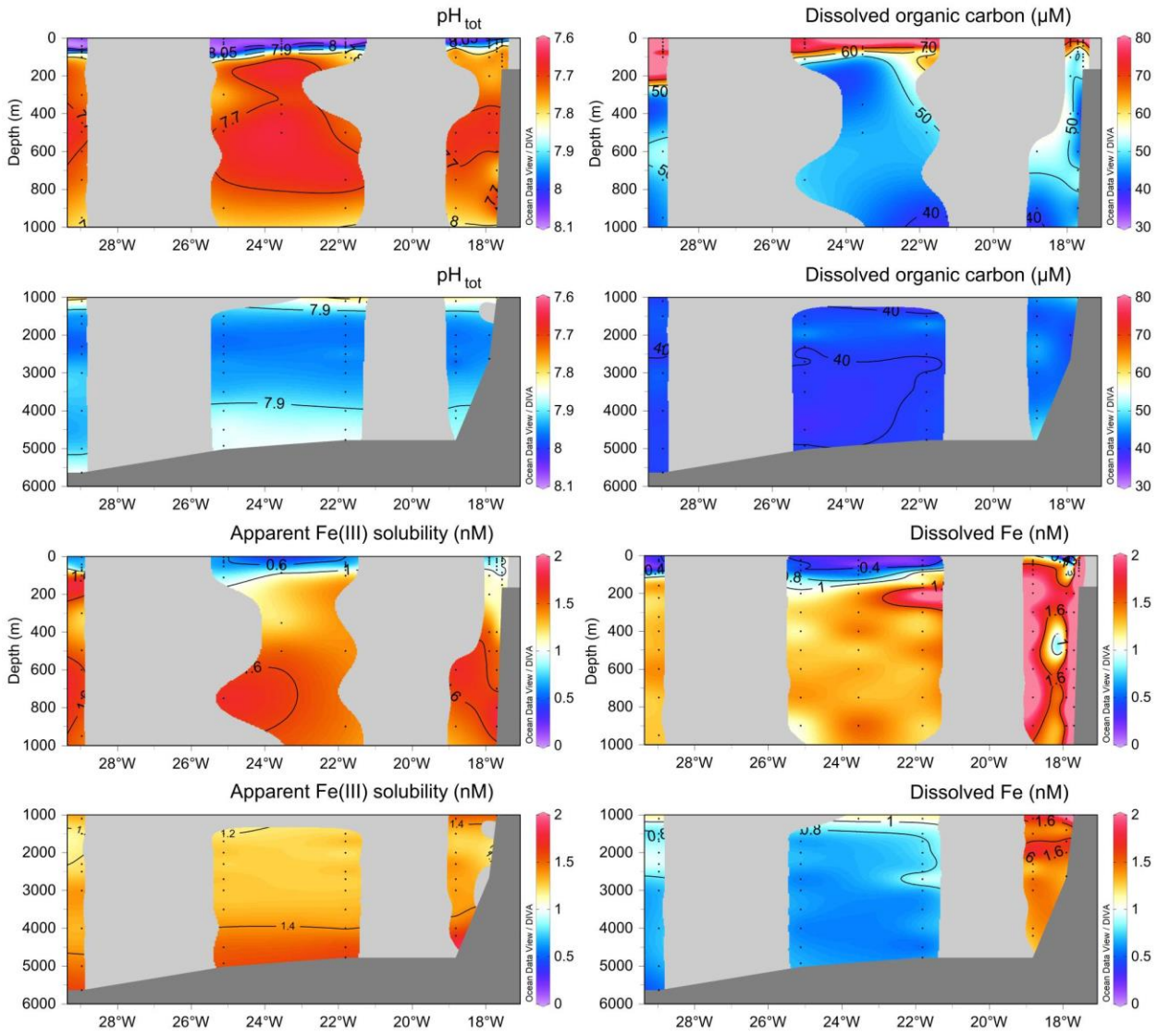

Figure 3. The distributions of pH_{tot} (total scale), dissolved organic carbon (DOC), modelled apparent Fe(III) solubility ($SFe(III)_{app}$) and dissolved Fe, were shown for full datasets along a Subtropical North Atlantic transect (GA06). $SFe(III)_{app}$ was calculated using the NICA-Donnan model at ambient ocean temperature, pH_{NBS} (the NBS scale) and DOC concentrations.

5.3.2 Comparison of the apparent Fe(III) solubility and dissolved Fe in the Atlantic and Pacific Oceans

The distribution of DFe in the West Atlantic Ocean has been described previously (Figure 2) (Rijkenberg et al., 2014). Dissolved Fe concentrations were generally <0.4 nmol L^{-1} in the upper 200 m and increased with increasing depth to ca. 0.8 nmol L^{-1} at ~1000 m. There were

exceptions of elevated DFe concentrations observed in surface waters (<50 m) that related to lateral transport or atmospheric dust input. Elevated DFe concentrations were observed at ~100-1000 m between 0-20 °N, as a result of intense remineralization of sinking organic matter in the OMZ. Below 1000 m, DFe concentrations ranged from 0.4 to 0.8 nmol L^{-1}, and slightly decreased to <0.4 nmol L^{-1} below 4000 m. Hydrothermal vents were observed to strongly enhance DFe concentrations between 0-20°S over the 2000-3000 m depth range. A similar pattern was observed in the distributions of measured DFe and modelled $SFe(III)_{app}$ with $SFe(III)_{app}$ concentrations <0.4 nmol L^{-1} and <0.6 nmol L^{-1}, respectively, observed down to 500 m at ~10-40°N. Below 1000 m, values of $SFe(III)_{app}$ were overall twice as high as DFe.

In the Subtropical North Atlantic (Figure 3), surface DFe concentrations (<50 m) were low (<0.4 nmol L^{-1}) in offshore waters (in the west of 20°W), and enhanced near the coast. In the subsurface waters (~100-1000 m), DFe concentrations increased with increasing depth to ca. 1.2 nmol L^{-1} at 1000 m in offshore waters. Elevated DFe concentrations were observed (>1.2 nmol L^{-1}) between 100-1000 m near the coast. Below 1000 m, DFe concentrations slightly decreased with increasing depth (<0.8 nmol L^{-1}) in offshore waters, while DFe concentrations were consistently high (>1.2 nmol L^{-1}) near the coast. A similar pattern was observed in the distributions of measured DFe and modelled $SFe(III)_{app}$ in the top 1000 m. Below 1000 m, DFe concentrations slightly decreased to <0.8 nmol L^{-1}, while $SFe(III)_{app}$ increased to values >1.4 nmol L^{-1}.

The distribution of DFe along the Southeast Pacific transect (Figure 4) has been described previously (Resing et al., 2015; Fitzsimmons et al., 2016). Dissolved Fe concentrations were generally <0.4 nmol L^{-1} in the top 1000 m. There were exceptions of elevated DFe concentrations near the coast, as a result of inputs from suboxic sediments on the Peruvian shelf (Heller et al., 2017; Cutter et al., 2018; Rapp et al., 2020). Below 1000 m, a significant input of DFe from hydrothermal vents was found at mid depth (~2500 m) to the west of the east Pacific Rise, and extended to the western end of the transect (Fitzsimmons et al., 2014, 2016; Resing et al., 2015). A similar pattern was observed in the distributions of measured DFe and modelled $SFe(III)_{app}$ in the top 1000 m. Near the coast, both DFe and $SFe(III)_{app}$ showed lower values in surface waters (<50 m) and increased with depth down to 1000 m. Offshore (in the west of

90°W), lower values were observed in the distribution of DFe and $SFe(III)_{app}$ in the upper ~300 m, which increased with increasing depth down to 1000 m. Below 1000 m, DFe concentrations ranged from 0.4 to 0.8 nmol L^{-1} with elevated values from hydrothermal vents, while the $SFe(III)_{app}$ generally showed twice the DFe concentration with a slight decrease to the west of the section.

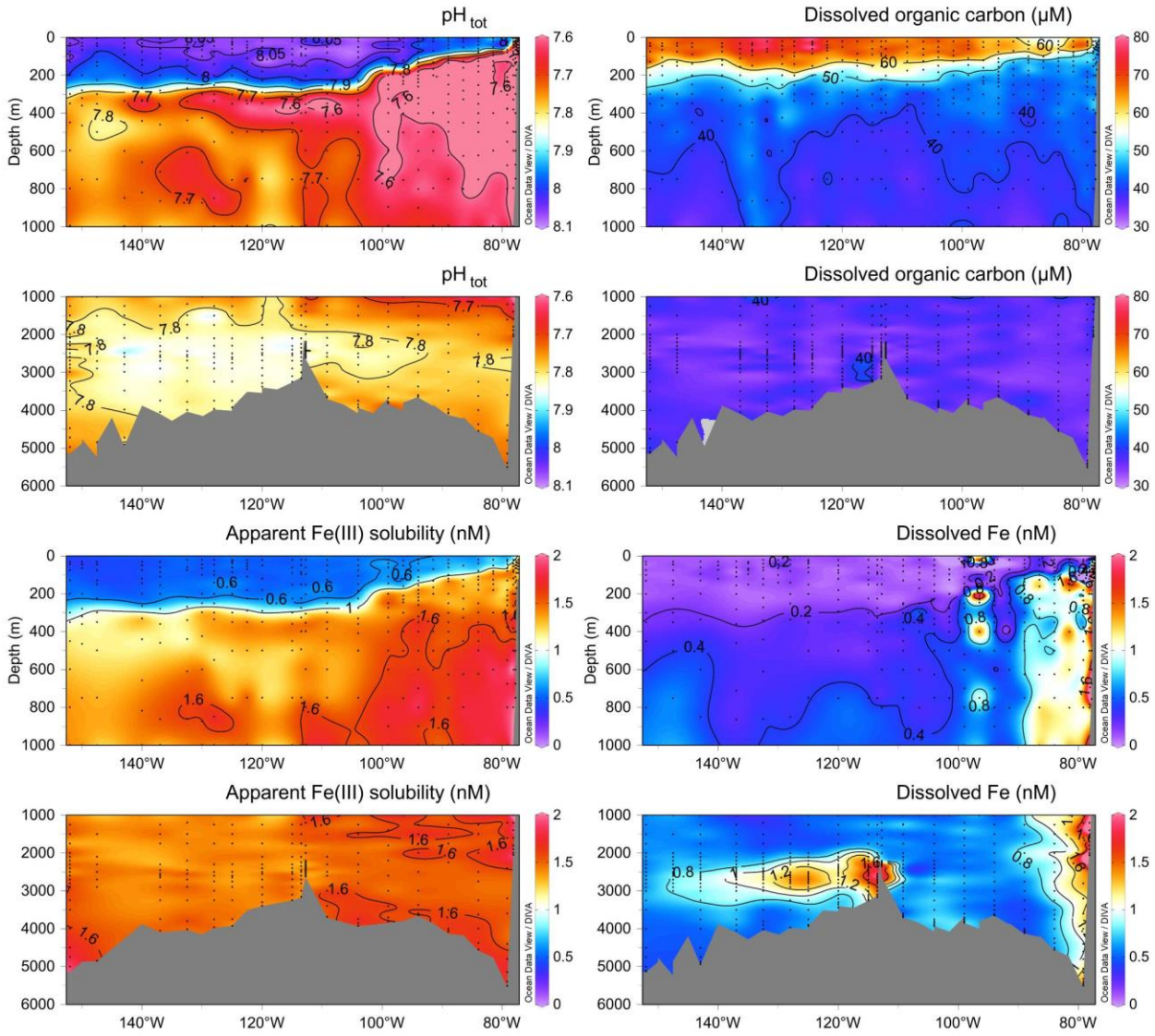

Figure 4. The distributions of pH_{tot} (total scale), dissolved organic carbon (DOC), modelled apparent Fe(III) solubility ($SFe(III)_{app}$) and dissolved Fe, were shown for full datasets along a Southeast Pacific transect (GP16). $SFe(III)_{app}$ was calculated using the NICA-Donnan model at ambient ocean temperature, pH_{NBS} (the NBS scale) and DOC concentrations.

5.4 Discussion

5.4.1 Underlying distributions of dissolved Fe associated with relative changes in the apparent Fe(III) solubility at basin scales

Johnson et al. (1997) suggested that the DFe distribution in the ocean is maintained by a mechanism that reduces the scavenging rate of DFe at concentrations less than the apparent solubility of Fe(III) (~0.6 nM), with apparent solubility of Fe(III) set by organic Fe complexation. However, determination of the organic Fe complexation via CLE-AdCSV show conditional ligand concentrations (i.e. conditional on pH) that generally exceed DFe concentrations by ca. 1 nmol L^{-1} (Caprara et al., 2016). The determination of the Fe(III) hydroxide solubility in filtered seawater samples (<0.025 µm) at temperature 20°C and pH_{NBS} range 8-8.2, suggests Fe is oversaturated with respect to the Fe(III) hydroxide solubility in seawater (Kuma et al., 1996, 1998, 2003). Both interpretations of the speciation and solubility of Fe do not account for the impact of ambient seawater conditions such as pH and temperature, even though pH is known to strongly affect inorganic complexation of trace metals (Millero et al., 2009).

In this work, overall values of modelled $SFe(III)_{app}$ were higher than measured DFe concentrations through the water column in the Atlantic and Pacific Oceans (Figure 2, 3 and 4). This is not unexpected, since traditional titrations via CLE-AdCSV, show total ligand concentrations generally exceed the DFe concentrations in the West Atlantic and Southeast Pacific (Gerringa et al., 2015; Buck et al., 2018). The similarities and differences between measured DFe and modelled $SFe(III)_{app}$ in both ocean basins suggest a strong influence of point sources on the DFe distribution, but the underlying distribution of DFe shows some correspondence to changes in the $SFe(III)_{app}$, particularly when considering the vertical distribution. This confirms earlier findings that DFe depth profiles are governed by release of DFe from remineralized organic matter, scavenging and Fe(III) hydroxide solubility (Kuma et al., 2003, 1998). To further explore this comparison, we plotted depth profiles in the Atlantic Ocean of horizontally averaged measured DFe and predicted $SFe(III)_{app}$ (Figure 5, panel A, n= 1079 and 798 profiles for DFe and $SFe(III)_{app}$, respectively) and Pacific Ocean (Figure 5, panel B, n= 492 and 555 profiles for DFe and $SFe(III)_{app}$, respectively). We omitted measured DFe

profiles that were strongly influenced by source signatures from e.g. hydrothermal vents, atmospheric dust and suboxic sediment inputs in both ocean basins (Fitzsimmons et al., 2014; Rijkenberg et al., 2014; Milne et al., 2017).

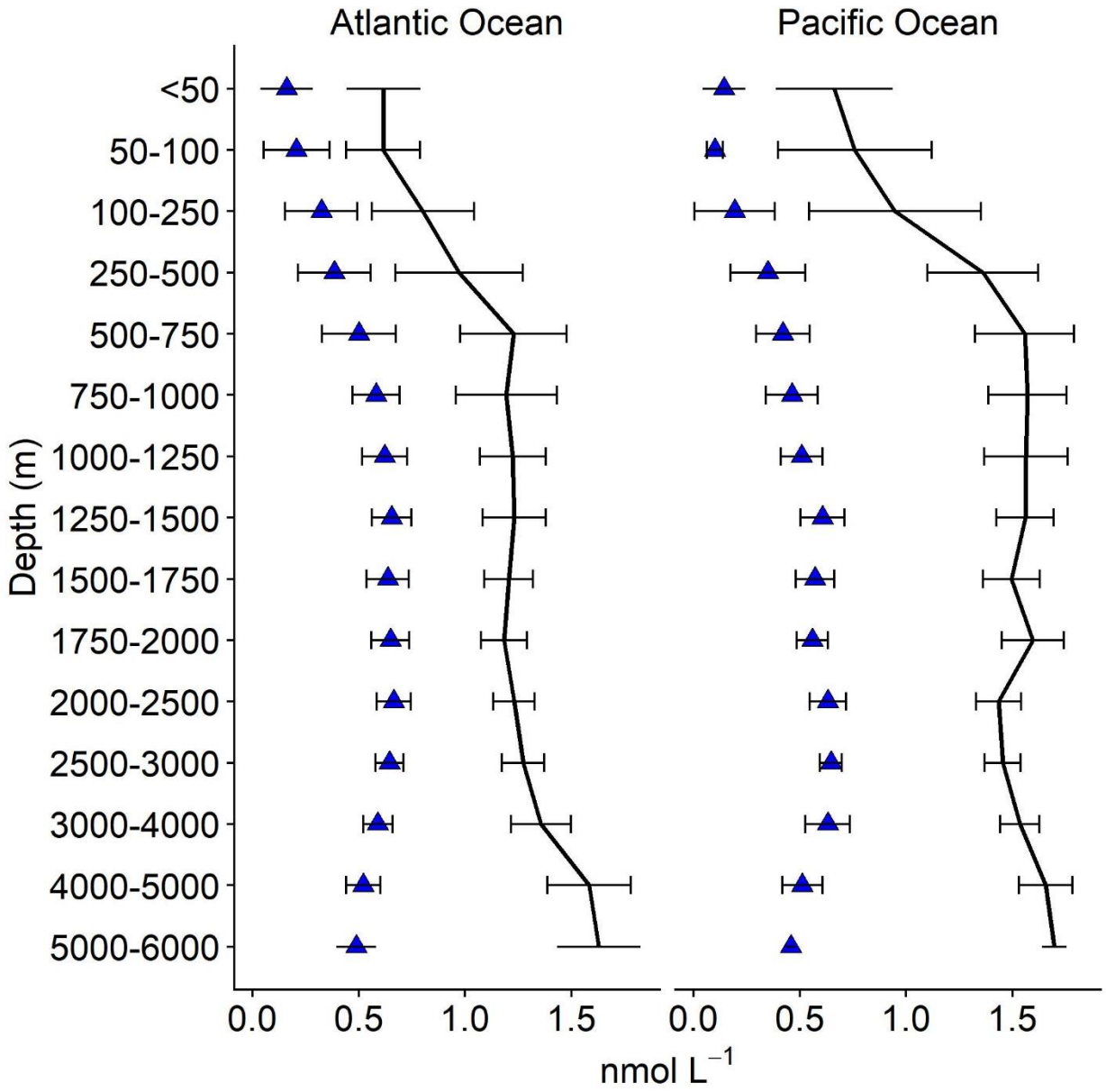

Figure 5. The depth profiles of horizontally averaged apparent Fe(III) solubility ($SFe(III)_{app}$, solid line) and dissolved Fe (DFe, blue triangle points). $SFe(III)_{app}$ was calculated using the NICA-Donnan model at ambient ocean pH, temperature and dissolved organic carbon concentrations for the Atlantic Ocean (a West Atlantic transect and Subtropical North Atlantic transect) and Pacific Ocean (a Southeast Pacific transect). Panel A, n= 1079 and 798 profiles for

DFe and $SFe(III)_{app}$, respectively; panel B, n= 492 and 555 profiles for DFe and $SFe(III)_{app}$, respectively. We omitted measured DFe profiles that were strongly influenced by source signatures from e.g. hydrothermal vents, atmospheric dust and suboxic sediment inputs in both ocean basins (Fitzsimmons et al., 2014; Rijkenberg et al., 2014; Milne et al., 2017).

We observed a similar trend in the vertical distributions of horizontally averaged DFe and $SFe(III)_{app}$ in the top 2000 m at the basin scale, i.e. both DFe and $SFe(III)_{app}$ have regeneration-like depth profiles (Figure 5). There were similar correlation coefficients between DFe to nutrients ($r_{(DFe\text{-}phosphate)} = 0.44$; $r_{(DFe\text{-}silicate)} = 0.55$), and DFe to $SFe(III)_{app}$ ($r_{(DFe\text{-}SFe(III)app)} = 0.5$) (Figure S1). Regeneration-like (or nutrient-like) profiles are assumed to arise from remineralized organic matter, which transfers particulate elements to dissolved phase. However, the low solubility and particle reactivity of Fe leads to a hybrid type distribution indicating that Fe is also removed from dissolved phase via scavenging or precipitation. Figure 5 shows that the apparent solubility of Fe increases with depth in parallel with remineralization of organic matter. Remineralization simultaneously releases C_T and reduces the pH of water column. Whilst ambient temperature decreases with increasing depth. The depth profiles of DFe thus likely lies within a range defined at the lower limit by supply from remineralization and the upper limit by the apparent solubility of Fe.

We also calculated the ratios of measured DFe to predicted $SFe(III)_{app}$ across our transects. The overall relationships of modelled $SFe(III)_{app}$ and measured DFe was $DFe = 0.29\pm0.02*SFe(III)_{app} + 0.15\pm0.03$ ($r^2 = 0.29$, $p<0.001$, n= 439 profiles) for the Atlantic Ocean, and $DFe = 0.44\pm0.02*SFe(III)_{app} - 0.14\pm0.02$ ($r^2 = 0.71$, $p<0.001$, n= 333 profiles) for the Pacific Ocean. Figure 6 shows that distributions of the ratios of measured DFe to predicted $SFe(III)_{app}$ were apparently influenced by source signatures, such as atmospheric dust input and hydrothermal vents in the West Atlantic leading to ratios of DFe/DFe > 0.7, or sediments fluxes and hydrothermal vents in the Southeast Pacific leading to values >0.6. However, away from these source-influenced waters, similar values of $DFe/SFe(III)_{app}$ through the water column indicated that DFe depth profiles likely reflected relative changes in the $SFe(III)_{app}$. Differences in the upper 200 m could be associated with biological uptake of Fe in the (sub)surface layer (Cullen, 2015). In addition, a potential dilution of the Fe-binding DOM pool by enhanced primary

production, could invalidate the assumption that binding sites scale to DOC (see Chapter 3). Below 2000 m, there could be several reasons for the differences between $SFe(III)_{app}$ and DFe. Firstly, the solubility constants of Fe hydroxide ($Fe(OH)_3(s)$, as ferrihydrite assumed in the work) applied in our calculations are representative of relatively fresh (one week old) precipitates and thus comprise an upper limit for Fe solubility in seawater (Byrne et al., 2000; Liu and Millero, 2002). Aging of ferrihydrite leads to conformational changes within the minerals that decreases solubility with time (Raiswell et al., 2010). Furthermore, the impact of temperature strongly affects the vertical distribution of Fe(III) hydroxide solubility based on derived solubility constants of $Fe(OH)_3(s)$ derived from Liu and Millero (1999). Secondly, although a major fraction of the marine DOM pool is thought to be recalcitrant, especially in deep old waters (Hansell, 2013), the diversity of functional groups are likely to be subject to spatial-temporal changes (Hansman et al., 2015; Medeiros et al., 2015). Such variability could result in differences in predicted $SFe(III)_{app}$, since the NICA constants used to calculate $SFe(III)_{app}$ in this work were derived from titrations undertaken on samples dominated by waters <800 m (see Chapter 4). Thirdly, differences in trends in the distributions of $SFe(III)_{app}$ and DFe in deep waters could also be related to source signatures of the transported water masses. For example, Antarctic Bottom Water formed in the Southern Ocean reflects low DFe concentrations in source waters (Figure 2). Furthermore, our calculations of $SFe(III)_{app}$ do not included non-equilibrium process, such as the scavenging (Johnson et al., 1997; Tagliabue et al., 2016; Ye et al., 2020).

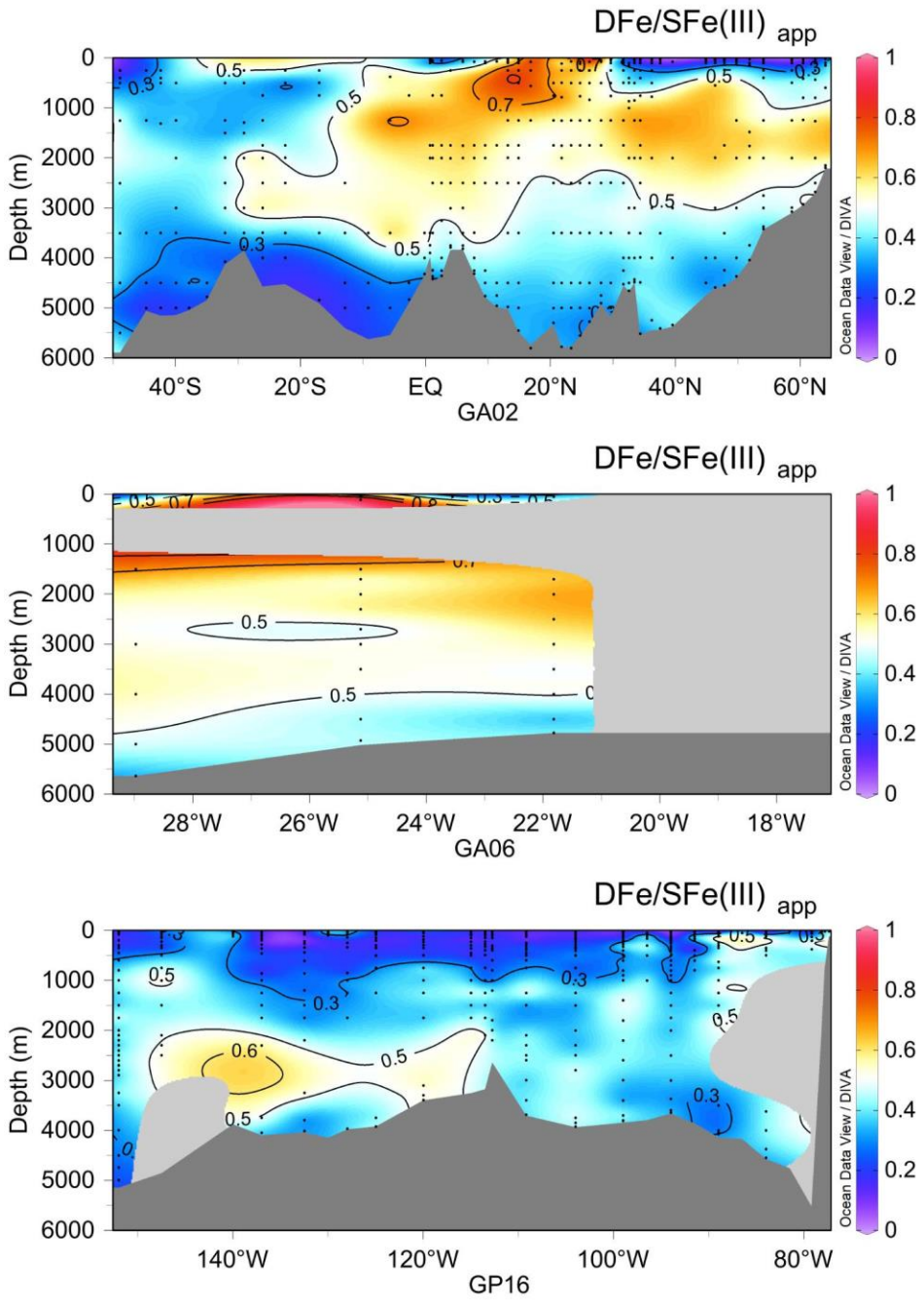

Figure 6. Ratios of measured dissolved Fe (DFe) to modelled apparent Fe(III) solubility ($SFe(III)_{app}$) that was calculated using the NICA-Donnan model at ambient ocean pH, temperature and dissolved organic carbon concentrations, shown for a West Atlantic transect (GA02), Subtropical North Atlantic transect (GA06) and Southeast Pacific transect (GP16). We omitted measured DFe profiles that strongly influenced by source signatures from e.g.

hydrothermal vents, atmospheric dust and suboxic sediment inputs in both ocean basins (Fitzsimmons et al., 2014; Rijkenberg et al., 2014; Milne et al., 2017).

5.4.2 Both pH and temperature affect the apparent iron solubility in the deep ocean

A global biogeochemical model (REcoM) combined the parameterized constants calculated using the NICA-Donnan model, and suggests pH is more important than DOC for determining the speciation and solubility of Fe in seawater (Ye et al., 2020). Here we investigated the factors influencing the $SFe(III)_{app}$ at the basin scale, using data obtained from the Atlantic and Pacific Oceans, in order to understand which physico-chemical parameters (pH, temperature) have the most impact on $SFe(III)_{app}$ and thus have the potential to further impact on the DFe inventory.

Figures 2, 3 and 4 show that a large gradient was observed in pH distributions through the water column, while distributions of DOC concentrations mostly varied in the upper 200 m and DOC concentrations were 41.9±6.2 µmol L^{-1}, n= 1085 below 200 m. In addition, ambient ocean temperature showed a strong vertical gradient that decreased from >20°C in surface waters (>50 m) to <2.5 °C below ~3000 m in the Atlantic Ocean, and below ~2000 m in the Pacific Ocean (Figure S2). We plotted $SFe(III)_{app}$ versus pH_{tot} using the data collected below 200 m, with points colored according to ambient temperature. Our results showed that modelled $SFe(III)_{app}$ increased with decreasing pH_{tot} from the Atlantic (West Atlantic transect and Subtropical North Atlantic transect) to the Pacific (Southeast Pacific transect), as well as from intermediate waters (~200-2000 m) to deep waters (>2000 m) (Figure 7). The negative slopes for pH-$SFe(III)_{app}$ were similar between the Atlantic Ocean and Pacific Ocean, and decreased from intermediate waters (Atlantic Ocean: y= -1.22±0.12 x + 10.8±0.93, r^2= 0.30; Pacific Ocean: y= -1.69±0.13 x + 14.5±1.0, r^2= 0.41) to deep waters (Atlantic Ocean: y= -3.04±0.11 x + 25.4±0.87, r^2= 0.75; Pacific Ocean: y= -3.18±0.14 x + 26.3±1.08, r^2= 0.78). These differences between slopes for pH-$SFe(III)_{app}$, likely reflect the relative changes in temperature distributions (Byrne et al., 2000; Liu and Millero, 2002; Raiswell et al., 2010). Our results suggest the increase in $SFe(III)_{app}$ with decreasing pH would be mitigated by lower solubility of Fe hydroxide in warmer seawaters. The impact of pH on $SFe(III)_{app}$ is not unexpected, since DFe concentrations has been observed to be

enhanced in the presence of excess particulate Fe, with decreasing pH as a result of ocean acidification during a coastal mesocosm experiment (Breitbarth et al., 2010).

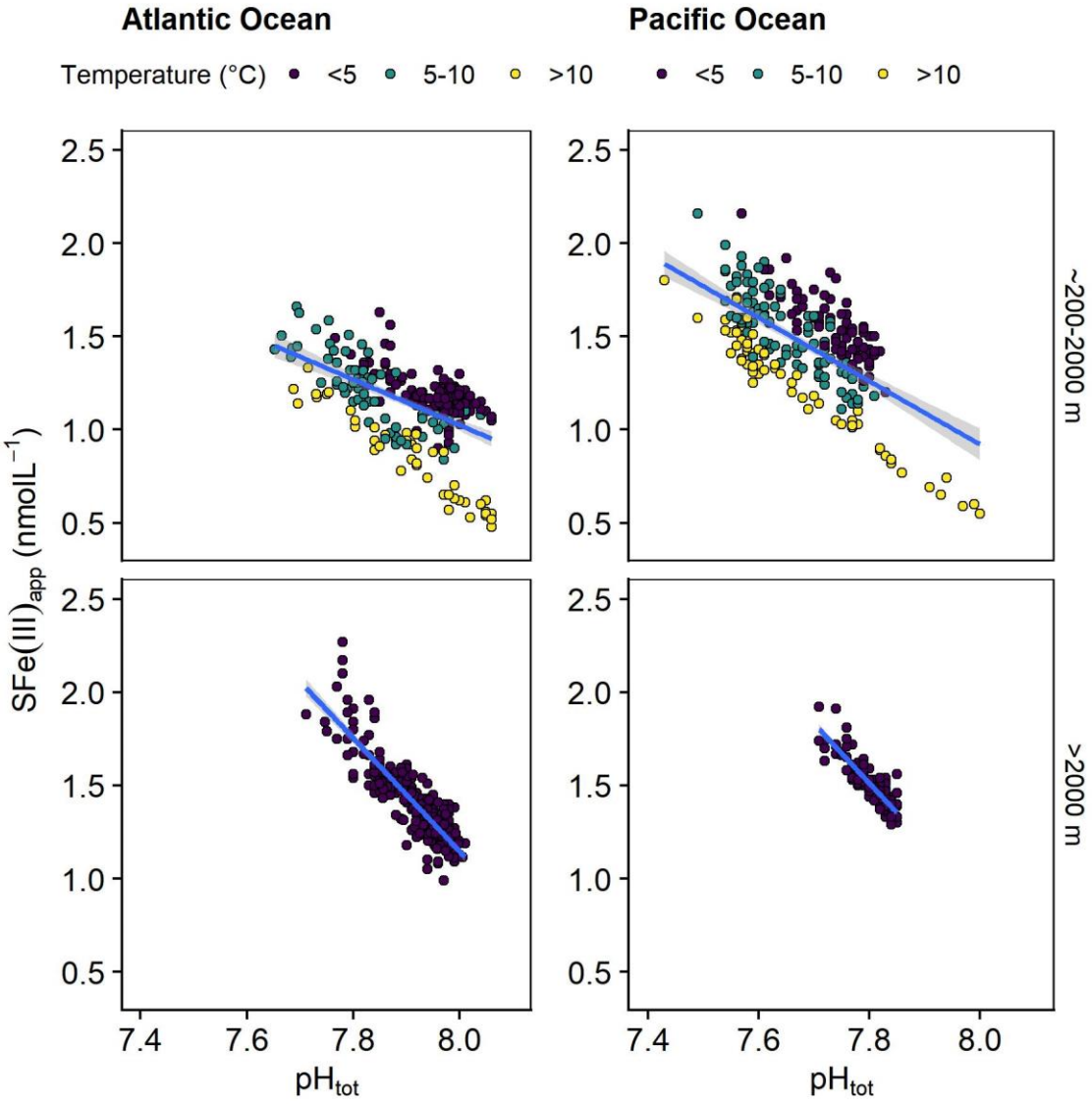

Figure 7. Apparent Fe(III) solubilities ($SFe(III)_{app}$) were calculated using the NICA-Donnan model in the ambient water column using the data collected below 200 m. $SFe(III)_{app}$ were plotted versus pH_{tot} (total scale) at the basin scale, which points are colored according to ambient temperature. Left: Atlantic Ocean (West Atlantic transect and Subtropical North Atlantic transect); Right: Pacific Ocean (Southeast Pacific transect).

To understand the combined impact of pH and temperature on $SFe(III)_{app}$, we further did a sensitivity analysis by doubling H^+ concentrations, resulting in a 0.3 unit decrease in pH_{tot}, and

calculated the $SFe(III)_{app}$ at ambient temperature and DOC concentrations. We used the data collected below 200 m in the Atlantic and Pacific Oceans (West Atlantic transect, Subtropical North Atlantic transect and Southeast Pacific transect). Figure 8 shows that relative changes in predicted $SFe(III)_{app}$ ($\Delta SFe(III)_{app}$) ranged from increases of 21% to 164%. An increase over 150% in $\Delta SFe(III)_{app}$ was observed when ambient pH_{tot} and temperature both showed lower values (<7.8 and <5 °C, respectively). Condisdering ambient temperature was between 10-15 °C, the decrease in pH_{tot} resulted in a doubling of $\Delta SFe(III)_{app}$. On the other hand, when ambient temperature was higher e.g. over 20°C, the $\Delta SFe(III)_{app}$ was strongly influenced by the relative change in pH at basin scales, but the impact of decreasing pH was mitigated by low solubility of Fe hydroxide that driven by high temperature. Overall, our results indicate that pH has a strong impact on $SFe(III)_{app}$, although increased temperature (or warmer waters) reduces the solubility of Fe hydroxide and thus mitigates that impact of decreasing pH in seawater.

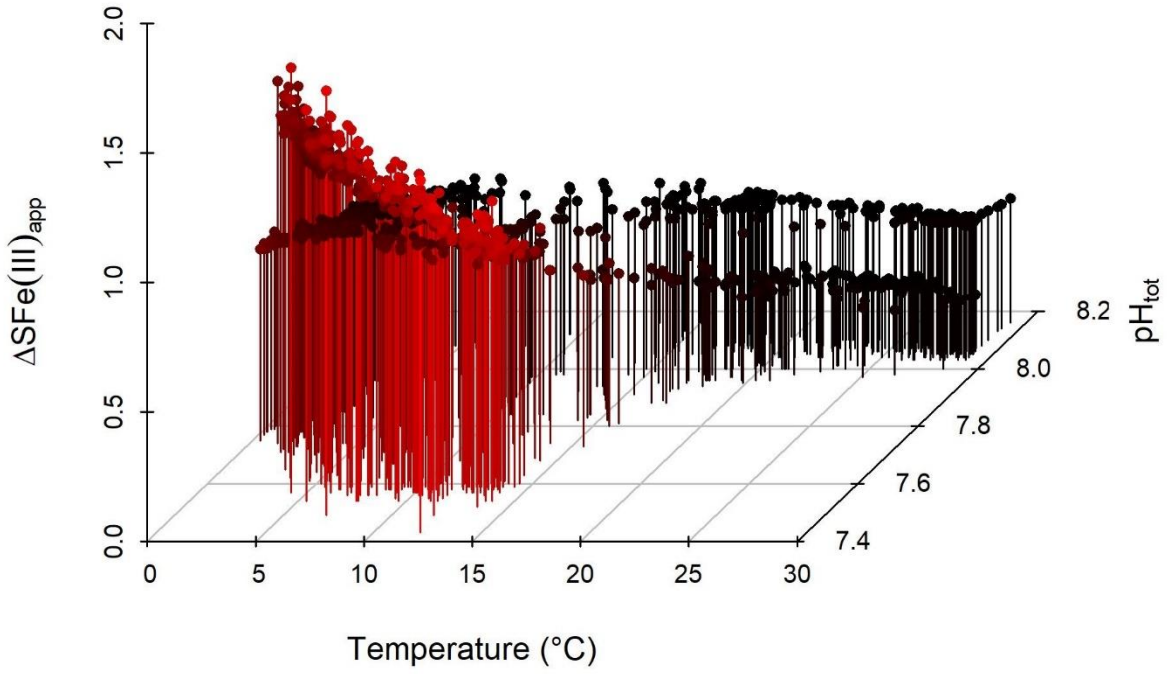

Figure 8. Visualization of the sensitivity of change in the apparent Fe(III) solubility ($\Delta SFe(III)_{app}$) for a doubling of H^+ concentration, as a function of ambient temperature and pH_{tot}, using the data collected below 200 m in the Atlantic and Pacific Oceans (West Atlantic transect, Subtropical North Atlantic transect and Southeast Pacific transect). The point color is highlighted with respect to the pH_{tot} scale, where decreasing pH shown as changing from black to red.

5.4.3 The combined impact of pH and low oxygen conditions in the Subtropical North Atlantic and Peruvian shelf and slope

The ocean is currently experiencing warming, acidification and deoxygenation. Increasing temperatures decrease the solubility of oxygen in surface waters and enhance stratification with a consequent reduction in the ventilation of the ocean interior (Bopp et al., 2002; Stramma et al., 2009). (Stramma et al., 2008b) reported a vertical expansion of the OMZ in the eastern tropical Atlantic and equatorial Pacific. Previous work using the NICA-Donnan model has shown that decreasing pH values as a result of intense remineralization of organic matter and ocean acidification could increase the apparent solubility of Fe with consequences for the surface DFe inventory of the Peruvian shelf and slope region (see Chapter 4). Here we further investigate this combined impact of pH and low oxygen conditions on the apparent solubility of Fe, by comparing the calculations in the Subtropical North Atlantic and Peruvian shelf and slope.

In surface waters (<50 m), overall, modelled $SFe(III)_{app}$ showed lower values (<0.4 nmol L^{-1}) in the Subtropical North Atlantic (Figure 3) than on the Peruvian shelf and slope (ca. 0.9 nmol L^{-1}). In the interior of OMZs, values of modelled $SFe(III)_{app}$ were similar for the Subtropical North Atlantic and Peruvian shelf and slope, but the highest value of $SFe(III)_{app}$ predicted over the Peruvian shelf and slope was up to ca. 3 nmol L^{-1}, and ca. 1.7 nmol L^{-1} for the Subtropical North Atlantic. Differences in the distributions of $SFe(III)_{app}$ between in the Subtropical North Atlantic and Peruvian shelf and slope were predominantly determined by variations in pH distributions. The pH_{tot} values observed in the Subtropical North Atlantic (Figure 3) were ca. pH_{tot} 8.1 in surface waters and ca. pH_{tot} 7.7 in the interior of the OMZ , and ca. pH_{tot} 8.0 in surface waters and ca. pH_{tot} 7.2 in the interior of the OMZ of the Peruvian shelf and slope (see Chapter 4). The distributions of DOC concentrations and temperature were similar across these regions (Figure 4, S2 and see Chapter 4). The higher modelled $SFe(III)_{app}$ observed in surface waters (<50 m) of the Peruvian shelf and slope resulted from low pH values as a consequence of upwelled acidic subsurface waters (Bates 2018).

Milne et al. (2017) compared the distributions of particulate Fe, labile particulate Fe and DFe in the Subtropical North Atlantic, suggesting a dynamic equilibrium between labile particulate and DFe phases whereby particles buffer the DFe and maintain elevated DFe concentrations especially in the open ocean waters. Here we compared the distributions of modelled $SFe(III)_{app}$ and measured DFe for the Subtropical North Atlantic (Figure 9). As observed for the Peruvian shelf and slope region, predicted $SFe(III)_{app}$ was similar to DFe measured in the upper 200 m and ~200-1000 m in offshore waters. Our work thus supports equilibrium conditions in the open ocean waters as reported by (Milne et al., 2017). In addition, Milne et al. (2017) showed lateral shelf fluxes of labile particulate Fe were similar in magnitude to observed soluble aerosol-Fe deposition. However, values of DFe and $SFe(III)_{app}$ were both higher in the OMZ (~200-1000 m) than that in the upper 200 m in offshore waters. This indicates that decreasing pH due to remineralization of organic matter, in combination with decreasing temperatures could increase the apparent solubility of Fe, and thus enhance the cap of Fe dissolved in the ambient water column.

Near the coast, elevated DFe was observed throughout the water column as a result of atmospheric dust inputs (Powell et al., 2015) and benthic release, and mostly exceeded the maximum predicted values of $SFe(III)_{app}$,. Considering those comparisons in the Subtropical North Atlantic and Peruvian shelf and slope, our results suggest the non-equilibrium process such as the production of Fe(II) and particulate Fe play a key role in maintaining elevated DFe concentrations, with enhanced $SFe(III)_{app}$ due to low pH values and an increase in solubility of Fe hydroxide by low temperatures.

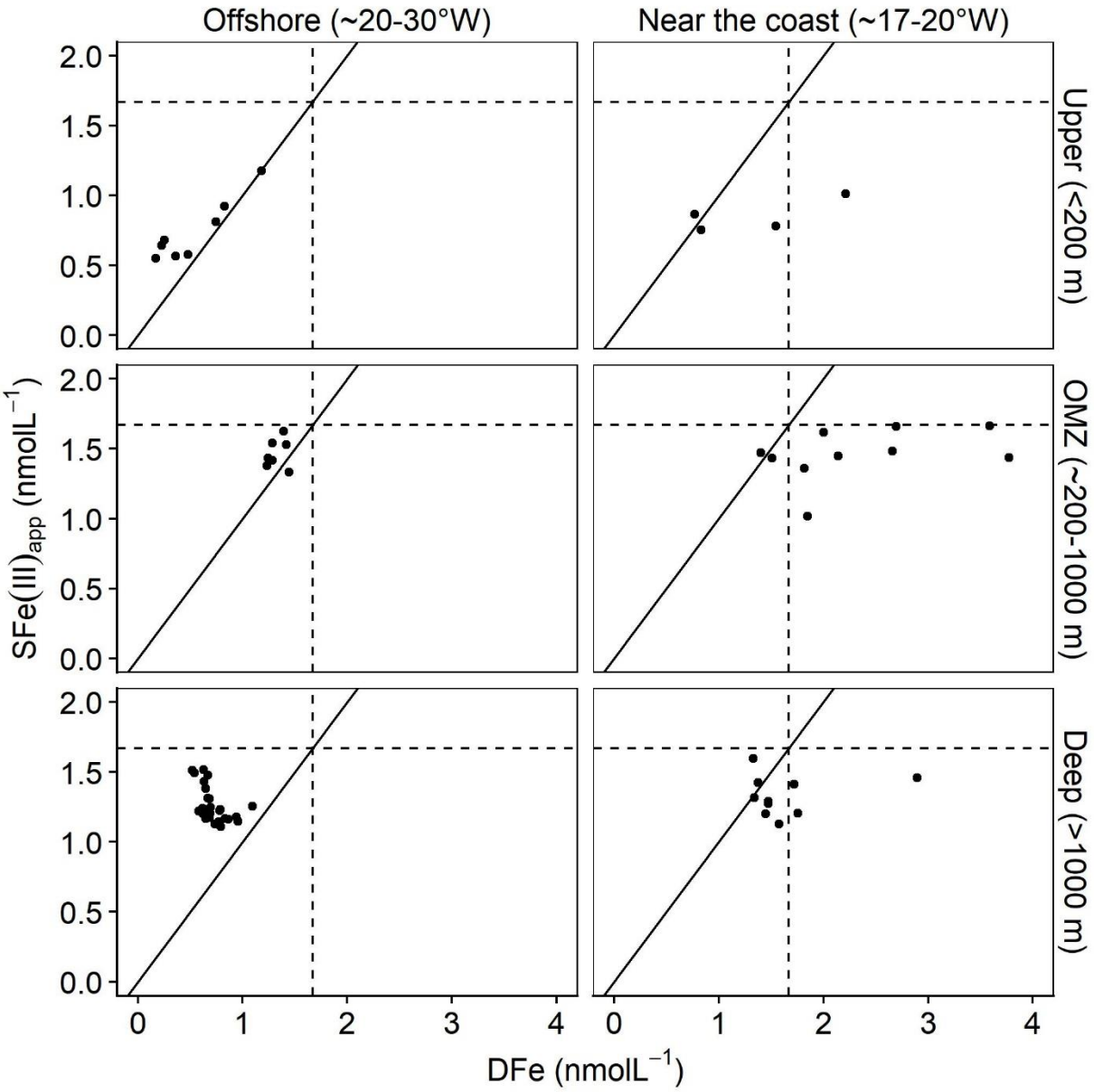

Figure 9. Apparent Fe solubilities ($SFe(III)_{app}$) calculated using the NICA-Donnan model in the ambient water column, plotted versus measured dissolved Fe (DFe) in the Subtropical North Atlantic. The solid lines have a slope of 1, while the dashed lines are equal to the maximum concentrations of modelled $SFe(III)_{app}$ (1.67 nmol L^{-1}).

5.4.4 Implications for future changes in ocean pH

Shi et al. (2010) reported a decrease in Fe bioavailability as a result of ocean acidification from laboratory culture experiments using various Fe chelates. The Fe requirement of model phytoplankton remained unchanged with increasing CO_2, however a slower uptake by a model diatom with decreasing pH was observed in the experiments. This indicates that decreased Fe availability was a result of changes in Fe speciation rather than changes in the uptake process. A few studies have addressed the impact on trace metals speciation of a decrease in pH as a result of ocean acidification. Millero et al. (2009) used a Pitzer interaction model, and examined the effect of ocean acidification on inorganic complexation of trace metals. They indicated a 40% increase in solubility of inorganic Fe(III) with pH_{NBS} decreasing from 8.1 to 7.4. However changes in organic complexation of Fe that controls Fe speciation remains largely unclear. Using the NICA-Donnan model with generic constants, Gledhill et al. (2015) suggested a decrease in Fe(III) binding to organic matter and an 3-fold increase in inorganic Fe(III) complexes at lower pH_{NBS} (7.41) compared to pH_{NBS} 8.18. This is in contrast to results by Stockdale et al. (2016) who used the WHAM/Model VII and showed an increase in the organic Fe(III) binding fraction and free Fe (Fe^{3+}) concentration and decreases in inorganic complexes as a result of ocean acidification. Both model results suggested Fe may become more available for marine organisms responding to ocean acidification.

Our work aims to mechanistically describe relative changes in the apparent Fe(III) solubility as a function of pH, temperature and DOM with potential impact on the overall DFe inventory. This provides a way to assess the maximum dissolved Fe concentrations under the ambient seawater condition, rather than describing certain changes in different Fe species. To date, Zark et al. (2015) has shown effects of ocean acidification on marine DOM are not detectable over a succession phytoplankton growth during mesocosm experiments, suggesting relative changes in DOM composition could be less to include into the calculation over a temporal period.

Considering our results, a 0.3 unit decrease in pH_{tot} could result in 21% to 164% increase in $SFe(III)_{app}$, while the increases are affected by the solubility gradient of Fe hydroxide that is driven by ambient temperature across ocean basins. For example, the Southern Ocean is one of most important sinks of natural and anthropogenic CO_2 (Sabine et al., 2004; Gruber et al., 2009). Fe limitation has been observed in the Southern Ocean (Boyd et al. 2007). Icebergs are thought

to be one of the largest Fe sources (3.9-30.5 Gmol Fe yr^{-1}) to both the Arctic and Southern Oceans (Boyd et al., 2012). Smith et al. (2007) reported increased iceberg fluxes could result in enrichment of iceberg derived terrigenous material (e.g. organic matter and Fe), and thus increase the abundance of phytoplankton. As a pH decrease combined with a higher solubility of Fe hydroxide resulting from low temperatures in sub surface waters, then increases in $SFe(III)_{app}$ could enhance caps of the maximum DFe concentrations and therefore facilitate the supply of DFe to surface waters. However, increasing ocean surface temperature could reversely reduce those impacts of decreasing pH on surface DFe inventories. Therefore, the way of calculating the apparent solubility of Fe(III) could be used to combine with other global biogeochemical models, to modify relative changes in the primary productivity.

5.5 Conclusions

We derived the apparent Fe(III) solubility at ambient ocean temperature, pH and DOC concentrations, using the NICA-Donnan model applying the newly derived proton/Fe(III) NICA constants for marine DOM. Using data obtained during a series of GEOTRACES cruises, we investigated the correlations between modelled $SFe(III)_{app}$ and measured DFe at basin scales. A similar trend was observed in the vertical distributions of horizontally averaged $SFe(III)_{app}$ and DFe, especially in the top 2000 m, suggesting DFe distributions were largely influenced by sources, but the underlying distributions of DFe could also be potentially regulated by $SFe(III)_{app}$. Statistical analysis suggests that vertical DFe distributions are determined by remineralization of sinking organic matter, and also by relative changes in ambient pH and temperature. We observed large gradients in the vertical and horizontal distributions of ocean pH and temperature, compared to rather constant distributions of DOC concentrations especially observed below 200 m (41.9±6.2 μmol L^{-1}). A further sensitivity test indicates pH largely affected the $SFe(III)_{app}$ through the water column, based on a solubility gradient of Fe hydroxide influenced by ambient temperature especially in deep waters (>2000 m). Our results reaffirm that considerations of the impact of changes in ambient pH and temperature are important for Fe cycling in the ocean. We highlight that the calculation of the apparent Fe(III) solubility is useful for constraining the maximum potential DFe concentrations, based on the dynamic equilibrium of the production of Fe and scavenging process. However, given the uncertainties of acid-base

properties of marine DOM and Fe-binding constants used in the NICA-Donnan model, and also the solubility constants of Fe hydroxide (as ferrihydrite assumed in our calculations), it is difficult to conclude how the apparent solubility of Fe will change in response to decreasing pH as a result of ocean acidification. Therefore, further work is needed to characterize the behaviour of proton-/Fe- binding to marine DOM via such ion paring – organic matter model, e.g. NICA-Donnan and WHAM/Model VII.

Supporting Information

Figure S1. The correlation matrix among the apparent Fe(III) solubility ($SFe(III)_{app}$) that calculated using the NICA-Donnan model, measured dissolved Fe (DFe), pH_{tot} (total scale), temperature and dissolved organic carbon (DOC) concentrations, nutrients (phosphate and silicate), were shown using data obtained in the Atlantic and Pacific Oceans. We omitted measured DFe profiles that strongly influenced by source signatures from e.g. hydrothermal vents, atmospheric dust and suboxic sediment inputs in both ocean basins (Fitzsimmons et al., 2014; Rijkenberg et al., 2014; Milne et al., 2017).

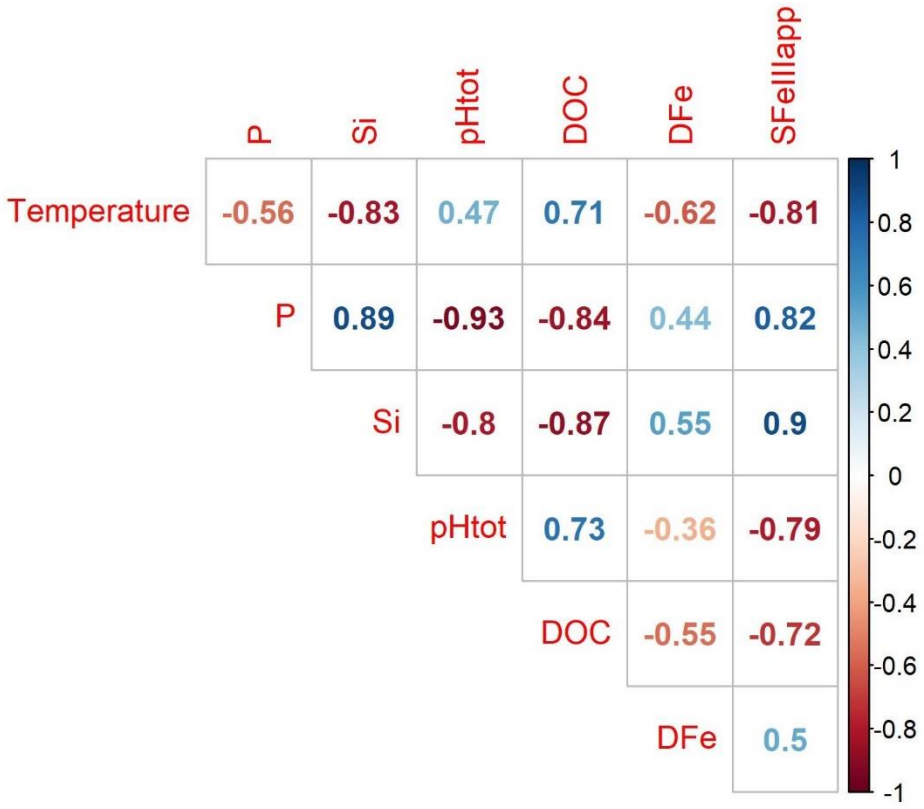

Figure S2. Distributions of ambient ocean temperature were shown for a West Atlantic transect (GA02), Subtropical North Atlantic transect (GA06) and Southeast Pacific transect (GP16).

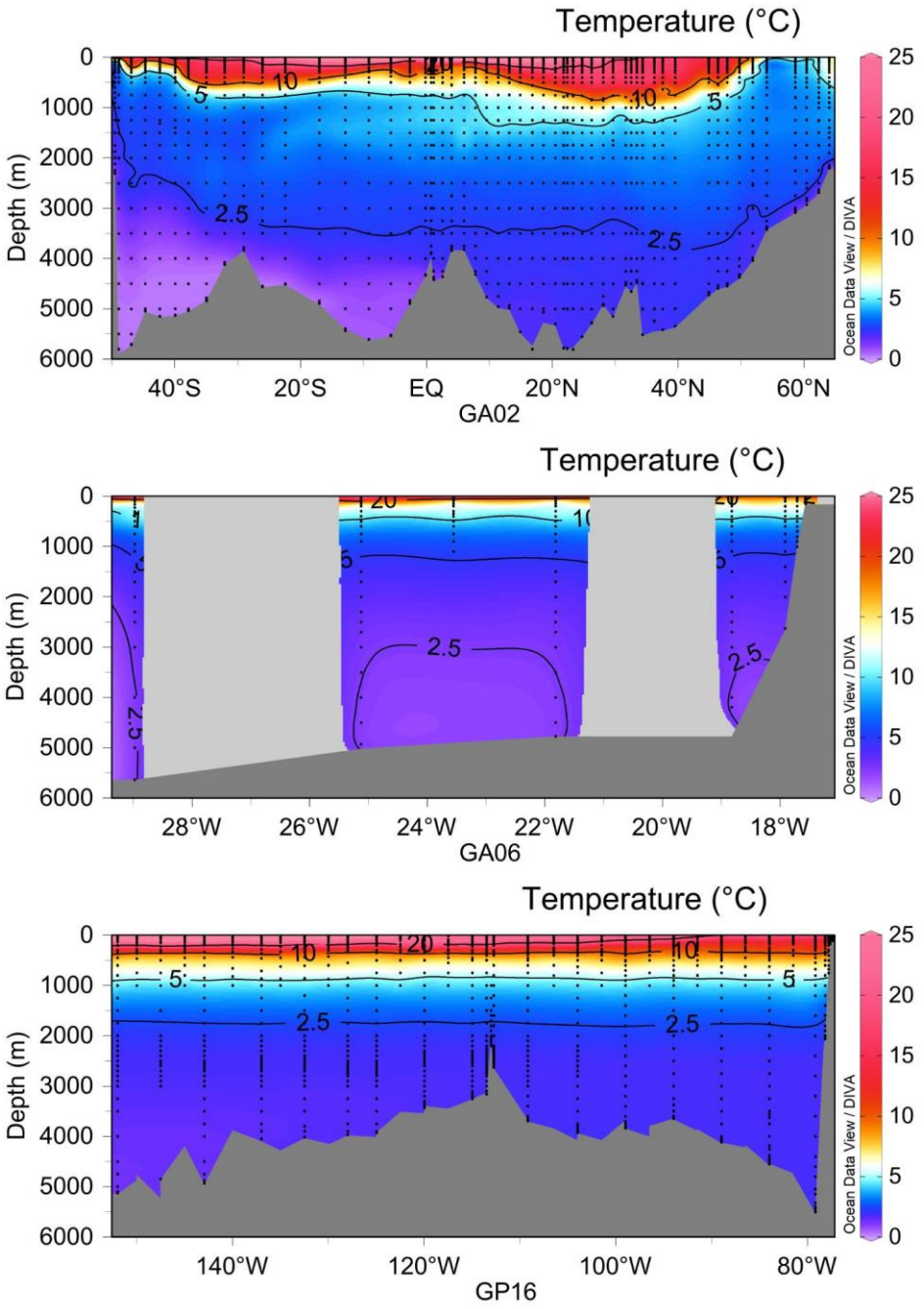

6 Conclusions and future works

The overall aim of this PhD project was to use an ion-paring-organic matter model (NICA-Donnan) to account for the impact of relative changes in seawater chemistry, such as pH, temperature and DOM, on the speciation and solubility of Fe, in order to better understand Fe biogeochemical cycling with respect to e.g. ocean warming, acidification and deoxygenation. I derived the apparent solubility of Fe(III) ($SFe(III)_{app}$) by setting the total Fe(III) to 10 nmol L^{-1} using ambient ocean pH, temperature and DOC concentrations. The $SFe(III)_{app}$ is defined as the sum of aqueous inorganic Fe(III) species and Fe(III) bound to DOM at a free Fe (Fe^{3+}) concentration equal to the limiting solubility of Fe hydroxide ($Fe(OH)_3(s)$). The term $SFe(III)_{app}$, therefore represents caps of the maximum Fe could be dissolved at equilibrium in the ambient water column.

6.1 Conclusions

In the absence of organic matter, I simulated pH-Fe titrations using a set of ion paring models via ORCHESTRA (Meeussen, 2003), and compared those results to determined titrations via CLE-AdCSV in UV-irradiated seawater (Chapter 3). The determined species of voltammetric analysis ($FeNN_3$) and most sensitive species (free Fe^{3+}) were regarded as the criteria to optimize the stability constant of $k_{FeNN3,H+}$ that would account for competition between NN^-, H^+, Fe^{3+} and OH^- at the ionic strengths and pH relevant to this thesis. The results indicated that titration experiments - speciation calculation framework were of adequate consistency within the time frame, though uncertainties of both equilibrium conditions during titration and underestimations of ionic strength using the Debye-Hückel equation would be expected to have an impact on the comparisons.

In the presence of organic matter, I simulated pH-Fe titrations using an ion paring-organic matter model (NICA-Donnan) via ORCHESTRA, and compared those results to determined titrations via CLE-AdCSV in seawater samples collected in the Celtic Sea (Chapter 3). The determined species in voltammetric analysis ($FeNN_3$), most sensitive species (free Fe^{3+}) and non-labile fraction of Fe (DFe*=total Fe- FeNN3), were regarded as the criteria to optimize the model with

four different NICA parameter sets representing a range of binding site strengths and heterogeneities. I also examined the assumption that the binding sites used in the NICA-Donnan model scale proportionally to DOC concentrations. The results showed that fits improved on application of a constant low DOC concentration of 43.7 µmol L^{-1} across the data set, rather than assuming that binding scaled to ambient DOC concentrations. This suggests that binding sites could be diluted by fresh inputs of DOM that result from phytoplankton productivity, and may be more strongly linked to the refractory component of marine DOM. The results highlight an important role of pH in the derivations of NICA constants for Fe(III) binding to marine DOM.

In Chapter 3, using the NICA-Donnan parameters that fitted most closely to our titration data, calculated $SFe(III)_{app}$ concentrations (ca. 0.9 nmol L^{-1}) were within the range of the water column DFe concentrations observed on the Celtic shelf following winter mixing and also within the range of DFe concentrations for the furthest off-shore deep waters. In surface waters DFe concentrations were lower than $SFe(III)_{app}$ as result of the drawdown of DFe by phytoplankton. On the shelf in July and November and over the shelf break, DFe exceeded $SFe(III)_{app}$ in deeper waters close to the seafloor, which could potentially be ascribed to inputs of DFe from remineralization and sediments. The results shown in the Celtic Sea supports the hypothesis that distributions of DFe likely reflect the interplay between regeneration of Fe from remineralization of organic matter, the scavenging process and the solubility of Fe .

The use of intrinsic binding parameters for Fe binding to DOM (e.g. via the NICA-Donnan model) has been shown to allow for more confident disentangling of the different processes affecting the DFe inventory. Therefore, in Chapter 4, I applied a novel two dimensional pH-Fe titration experimental design that incorporates changes in pH. Using newly derived total amounts of binding sites ($Q_{max,H+,1or2}$) from marine DOM preconcentrated from the brackish Baltic Sea (Lodeiro et al., 2020), I derived NICA constants for Fe(III) binding to marine DOM from samples collected in the Peruvian shelf and slope region, via the approach PEST-ORCHESTRA (Janot et al., 2017). The derived Fe(III) NICA constants suggest Fe(III) binding to marine DOM behaves more ideally, compared to generic constants derived from fresh water environment (Milne et al., 2003).

In Chapter 4 and 5, using the newly derived proton/Fe(III) constants for marine DOM (Lodeiro et al., 2020, Zhu et al. Submitted), I investigated the speciation and solubility of Fe in the ambient water column from the Peruvian shelf and slope region to basin scales. In the Peruvian shelf and slope region (Chapter 4), modelled $SFe(III)_{app}$ showed a ca. 2 fold increase in OMZ compared to surface waters. The increase results from one order of magnitude decrease in pH, which impacts both the solubility of Fe hydroxide and organic Fe complexation. The results highlight an important role of pH and temperature on iron speciation and solubility, similarly as the DOM pool (or Fe-binding ligands). Also, the redox process has been reported to strongly affect the DFe pool on the Peruvian shelf (Croot et al., 2019). Thus I adopted a new way to account for that impact of Fe(II) production by calculating the dissolved Fe(III) concentrations (DFe-FeII). Comparisons of modelled $SFe(III)_{app}$ and measured DFe(III), with a further correlations test, indicate the underlying distribution of DFe(III) likely reflects changes in ambient pH and temperature.

The role of pH and temperature on the speciation and solubility has been further examined at basin scales (Chapter 5). Using data obtained during a series of GEOTRACES cruises, a similar trend was observed in the vertical distributions of horizontally averaged $SFe(III)_{app}$ and DFe, especially in the top 2000 m, suggesting DFe distributions were largely influenced by sources, but the underlying distributions of DFe could also be potentially regulated by $SFe(III)_{app}$. Statistical analysis suggested that DFe vertical distributions are determined by remineralization of sinking organic matter, and also by relative changes in ambient pH and temperature.

Large gradients in the vertical and horizontal distributions of ocean pH and temperature were observed at basin scales, compared to rather constant distributions of DOC concentrations especially observed below 200 m. The results show pH has a large impact on the $SFe(III)_{app}$ through the water column, based on a solubility gradient of Fe hydroxide influenced by ambient temperature especially in deep waters (>2000 m). This reaffirms that considerations of the impact of changes in ambient pH and temperature is as important for Fe cycling in the ocean.

This thesis highlights the way of calculating the apparent Fe(III) solubility that accounts for the impact of relative changes in ambient ocean pH, temperature and DOC concentrations, is useful

for constraining the maximum potential DFe concentrations, based on the dynamic equilibrium of the production of Fe and the scavenging process. Combining with other global biogeochemical models, it would be helpful to improve our understanding of Fe cycling in seawater, e.g. a preliminary work described in (Ye et al., 2020). To date, Those calculations made in the thesis are a simplification of the real system since it does not account for non-equilibrium processes and the physical size of our $SFe(III)_{app}$ fraction may not map directly onto the DFe concentration.

6.2 Future works

Ion paring-organic matter models (e.g. using NICA-Donnan or WHAM/Model VII) have been shown to provide consistent results with determinations of metal speciation in seawater (Hiemstra and van Riemsdijk, 2006; Stockdale et al., 2011, 2015; Gledhill et al., 2015; Avendaño et al., 2016). On the other hand, calculations of the speciation and solubility of Fe shown in this thesis provide a way to improve our understanding of Fe biogeochemical cycling under changing ocean chemistry conditions. Future research should therefore focus on calculations of the ion paring-organic matter model (e.g. using NICA-Donnan or WHAM/Model VII) applied in seawater.

Firstly, studies of the chemical speciation of any metal require calculations of both inorganic and organic speciation, which are typically performed using equilibrium calculation tools. In chemical equilibrium calculations, activity is a key parameter that describes how ions in solution interact with each other as well as with water molecules. The importance of these interactions increases with salt concentration. At higher ionic strength, ions behave chemically like they are less concentrated than they really are, and the activity coefficient is used to calculate the actual concentration. The impact of the ion pairing approach is illustrated by an approximate 15% underestimation in ionic strength in the calculation (I=0.6 M) based on the extended Debye-Hückel equation. This is consistent with previous estimates of the error introduced by application of the Debye-Hückel equation (Stockdale et al., 2016). Gledhill et al. (2015) has shown this leads to underestimation of carbonate concentration in visual MINTEQ that would result in a bias for copper speciation since the inorganic speciation of copper is strongly influenced by carbonate

complexation (Millero et al., 2009). Many efforts have been made to develop the Pitzer interaction model and subsequently calculate dissolved components in seawater (Turner et al., 2016). However, the application of the Pitzer interaction model in combination with metal-organic matter model is much more complex, since the difficulties present in the execution program of chemical speciation calculation tools. Recently, a chemical speciation tool, ORCHESTRA (Meeussen, 2003), has been shown that an alternative ion activity model (i.e. specific ion interaction theory, SIT) is successfully testified instead of using the Davies equation. Similarly, the flexible definitions in ORCHESTRA provide an opportunity to allow the combination of the Pitzer interaction model and NICA-Donnan model to calculate Fe speciation at high ionic strength in seawater.

In addition, in the presence of organic matter, such calculations using the NICA-Donnan model in this thesis assumes that the bulk properties of marine DOM can be represented by a limited number of binding site coefficients that describe intrinsic affinities between cations and different types or groups of binding sites. Furthermore, it is assumed that both groups of marine DOM binding sites (i.e. via the NICA-Donnan model) scale proportionally with DOC. Marine DOM has been shown to have a lower total amount of available proton binding sites within both the carboxylic and phenolic fractions (Lodeiro et al., 2020) in comparison to generic fulvic acid (Milne et al., 2001), though those constants for marine DOM are only evaluated from the brackish Baltic Sea. A study of individual molecular component of DOM from a set of four marine and one freshwater environments, indicates there is likely a universal background of DOM structures as a result of a cascade of degradation processes or common synthetic pathways (Zark and Dittmar, 2018). Further work could be useful to investigate the acid-base properties of marine DOM from surface to deep waters, coastal to open ocean, though there are still challenges with the efficiency on the preconcentrated marine DOM (Li et al., 2016, 2017).

Also, the fully understanding of Fe biogeochemical cycling should consider the ambient physico-chemical speciation of Fe. For example, size-fractionation of the DFe pool suggests that as much as 50 % of the DFe pool could be present as colloids (0.02-0.2 μm) (Cullen et al., 2006; Boye et al., 2010; Fitzsimmons et al., 2015). The non-equilibrium processes have also an important impact on DFe inventories, e.g. the production of Fe(II) strongly influences the distribution of

DFe in the Peruvian shelf (Croot et al., 2019). However, given our DOM fraction was determined as the <0.7 µm fraction, it is not straightforward to map the chemical speciation calculations we made in this study onto size fractions (soluble, colloidal, dissolved) that are typically determined in field studies. Therefore, further considerations of those impact on the speciation and solubility of Fe should be examined, e.g. calculating the dissolved Fe(III) (DFe-FeII) to accounts for the impact of Fe(II) production when comparing the modelled and measured results in the Peruvian OMZ (Chapter 4).

Finally, the way shown in this thesis could be further applied for other metals that binding to organic matter in seawater. The biogeochemistry of the transition metals (TMs) manganese (Mn), iron (Fe), cobalt (Co), nickel (Ni), copper (Cu), zinc (Zn), cadmium (Cd) and lead (Pb) have been shown to be either important essential trace nutrients (TM-nuts) for microbial growth (Mn, Fe, Co, Cu, Ni, Zn (Moore et al., 2013)) or toxic (TM-tox) at elevated concentrations (Cu, Cd, Pb, Zn). For example, in most surface waters, organic complexation dominates the speciation of Zn and reduces the fractions of free ions Zn^{2+} to levels as low as 1 pmol L^{-1} (Bruland et al., 1991; Ellwood and Van den Berg, 2000). Such calculations using an ion paring-organic matter model (NICA-Donnan), account for the impact of changes in the ambient water column and therefore predict the relative changes in Zn concentrations that would be as nutrient or toxic element for phytoplankton and bacteria (Sunda and Huntsman, 1996, 1998).

Future works on trace metals speciation should therefore couple different approaches, e.g. investigations on the structure (Koch et al., 2005), and acid-base properties of marine DOM (Lodeiro et al., 2020). In addition, interactions of trace metals complexed to organic matter would be possibly indirectly examined using mass spectrometry e.g. ICP-MS, in combination with thermodynamic calculations in future works. This may provide a way to investigate the organic complexation of more than one single trace metal at the same time, and therefore be useful to understand of the toxicity and bioavailability of trace metals with response to ocean acidification. In the future, trace metals speciation would be likely examined using intrinsic constants with collected data of pH, temperature and DOC concentrations. The calculations could be therefore associated with biogeochemical models, and enhance fully understanding of the cycling of trace metals.

References

Abraham, J. P., Baringer, M., Bindoff, N. L., Boyer, T., Cheng, L. J., Church, J. A., et al. (2013). A review of global ocean temperature observations: Implications for ocean heat content estimates and climate change. *Rev. Geophys.* 51, 450–483.

Abualhaija, M. M., and van den Berg, C. M. G. G. (2014). Chemical speciation of iron in seawater using catalytic cathodic stripping voltammetry with ligand competition against salicylaldoxime. *Mar. Chem.* 164, 60–74. doi:10.1016/j.marchem.2014.06.005.

Achterberg, E. P., Braungardt, C. B., Sandford, R. C., and Worsfold, P. J. (2001a). UV digestion of seawater samples prior to the determination of copper using flow injection with chemiluminescence detection. *Anal. Chim. Acta* 440, 27–36. doi:10.1016/S0003-2670(01)00824-8.

Achterberg, E. P., Holland, T. W., Bowie, A. R., Mantoura, R. F. C., and Worsfold, P. J. (2001b). Determination of iron in seawater. *Anal. Chim. Acta* 442, 1–14. doi:10.1016/S0003-2670(01)01091-1.

Achterberg, E. P., Moore, C. M., Henson, S. A., Steigenberger, S., Stohl, A., Eckhardt, S., et al. (2013). Natural iron fertilization by the Eyjafjallajökull volcanic eruption. *Geophys. Res. Lett.* 40, 921–926. doi:10.1002/grl.50221.

Achterberg, E. P., Steigenberger, S., Marsay, C. M., Lemoigne, F. A. C., Painter, S. C., Baker, A. R., et al. (2018). Iron Biogeochemistry in the High Latitude North Atlantic Ocean. *Sci. Rep.* 8. doi:10.1038/s41598-018-19472-1.

Adusei-Gyamfi, J., Ouddane, B., Rietveld, L., Cornard, J. P., and Criquet, J. (2019). Natural organic matter-cations complexation and its impact on water treatment: A critical review. *Water Res.* 160, 130–147. doi:10.1016/j.watres.2019.05.064.

Allen, A. E., LaRoche, J., Maheswari, U., Lommer, M., Schauer, N., Lopez, P. J., et al. (2008). Whole-cell response of the pennate diatom Phaeodactylum tricornutum to iron starvation. *Proc. Natl. Acad. Sci. U. S. A.* 105, 10438–10443. doi:10.1073/pnas.0711370105.

Ardiningsih, I., Zhu, K., Lodeiro, P., Gledhill, M., Reichart, G.-J., Achterberg, E. P., et al. (2021). Iron Speciation in Fram Strait and Over the Northeast Greenland Shelf: An Inter-Comparison Study of Voltammetric Methods. *Front. Mar. Sci.* 7, 1203. doi:10.3389/fmars.2020.609379.

Avendaño, L., Gledhill, M., Achterberg, E. P., Rérolle, V. M. C. C., and Schlosser, C. (2016). Influence of ocean acidification on the organic complexation of iron and copper in Northwest European shelf seas; a combined observational and model study. *Front. Mar. Sci.* 3, 1–19. doi:10.3389/fmars.2016.00058.

Badr, E. S. A., Achterberg, E. P., Tappin, A. D., Hill, S. J., and Braungardt, C. B. (2003). Determination of dissolved organic nitrogen in natural waters using high-temperature catalytic oxidation. *TrAC - Trends Anal. Chem.* 22, 819–827. doi:10.1016/S0165-9936(03)01202-0.

Barbeau, K. (2006). Photochemistry of organic iron (III) complexing ligands in oceanic systems. *Photochem. Photobiol.* 82, 1505–1516.

Barbeau, K., Rue, E. L., Trick, C. G., Bruland, K. W., and Butler, A. (2003). Photochemical reactivity of siderophores produced by marine heterotrophic bacteria and cyanobacteria based on characteristic Fe(III)

binding groups. *Limnol. Oceanogr.* 48, 1069–1078. doi:10.4319/lo.2003.48.3.1069.

Barrón, C., and Duarte, C. M. (2015). Dissolved organic carbon pools and export from the coastal ocean. *Global Biogeochem. Cycles* 29, 1725–1738. doi:https://doi.org/10.1002/2014GB005056.

Bates, N. R. (2018). Seawater carbonate chemistry distributions across the Eastern South Pacific Ocean sampled as part of the GEOTRACES project and changes in marine carbonate chemistry over the past 20 years. *Front. Mar. Sci.* 9, 1–18. doi:10.3389/fmars.2018.00398.

Benedetti, M. F. F., Van Riemsdijk, W. H. H., and Koopal, L. K. K. (1996). Humic substances considered as a heterogeneous Donnan gel phase. *Environ. Sci. Technol.* 30, 1805–1813. doi:10.1021/es950012y.

Bennett, S. A., Achterberg, E. P., Connelly, D. P., Statham, P. J., Fones, G. R., and German, C. R. (2008). The distribution and stabilisation of dissolved Fe in deep-sea hydrothermal plumes. *Earth Planet. Sci. Lett.* 270, 157–167. doi:10.1016/j.epsl.2008.01.048.

Berg, C. M. G. Van Den, and van den Berg, C. M. G. (2006). Chemical Speciation of Iron in Seawater by Cathodic Stripping Voltammetry with Dihydroxynaphthalene Chemical Speciation of Iron in Seawater by Cathodic Stripping Voltammetry with. *Anal. Chem.* 78, 156–63. doi:10.1021/ac051441.

Bergquist, B. A., and Boyle, E. A. (2006). Dissolved iron in the tropical and subtropical Atlantic Ocean. *Global Biogeochem. Cycles* 20, 1–14. doi:10.1029/2005GB002505.

Birchill, A. J., Milne, A., Woodward, E. M. S., Harris, C., Annett, A., Rusiecka, D., et al. (2017). Seasonal iron depletion in temperate shelf seas. *Geophys. Res. Lett.* 44, 8987–8996. doi:10.1002/2017GL073881.

Blain, S., Guieu, C., Claustre, H., Leblanc, K., Moutin, T., Quéguiner, B., et al. (2004). Availability of iron and major nutrients for phytoplankton in the northeast Atlantic Ocean. *Limnol. Oceanogr.* 49, 2095–2104. doi:10.4319/lo.2004.49.6.2095.

Boiteau, R. M., Mende, D. R., Hawco, N. J., McIlvin, M. R., Fitzsimmons, J. N., Saito, M. A., et al. (2016). Siderophore-based microbial adaptations to iron scarcity across the eastern Pacific Ocean. *Proc. Natl. Acad. Sci. U. S. A.* 113, 14237–14242. doi:10.1073/pnas.1608594113.

Bopp, L., Le Quéré, C., Heimann, M., Manning, A. C., and Monfray, P. (2002). Climate-induced oceanic oxygen fluxes: Implications for the contemporary carbon budget. *Global Biogeochem. Cycles* 16, 6-1-6–13. doi:10.1029/2001gb001445.

Boyd, P. W., Arrigo, K. R., Strzepek, R., and Van Dijken, G. L. (2012). Mapping phytoplankton iron utilization: Insights into Southern Ocean supply mechanisms. *J. Geophys. Res. Ocean.* 117.

Boyd, P. W., and Ellwood, M. J. (2010). The biogeochemical cycle of iron in the ocean. *Nat. Geosci.* 3, 675–682. doi:10.1038/ngeo964.

Boyd, P. W., Jickells, T., Law, C. S., Blain, S., Boyle, E. A., Buesseler, K. O., et al. (2007). Mesoscale iron enrichment experiments 1993-2005: Synthesis and future directions. *Science (80-.).* 315, 612–617. doi:10.1126/science.1131669.

Boye, M., Aldrich, A. P. A. P., van den Berg, C. M. G. C. M. G., de Jong, J. T. M. J. T. M., Veldhuis, M., and De Baar, H. J. W. H. J. W. (2003). Horizontal gradient of the chemical speciation of iron in surface waters of the northeast Atlantic Ocean. *Mar. Chem.* 80, 129–143. doi:10.1016/S0304-4203(02)00102-0.

Boye, M., Nishioka, J., Croot, P., Laan, P., Timmermans, K. R., Strass, V. H., et al. (2010). Significant portion of dissolved organic Fe complexes in fact is Fe colloids. *Mar. Chem.* 122, 20–27. doi:10.1016/j.marchem.2010.09.001.

Boye, M., Van Den Berg, C. M. G., De Jong, J. T. M., Leach, H., Croot, P., and De Baar, H. J. W. (2001). Organic complexation of iron in the Southern Ocean. *Deep. Res. Part I Oceanogr. Res. Pap.* 48, 1477–1497. doi:10.1016/S0967-0637(00)00099-6.

Boyle, E. A., Edmond, J. M., and Sholkovitz, E. R. (1977). The mechanism of iron removal in estuaries. *Geochim. Cosmochim. Acta* 41, 1313–1324. doi:10.1016/0016-7037(77)90075-8.

Brandt, P., Bange, H. W., Banyte, D., Dengler, M., Didwischus, S. H., Fischer, T., et al. (2015). On the role of circulation and mixing in the ventilation of oxygen minimum zones with a focus on the eastern tropical North Atlantic. *Biogeosciences* 12, 489–512. doi:10.5194/bg-12-489-2015.

Breitbarth, E., Bellerby, R. J., Neill, C. C., Ardelan, M. V., Meyerhöfer, M., Zöllner, E., et al. (2010). Ocean acidification affects iron speciation during a coastal seawater mesocosm experiment. *Biogeosciences* 7, 1065–1073. doi:10.5194/bg-7-1065-2010.

Browning, T. J., Achterberg, E. P., Rapp, I., Engel, A., Bertrand, E. M., Tagliabue, A., et al. (2017). Nutrient co-limitation at the boundary of an oceanic gyre. *Nature* 551, 242–246. doi:10.1038/nature24063.

Browning, T. J. J., Rapp, I., Schlosser, C., Gledhill, M., Achterberg, E. P. P., Bracher, A., et al. (2018). Influence of Iron, Cobalt, and Vitamin B12 Supply on Phytoplankton Growth in the Tropical East Pacific During the 2015 El Niño. *Geophys. Res. Lett.* 45, 6150–6159. doi:10.1029/2018GL077972.

Bruland, K. W., Donat, J. R., and Hutchins, D. A. (1991). Interactive influences of bioactive trace metals on biological production in oceanic waters. *Limnol. Oceanogr.* 36, 1555–1577. doi:10.4319/lo.1991.36.8.1555.

Bruland, K. W. K. W., Rue, E. L. E. L., Smith, G. J. G. J., and DiTullio, G. R. G. R. (2005). Iron, macronutrients and diatom blooms in the Peru upwelling regime: Brown and blue waters of Peru. *Mar. Chem.* 93, 81–103. doi:10.1016/j.marchem.2004.06.011.

Bruland, K. W., and Lohan, M. C. (2006). Controls of trace metals in seawater. *Ocean. Mar. geochemistry* 6, 23–47.

Buck, K. N., Moffett, J., Barbeau, K. A., Bundy, R. M., Kondo, Y., and Wu, J. (2012). The organic complexation of iron and copper: An intercomparison of competitive ligand exchange-adsorptive cathodic stripping voltammetry (CLE-ACSV) techniques. *Limnol. Oceanogr. Methods* 10, 496–515. doi:10.4319/lom.2012.10.496.

Buck, K. N., Sedwick, P. N., Sohst, B., and Carlson, C. A. (2018). Organic complexation of iron in the eastern tropical South Pacific: Results from US GEOTRACES Eastern Pacific Zonal Transect (GEOTRACES cruise GP16). *Mar. Chem.* 201, 229–241. doi:10.1016/j.marchem.2017.11.007.

Buck, K. N., Sohst, B., and Sedwick, P. N. (2015). The organic complexation of dissolved iron along the U.S. GEOTRACES (GA03) North Atlantic Section. *Deep. Res. Part II Top. Stud. Oceanogr.* 116, 152–165. doi:10.1016/j.dsr2.2014.11.016.

Bundy, R. M., Boiteau, R. M., McLean, C., Turk-Kubo, K. A., McIlvin, M. R., Saito, M. A., et al. (2018). Distinct siderophores contribute to iron cycling in the mesopelagic at station ALOHA. *Front. Mar. Sci.* 5, 1–15.

doi:10.3389/fmars.2018.00061.

Byrne, R. H., and Kester, D. R. (1976). Solubility of hydrous ferric oxide and iron speciation in seawater. *Mar. Chem.* 4, 255–274. doi:https://doi.org/10.1016/0304-4203(76)90012-8.

Byrne, R. H., Luo, Y.-R. R., and Young, R. W. (2000). Iron hydrolysis and solubility revisited: observations and comments on iron hydrolysis characterizations. *Mar. Chem.* 70, 23–35. doi:10.1016/S0304-4203(00)00012-8.

Caldeira, K., and Wickett, M. E. M. E. (2003). Anthropogenic carbon and ocean pH. *Nature* 425, 365. doi:10.1038/425365a.

Caprara, S., Buck, K. N., Gerringa, L. J. A. A., Rijkenberg, M. J. A. A., and Monticelli, D. (2016). A compilation of iron speciation data for open oceanic waters. *Front. Mar. Sci.* 3, 1–7. doi:10.3389/fmars.2016.00221.

Carlson, C. A., Giovannoni, S. J., Hansell, D. A., Goldberg, S. J., Parsons, R., and Vergin, K. (2004). Interactions among dissolved organic carbon, microbial processes, and community structure in the mesopelagic zone of the northwestern Sargasso Sea. *Limnol. Oceanogr.* 49, 1073–1083. doi:10.4319/lo.2004.49.4.1073.

Carr, M. E. (2001). Estimation of potential productivity in Eastern Boundary Currents using remote sensing. *Deep. Res. Part II Top. Stud. Oceanogr.* 49, 59–80. doi:10.1016/S0967-0645(01)00094-7.

Carr, M. E., and Kearns, E. J. (2003). Production regimes in four Eastern Boundary Current systems. *Deep. Res. Part II Top. Stud. Oceanogr.* 50, 3199–3221. doi:10.1016/j.dsr2.2003.07.015.

Carr, N., Davis, C. E., Blackbird, S., Daniels, L. R., Preece, C., Woodward, M., et al. (2019). Seasonal and spatial variability in the optical characteristics of DOM in a temperate shelf sea. *Prog. Oceanogr.* 177. doi:10.1016/j.pocean.2018.02.025.

Christensen, J. B., Tipping, E., Kinniburgh, D. G., Grøn, C., and Christensen, T. H. (1998). Proton binding by groundwater fulvic acids of different age, origins, and structure modeled with the model V and NICA-Donnan model. *Environ. Sci. Technol.* 32, 3346–3355. doi:10.1021/es971134o.

Cismasu, A. C., Michel, F. M., Tcaciuc, A. P., Tyliszczak, T., and Brown Jr, G. E. (2011). Composition and structural aspects of naturally occurring ferrihydrite. *Comptes Rendus Geosci.* 343, 210–218.

Coale, T. H., Moosburner, M., Horák, A., Oborník, M., Barbeau, K. A., and Allen, A. E. (2019). Reduction-dependent siderophore assimilation in a model pennate diatom. *Proc. Natl. Acad. Sci. U. S. A.* 116, 23609–23617. doi:10.1073/pnas.1907234116.

Croot, P. L., Andersson, K., Öztürk, M., and Turner, D. R. (2004a). The distribution and speciation of iron along 6°E in the Southern Ocean. *Deep. Res. Part II Top. Stud. Oceanogr.* 51, 2857–2879. doi:10.1016/j.dsr2.2003.10.012.

Croot, P. L., Bluhm, K., Schlosser, C., Streu, P., Breitbarth, E., Frew, R., et al. (2008). Regeneration of Fe(II) during EIFeX and SOFeX. *Geophys. Res. Lett.* 35. doi:10.1029/2008GL035063.

Croot, P. L., and Heller, M. I. (2012). The importance of kinetics and redox in the biogeochemical cycling of iron in the surface ocean. *Front. Microbiol.* 3, 1–15. doi:10.3389/fmicb.2012.00219.

Croot, P. L., Heller, M. I., and Wuttig, K. (2019). Redox Processes Impacting the Flux of Iron(II) from Shelf Sediments to the OMZ along the Peruvian Shelf. *ACS Earth Sp. Chem.* 3, 537–549. doi:10.1021/acsearthspacechem.8b00203.

Croot, P. L., and Johansson, M. (2000). Determination of iron speciation by cathodic stripping voltammetry in seawater using the competing ligand 2-(2-thiazolylazo)-p-cresol (TAC). *Electroanalysis* 12, 565–576. doi:10.1002/(SICI)1521-4109(200005)12:8<565::AID-ELAN565>3.0.CO;2-L.

Croot, P. L., and Laan, P. (2002). Continuous shipboard determination of Fe(II) in polar waters using flow injection analysis with chemiluminescence detection. *Anal. Chim. Acta* 466, 261–273. doi:10.1016/S0003-2670(02)00596-2.

Croot, P. L., Streu, P., and Baker, A. R. (2004b). Short residence time for iron in surface seawater impacted by atmospheric dry deposition from Saharan dust events. *Geophys. Res. Lett.* 31, 1–4. doi:10.1029/2004GL020153.

Cullen, J. J. (2015). Subsurface chlorophyll maximum layers: Enduring enigma or mystery solved? *Ann. Rev. Mar. Sci.* 7, 207–239. doi:10.1146/annurev-marine-010213-135111.

Cullen, J. T., Bergquist, B. A., and Moffett, J. W. (2006). Thermodynamic characterization of the partitioning of iron between soluble and colloidal species in the Atlantic Ocean. *Mar. Chem.* 98, 295–303. doi:10.1016/j.marchem.2005.10.007.

Cutter, G. A., Moffett, J. G., Nielsdóttir, M. C., and Sanial, V. (2018). Multiple oxidation state trace elements in suboxic waters off Peru: In situ redox processes and advective/diffusive horizontal transport. *Mar. Chem.* 201, 77–89. doi:10.1016/j.marchem.2018.01.003.

Cutter, G., Casciotti, K., Croot, P., Geibert, W., Heimbürger, L.-E., Lohan, M., et al. (2017). Sampling and Sample-handling Protocols for GEOTRACES Cruises. Version 3, August 2017. 139pp. & Appendices. doi:http://dx.doi.org/10.25607/OBP-2.

Dai, M. H., and Martin, J. M. (1995). First data on trace metal level and behaviour in two major Arctic river-estuarine systems (Ob and Yenisey) and in the adjacent Kara Sea, Russia. *Earth Planet. Sci. Lett.* 131, 127–141. doi:10.1016/0012-821X(95)00021-4.

Dale, A. W., Graco, M., and Wallmann, K. (2017). Strong and dynamic benthic-pelagic coupling and feedbacks in a coastal upwelling system (Peruvian Shelf). *Front. Mar. Sci.* 4, 1–17. doi:10.3389/fmars.2017.00029.

Davis, C. E., Blackbird, S., Wolff, G., Woodward, M., and Mahaffey, C. (2018). Seasonal organic matter dynamics in a temperate shelf sea. *Prog. Oceanogr.* doi:10.1016/J.POCEAN.2018.02.021.

de Baar, H. J. W., Boyd, P. W., Coale, K. H., Landry, M. R., Tsuda, A., Assmy, P., et al. (2005). Synthesis of iron fertilization experiments: From the iron age in the age of enlightenment. *J. Geophys. Res. C Ocean.* 110, 1–24. doi:10.1029/2004JC002601.

de Wit, J. C. M., van Riemsdijk, W. H., and Koopal, L. K. (1993). Proton Binding to Humic Substances. 2. Chemical Heterogeneity and Adsorption Models. *Environ. Sci. Technol.* 27, 2015–2022. doi:10.1021/es00047a005.

Dickson, A. G. (2010). Part 1 : Seawater carbonate chemistry The carbon dioxide system in seawater : equilibrium chemistry and measurements. *Guid. to best Pract. Ocean Acidif. Res. data Report.*, 1–40. doi:10.2777/66906.

Dickson, A. G., Afghan, J. D., and Anderson, G. C. (2003). Reference materials for oceanic CO2 analysis: a method for the certification of total alkalinity. *Mar. Chem.* 80, 185–197.

Dickson, A. G. G. G. (1990). Standard potential of the reaction: AgCl(s) + 1 2H2(g) = Ag(s) + HCl(aq), and and the standard acidity constant of the ion HSO4- in synthetic sea water from 273.15 to 318.15 K. *J. Chem. Thermodyn.* 22, 113–127. doi:10.1016/0021-9614(90)90074-Z.

Dickson, A. G., and Millero, F. J. (1987). A comparison of the equilibrium constants for the dissociation of carbonic acid in seawater media. *Deep Sea Res. Part A, Oceanogr. Res. Pap.* 34, 1733–1743. doi:10.1016/0198-0149(87)90021-5.

Dickson, A. G., Sabine, C. L., and Christian, J. R. (Eds) (2007). *Guide to best practices for ocean CO2 measurements, PICES Special Publication 3*. Available at: http://cdiac.ornl.gov/ftp/oceans/Handbook_2007/.

Dittmar, T., and Kattner, G. (2003). Recalcitrant dissolved organic matter in the ocean : major contribution of small amphiphilics. 82, 115–123. doi:10.1016/S0304-4203(03)00068-9.

Doherty, J. (2019). PEST, Model-Independent Parameter Estimation, User Manual Part I. Available at: http://www.pesthomepage.org/.

Doney, S. C. S. C. (2006). The dangers of Ocean acidification. *Sci. Am.* 294, 58–65. doi:10.1097/01.NME.0000432872.67463.f4.

Dudal, Y., and Gérard, F. (2004). Accounting for natural organic matter in aqueous chemical equilibrium models: A review of the theories and applications. *Earth-Science Rev.* 66, 199–216. doi:10.1016/j.earscirev.2004.01.002.

Ellwood, M. J., and Van den Berg, C. M. G. G. (2000). Zinc speciation in the northeastern Atlantic Ocean. *Mar. Chem.* 68, 295–306. doi:10.1016/S0304-4203(99)00085-7.

Engel, A., and Galgani, L. (2016). The organic sea-surface microlayer in the upwelling region off the coast of Peru and potential implications for air-sea exchange processes. *Biogeosciences* 13, 989–1007. doi:10.5194/bg-13-989-2016.

Feely, R. A., Doney, S. C., and Sarah, C. R. (2009). Present Conditions and Future Changes in a High-CO2 World. *Oceanography* 22, 36–47. doi:10.4337/9781781004777.00032.

Feely, R. A., Okazaki, R. R., Cai, W. J., Bednaršek, N., Alin, S. R., Byrne, R. H., et al. (2018). The combined effects of acidification and hypoxia on pH and aragonite saturation in the coastal waters of the California current ecosystem and the northern Gulf of Mexico. *Cont. Shelf Res.* 152, 50–60. doi:10.1016/j.csr.2017.11.002.

Feely, R. A., Sabine, C. L., Hernandez-Ayon, J. M., Ianson, D., and Hales, B. (2008). Evidence for upwelling of corrosive “acidified” water onto the continental shelf. *Science (80-.).* 320, 1490–1492. doi:10.1126/science.1155676.

Feely, R. A., Sabine, C. L., Lee, K., Berelson, W., Kleypas, J., Fabry, V. J., et al. (2004). Impact of anthropogenic CO2 on the CaCO3 system in the oceans. *Science (80-.).* 305, 362–366. doi:10.1126/science.1097329.

Fitzsimmons, J. N., Boyle, E. A., and Jenkins, W. J. (2014). Distal transport of dissolved hydrothermal iron in the deep South Pacific Ocean. *Proc. Natl. Acad. Sci. U. S. A.* 111, 16654–16661. doi:10.1073/pnas.1418778111.

Fitzsimmons, J. N., Carrasco, G. G., Wu, J., Roshan, S., Hatta, M., Measures, C. I., et al. (2015). Partitioning of dissolved iron and iron isotopes into soluble and colloidal phases along the GA03 GEOTRACES North Atlantic Transect. *Deep. Res. Part II Top. Stud. Oceanogr.* 116, 130–151. doi:10.1016/j.dsr2.2014.11.014.

Fitzsimmons, J. N., Conway, T. M., Lee, J. M., Kayser, R., Thyng, K. M., John, S. G., et al. (2016). Dissolved iron

and iron isotopes in the southeastern Pacific Ocean. *Global Biogeochem. Cycles* 30, 1372–1395. doi:10.1002/2015GB005357.

Fitzsimmons, J. N., John, S. G., Marsay, C. M., Hoffman, C. L., Nicholas, S. L., Toner, B. M., et al. (2017). Iron persistence in a distal hydrothermal plume supported by dissolved–particulate exchange. *Nat. Geosci.* 10, 195–201. doi:10.1038/ngeo2900.

Fitzsimmons, J. N., Zhang, R., and Boyle, E. A. (2013). Dissolved iron in the tropical North Atlantic Ocean. *Mar. Chem.* 154, 87–99. doi:10.1016/j.marchem.2013.05.009.

Gerringa, L. J. A., Rijkenberg, M. J. A., Schoemann, V., Laan, P., and de Baar, H. J. W. (2015). Organic complexation of iron in the West Atlantic Ocean. *Mar. Chem.* 177, 434–446. doi:10.1016/j.marchem.2015.04.007.

Gerringa, L. J. A., Rijkenberg, M. J. A., Thuróczy, C. E., and Maas, L. R. M. (2014). A critical look at the calculation of the binding characteristics and concentration of iron complexing ligands in seawater with suggested improvements. *Environ. Chem.* 11, 114–136. doi:10.1071/EN13072.

Gerringa, L. J. A., Veldhuis, M. J. W., Timmermans, K. R., Sarthou, G., and de Baar, H. J. W. (2006). Co-variance of dissolved Fe-binding ligands with phytoplankton characteristics in the Canary Basin. *Mar. Chem.* 102, 276–290. doi:10.1016/j.marchem.2006.05.004.

Gledhill, M., Achterberg, E. P., Li, K., Mohamed, K. N., and Rijkenberg, M. J. A. A. (2015). Influence of ocean acidification on the complexation of iron and copper by organic ligands in estuarine waters. *Mar. Chem.* 177, 421–433. doi:10.1016/j.marchem.2015.03.016.

Gledhill, M., and Buck, K. N. (2012). The organic complexation of iron in the marine environment: A review. *Front. Microbiol.* 3, 69. doi:10.3389/fmicb.2012.00069.

Gledhill, M., and Gerringa, L. J. A. A. (2017). The effect of metal concentration on the parameters derived from complexometric titrations of trace elements in seawater—a model study. *Front. Mar. Sci.* 4, 254. doi:10.3389/fmars.2017.00254.

Gledhill, M., and van den Berg, C. M. G. (1994). Determination of complexation of iron(III) with natural organic complexing ligands in seawater using cathodic stripping voltammetry. *Mar. Chem.* 47, 41–54. doi:10.1016/0304-4203(94)90012-4.

Gran, H. H. (1931). On the conditions for the production of plankton in the sea. *Cons. Perm. Internat. pour I'Explor. la Mer. Rapp. Proces-Verb.* 75, 37–46.

Gruber, N., Gloor, M., Mikaloff Fletcher, S. E., Doney, S. C., Dutkiewicz, S., Follows, M. J., et al. (2009). Oceanic sources, sinks, and transport of atmospheric CO2. *Global Biogeochem. Cycles* 23, 1–21. doi:10.1029/2008GB003349.

Gustafsson, J. P. (2001). Modeling the Acid–Base Properties and Metal Complexation of Humic Substances with the Stockholm Humic Model. *J. Colloid Interface Sci.* 244, 102–112. doi:https://doi.org/10.1006/jcis.2001.7871.

Gustafsson, J. P. (2014). Visual MINTEQ 3.1 user guide. *Dep. L. Water Resour. Eng. R. Inst. Technol. Stokholm, Sweden*, 1–73. Available at: https://vminteq.lwr.kth.se/.

Hans Wedepohl, K. (1995). The composition of the continental crust. *Geochim. Cosmochim. Acta* 59, 1217–1232.

doi:10.1016/0016-7037(95)00038-2.

Hansell, D. A. (2013). Recalcitrant dissolved organic carbon fractions. *Ann. Rev. Mar. Sci.* 5, 421–445. doi:10.1146/annurev-marine-120710-100757.

Hansell, D. A., and Carlson, C. A. (2001). Marine dissolved organic matter and the carbon cycle. *Oceanography* 14, 41–49. doi:10.5670/oceanog.2001.05.

Hansell, D. A., and Carlson, C. A. (2002). *Biogeochemistry of Marine Dissolved Organic Matter*. Academic Press doi:10.1017/CBO9781107415324.004.

Hansell, D. A., Carlson, C. A., Repeta, D. J., and Schlitzer, R. (2009). Dissolved organic matter in the ocean a controversy stim ulates new insights. *Oceanography* 22, 202–211. doi:10.5670/oceanog.2009.109.

Hansen, A. M., Kraus, T. E. C., Pellerin, B. A., Fleck, J. A., Downing, B. D., and Bergamaschi, B. A. (2016). Optical properties of dissolved organic matter (DOM): Effects of biological and photolytic degradation. *Limnol. Oceanogr.* 61, 1015–1032. doi:10.1002/lno.10270.

Hansman, R. L., Dittmar, T., and Herndl, G. J. (2015). Conservation of dissolved organic matter molecular composition during mixing of the deep water masses of the northeast Atlantic Ocean. *Mar. Chem.* 177, 288–297. doi:10.1016/j.marchem.2015.06.001.

Hart, T. J. (1934). *On the phytoplankton of the south-west Atlantic and the Bellingshausen Sea, 1929-31*. Cambridge: University Press.

Hassler, C. S. C. S., Schoemann, V., Nichols, C. M. C. M., Butler, E. C. V. E. C. V., and Boyd, P. W. P. W. (2011a). Saccharides enhance iron bioavailability to southern ocean phytoplankton. *Proc. Natl. Acad. Sci. U. S. A.* 108, 1076–1081. doi:10.1073/pnas.1010963108.

Hassler, C. S. S., Alasonati, E., Nichols, C. A. M., Slaveykova, V. I. I., Mancuso Nichols, C. A., and Slaveykova, V. I. I. (2011b). Exopolysaccharides produced by bacteria isolated from the pelagic Southern Ocean - Role in Fe binding, chemical reactivity, and bioavailability. *Mar. Chem.* 123, 88–98. doi:10.1016/j.marchem.2010.10.003.

Hawkes, J. A., Connelly, D. P., Gledhill, M., and Achterberg, E. P. (2013). The stabilisation and transportation of dissolved iron from high temperature hydrothermal vent systems. *Earth Planet. Sci. Lett.* 375, 280–290. doi:10.1016/j.epsl.2013.05.047.

Heller, M. I., Lam, P. J., Moffett, J. W., Till, C. P., Lee, J. M., Toner, B. M., et al. (2017). Accumulation of Fe oxyhydroxides in the Peruvian oxygen deficient zone implies non-oxygen dependent Fe oxidation. *Geochim. Cosmochim. Acta* 211, 174–193. doi:10.1016/j.gca.2017.05.019.

Hiemstra, T., and van Riemsdijk, W. H. (2002). On the relationship between surface structure and ion complexation of oxide-solution interfaces. *Surf. complexation Miner. interfaces Multisite Charg. Distrib. approach*, 15.

Hiemstra, T., and van Riemsdijk, W. H. (2006). Biogeochemical speciation of Fe in ocean water. *Mar. Chem.* 102, 181–197. doi:10.1016/j.marchem.2006.03.008.

Hogle, S. L., Dupont, C. L., Hopkinson, B. M., King, A. L., Buck, K. N., Roe, K. L., et al. (2018). Pervasive iron limitation at subsurface chlorophyll maxima of the California Current. *Proc. Natl. Acad. Sci. U. S. A.* 115, 13300–13305. doi:10.1073/pnas.1813192115.

Homoky, W. B., Severmann, S., McManus, J., Berelson, W. M., Riedel, T. E., Statham, P. J., et al. (2012). Dissolved oxygen and suspended particles regulate the benthic flux of iron from continental margins. *Mar. Chem.* 134–135, 59–70. doi:10.1016/j.marchem.2012.03.003.

Hong, H., and Kester, D. R. D. R. (1986). Redox state of iron in the offshore waters of Peru. *Limnol. Oceanogr.* 31, 612–626. doi:10.4319/lo.1986.31.3.0612.

Hopkinson, B. M., and Barbeau, K. A. (2007). Organic and redox speciation of iron in the eastern tropical North Pacific suboxic zone. *Mar. Chem.* 106, 2–17. doi:10.1016/j.marchem.2006.02.008.

Hopwood, M. J., Birchill, A. J., Gledhill, M., Achterberg, E. P., Klar, J. K., and Milne, A. (2017). A Comparison between four analytical methods for the measurement of Fe(II) at nanomolar concentrations in coastal seawater. *Front. Mar. Sci.* 4. doi:10.3389/fmars.2017.00192.

Hopwood, M. J., Carroll, D., Höfer, J., Achterberg, E. P., Meire, L., Le Moigne, F. A. C., et al. (2019). Highly variable iron content modulates iceberg-ocean fertilisation and potential carbon export. *Nat. Commun.* 10, 5261. doi:10.1038/s41467-019-13231-0.

Hudson, R. J. M. M., Rue, E. L., and Bruland, K. W. (2003). Modeling complexometric titrations of natural water samples. *Environ. Sci. Technol.* 37, 1553–1562. doi:10.1021/es025751a.

Hummel, W., Filella, M., and Rowland, D. (2019). Where to find equilibrium constants? *Sci. Total Environ.* 692, 49–59. doi:10.1016/j.scitotenv.2019.07.161.

Humphreys, M. P., Achterberg, E. P., Hopkins, J. E., Chowdhury, M. Z. H., Griffiths, A. M., Hartman, S. E., et al. (2019). Mechanisms for a nutrient-conserving carbon pump in a seasonally stratified, temperate continental shelf sea. *Prog. Oceanogr.* 177. doi:10.1016/j.pocean.2018.05.001.

Hunter, K. A. (2005). Comment on "measuring marine iron(III) complexes by CLE-AdSV." *Environ. Chem.* 2, 80–84. doi:10.1071/EN05021.

Hunter, K. A. K. A., and Boyd, P. W. P. W. (2007). Iron-binding ligands and their role in the ocean biogeochemistry of iron. *Environ. Chem.* 4, 221–232. doi:10.1071/EN07012.

Hunter, K. A., and Leonard, M. W. (1988). Colloid stability and aggregation in estuaries: 1. Aggregation kinetics of riverine dissolved iron after mixing with seawater. *Geochim. Cosmochim. Acta* 52, 1123–1130. doi:10.1016/0016-7037(88)90266-9.

Hutchins, D. A. A., and Boyd, P. W. W. (2016). Marine phytoplankton and the changing ocean iron cycle. *Nat. Clim. Chang.* 6, 1072–1079. doi:10.1038/nclimate3147.

Hutchins, D. A., and Bruland, K. W. (1998). Iron-limited diatom growth and Si:N uptake ratios in a coastal upwelling regime. *Nature* 393, 561–564. doi:10.1038/31203.

Hutchins, D. A. D. A., Witter, A. E. A. E., Butler, A., Luther III, G. W., Luther, G. W., and Luther III, G. W. (1999). Competition among marine phytoplankton for different chelated iron species. *Nature* 400, 858–861. doi:10.1038/23680.

Hutchins, D. A., Hare, C. E., Weaver, R. S., Zhang, Y., Firme, G. F., DiTullio, G. R., et al. (2002). Phytoplankton iron limitation in the Humboldt Current and Peru Upwelling. *Limnol. Oceanogr.* 47, 997–1011. doi:10.4319/lo.2002.47.4.0997.

Hwang, J., Druffel, E. R. M., Griffin, S., Smith, K. L., Baldwin, R. J., and Bauer, J. E. (2004). Temporal variability of Δ14C, δ13C, and C/N in sinking particulate organic matter at a deep time series station in the northeast Pacific Ocean. *Global Biogeochem. Cycles* 18, 1–9. doi:10.1029/2004GB002221.

Janney, D. E., Cowley, J. M., and Buseck, P. R. (2000). Transmission Electron Microscopy of Synthetic 2- and 6-Line Ferrihydrite. *Clays Clay Miner.* 48, 111–119. doi:10.1346/CCMN.2000.0480114.

Janot, N., Pinheiro, J. P., Botero, W. G., Meeussen, J. C. L., and Groenenberg, J. E. (2017). PEST-ORCHESTRA, a tool for optimising advanced ion-binding model parameters: Derivation of NICA-Donnan model parameters for humic substances reactivity. *Environ. Chem.* 14, 31–38. doi:10.1071/EN16039.

Jiang, L. Q., Carter, B. R., Feely, R. A., Lauvset, S. K., and Olsen, A. (2019). Surface ocean pH and buffer capacity: past, present and future. *Sci. Rep.* 9, 1–11. doi:10.1038/s41598-019-55039-4.

Jiao, N., Herndl, G. J., Hansell, D. A., Benner, R., Kattner, G., Wilhelm, S. W., et al. (2010). Microbial production of recalcitrant dissolved organic matter: Long-term carbon storage in the global ocean. *Nat. Rev. Microbiol.* 8, 593–599. doi:10.1038/nrmicro2386.

Jickells, T. D., An, Z. S., Andersen, K. K., Baker, A. R., Bergametti, C., Brooks, N., et al. (2005). Global iron connections between desert dust, ocean biogeochemistry, and climate. *Science (80-.).* 308, 67–71. doi:10.1126/science.1105959.

John, S. G., Helgoe, J., Townsend, E., Weber, T., DeVries, T., Tagliabue, A., et al. (2018). Biogeochemical cycling of Fe and Fe stable isotopes in the Eastern Tropical South Pacific. *Mar. Chem.* 201, 66–76. doi:10.1016/j.marchem.2017.06.003.

Johnson, K. S., Gordon, R. M., and Coale, K. H. (1997). What controls dissolved iron in the world ocean? *Mar. Chem.* 57, 137–161.

Karstensen, J., Stramma, L., and Visbeck, M. (2008). Oxygen minimum zones in the eastern tropical Atlantic and Pacific oceans. *Prog. Oceanogr.* 77, 331–350. doi:10.1016/j.pocean.2007.05.009.

Kazamia, E., Sutak, R., Paz-Yepes, J., Dorrell, R. G., Vieira, F. R. J., Mach, J., et al. (2018). Endocytosis-mediated siderophore uptake as a strategy for Fe acquisition in diatoms. *Sci. Adv.* 4. doi:10.1126/sciadv.aar4536.

Kinniburgh, D. G. G. D. G., Milne, C. J. C. J. C. J., Benedetti, M. F., Pinheiro, J. P. J. P. P., Filius, J., Koopal, L. K. L. K. K., et al. (1996). Metal ion binding by humic acid: Application of the NICA-Donnan model. *Environ. Sci. Technol.* 30, 1687–1698. doi:10.1021/es950695h.

Kinniburgh, D. G., Van Riemsdijk, W. H., Koopal, L. K., Borkovec, M., Benedetti, M. F., and Avena, M. J. (1999). Ion binding to natural organic matter: Competition, heterogeneity, stoichiometry and thermodynamic consistency. *Colloids Surfaces A Physicochem. Eng. Asp.* 151, 147–166. doi:10.1016/S0927-7757(98)00637-2.

Kleint, C., Hawkes, J. A., Sander, S. G., and Koschinsky, A. (2016). Voltammetric investigation of hydrothermal iron speciation. *Front. Mar. Sci.* 3, 1–11. doi:10.3389/fmars.2016.00075.

Koch, B. P. B. P., Witt, M. M. R., Engbrodt, R., Dittmar, T., and Kattner, G. (2005). Molecular formulae of marine and terrigenous dissolved organic matter detected by electrospray ionization Fourier transform ion cyclotron resonance mass spectrometry. *Geochim. Cosmochim. Acta* 69, 3299–3308. doi:10.1016/j.gca.2005.02.027.

Koch, B. P., and Dittmar, T. (2006). From mass to structure: An aromaticity index for high-resolution mass data of natural organic matter. *Rapid Commun. Mass Spectrom.* 20, 926–932. doi:10.1002/rcm.2386.

Koch, B. P., Ludwichowski, K. U., Kattner, G., Dittmar, T., and Witt, M. (2008). Advanced characterization of marine dissolved organic matter by combining reversed-phase liquid chromatography and FT-ICR-MS. *Mar. Chem.* 111, 233–241. doi:10.1016/j.marchem.2008.05.008.

Kogut, M. B. B., and Voelker, B. M. M. (2001). Strong copper-binding behavior of terrestrial humic substances in seawater. *Environ. Sci. Technol.* 35, 1149–1156. doi:10.1021/es0014584.

Kondo, Y., Bamba, R., Obata, H., Nishioka, J., and Takeda, S. (2021). Distinct profiles of size-fractionated iron-binding ligands between the eastern and western subarctic Pacific. *Sci. Rep.* 11, 1–9. doi:10.1038/s41598-021-81536-6.

Kondo, Y., and Moffett, J. W. (2015). Iron redox cycling and subsurface offshore transport in the eastern tropical South Pacific oxygen minimum zone. *Mar. Chem.* 168, 95–103. doi:10.1016/j.marchem.2014.11.007.

Koopal, L. K. K. K., Saito, T., Pinheiro, J. P. P. P., and van Riemsdijk, W. H. H. H. (2005). Ion binding to natural organic matter: General considerations and the NICA-Donnan model. *Colloids Surfaces A Physicochem. Eng. Asp.* 265, 40–54. doi:10.1016/j.colsurfa.2004.11.050.

Kuma, K., Isoda, Y., and Nakabayashi, S. (2003). Control on dissolved iron concentrations in deep waters in the western North Pacific: Iron (III) hydroxide solubility. *J. Geophys. Res. C Ocean.* 108, 5–1. doi:10.1029/2002jc001481.

Kuma, K., Katsumoto, A., Kawakami, H., Takatori, F., and Matsunaga, K. (1998). Spatial variability of Fe(III) hydroxide solubility in the water column of the northern North Pacific Ocean. *Deep. Res. Part I Oceanogr. Res. Pap.* 45, 91–113. doi:10.1016/S0967-0637(97)00067-8.

Kuma, K., Katsumoto, A., Shiga, N., Sawabe, T., and Matsunaga, K. (2000). Variation of size-fractionated Fe concentrations and Fe(III) hydroxide solubilities during a spring phytoplankton bloom in Funka Bay (Japan). *Mar. Chem.* 71, 111–123. doi:10.1016/S0304-4203(00)00044-X.

Kuma, K., Nishioka, J., and Matsunaga, K. (1996). Controls on iron(III) hydroxide solubility in seawater: The influence of pH and natural organic chelators. *Limnol. Oceanogr.* 41, 396–407. doi:10.4319/lo.1996.41.3.0396.

Laès, A., Blain, S., Laan, P., Ussher, S. J. J., Achterberg, E. P. E. P., Tréguer, P., et al. (2007). Sources and transport of dissolved iron and manganese along the continental margin of the Bay of Biscay. *Biogeosciences (BG)* 4, 181–194. doi:10.5194/bg-4-181-2007.

Laglera, L. M., Battaglia, G., and van den Berg, C. M. G. (2007). Determination of humic substances in natural waters by cathodic stripping voltammetry of their complexes with iron. *Anal. Chim. Acta* 599, 58–66. doi:10.1016/j.aca.2007.07.059.

Laglera, L. M., Battaglia, G., and van den Berg, C. M. G. (2011). Effect of humic substances on the iron speciation in natural waters by CLE/CSV. *Mar. Chem.* 127, 134–143. doi:10.1016/j.marchem.2011.09.003.

Laglera, L. M. M., and Filella, M. (2015). The relevance of ligand exchange kinetics in the measurement of iron speciation by CLE-AdCSV in seawater. *Mar. Chem.* 173, 100–113. doi:10.1016/j.marchem.2014.09.005.

Laglera, L. M., and van den Berg, C. M. G. G. (2009). Evidence for geochemical control of iron by humic substances in seawater. *Limnol. Oceanogr.* 54, 610–619. doi:10.4319/lo.2009.54.2.0610.

Lewis, E., and Wallace, D. (1998). Program developed for CO2 system calculations. *Ornl/Cdiac-105*, 1–21. doi:4735.

Li, G., Cheng, L., Zhu, J., Trenberth, K. E., Mann, M. E., and Abraham, J. P. (2020). Increasing ocean stratification over the past half-century. *Nat. Clim. Chang.* doi:10.1038/s41558-020-00918-2.

Li, Y., Harir, M., Lucio, M., Kanawati, B., Smirnov, K., Flerus, R., et al. (2016). Proposed Guidelines for Solid Phase Extraction of Suwannee River Dissolved Organic Matter. *Anal. Chem.* 88, 6680–6688. doi:10.1021/acs.analchem.5b04501.

Li, Y., Harir, M., Uhl, J., Kanawati, B., Lucio, M., Smirnov, K. S., et al. (2017). How representative are dissolved organic matter (DOM) extracts? A comprehensive study of sorbent selectivity for DOM isolation. *Water Res.* 116, 316–323. doi:10.1016/j.watres.2017.03.038.

Liu, X., and Millero, F. J. (2002). The solubility of iron in seawater. *Mar. Chem.* 77, 43–54. doi:10.1016/S0304-4203(01)00074-3.

Liu, X., and Millero, F. J. J. (1999). The solubility of iron hydroxide in sodium chloride solutions. *Geochim. Cosmochim. Acta* 63, 3487–3497. doi:10.1016/S0016-7037(99)00270-7.

Lodeiro, P., Rey-Castro, C., David, C., Achterberg, E. P., Puy, J., and Gledhill, M. (2020). Acid-base properties of dissolved organic matter extracted from the marine environment. *Sci. Total Environ.* 729, 138437. doi:10.1016/j.scitotenv.2020.138437.

Loginova, A. N., Thomsen, S., Dengler, M., Lüdke, J., and Engel, A. (2019). Diapycnal dissolved organic matter supply into the upper Peruvian oxycline. *Biogeosciences* 16, 2033–2047. doi:10.5194/bg-16-2033-2019.

Loginova, A. N., Thomsen, S., and Engel, A. (2016). Chromophoric and fluorescent dissolved organic matter in and above the oxygen minimum zone off Peru. *J. Geophys. Res. Ocean.* 121, 7973–7990. doi:10.1002/2016JC011906.

Lønborg, C., Carreira, C., Jickells, T., and Álvarez-Salgado, X. A. (2020). Impacts of Global Change on Ocean Dissolved Organic Carbon (DOC) Cycling. *Front. Mar. Sci.* 7, 466. doi:10.3389/fmars.2020.00466.

Maldonado, M. T., Allen, A. E., Chong, J. S., Lin, K., Leus, D., Karpenko, N., et al. (2006). Copper-dependent iron transport in coastal and oceanic diatoms. *Limnol. Oceanogr.* 51, 1729–1743. doi:10.4319/lo.2006.51.4.1729.

Maldonado, M. T., and Price, N. M. (2001). Reduction and transport of organically bound iron by Thalassiosira oceanica (Bacillariophyceae). *J. Phycol.* 37, 298–309. doi:10.1046/j.1529-8817.2001.037002298.x.

Mark Moore, C., Mills, M. M., Achterberg, E. P., Geider, R. J., Laroche, J., Lucas, M. I., et al. (2009). Large-scale distribution of Atlantic nitrogen fixation controlled by iron availability. *Nat. Geosci.* 2, 867–871. doi:10.1038/ngeo667.

Marsay, C. M., Barrett, P. M., McGillicuddy, D. J., and Sedwick, P. N. (2017). Distributions, sources, and transformations of dissolved and particulate iron on the Ross Sea continental shelf during summer. *J. Geophys. Res. Ocean.* 122, 6371–6393. doi:10.1002/2017JC013068.

Martin, J. H. (1990). Glacial-interglacial CO2 change: The Iron Hypothesis. *Paleoceanography* 5, 1–13.

doi:10.1029/PA005i001p00001.

Matear, R. J., Hirst, A. C., and McNeil, B. I. (2000). Changes in dissolved oxygen in the Southern Ocean with climate change. *Geochemistry, Geophys. Geosystems* 1.

Mawji, E., Gledhill, M., Milton, J. A. A. J. A., Tarran, G. A. G. A. G. A., Ussher, S., Thompson, A., et al. (2008). Hydroxamate siderophores: Occurrence and importance in the Atlantic Ocean. *Environ. Sci. Technol.* 42, 8675–8680. doi:10.1021/es801884r.

Mawji, E., Gledhill, M., Milton, J. A. J. A., Zubkov, M. V. M. V, Thompson, A., Wolff, G. A. G. A., et al. (2011). Production of siderophore type chelates in Atlantic Ocean waters enriched with different carbon and nitrogen sources. *Mar. Chem.* 124, 90–99. doi:10.1016/j.marchem.2010.12.005.

Medeiros, P. M., Seidel, M., Powers, L. C., Dittmar, T., Hansell, D. A., and Miller, W. L. (2015). Dissolved organic matter composition and photochemical transformations in the northern North Pacific Ocean. *Geophys. Res. Lett.* 42, 863–870. doi:10.1002/2014GL062663.

Meeussen, J. C. L. (2003). Orchestra: An object-oriented framework for implementing chemical equilibrium models. *Environ. Sci. Technol.* 37, 1175–1182. doi:10.1021/es025597s.

Mehrbach, C., Culberson, C. H., Hawley, J. E., Pytkowicx, R. M., and Pytkowicz, R. M. (1973). Measurement of the Apparent Dissociation Constants of Carbonic Acid in Seawater At Atmospheric Pressure. *Limnol. Oceanogr.* 18, 897–907. doi:10.4319/lo.1973.18.6.0897.

Millero, F. J., and Sotolongo, S. (1989). The oxidation of Fe(II) with H2O2 in seawater. *Geochim. Cosmochim. Acta* 53, 1867–1873. doi:10.1016/0016-7037(89)90307-4.

Millero, F. J., Sotolongo, S., and Izaguirre, M. (1987). The kinetics of oxidation of Fe (II) in seawater. *Geochim. Cosmochim. Acta* 51, 793–801.

Millero, F. J., Woosley, R., Ditrolio, B., and Waters, J. (2009). Effect of ocean acidification on the speciation of metals in seawater. *Oceanography* 22, 72–85. doi:10.5670/oceanog.2009.98.

Milne, A., Schlosser, C., Wake, B. D., Achterberg, E. P., Chance, R., Baker, A. R., et al. (2017). Particulate phases are key in controlling dissolved iron concentrations in the (sub)tropical North Atlantic. *Geophys. Res. Lett.* 44, 2377–2387. doi:10.1002/2016GL072314.

Milne, C. J., Kinniburgh, D. G., de Wit, J. C. M., van Riemsdijk, W. H., and Koopal, L. K. (1995). Analysis of metal-ion binding by a peat humic acid using a simple electrostatic model. *J. Colloid Interface Sci.* 175, 448–460. doi:10.1006/jcis.1995.1475.

Milne, C. J., Kinniburgh, D. G., and Tipping, E. (2001). Generic NICA-Donnan model parameters for proton binding by humic substances. *Environ. Sci. Technol.* 35, 2049–2059. doi:10.1021/es000123j.

Milne, C. J., Kinniburgh, D. G., Van Riemsdijk, W. H., and Tipping, E. (2003). Generic NICA - Donnan model parameters for metal-ion binding by humic substances. *Environ. Sci. Technol.* 37, 958–971. doi:10.1021/es0258879.

Moore, C. M., Mills, M. M., Arrigo, K. R., Berman-Frank, I., Bopp, L., Boyd, P. W., et al. (2013). Processes and patterns of oceanic nutrient limitation. *Nat. Geosci.* 6, 701–710. doi:10.1038/ngeo1765.

Moore, J. K., and Braucher, O. (2007). Observations of dissolved iron concentrations in the World Ocean:

implications and constraints for ocean biogeochemical models. *Biogeosciences Discuss.* 4, 1241–1277. doi:10.5194/bgd-4-1241-2007.

Moore, J. K., Doney, S. C., and Lindsay, K. (2004). Upper ocean ecosystem dynamics and iron cycling in a global three-dimensional model. *Global Biogeochem. Cycles* 18, 1–21. doi:10.1029/2004GB002220.

Moore, R. M., and Millward, G. E. (1984). Dissolved-particulate interactions of aluminium in ocean waters. *Geochim. Cosmochim. Acta* 48, 235–241.

Morel, F. M. M., Kustka, A. B., and Shaked, Y. (2008). The role of unchelated Fe in the iron nutrition of phytoplankton. *Limnol. Oceanogr.* 53, 400–404. doi:10.4319/lo.2008.53.1.0400.

Mosch, T., Sommer, S., Dengler, M., Noffke, A., Bohlen, L., Pfannkuche, O., et al. (2012). Factors influencing the distribution of epibenthic megafauna across the Peruvian oxygen minimum zone. *Deep. Res. Part I Oceanogr. Res. Pap.* 68, 123–135. doi:10.1016/j.dsr.2012.04.014.

Muller-Karger, F. E., Varela, R., Thunell, R., Luerssen, R., Hu, C., and Walsh, J. J. (2005). The importance of continental margins in the global carbon cycle. *Geophys. Res. Lett.* 32, 1–4. doi:10.1029/2004GL021346.

Muller, F. L. L. (2018). Exploring the potential role of terrestrially derived humic substances in the marine biogeochemistry of iron. *Front. Earth Sci.* 6, 1–20. doi:10.3389/feart.2018.00159.

Ndungu, K. (2012). Model Predictions of Copper Speciation in Coastal Water Compared to Measurements by Analytical Voltammetry. *Environ. Sci. Technol.* 46, 7644–7652. doi:10.1021/es301017x.

Nedelec, F., Statham, P. J. J., Mowlem, M., Nédélec, F., Statham, P. J. J., and Mowlem, M. (2007). Reprint of "Processes influencing dissolved iron distributions below the surface at the Atlantic Ocean-Celtic Sea shelf edge." *Mar. Chem.* 106, 365–379. doi:10.1016/j.marchem.2007.06.010.

Noffke, A., Hensen, C., Sommer, S., Scholz, F., Bohlen, L., Mosch, T., et al. (2012). Benthic iron and phosphorus fluxes across the Peruvian oxygen minimum zone. *Limnol. Oceanogr.* 57, 851–867. doi:10.4319/lo.2012.57.3.0851.

Norman, L., Worms, I. A. M., Angles, E., Bowie, A. R., Nichols, C. M., Ninh Pham, A., et al. (2015). The role of bacterial and algal exopolymeric substances in iron chemistry. *Mar. Chem.* 173, 148–161. doi:10.1016/j.marchem.2015.03.015.

Obata, H., Karatani, H., and Nakayama, E. (1993). Automated Determination of Iron in Seawater by Chelating Resin Concentration and Chemiluminescence Detection. *Anal. Chem.* 65, 1524–1528. doi:10.1021/ac00059a007.

Orr, J. C., Fabry, V. J., Aumont, O., Bopp, L., Doney, S. C., Feely, R. A., et al. (2005). Anthropogenic ocean acidification over the twenty-first century and its impact on calcifying organisms. *Nature* 437, 681–686. doi:10.1038/nature04095.

Osborne, E. B., Thunell, R. C., Gruber, N., Feely, R. A., and Benitez-Nelson, C. R. (2019). Decadal variability in twentieth-century ocean acidification in the California Current Ecosystem. *Nat. Geosci.* 13. doi:10.1038/s41561-019-0499-z.

Paulmier, A., and Ruiz-Pino, D. (2009). Oxygen minimum zones (OMZs) in the modern ocean. *Prog. Oceanogr.* 80, 113–128. doi:10.1016/j.pocean.2008.08.001.

Paulmier, A., Ruiz-Pino, D., and Garçon, V. (2011). CO2 maximum in the oxygen minimum zone (OMZ). *Biogeosciences* 8, 239–252. doi:10.5194/bg-8-239-2011.

Perdue, E. M. (1985). Acidic functional groups of humic substances.

Pierrot, D., Lewis, E., and Wallace, D. W. R. (2006). MS Excel program developed for CO_2 system calculations. *ORNL/CDIAC-105a. Carbon Dioxide Inf. Anal. Center, Oak Ridge Natl. Lab. US Dep. Energy, Oak Ridge, Tennessee*.

Pinheiro, J. P., Rotureau, E., and Duval, J. F. L. (2021). Addressing the electrostatic component of protons binding to aquatic nanoparticles beyond the Non-Ideal Competitive Adsorption (NICA)-Donnan level: Theory and application to analysis of proton titration data for humic matter. *J. Colloid Interface Sci.* 583, 642–651. doi:10.1016/j.jcis.2020.09.059.

Pitzer, K. S. (2018). *Activity coefficients in electrolyte solutions*. CRC press.

Pižeta, I., Sander, S. G., Hudson, R. J. M., Omanović, D., Baars, O., Barbeau, K. A., et al. (2015). Interpretation of complexometric titration data: An intercomparison of methods for estimating models of trace metal complexation by natural organic ligands. *Mar. Chem.* 173, 3–24. doi:10.1016/j.marchem.2015.03.006.

Plass, A., Schlosser, C., Sommer, S., Dale, A. W., and Eric, P. (2019). The control of hydrogen sulfide on benthic iron and cadmium fluxes in the oxygen minimum zone off Peru. 1–52.

Plavšić, M., Krznarić, D., and Branica, M. (1982). Determination of the apparent copper complexing capacity of seawater by anodic stripping voltammetry. *Mar. Chem.* 11, 17–31. doi:10.1016/0304-4203(82)90045-7.

Poorvin, L., Sander, S. G., Velasquez, I., Ibisanmi, E., LeCleir, G. R., and Wilhelm, S. W. (2011). A comparison of Fe bioavailability and binding of a catecholate siderophore with virus-mediated lysates from the marine bacterium Vibrio alginolyticus PWH3a. *J. Exp. Mar. Bio. Ecol.* 399, 43–47. doi:10.1016/j.jembe.2011.01.016.

Powell, C. F., Baker, A. R., Jickells, T. D., W. Bange, H., Chance, R. J., and Yodle, C. (2015). Estimation of the atmospheric flux of nutrients and trace metals to the eastern tropical North Atlantic Ocean. *J. Atmos. Sci.* 72, 4029–4045. doi:10.1175/JAS-D-15-0011.1.

Powell, R. T., and Wilson-Finelli, A. (2003). Importance of organic Fe complexing ligands in the Mississippi River plume. *Estuar. Coast. Shelf Sci.* 58, 757–763. doi:10.1016/S0272-7714(03)00182-3.

Raiswell, R., and Canfield, D. E. (2012). The iron biogeochemical cycle past and present. *Geochemical Perspect.* 1, 1–232. doi:10.7185/geochempersp.1.1.

Raiswell, R., Vu, H. P., Brinza, L., and Benning, L. G. (2010). The determination of labile Fe in ferrihydrite by ascorbic acid extraction: Methodology, dissolution kinetics and loss of solubility with age and de-watering. *Chem. Geol.* 278, 70–79. doi:10.1016/j.chemgeo.2010.09.002.

Rapp, I., Schlosser, C., Browning, T. J., Wolf, F., Le Moigne, F. A. C., Gledhill, M., et al. (2020). El Niño-driven oxygenation impacts Peruvian shelf iron supply to the South Pacific Ocean. *Geophys. Res. Lett.* 47. doi:10.1029/2019gl086631.

Rapp, I., Schlosser, C., Rusiecka, D., Gledhill, M., and Achterberg, E. P. (2017). Automated preconcentration of Fe, Zn, Cu, Ni, Cd, Pb, Co, and Mn in seawater with analysis using high-resolution sector field inductively-coupled plasma mass spectrometry. *Anal. Chim. Acta* 976, 1–13. doi:10.1016/j.aca.2017.05.008.

Resing, J. A., Sedwick, P. N., German, C. R., Jenkins, W. J., Moffett, J. W., Sohst, B. M., et al. (2015). Basin-scale transport of hydrothermal dissolved metals across the South Pacific Ocean. *Nature* 523, 200–203. doi:10.1038/nature14577.

Rickard, D., and Luther, G. W. (2007). Chemistry of Iron Sulfides. *Chem. Rev.* 107, 514–562. doi:10.1021/cr0503658.

Rijkenberg, M. J. A., Gerringa, L. J. A., Carolus, V. E., Velzeboer, I., and de Baar, H. J. W. (2006a). Enhancement and inhibition of iron photoreduction by individual ligands in open ocean seawater. *Geochim. Cosmochim. Acta* 70, 2790–2805. doi:10.1016/j.gca.2006.03.004.

Rijkenberg, M. J. A., Gerringa, L. J. A., Velzeboer, I., Timmermans, K. R., Buma, A. G. J., and de Baar, H. J. W. (2006b). Iron-binding ligands in Dutch estuaries are not affected by UV induced photochemical degradation. *Mar. Chem.* 100, 11–23. doi:10.1016/j.marchem.2005.10.005.

Rijkenberg, M. J. A., Middag, R., Laan, P., Gerringa, L. J. A., Van Aken, H. M., Schoemann, V., et al. (2014). The distribution of dissolved iron in the West Atlantic Ocean. *PLoS One* 9, 1–14. doi:10.1371/journal.pone.0101323.

Ringbom, A., and Still, E. (1972). The calculation and use of a coefficients. *Anal. Chim. Acta* 59, 143–146.

Rose, A. L., and Waite, T. D. (2002). Kinetic model for FE(II) oxidation in seawater in the absence and presence of natural organic matter. *Environ. Sci. Technol.* 36, 433–444. doi:10.1021/es0109242.

Rose, A. L., and Waite, T. D. (2005). Reduction of organically complexed ferric iron by superoxide in a simulated natural water. *Environ. Sci. Technol.* 39, 2645–2650. doi:10.1021/es048765k.

Rue, E. L., and Bruland, K. W. (1995). Complexation of iron(III) by natural organic ligands in the Central North Pacific as determined by a new competitive ligand equilibration/adsorptive cathodic stripping voltammetric method. *Mar. Chem.* 50, 117–138. doi:10.1016/0304-4203(95)00031-L.

Rusiecka, D., Gledhill, M., Milne, A., Achterberg, E. P., Annett, A. L., Atkinson, S., et al. (2018). Anthropogenic Signatures of Lead in the Northeast Atlantic. *Geophys. Res. Lett.* 45, 2734–2743. doi:10.1002/2017GL076825.

Ruud, J. T. (1930). Nitrates and phosphates in the southern seas. *ICES J. Mar. Sci.* 5, 347–360. doi:10.1093/icesjms/5.3.347.

Sabine, C. L., Feely, R. A., Gruber, N., Key, R. M., Lee, K., Bullister, J. L., et al. (2004). The oceanic sink for anthropogenic CO2. *Science (80-.).* 305, 367–371. doi:10.1126/science.1097403.

Saito, M. A., Noble, A. E., Tagliabue, A., Goepfert, T. J., Lamborg, C. H., and Jenkins, W. J. (2013). Slow-spreading submarine ridges in the South Atlantic as a significant oceanic iron source. *Nat. Geosci.* 6, 775–779. doi:10.1038/ngeo1893.

Sander, S. G., Buck, K. N., and Wells, M. (2015). The effect of natural organic ligands on trace metal speciation in San Francisco Bay: Implications for water quality criteria. *Mar. Chem.* 173, 269–281. doi:10.1016/j.marchem.2014.09.015.

Sander, S. G., Hunter, K. A., Harms, H., and Wells, M. (2011). Numerical approach to speciation and estimation of parameters used in modeling trace metal bioavailability. *Environ. Sci. Technol.* 45, 6388–6395. doi:10.1021/es200113v.

Sarthou, G., Baker, A. R., Blain, S., Achterberg, E. P., Boye, M., Bowie, A. R., et al. (2003). Atmospheric iron deposition and sea-surface dissolved iron concentrations in the eastern Atlantic Ocean. *Deep. Res. Part I Oceanogr. Res. Pap.* 50, 1339–1352. doi:10.1016/S0967-0637(03)00126-2.

Schlitzer, R. (2015). Ocean Data View, odv. awi. de.

Schlitzer, R., Anderson, R. F., Dodas, E. M., Lohan, M., Geibert, W., Tagliabue, A., et al. (2018). The GEOTRACES Intermediate Data Product 2017. *Chem. Geol.* 493, 210–223. doi:10.1016/j.chemgeo.2018.05.040.

Schlosser, C., Klar, J. K., Wake, B. D., Snow, J. T., Honey, D. J., Woodward, E. M. S., et al. (2014). Seasonal ITCZ migration dynamically controls the location of the (sub)tropical Atlantic biogeochemical divide. *Proc. Natl. Acad. Sci. U. S. A.* 111, 1438–1442. doi:10.1073/pnas.1318670111.

Schlosser, C., Streu, P., Frank, M., Lavik, G., Croot, P. L., Dengler, M., et al. (2018). H2S events in the Peruvian oxygen minimum zone facilitate enhanced dissolved Fe concentrations. *Sci. Rep.* 8, 1–8. doi:10.1038/s41598-018-30580-w.

Scholz, F., Hensen, C., Noffke, A., Rohde, A., Liebetrau, V., and Wallmann, K. (2011). Early diagenesis of redox-sensitive trace metals in the Peru upwelling area - response to ENSO-related oxygen fluctuations in the water column. *Geochim. Cosmochim. Acta* 75, 7257–7276. doi:10.1016/j.gca.2011.08.007.

Scholz, F., Löscher, C. R., Fiskal, A., Sommer, S., Hensen, C., Lomnitz, U., et al. (2016). Nitrate-dependent iron oxidation limits iron transport in anoxic ocean regions. *Earth Planet. Sci. Lett.* 454, 272–281. doi:10.1016/j.epsl.2016.09.025.

Scholz, F., Mcmanus, J., Mix, A. C., Hensen, C., and Schneider, R. R. (2014). The impact of ocean deoxygenation on iron release from continental margin sediments. *Nat. Geosci.* 7, 433–437. doi:10.1038/ngeo2162.

Seidel, M., Manecki, M., Herlemann, D. P. R., Deutsch, B., Schulz-Bull, D., Jürgens, K., et al. (2017). Composition and transformation of dissolved organic matter in the Baltic sea. *Front. Earth Sci.* 5, 1–20. doi:10.3389/feart.2017.00031.

Shaked, Y., Kustka, A. B., and Morel, F. M. M. (2005). A general kinetic model for iron acquisition by eukaryotic phytoplankton. *Limnol. Oceanogr.* 50, 872–882. doi:10.4319/lo.2005.50.3.0872.

Shaked, Y., and Lis, H. (2012). Disassembling iron availability to phytoplankton. *Front. Microbiol.* 3, 1–26. doi:10.3389/fmicb.2012.00123.

Shi, D., Xu, Y., Hopkinson, B. M., and Morel, F. M. M. F. M. M. (2010). Effect of ocean acidification on iron availability to marine phytoplankton. *Science (80-.).* 327, 676–679. doi:10.1126/science.1183517.

Sholkovitz, E. R., Boyle, E. A., and Price, N. B. (1978). The removal of dissolved humic acids and iron during estuarine mixing. *Earth Planet. Sci. Lett.* 40, 130–136. doi:10.1016/0012-821X(78)90082-1.

Siegenthaler, U., and Sarmiento, J. L. (1993). Atmospheric carbon dioxide and the ocean. *Nature* 365, 119–125.

Smith, K. L., Robison, B. H., Helly, J. J., Kaufmann, R. S., Ruhl, H. A., Shaw, T. J., et al. (2007). Free-drifting icebergs: Hot spots of chemical and biological enrichment in the Weddell Sea. *Science (80-.).* 317, 478–482. doi:10.1126/science.1142834.

Smith, R. M., Martell, A. E., and Motekaitis, R. J. (2004). NIST critically selected stability constants of metal

complexes database. *NIST Stand. Ref. Database 46*, National Institute of Standard and Technology, Gai. Available at: https://www.nist.gov/document-14894.

Stockdale, A., Tipping, E., Hamilton-Taylor, J., and Lofts, S. (2011). Trace metals in the open oceans: Speciation modelling based on humic-type ligands. *Environ. Chem.* 8, 304–319. doi:10.1071/EN11004.

Stockdale, A., Tipping, E., and Lofts, S. (2015). Dissolved trace metal speciation in estuarine and coastal waters: Comparison of WHAM/Model VII predictions with analytical results. *Environ. Toxicol. Chem.* 34, 53–63. doi:10.1002/etc.2789.

Stockdale, A., Tipping, E., Lofts, S., and Mortimer, R. J. G. (2016). Effect of Ocean Acidification on Organic and Inorganic Speciation of Trace Metals. *Environ. Sci. Technol.* 50, 1906–1913. doi:10.1021/acs.est.5b05624.

Stocker, T. F., Qin, D., Plattner, G.-K., Tignor, M., Allen, S. K., Boschung, J., et al. (2013). Climate change 2013: The physical science basis. *Contrib. Work. Gr. I to fifth Assess. Rep. Intergov. panel Clim. Chang.* 1535.

Stramma, L., Brandt, P., Schafstall, J., Schott, F., Fischer, J., and Körtzinger, A. (2008a). Oxygen minimum zone in the North Atlantic south and east of the Cape Verde Islands. *J. Geophys. Res. Ocean.* 113. doi:10.1029/2007JC004369.

Stramma, L., Johnson, G. C. G. C., Sprintall, J., and Mohrholz, V. (2008b). Expanding oxygen-minimum zones in the tropical oceans. *Science (80-.).* 320, 655–658. doi:10.1126/science.1153847.

Stramma, L., Visbeck, M., Brandt, P., Tanhua, T., and Wallace, D. (2009). Deoxygenation in the oxygen minimum zone of the eastern tropical North Atlantic. *Geophys. Res. Lett.* 36. doi:https://doi.org/10.1029/2009GL039593.

Strub, P. T., Mesías, M. J., Montecino, V., Rutllant, J., and Salinas, S. (1998). "Coastal ocean circulation off western South America coastal segment," in *The Sea*, 273–313.

SUNDA, W. G. (2001). Bioavailability and bioaccumulation of iron in the sea. *Biogeochem. iron seawater*, 41–84.

Sunda, W. G., and Huntsman, S. A. (1995). Iron uptake and growth limitation in oceanic and coastal phytoplankton. *Mar. Chem.* 50, 189–206. doi:10.1016/0304-4203(95)00035-P.

Sunda, W. G., and Huntsman, S. A. (1996). Antagonisms between cadmium and zinc toxicity and manganese limitation in a coastal diatom. *Limnol. Oceanogr.* 41, 373–387.

Sunda, W. G., and Huntsman, S. A. (1998). Interactions among Cu2+, Zn2+, and Mn2+ in controlling cellular Mn, Zn, and growth rate in the coastal alga Chlamydomonas. *Limnol. Oceanogr.* 43, 1055–1064.

Tagliabue, A., Aumont, O., Death, R., Dunne, J. P., Dutkiewicz, S., Galbraith, E., et al. (2016). How well do global ocean biogeochemistry models simulate dissolved iron distributions? *Global Biogeochem. Cycles* 30, 149–174. doi:10.1002/2015GB005289.

Tagliabue, A., Bowie, A. R., DeVries, T., Ellwood, M. J., Landing, W. M., Milne, A., et al. (2019). The interplay between regeneration and scavenging fluxes drives ocean iron cycling. *Nat. Commun.* 10, 1–8. doi:10.1038/s41467-019-12775-5.

Tagliabue, A., Williams, R. G., Rogan, N., Achterberg, E. P., and Boyd, P. W. (2014). A ventilation-based framework to explain the regeneration-scavenging balance of iron in the ocean. *Geophys. Res. Lett.* 41, 7227–7236. doi:10.1002/2014GL061066.

Takahashi, T., Sutherland, S. C., Chipman, D. W., Goddard, J. G., and Ho, C. (2014). Climatological distributions of pH, pCO2, total CO2, alkalinity, and CaCO3 saturation in the global surface ocean, and temporal changes at selected locations. *Mar. Chem.* 164, 95–125. doi:10.1016/j.marchem.2014.06.004.

Thompson, M., and Howarth, R. J. (1973). The rapid estimation and control of precision by duplicate determinations. *Analyst* 98, 153–160.

Timmermans, K. R., van der Wagt, B., Veldhuis, M. J. W. W., Maatman, A., and De Baar, H. J. W. W. (2005). Physiological responses of three species of marine pico-phytoplankton to ammonium, phosphate, iron and light limitation. *J. Sea Res.* 53, 109–120. doi:10.1016/j.seares.2004.05.003.

Tipping, E., Lofts, S., and Sonke, J. E. (2011). Humic Ion-Binding Model VII: a revised parameterisation of cation-binding by humic substances. *Environ. Chem* 8, 225–235. doi:10.1071/EN11016.

Tipping, E., Lofts, S., and Stockdale, A. (2016). Metal speciation from stream to open ocean: Modelling v. measurement. *Environ. Chem.* 13, 464–477. doi:10.1071/EN15111.

Town, R. M. R. M., and Filella, M. (2000). Dispelling the myths: Is the existence of L1 and L2 ligands necessary to explain metal ion speciation in natural waters? *Limnol. Oceanogr.* 45, 1341–1357. doi:10.4319/lo.2000.45.6.1341.

Town, R. M., and Van Leeuwen, H. P. (2016). Metalion-humic acid nanoparticle interactions: Role of both complexation and condensation mechanisms. *Phys. Chem. Chem. Phys.* 18, 18024–18032. doi:10.1039/c6cp02634f.

Town, R. M., Van Leeuwen, H. P., and Duval, J. F. L. (2019). Rigorous Physicochemical Framework for Metal Ion Binding by Aqueous Nanoparticulate Humic Substances: Implications for Speciation Modeling by the NICA-Donnan and WHAM Codes. *Environ. Sci. Technol.* 53, 8516–8532. doi:10.1021/acs.est.9b00624.

Turner, D. R., Achterberg, E. P., Chen, C.-T. A. T. A., Clegg, S. L., Hatje, V., Maldonado, M. T., et al. (2016). Toward a quality-controlled and accessible pitzer model for seawater and related systems. *Front. Mar. Sci.* 3, 139. doi:10.3389/fmars.2016.00139.

Turner, D. R., and Hunter, K. A. (2001). *The biogeochemistry of iron in seawater*. Wiley Chichester, UK.

Tynan, E., Clarke, J. S., Humphreys, M. P., Ribas-Ribas, M., Esposito, M., Rérolle, V. M. C., et al. (2016). Physical and biogeochemical controls on the variability in surface pH and calcium carbonate saturation states in the Atlantic sectors of the Arctic and Southern Oceans. *Deep. Res. Part II Top. Stud. Oceanogr.* 127, 7–27. doi:10.1016/j.dsr2.2016.01.001.

Ulfsbo, A., Kuliński, K., Anderson, L. G., and Turner, D. R. (2015). Modelling organic alkalinity in the Baltic Sea using a Humic-Pitzer approach. *Mar. Chem.* 168, 18–26. doi:10.1016/j.marchem.2014.10.013.

Uppström, L. R. (1974). The boron/chlorinity ratio of deep-sea water from the Pacific Ocean. *Deep. Res. Oceanogr. Abstr.* 21, 161–162. doi:10.1016/0011-7471(74)90074-6.

Ussher, S. J., Worsfold, P. J., Achterberg, E. P., Laës, A., Blain, S., Laan, P., et al. (2007). Distribution and redox speciation of dissolved iron on the European continental margin. *Limnol. Oceanogr.* 52, 2530–2539. doi:10.4319/lo.2007.52.6.2530.

van den Berg, C. M. G. (1991). Potentials and potentialities of cathodic stripping voltammetry of trace elements in

natural waters. *Anal. Chim. Acta* 250, 265–276. doi:https://doi.org/10.1016/0003-2670(91)85075-4.

van den Berg, C. M. G. (1995). Evidence for organic complexation of iron in seawater. *Mar. Chem.* 50, 139–157. doi:10.1016/0304-4203(95)00032-M.

Van Den Berg, C. M. G. (1984). Determination of copper in sea water by cathodic stripping voltammetry of complexes with catechol. *Anal. Chim. Acta* 164, 195–207. doi:10.1016/S0003-2670(00)85631-7.

van den Berg, C. M. G., and Donat, J. R. (1992). Determination and data evaluation of copper complexation by organic ligands in sea water using cathodic stripping voltammetry at varying detection windows. *Anal. Chim. Acta* 257, 281–291. doi:10.1016/0003-2670(92)85181-5.

Van Den Berg, C. M. G., Nimmo, M., Daly, P., and Turner, D. R. (1990). Effects of the detection window on the determination of organic copper speciation in estuarine waters. *Anal. Chim. Acta* 232, 149–159. doi:10.1016/S0003-2670(00)81231-3.

Van Leeuwen, H. P., and Town, R. M. (2005). Kinetic limitations in measuring stabilities of metal complexes by competitive ligand exchange-adsorptive stripping voltammetry (CLE-AdSV). *Environ. Sci. Technol.* 39, 7217–7225. doi:10.1021/es050367+.

Vedamati, J., Goepfert, T., and Moffett, J. W. (2014). Iron speciation in the eastern tropical south pacific oxygen minimum zone off peru. *Limnol. Oceanogr.* 59, 1945–1957. doi:10.4319/lo.2014.59.6.1945.

Vieira, L. H., Krisch, S., Hopwood, M. J., Beck, A. J., Scholten, J., Liebetrau, V., et al. (2020). Unprecedented Fe delivery from the Congo River margin to the South Atlantic Gyre. *Nat. Commun.* 11, 1–8. doi:10.1038/s41467-019-14255-2.

Vraspir, J. M. J. M., and Butler, A. (2009). Chemistry of Marine Ligands and Siderophores. *Ann. Rev. Mar. Sci.* 1, 43–63. doi:10.1146/annurev.marine.010908.163712.

Waska, H., Koschinsky, A., and Dittmar, T. (2016). Fe- and Cu-complex formation with artificial ligands investigated by ultra-high resolution fourier-transform ion cyclotron resonance mass spectrometry (FT-ICR-MS): Implications for natural metal-organic complex studies. *Front. Mar. Sci.* 3, 1–19. doi:10.3389/fmars.2016.00119.

Wen, L. S., Santschi, P., Gill, G., and Paternostro, C. (1999). Estuarine trace metal distributions in Galveston Bay: Importance of colloidal forms in the speciation of the dissolved phase. *Mar. Chem.* 63, 185–212. doi:10.1016/S0304-4203(98)00062-0.

Witter, A. E., Lewis, B. L., and Luther, G. W. (2000). Iron speciation in the Arabian Sea. *Deep. Res. Part II Top. Stud. Oceanogr.* 47, 1517–1539. doi:10.1016/S0967-0645(99)00152-6.

Worms, I., Simon, D. F., Hassler, C. S., and Wilkinson, K. J. (2006). Bioavailability of trace metals to aquatic microorganisms: importance of chemical, biological and physical processes on biouptake. *Biochimie* 88, 1721–1731. doi:10.1016/j.biochi.2006.09.008.

Worsfold, P. J., Achterberg, E. P., Birchill, A. J., Clough, R., Leito, I., Lohan, M. C., et al. (2019). Estimating uncertainties in oceanographic trace element measurements. *Front. Mar. Sci.* 6, 1–9. doi:10.3389/fmars.2018.00515.

Wu, J., Boyle, E., Sunda, W., and Wen, L. S. (2001). Soluble and colloidal iron in the oligotrophic North Atlantic

and North Pacific. *Science (80-.).* 293, 847–849. doi:10.1126/science.1059251.

Wu, J., Luther III, G. W., and Luther, G. W. (1994). Size-fractionated iron concentrations in the water column of the western North Atlantic Ocean. *Limnol. Oceanogr.* 39, 1119–1129. doi:10.4319/lo.1994.39.5.1119.

Wu, J., Luther III, G. W., and Luther, G. W. (1995). Complexation of Fe(III) by natural organic ligands in the Northwest Atlantic Ocean by a competitive ligand equilibration method and a kinetic approach. *Mar. Chem.* 50, 159–177. doi:10.1016/0304-4203(95)00033-N.

Xia, K., Bleam, W., and Helmke, P. A. (1997). Studies of the nature of binding sites of first row transition elements bound to aquatic and soil humic substances using X-ray absorption spectroscopy. *Geochim. Cosmochim. Acta* 61, 2223–2235. doi:10.1016/S0016-7037(97)00080-X.

Yamashita, Y., Nishioka, J., Obata, H., and Ogawa, H. (2020). Shelf humic substances as carriers for basin-scale iron transport in the North Pacific. *Sci. Rep.* 10, 1–10. doi:10.1038/s41598-020-61375-7.

Ye, Y., Völker, C., and Gledhill, M. (2020). Exploring the Iron-Binding Potential of the Ocean Using a Combined pH and DOC Parameterization. *Global Biogeochem. Cycles* 34, e2019GB006425. doi:https://doi.org/10.1029/2019GB006425.

Zark, M., and Dittmar, T. (2018). Universal molecular structures in natural dissolved organic matter. *Nat. Commun.* 9, 1–8. doi:10.1038/s41467-018-05665-9.

Zark, M., Riebesell, U., and Dittmar, T. (2015). Effects of ocean acidification on marine dissolved organic matter are not detectable over the succession of phytoplankton blooms. *Sci. Adv.* 1, 1–7. doi:10.1126/sciadv.1500531.

Zhang, J., Kattner, G., and Koch, B. P. (2019). Interactions of trace elements and organic ligands in seawater and implications for quantifying biogeochemical dynamics: A review. *Earth-Science Rev.* 192, 631–649. doi:10.1016/j.earscirev.2019.03.007.

Statement of declaration

I, Kechen Zhu, hereby declare that I have written this Ph.D. thesis independently, under compliance of the rules for good scientific practice of the German Research Foundation. I declare that I have used only the sources, the data and the support that I have clearly mentioned. Moreover, I assure that this Ph.D. thesis has not been submitted for the conferral of a degree elsewhere, and that none of my academic degrees has ever been withdrawn. Published or submitted for publication manuscripts are identified at the relevant places.

Kechen Zhu Kiel, 19.05.2021